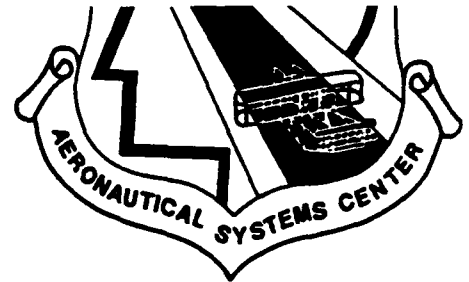


ASC-TR-93-5005

AN UNCERTAINTY ANALYSIS OF INLET
DYNAMIC FLOW DISTORTION USING AN
ANALOG/DIGITAL HYBRID EDITING SYSTEM

AD-A266 924



MARYANN ZELENAK

FLIGHT TECHNOLOGY BRANCH
FLIGHT SYSTEMS ENGINEERING DIVISION

MARCH 1993

FINAL REPORT FOR 02/01/91-12/31/92

APPROVED FOR PUBLIC RELEASE; DISTRIBUTION IS UNLIMITED.



INTEGRATED ENGINEERING & TECHNICAL MANAGEMENT DIRECTORATE
AERONAUTICAL SYSTEMS CENTER
AIR FORCE MATERIEL COMMAND
WRIGHT PATTERSON AFB OH 45433-7126

93-15821



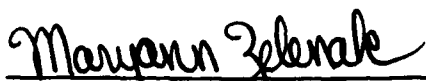
93 7 13 01 2

NOTICE

When Government drawings, specifications, or other data are used for any purpose other than in connection with a definitely Government-related procurement, the United States Government incurs no responsibility or any obligation whatsoever. The fact that the government may have formulated or in any way supplied the said drawings, specifications, or other data, is not to be regarded by implication, or otherwise in any manner construed, as licensing the holder, or any other person or corporation; or as conveying any rights or permission to manufacture, use, or sell any patented invention that may in any way be related thereto.

This report is releasable to the National Technical Information Service (NTIS). At NTIS, it will be available to the general public, including foreign nations.

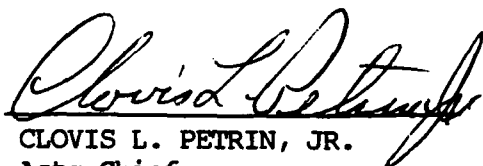
This technical report has been reviewed and is approved for publication.



MARYANN ZELENAR
Aerodynamics & Performance Section
Flight Technology Branch
Flight Systems Engineering Division



RIMANTAS LIAUGMINAS, Chief
Aerodynamics & Performance Section
Flight Technology Branch
Flight Systems Engineering Division



CLOVIS L. PETRIN, JR.
Actg Chief
Flight Systems Engineering Division

If your address has changed, if you wish to be removed from our mailing list, or if the addressee is no longer employed by your organization please notify ASC/ENFTA, WPAFB, OH 45433-7809 to help us maintain a current mailing list.

Copies of this report should not be returned unless return is required by security considerations, contractual obligations, or notice on a specific document.

REPORT DOCUMENTATION PAGE			Form Approved OMB No. 0704-0188	
Public reporting burden for this collection of information is estimated to average 1 hour per response, including the time for reviewing instructions, searching existing data sources, gathering and maintaining the data needed, and completing and reviewing the collection of information. Send comments regarding this burden estimate or any other aspect of this collection of information, including suggestions for reducing this burden, to Washington Headquarters Services, Directorate for Information Operations and Reports, 1215 Jefferson Davis Highway, Suite 1204, Arlington, VA 22202-4302, and to the Office of Management and Budget, Paperwork Reduction Project (0704-0188), Washington, DC 20503.				
1. AGENCY USE ONLY (Leave blank)	2. REPORT DATE March 1993	3. REPORT TYPE AND DATES COVERED Final - Feb 1991 thru Dec 1992		
4. TITLE AND SUBTITLE An Uncertainty Analysis of Inlet Dynamic Flow Distortion Using an Analog/Digital Hybrid Editing System		5. FUNDING NUMBERS		
6. AUTHOR(S) Zelenak, Maryann				
7. PERFORMING ORGANIZATION NAME(S) AND ADDRESS(ES) Aerodynamics and Performance Section (ASC/ENFTA) Integrated Engineering and Technical Management Directorate Aeronautical Systems Center Air Force Materiel Command Wright Patterson AFB OH 45433-7809		8. PERFORMING ORGANIZATION REPORT NUMBER ASC-TR-93-5005		
9. SPONSORING/MONITORING AGENCY NAME(S) AND ADDRESS(ES) Aerodynamics and Performance Section (ASC/ENFTA) Integrated Engineering and Technical Management Directorate Aeronautical Systems Center Air Force Materiel Command Wright-Patterson AFB OH 45433-7809		10. SPONSORING/MONITORING AGENCY REPORT NUMBER ASC-TR-93-5005		
11. SUPPLEMENTARY NOTES				
12a. DISTRIBUTION / AVAILABILITY STATEMENT Approved for Public Release; Distribution is Unlimited			12b. DISTRIBUTION CODE	
13. ABSTRACT (Maximum 200 words) The objectives of this analysis were to establish precision and bias errors for an analog/digital hybrid computer system (DYNADEC) used in the dynamic data editing phase of inlet wind tunnel testing. An uncertainty analysis was initiated to evaluate the system using inlet data from the Aeronautical Systems Center (ASC)/Arnold Engineering Development Center (AEDC) Freejet Development program. Three test points from a subscale freejet test and three test points from a wind tunnel test of the same F-15 inlet model were selected to cover a wide range of test conditions and turbulence levels. Precision errors of the 40 total pressure probes at the location of the engine face were 1-2% of the 40 total pressure recovery magnitudes. Precision errors of the Pratt and Whitney K_{a2} distortion index, the parameter used to edit the data on DYNADEC, were also investigated. These results indicated that K_{a2} precision errors decreased with higher turbulence levels. Static bias errors were also computed by sending known signal through the DYNADEC system and measuring the output quantity. Static bias errors were much smaller in comparison to the precision error magnitudes and may be considered negligible.				
14. SUBJECT TERMS Distortion Bias Uncertainty Precision Error Inlet			15. NUMBER OF PAGES 334	
			16. PRICE CODE	
17. SECURITY CLASSIFICATION OF REPORT Unclassified	18. SECURITY CLASSIFICATION OF THIS PAGE Unclassified	19. SECURITY CLASSIFICATION OF ABSTRACT Unclassified	20. LIMITATION OF ABSTRACT UL	

DTIC QUALITY INSPECTED 5

TABLE OF CONTENTS

NTIS	CRA&I	<input checked="" type="checkbox"/>
DTIC	TAB	<input type="checkbox"/>
Unannounced		<input type="checkbox"/>
Justification		
By		
Distribution/		
Availability Codes		
Dist	Avail and/or Special	
A-1		

LIST OF FIGURES.....	iv
LIST OF TABLES.....	xi
ACKNOWLEDGMENTS.....	xiii
LIST OF SYMBOLS.....	xiv
CHAPTER	PAGE
Introduction.....	1
I Inlet Aerodynamics and Test Methods.....	5
1.1 Inlet Design Parameters.....	5
1.2 Inlet Distortion.....	10
1.3 Test Techniques.....	14
1.4 Instrumentation and Data Reduction.....	24
1.5 Statistical Prediction Methods.....	36
II Data Background and Evaluation Methods.....	42
2.1 ASTF Freejet Development Program.....	42
2.2 DYNADEC Analog-Digital Computer Set Up...	57
2.3 Basic Uncertainty Methodology.....	63
2.4 Uncertainty Analysis Applied to Data Set.	71
III Discussion of Results.....	99
3.1 Level 1 Analysis.....	99
3.2 Level 2 Analysis.....	104
3.3 Level 3 Analysis.....	118
3.4 Level 4 Analysis.....	169
IV Conclusions and Recommendations.....	176
APPENDICES	
A. Pratt and Whitney and AIR 1419 Distortion Parameters.....	181
B. Precision Index Data.....	189
C. Bias Error Data.....	273
LIST OF REFERENCES.....	317

LIST OF FIGURES

FIGURES	PAGE
1. Variable Geometry Inlet Examples.....	6
2. Cowl Lip Geometry Effect on Additive Drag.....	7
3. Diffuser Design Considerations.....	8
4. Temperature-Entropy Diagram for an Ideal Turbine Engine.....	9
5. Compressor Stall Example.....	11
6. Inlet Development Test Models.....	15
7. Aerodynamic Interface Plane Instrumentation Rake..	16
8. Inlet Verification Test Mass Flow Plug Example....	18
9. Direct Connect Test Facility.....	19
10. Distortion Screen Examples.....	19
11. Air Jet Distortion Generator Set Up.....	21
12. Forebody Simulator Example.....	23
13. Inlet Reference Plane Location.....	24
14. 40 Probe Rake Configuration.....	26
15. Data Acquisition System Set Up.....	28
16. Dual-Probe Rake Configuration.....	30
17. Example of Power Spectral Density Plot.....	31
18. Examples of Various Signal Types.....	32
19. Dynamic Signal Representation.....	39

FIGURES	PAGE
20. ASTF Freejet Set Up.....	42
21. ASTF Freejet Development Program F-15 Test Matrix.	44
22. Subscale Freejet.....	45
23. ASTF Subscale Freejet Nozzles.....	46
24. F-15 Aircraft.....	47
25. F-15 16% Scale Inlet Model.....	48
26. ASTF Freejet Forebody Simulators.....	49
27. AIP Rake.....	50
28. F-15 IRP Rake Set Up.....	51
29. ASTF Freejet Dynamic Criteria.....	54
30. DYNADEC Equipment Set Up.....	58
31. DYNADEC Analog Wiring.....	59
32. DYNADEC Peak Detector Set Up.....	60
33. DYNADEC Example Output.....	61
34. Bias Error.....	64
35. Measurement Errors.....	65
36. Precision Error.....	66
37. Bias Error Determination.....	68
38. Uncertainty Interval about the Mean.....	70
39. Amplitude Variation with Turbulence Level.....	73
40. Probe Bias Error Signal Locations.....	86
41. Distortion Parameter Bias Error Signal Locations..	92
42. Probe Bias Error Signal Locations from Static Checks of Test Points.....	97
43. FJ72.067 Six Probe Distributions.....	101
44. Level 1 Analysis Example Outlier Cases.....	102

FIGURES	PAGE
45. K _θ Digital-Analog Difference Vs. RMS Turbulence Level.....	110
46. K _{ra2} Digital-Analog Difference Vs. RMS Turbulence Level.....	113
47. K _{a2} Digital-Analog Difference Vs. RMS Turbulence Level.....	113
48. WT603.4 Outlier.....	114
49. WT563.4 Outliers.....	115
50. FJ72.067 Faulty Probe Distribution Example.....	117
51. K _θ Digital-Analog Difference Vs. RMS Turbulence Level, Outliers Eliminated.....	127
52. K _{ra2} Digital-Analog Difference Vs. RMS Turbulence Level, Outliers Eliminated.....	128
53. K _{a2} Digital-Analog Difference Vs. RMS Turbulence Level, Outliers Eliminated.....	128
54. FJ72.067 Faulty Probe Distributions.....	130
55. FJ14.148 Faulty Probe Distributions.....	131
56. FJ59.022 Faulty Probe Distributions.....	132
57. WT1170.1 Faulty Probe Distributions.....	133
58. Probe (5,4) Distributions from Six Test Cases.....	135
59. Sedlock Program Delta Recovery Vs. Run Time.....	139
60. FJ72.067 Sedlock Predicted Peak Distortion Pattern Evolution with Number of Samples, 4050 & 8050 Samples.....	141
61. FJ72.067 Sedlock Predicted Peak Distortion Pattern Evolution with Number of Samples, 16100 & 24150 Samples.....	142
62. WT603.4 Sedlock Predicted Peak Distortion Pattern Evolution with Number of Samples, 4050 & 8050 Samples.....	143

FIGURES

PAGE

63.	WT603.4 Sedlock Predicted Peak Distortion Pattern Evolution with Number of Samples, 16100 & 24150 Samples.....	144
64.	FJ14.148 Sedlock Predicted Peak Distortion Pattern Evolution with Number of Samples, 4050 & 8050 Samples.....	145
65.	FJ14.148 Sedlock Predicted Peak Distortion Pattern Evolution with Number of Samples, 16100 & 24150 Samples.....	146
66.	WT563.4 Sedlock Predicted Peak Distortion Pattern Evolution with Number of Samples, 4050 & 8050 Samples.....	147
67.	WT563.4 Sedlock Predicted Peak Distortion Pattern Evolution with Number of Samples, 16100 & 24150 Samples.....	148
68.	FJ59.022 Sedlock Predicted Peak Distortion Pattern Evolution with Number of Samples, 4050 & 8050 Samples.....	149
69.	FJ59.022 Sedlock Predicted Peak Distortion Pattern Evolution with Number of Samples, 16100 & 24150 Samples.....	150
70.	WT1170.1 Sedlock Predicted Peak Distortion Pattern Evolution with Number of Samples, 4050 & 8050 Samples.....	151
71.	WT1170.1 Sedlock Predicted Peak Distortion Pattern Evolution with Number of Samples, 16100 & 24150 Samples.....	152
72.	FJ72.067 Sedlock Predicted Peak Distortion Pattern at 4 sec Time Slice Vs. DYNADEC "Mean" Peak Distortion Pattern.....	154
73.	WT603.4 Sedlock Predicted Peak Distortion Pattern at 4 sec Time Slice Vs. DYNADEC "Mean" Peak Distortion Pattern.....	155
74.	FJ14.148 Sedlock Predicted Peak Distortion Pattern at 4 sec Time Slice Vs. DYNADEC "Mean" Peak Distortion Pattern.....	156

FIGURES

PAGE

75.	WT563.4 Sedlock Predicted Peak Distortion Pattern at 4 sec Time Slice Vs. DYNADEC "Mean" Peak Distortion Pattern.....	157
76.	FJ59.022 Sedlock Predicted Peak Distortion Pattern at 4 sec Time Slice Vs. DYNADEC "Mean" Peak Distortion Pattern.....	158
77.	WT1170.1 Sedlock Predicted Peak Distortion Pattern at 4 sec Time Slice Vs. DYNADEC "Mean" Peak Distortion Pattern.....	159
78.	FJ72.067 Strip Charts.....	163
79.	FJ72.067 and WT603.4 Forty Probe Precision Index Maps.....	165
80.	FJ14.148 and WT563.4 Forty Probe Precision Index Maps.....	166
81.	FJ59.022 and WT1170.1 Forty Probe Precision Index Maps.....	167
82.	Circumferential Intensity Definition.....	184
83.	FJ72.067 Analog Parameter Distributions.....	189
84.	FJ72.067 Digital Parameter Distributions.....	190
85.	FJ72.067 Dynamic Ring and Face Average Recovery Distributions.....	191
86.	FJ72.067 Probe Recovery Distributions.....	192
87.	FJ72.067 $\Delta P_c/P$, Intensity Distributions.....	199
88.	FJ72.067 MPR Distributions.....	200
89.	FJ72.067 Extent Distributions.....	201
90.	FJ72.067 $\Delta P_r/P$, IDR Distributions.....	202
91.	WT603.4 Analog Parameter Distributions.....	203
92.	WT603.4 Digital Paramter Distributions.....	204
93.	WT603.4 Dynamic Ring and Face Average Recovery Distributions.....	205

FIGURES	PAGE
94. WT603.4 Probe Recovery Distributions.....	206
95. WT603.4 Δ Pc/P, Intensity Distributions.....	213
96. WT603.4 MPR Distributions.....	214
97. WT603.4 Extent Distributions.....	215
98. WT603.4 Δ Pr/P, IDR Distributions.....	216
99. FJ14.148 Analog Parameter Distributions.....	217
100. FJ14.148 Digital Parameter Distributions.....	218
101. FJ14.148 Dynamic Ring and Face Average Recovery Distributions.....	219
102. FJ14.148 Probe Recovery Distributions.....	220
103. FJ14.148 Δ Pc/P, Intensity Distributions.....	227
104. FJ14.148 MPR Distributions.....	228
105. FJ14.148 Extent Distributions.....	229
106. FJ14.148 Δ Pr/P, IDR Distributions.....	230
107. WT563.4 Analog Parameter Distributions.....	231
108. WT563.4 Digital Parameter Distributions.....	232
109. WT563.4 Dynamic Ring and Face Average Recovery Distributions.....	233
110. WT563.4 Probe Recovery Distributions.....	234
111. WT563.4 Δ Pc/P, Intensity Distributions.....	241
112. WT563.4 MPR Distributions.....	242
113. WT563.4 Extent Distributions.....	243
114. WT563.4 Δ Pr/P, IDR Distributions.....	244
115. FJ59.022 Analog Parameter Distributions.....	245
116. FJ59.022 Digital Parameter Distributions.....	246

FIGURES	PAGE
117. FJ59.022 Dynamic Ring and Face Average Recovery Distributions.....	247
118. FJ59.022 Probe Recovery Distributions.....	248
119. FJ59.022 $\Delta P_c/P$, Intensity Distributions.....	255
120. FJ59.022 MPR Distributions.....	256
121. FJ59.022 Extent Distributions.....	257
122. FJ59.022 $\Delta P_r/P$, IDR Distributions.....	258
123. WT1170.1 Parameter Distributions.....	259
124. WT1170.1 Digital Parameter Distributions.....	260
125. WT1170.1 Dynamic Ring and Face Average Recovery Distributions.....	261
126. WT1170.1 Probe Recovery Distributions.....	262
127. WT1170.1 $\Delta P_c/P$, Intensity Distributions.....	269
128. WT1170.1 MPR Distributions.....	270
129. WT1170.1 Extent Distributions.....	271
130. WT1170.1 $\Delta P_r/P$, IDR Distributions.....	272

LIST OF TABLES

TABLE	PAGE
1. Primary Inlet Design Parameters.....	5
2. Sources of Flow Distortion.....	12
3. AIP Placement Guidelines.....	25
4. ASTF Freejet Validation Criteria.....	52
5. Acceptance Process.....	55
6. Student "T" Values.....	67
7. Steps for Determining In-Flight Thrust Uncertainty.....	71
8. Uncertainty Analysis Data Matrix.....	75
9. Uncertainty Analysis Run Log.....	76
10. Analysis Plan.....	78
11. Static Check Recovery Levels.....	85
12. Daily Static Check Example Output.....	88
13. Example Output from a Static Check Performed Before a Test Point is Edited.....	94
14. Preliminary Means and Precision Indices for Six Test Points.....	105
15. Analog and Digital K_0 Levels for Six Test Points.	110
16. K_{a2} Analog and Digital Magnitude Comparison, With Outliers.....	111
17. K_{a2} Analog and Digital Magnitude Comparison, With Outliers.....	112
18. Faulty Probe Log.....	116

TABLE	PAGE
19. Outliers Eliminated.....	119
20. Means and Precision Indices for Six Test Points..	122
21. K_0 Analog and Digital Magnitude Comparison, Outliers Eliminated.....	126
22. K_{a2} Analog and Digital Magnitude Comparison, Outliers Eliminated.....	126
23. K_{a2} Analog and Digital Magnitude Comparison, Outliers Eliminated.....	127
24. Probe (2,8) Precision Indices.....	134
25. Sedlock Program Inputs.....	136
26. Sedlock Program Run Times Simulated.....	153
27. FJ72.067 Run Schedule....	162
28. Wind Tunnel and Freejet Distortion Indices.....	168
29. DYNADEC System Bias Errors.....	172
30. DYNADEC System Bias Errors, Raw Output.....	273

ACKNOWLEDGMENTS

I would like to express my appreciation to my immediate supervisor, Dr. Rimas Liaugminas, for encouraging me to use my work in the Aerodynamics and Performance Section at Wright-Patterson Air Force Base, as a Masters thesis topic and as a basis for this technical report. Thanks go to my office's Technical Specialist, Steve Stumpfl, for his suggestions and comments. The technical assistance of Charlotte D. Coleman, Ellen R. Mayhew and William J. Dardis from Aeronautical Systems Center, Wright-Patterson Air Force Base and Dave K. Beale and Paul Kelly from is gratefully acknowledged.

LIST OF SYMBOLS

A_e	Nozzle Exit Area
ADC	Analog-Digital Converter
AIP	Aerodynamic Interface Plane
B	Bias Error
DYNADEC	Dynamic Data Editing and Computing
F_{gross}	Gross Thrust
F_{net}	Net Thrust
F_{ram}	Ram Drag
IDR	Radial Intensity, AIR 1419 Index Component
IRP	Inlet Reference Plane
K_{a2}	Pratt and Whitney Distortion Index
K_{ra2}	Pratt and Whitney Distortion Index
	Radial Component
K_{θ}	Pratt and Whitney Distortion Index
	Circumferential Component
M	Mach Number
MPR	Multiple-Per-Rev, AIR 1419 Index Component
P	Pressure
P_{t2}/P_{t0}	Total Pressure Recovery, Ratio of Total Pressure at Engine Face to Freestream Total Pressure
Re	Reynolds Number
RMS	Root Mean Square
RMSE	Root Mean Square Error
RN	Random Number
S	Precision Index
$2S/\bar{x}$	Precision Index as a Percentage of the Mean Value
T	Temperature
U_{add}	Additive Uncertainty
U_{rss}	Root-Sum-Squared Uncertainty
V	Velocity
VCO	Voltage Control Oscillator
WC2	Engine Corrected Airflow
W_{comp}	Compressor Work
W_{turb}	Turbine Work
Z1	DYNADEC Scaling Factor
C_p	Specific Heat at Constant Pressure
dval	Steady State Recovery Level Read in DYNADEC System

f	Frequency
m	Mass Flow
q/pt	Dynamic Pressure Head
ska2	DYNADEC Scaling Factor
skra2	DYNADEC Scaling Factor
skc	DYNADEC Scaling Factor
t	Time
\bar{x}	Mean or Average Value
zpss	Known Steady State Pressure Recovery
α	Angle of Attack
β	Angle of Sideslip
$\frac{\Delta (D-A)}{\text{Digital}}$	Difference between digital and analog reading as a percentage of digital reading
ΔDYN	Dynamic Adder Accounting for Test and Processing Uncertainty in Acceptance Criteria

Subscripts

e	Nozzle Exit Station
i	Individual Probe Reading
o	Freestream Quantity
t	Total Pressure
tdyn	Dynamic Component of Total Pressure
tss	Steady State Total Pressure
2	Compressor Face Engine Station
3	Compressor Exit Engine Station
4	Turbine Entrance Engine Station
5	Turbine Exit Engine Station

Superscripts

'	Non-Dimensionalized by Average Quantity
---	---

INTRODUCTION

Integration of an engine and airframe requires knowledge of more than just the engine's thrust producing capabilities. Extensive knowledge of the inlet's ability to deliver air to the engine is required, so that thrust penalties are minimized and aircraft maneuverability is not affected. This knowledge is acquired through numerical analysis, ground testing, and flight testing. The engine-airframe integrators responsibilities are further encumbered with the need to understand both the numerical methodology and test techniques.

Knowledge of test techniques is not restricted to understanding which physical quantities must be measured and where instrumentation should be placed to measure these quantities correctly. A measurement uncertainty analysis must be performed to ensure that the quantity measured is accurate enough to be interpreted correctly.

Precision and accuracy are the two primary goals of any measurement process. To ensure precise and accurate measurements during an aircraft flight test or wind tunnel test, a basic understanding of the instrumentation and data management techniques is required. This knowledge includes

operational methods and system mechanics, but should not be limited to these areas. Error sources in the instrumentation, data acquisition systems, data editing systems, and data reduction techniques should be quantified to fully understand how well a quantity is measured.

Error sources are usually divided into a bias, or fixed component, and a precision, or random component. Bias error is the difference between the actual value and the measured quantity. Precision error is the variation in the measured quantity as the measurement is taken repeatedly. This variation is usually compared to the average value of all repeat measurements.

Bias errors for instrumentation and recording devices can be supplied by the manufacturer. The integration of a number of different components (or error sources) requires on-site evaluation.

The objectives of this analysis were to establish precision and bias errors for an analog-digital hybrid computer used in the dynamic data editing phase of inlet wind tunnel testing. A Dynamic Data Editing and Computing (DYNADEC) System was developed in the early 1970's by the Flight Dynamics Laboratory at Wright-Patterson Air Force Base to screen large quantities of inlet dynamic pressure distortion data. An uncertainty analysis was initiated to

evaluate the current system equipment using inlet data from the Arnold Engineering Development Center (AEDC) Aeropropulsion System Test Facility (ASTF) Freejet Development Program. This program involved the evaluation of wind tunnel and subscale freejet dynamic inlet data in support of a full scale freejet in the ASTF C-2 test cell at AEDC, Tennessee. Results of this analysis will be integrated into the measurement uncertainty of the entire measurement process developed in the Freejet Development Program.

Precision and bias error magnitudes of dynamic total pressure readings at the engine face of an F-15 aircraft was computed. Precision and bias error magnitudes of mathematical formulas based on these total pressure readings, called distortion indices, was also computed. Distortion indices are used to predict "worst case" total pressure patterns at the engine face that deteriorate engine stability margins. A qualitative error analysis was also performed to ensure random number statistical methods were applicable to this data set and to gain a better understanding of overall system operation on a day to day basis.

Chapter I discusses basic inlet aerodynamic and inlet testing concepts used by engine-airframe integrators. Chapter II describes the history of the data set used in this analysis and the data evaluation methods applied to the data.

Chapter III is a discussion of the results from the uncertainty analysis and Chapter IV presents the recommendations and conclusions found during this analysis.

CHAPTER I
INLET AERODYNAMICS AND TESTING

1.1 Inlet Design Parameters

In an era of highly maneuverable aircraft, fighter configurations are requiring more precise engine-airframe integration with each leap in technology. Aircraft flight envelope and maneuvering capabilities can be restricted if engine-airframe integration issues are not properly addressed during in the design phase of the aircraft development program. The five primary design parameters used in the evaluation of potential engine-airframe configurations are described in the subsequent paragraphs and listed in Table 1.¹

Table 1.
Primary Inlet Design Parameters

Requirement	Parameter
1) The inlet must supply the amount of air required for proper engine operation	Airflow Level
2) The inlet's contribution to total aircraft drag is minimal	Inlet Drag
3) The inlet diffuser should reduce the velocity of incoming air in an efficient manner	Diffuser Geometry
4) The inlet has as small a loss in total pressure as possible.	Inlet Total Pressure Losses
5) The inlet provides uniform airflow to the inlet.	Inlet Distortion

The airflow levels required by the engine at off-design conditions can be achieved through various means. Inlet systems must include devices such as blow-in doors if additional air beyond the inlet's basic capabilities are required. If the inlet captures excessive amounts of air, the surplus air must be removed through bypass doors or bleed perforations. Airflow levels can also be regulated through the use of variable geometry which varies inlet ramp position or cone position to change the physical area available for air to enter (Figure 1.).



Figure 1. Variable Geometry Inlet Examples

Any amount of inlet drag detracts from an aircraft's installed thrust capabilities. Minimizing the various inlet drag components is of prime importance in the aircraft design phase. In addition to the ram drag penalty seen in the basic thrust equation;

$$F_{net} = F_{gross} - F_{ram} \quad (1)$$

$$= \dot{m}V_e + (P_e - P_o)A_e - \dot{m}V_o \quad (2)$$

drag penalties from the bleed/bypass system, boundary layer diverter, and skin friction are possible.² The change in momentum from freestream to the inlet face, as the inlet spills airflow outside the inlet capture tube, results in an "additive drag" penalty, as well.³ This effect is offset somewhat by a suction force around the inlet cowl lip; however, most modern fighter aircraft have sharp cowl lips that incur large additive drag penalties at off-design massflows (Figure 2.).

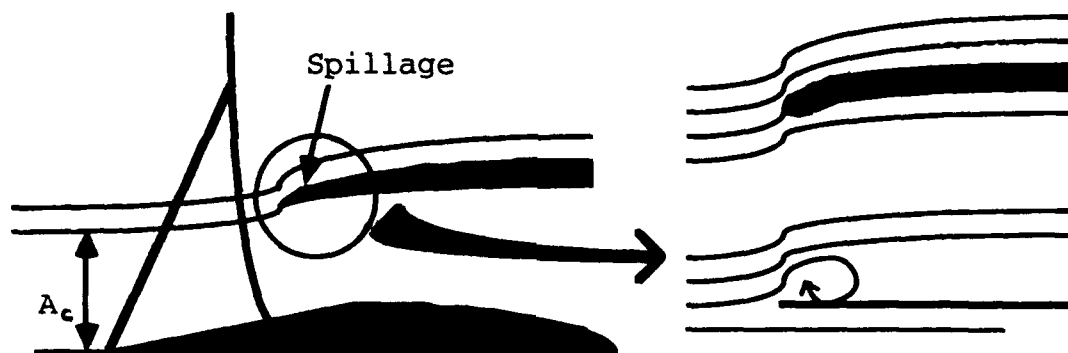


Figure 2. Cowl Lip Geometry Effect on Additive Drag

The third design parameter of importance is the need for a diffuser that efficiently delivers the incoming air to the compressor face. This means that turns and offsets in the diffuser (Figure 3.) should be designed to avoid flow separation.

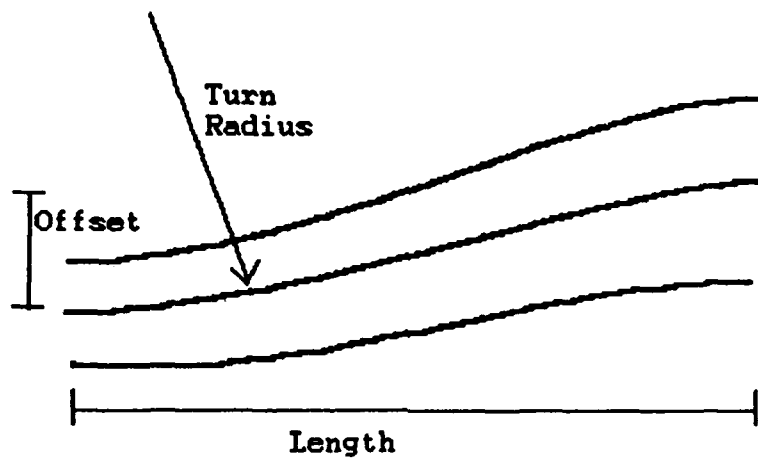


Figure 3. Diffuser Design Considerations

Diffuser lengths and expansion angles should be optimized for minimum friction and diffusion losses.³ The diffuser should additionally reduce air velocity to levels the engine requires in a uniform manner. Flow non-uniformities at the compressor face can result in engine stalls as will be discussed in more detail in subsequent paragraphs.

Flow non-uniformities are also directly associated with the fourth design parameter used to evaluate engine-airframe integration, inlet total pressure losses. Total pressure losses affect engine operation through a loss in thrust. This can be viewed on a temperature-entropy (T-S) diagram of an ideal turbine engine (Figure 4.).

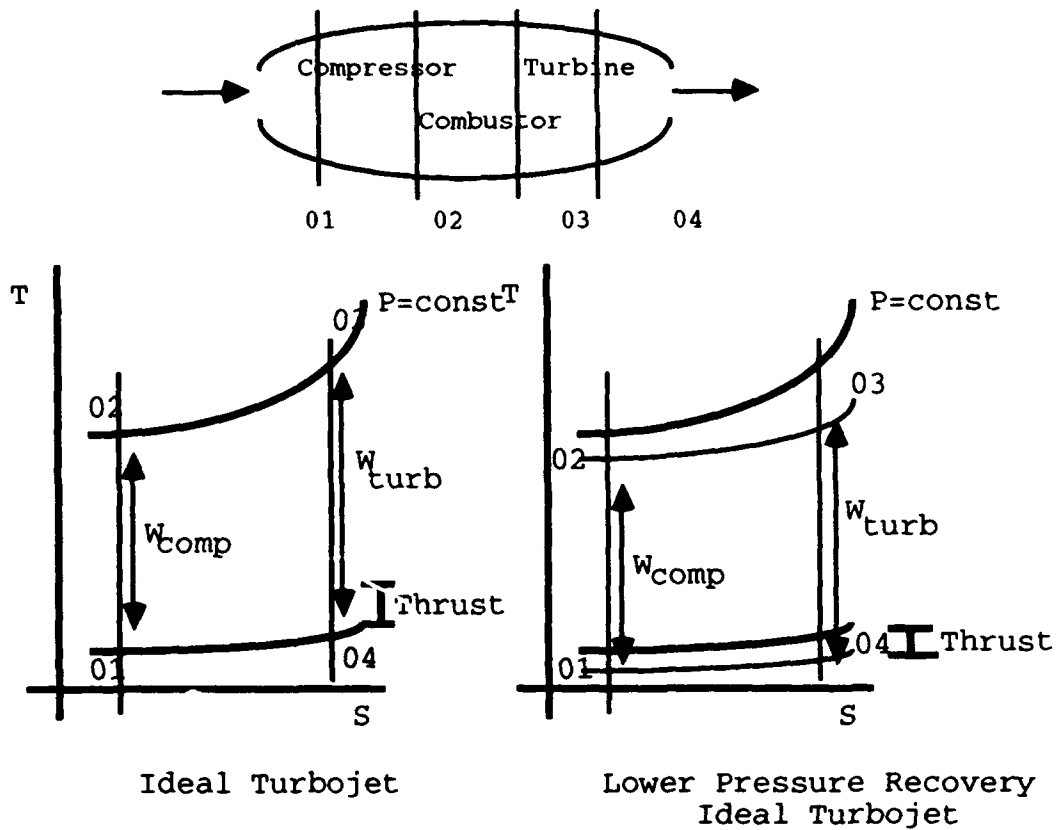


Figure 4. Temperature-Entropy Diagram for an Ideal Turbine Engine

The net work, or thrust, of this system is the turbine work less the work required to run the compressor:

$$W_{\text{turb}} = C_p(T_{03} - T_{04}) \quad (3)$$

$$W_{\text{comp}} = C_p(T_{02} - T_{01}) \quad (4)$$

$$W_{\text{net}} = W_{\text{turb}} - W_{\text{comp}} = \text{Thrust} = C_p(T_{03} + T_{01} - T_{02} - T_{04}) \quad (5)$$

As seen in Figure 4., air entering the compressor at a lower pressure will produce less net work (and thus thrust) because lines of constant pressure diverge on a T-S diagram. Thus,

the compressor work will be a larger percentage of turbine work at lower lines of constant pressure. Because the need for the inlet to "recover" as much of the freestream total pressure as possible is so important the aerospace community uses inlet pressure recovery, the ratio of total pressure at the engine face to freestream total pressure, as the primary means of evaluating inlet performance.

The sources of inlet total pressure losses are numerous, the most obvious being the total pressure loss from shocks at supersonic conditions. Normal shock losses can be alleviated efficiently through the use of a series of oblique shocks. Other causes of total pressure loss include boundary layer accumulation, separation and friction.³ The low energy boundary layer can be removed using bleed or bypass slots; however, these can be sources of total pressure loss themselves. Separation and friction can be minimized through an efficient diffuser design, as mentioned previously.

The fifth design parameter is inlet distortion or non-uniform airflow, which will be discussed in detail in the next section.

1.2 Inlet Distortion

So far, the effect of inlet total pressure losses on engine performance has been discussed on a global scale assuming a uniform total pressure distribution across the compressor face. Temperature, velocity and pressure non-

uniformities (distortion) entering the compressor can have catastrophic effects on various engine components. Isolated pockets of low velocity air enter the compressor at a corresponding low total pressure. The lower energy air approaches the compressor blades in non-ideal directions (Figure 5.).

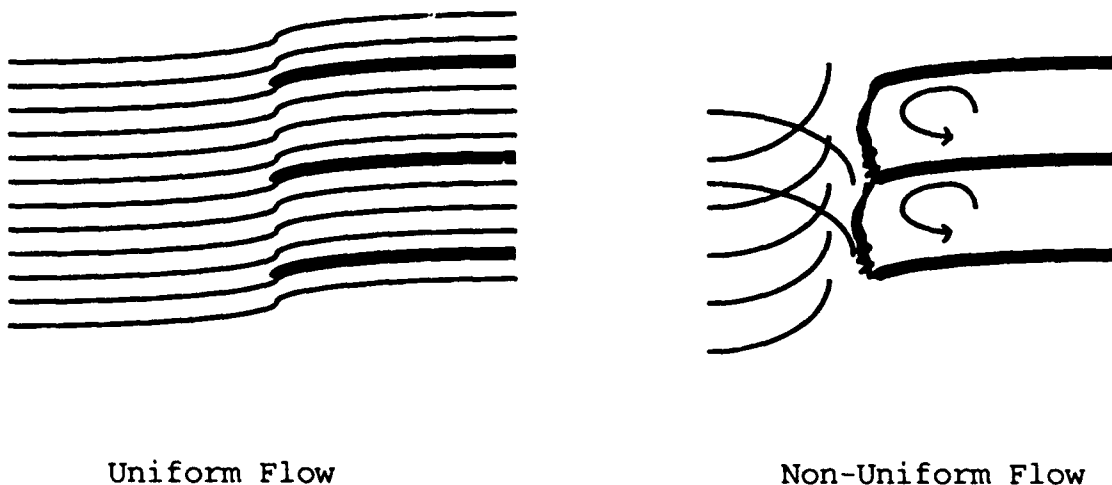


Figure 5. Compressor Stall Example

This increases the angle of incidence of the compressor blades in a direction opposite to the direction of blade rotation. If severe enough, the compressor blades will lose lift or stall, leading to blade failure, compressor vibration or a massive flow reversal (surge) as the compressor blades reach their load-carrying limits .⁴

Compressors can be designed to operate with a high tolerance to distortion. One solution is to reset stator inlet angles. This causes the incoming air to enter the

blades at a more ideal relative angle.¹ Unfortunately, design solutions which increase distortion tolerance must be traded-off with losses in overall engine performance.

An alternate solution is to examine the causes of the flow distortion entering the compressor and determine economical solutions. The primary causes of flow distortion are listed in Table 2.²

Table 2.
Sources of Flow Distortion

- Flow field non-uniformity
- Ingestion of low energy air
- Inlet shock system pressure gradients
- Shock/boundary layer interaction
- Inlet cowl lip separation
- Duct pressure losses and flow separation
- Secondary duct flows

Distortion can be avoided through inlet re-designs, a "re-scheduling" of cone or ramp positions in variable geometry inlets, or flight envelope restrictions. Generally, a design modification is a costly, last-resort solution. Inlet ramp schedule changes require some engineering analysis, but are considerably less costly. Flight envelope restrictions are simple to define, but overall aircraft capabilities are sacrificed.

In the preceding paragraphs, distortion has been discussed on a steady state basis. However, the primary causes of flow distortion listed are not steady state

phenomena. The time-dependent or dynamic nature of these events cause variations of compressor face distortion patterns with time. This is commonly referred to as turbulence, or instantaneous distortion. Because both steady state and dynamic distortion can be so detrimental to engine operation, the evaluation of these phenomena have become the most common method of assessing inlet-engine compatibility. More specifically, the overall goal for inlet design is to provide a stall-free operational environment at the most severe dynamic or peak distortion levels.⁵

The definition of worst case or peak distortion pattern varies from engine to engine and from airframe to airframe. Engines may be more sensitive to flow non-uniformities in either the radial direction or circumferential direction. A worst case pattern in one airframe-engine configuration may not exist in a configuration with a different airframe. The extent of maneuvering flight envelope required (angle of attack, α , and sideslip, β) will also influence the selection of the worst case pattern. Worst case patterns for most fighter aircraft occur near the outer limits of the aircraft maneuver envelope for a given Mach number and altitude.⁶

The effects of turbulence on engine operability directly depend upon the total pressure distribution or pattern, the time period that the compressor experiences the low energy air, compressor rotor speed, and airflow levels involved. Total pressure distributions across the compressor face are

measured in ground and flight tests. They are generally evaluated using the measured pressures and mathematical parameters defined by engine manufacturers called distortion indices. The time slices involved are usually on the order of the time needed for one revolution of the first stage of the compressor. Rotor speeds and airflow levels are a function of flight conditions. The methods used to determine engine operability limits will be described in subsequent paragraphs.

1.3 Test Techniques

There are numerous methods and objectives involved in assessing propulsion system performance. Rather than providing a lengthy description of the entire process, the following discussion will primarily focus on the evaluation of inlet distortion. Reference 7 gives a more detailed description of propulsion system performance evaluation

The following sentences taken, from Reference 7, provide a general description of distortion testing.

The primary objectives of distortion tests are to define the flow distortion characteristics of the inlet and to quantitatively determine the effects of distortion on the stability and performance of the engine. The scope of the test effort must be tailored to the specific needs of the propulsion system. The extent and type of the tests must be balanced with regard for system requirements, program milestones, program risk assessments, program schedules, engine and engine components, and the propulsion system.

The major categories of distortion testing are, 1) inlet development tests, 2) inlet verification tests, and 3) full scale, inlet compatibility tests. The levels of cost and risk involved usually force aircraft development programs to employ a limited combination of the three test techniques.

Inlet development tests use small-scale models of the isolated inlet or inlet/forebody combination (Figure 6.).

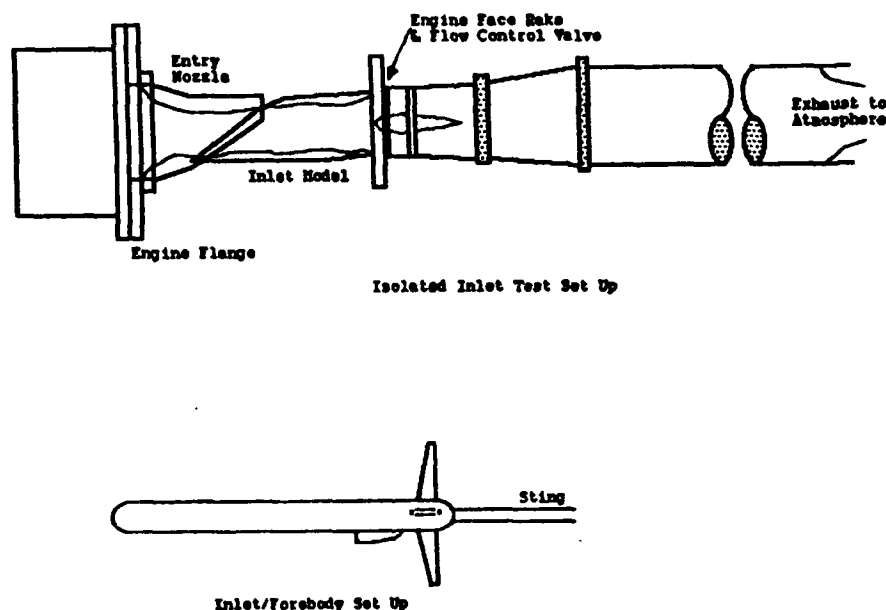


Figure 6. Inlet Development Test Models

The primary objective is to investigate alternate geometries, inlet placement and inlet drag in a series of wind tunnel tests to optimize the inlet configuration. Initial steady state and dynamic distortion data is taken to determine potential problems. Bypass/auxiliary inlet designs and the

influence of external stores on inlet performance may be evaluated, as well.

Instrumentation at this stage of inlet development is somewhat limited. Isolated inlet tests generally measure engine airflows, steady state total pressures and a limited amount of dynamic total pressure data at the aerodynamic interface plane (AIP) near the engine face station. Inlet/forebody tests measure inlet flow field data to optimize inlet placement and evaluate any aircraft forebody effects on flow entering the inlet. A limited amount of static pressure taps may be used to evaluate the diffuser, bleed, and bypass system performance. Steady state and dynamic distortion is determined using a total pressure rake at the AIP consisting of low and high response pressure transducers (probes) (Figure 7.).

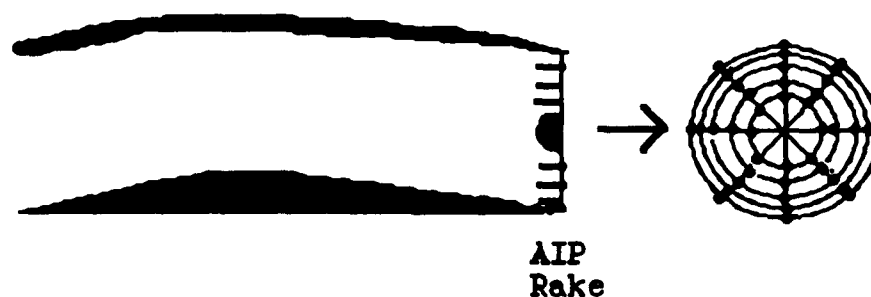


Figure 7. Aerodynamic Interface Plane Instrumentation Rake

Further details of AIP instrumentation and data recording will be given in the next section of this chapter.

Inlet verification tests use the optimized inlet/forebody configuration in a wind tunnel to evaluate performance characteristics throughout the aircraft's maneuver envelope and refine the inlet configuration. Usually model sizes are larger than models used in the development test phase because of the need to simulate all aircraft systems influencing inlet performance. Systems with a potential effect on performance include scoops, vents, auxiliary tanks or pods, and bypass/bleed systems.

Due to model complexity, extensive instrumentation is required in this test phase. Numerous static pressure taps are located throughout the diffuser, bleed and bypass systems and at the AIP. A mass flow plug located behind the simulated engine face regulates simulated engine airflow (Figure 8.).

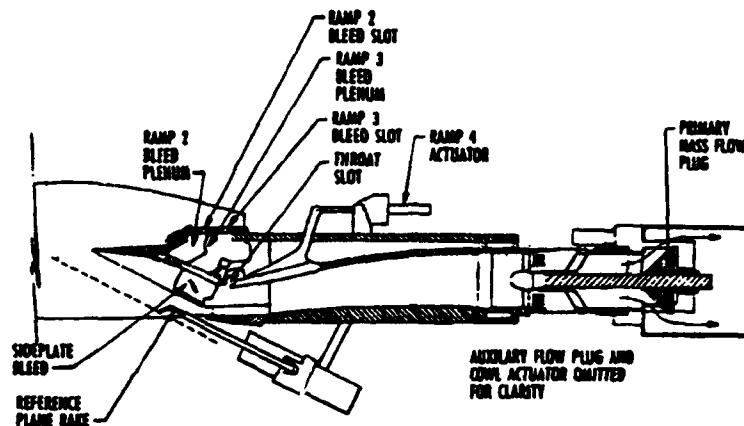


Figure 8. Inlet Verification Test Mass Flow Plug Example

Steady state and dynamic distortion are again measured using a total pressure rake at the AIP. Data taken from this series of tests should fix the inlet design and control schedules along with distortion levels and total pressure recoveries.

Full scale direct connect testing is usually performed in direct-connect test facilities to establish engine stability and performance (Figure 9.).

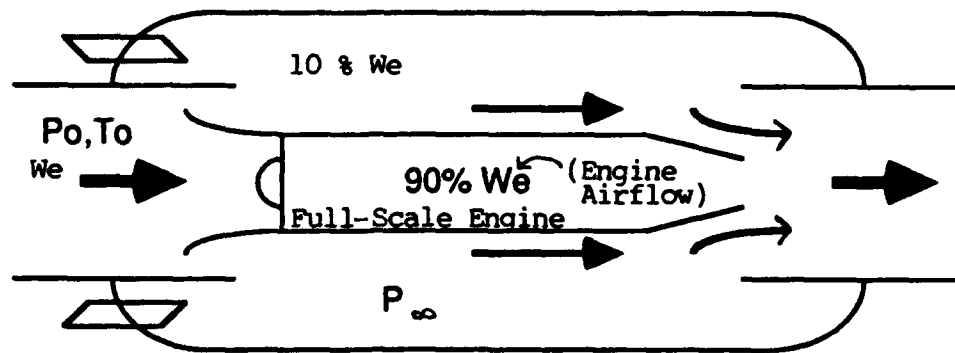
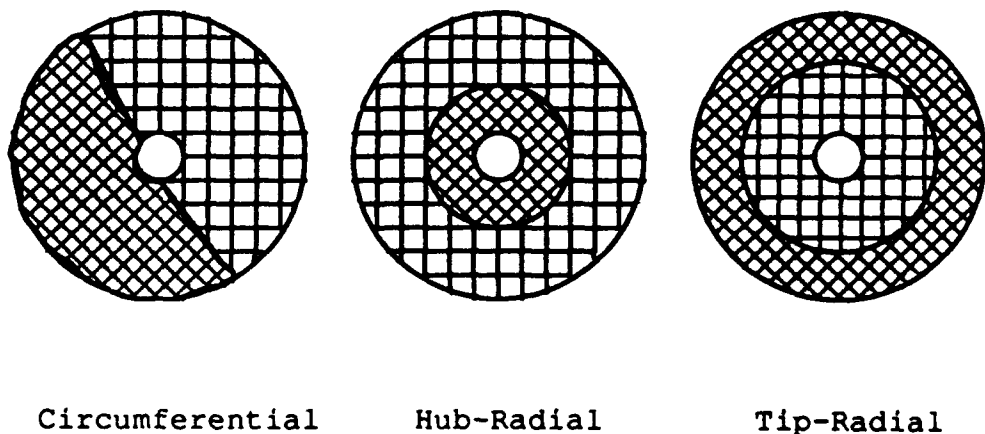


Figure 9. Direct-Connect Test Facility

Direct-connect facilities provide a controlled air source that simulates the influence of the full-scale inlet on air entering the compressor. This includes the production of steady-state and dynamic distortion. Two primary methods used to generate steady-state total pressure distortion are wire mesh screens and air jet distortion generators.

Wire mesh screens generate steady-state distortion by impeding the air entering the engine face (Figure 10.).



Circumferential

Hub-Radial

Tip-Radial

Figure 10. Distortion Screen Examples

Pressure variations are achieved by varying the density of the wire mesh in selected regions of the engine face. The levels of distortion generated depend upon the amount of blockage or porosity and the air velocity. Screens are simple to design and use. Calibrated screens can also be used in multiple facilities with the same engine configuration.

Classical and stylized screens are usually designed to generate a specific steady-state distortion pattern. Classical screens simulate basic distortion pattern characteristics to provide a parametric data base. The resultant distortion patterns may not necessarily occur in a field aircraft, but various combinations of the classical patterns will.

Classical screens in Figure 10 include circumferential, hub-radial, and tip-radial patterns. The classical circumferential distortion screens cause pressure variations around the circumference of the engine face. There are no pressure variations in the radial direction. Radial distortion screens produce pressure variations only in the radial direction with no circumferential variation. The terms hub and tip radial screens refer to the placement of the low pressure zones on the engine face.

Direct-connect tests also use stylized screens that create combinations of radial and circumferential distortions. An aircraft development program usually selects several distortion patterns of concern from prior subscale

inlet tests and fabricates associated screens for full scale engine tests. Because of the limited usable range for each screen, a considerable amount of test time can be sacrificed to changing screens if numerous patterns are required.

Air jets are an alternative method of producing steady state distortion. Air jets create jets of air in a direction that cancels part of the air momentum entering the engine (Figure 11.).

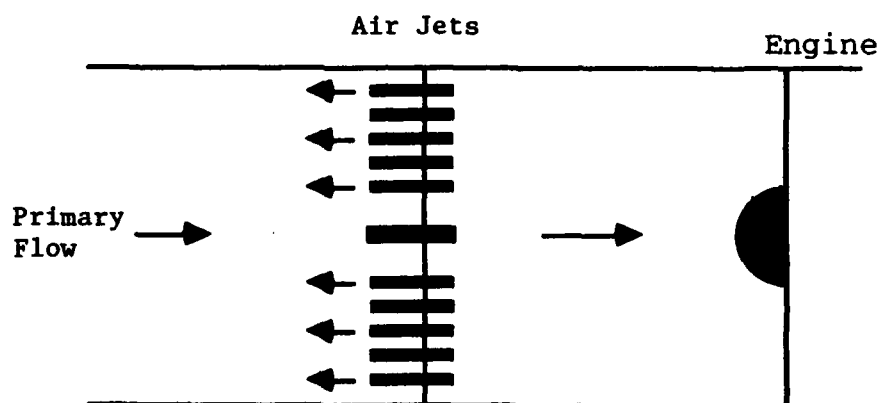


Figure 11. Air Jet Distortion Generator Set Up

The distortion pattern is regulated by remotely varying air jet velocities and quantities.

Dynamic distortion is generated in direct-connect tests to evaluate compressor/fan stability and performance and to determine the distortion patterns causing stall or surge events. Many dynamic distortion generators are variations on the screen and air jet techniques described previously. Air

jets can create dynamic distortion by varying the rate of counter airflow with time. Perforated plates can also be used to generate dynamic distortion by adjusting the distribution of the perforations. Details of other types of dynamic distortion generators for direct-connect tests can be found in Reference 7.

Two alternative full scale test techniques are full scale inlet/engine wind tunnel testing and freejet testing. Testing full scale inlet/engine configurations in wind tunnels has been done in the past. Full-scale wind tunnel testing is advantageous in that the inlet simulators required for direct-connect tests are avoided. The engine's effect on inlet airflow can also be evaluated. The level of risk involved in this type of testing is great in that a test failure could produce catastrophic results (the loss of a wind tunnel), thus full scale tests of this type are not as common as direct-connect tests.

Wind tunnel size dimensions limit the size of usable full scale configurations. Angle of attack and sideslip conditions are limited due to tunnel blockage. Configurations requiring forebody influences on engine performance limit size, as well. This can be alleviated using a forebody simulator (Figure 12.).

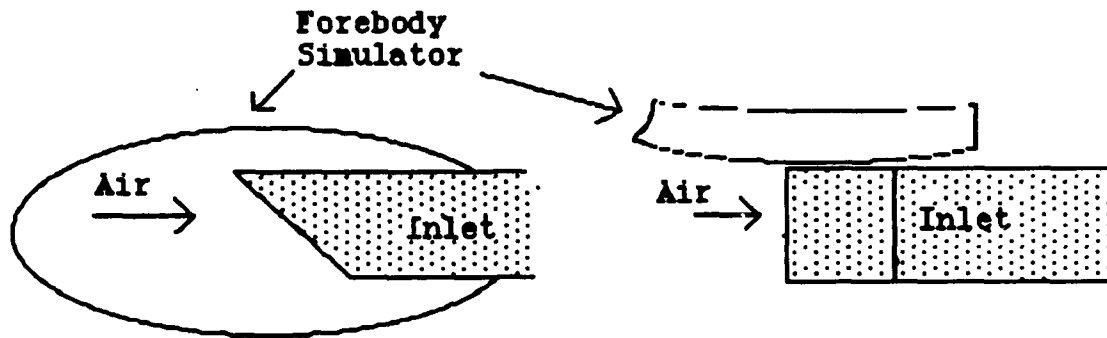


Figure 12. Forebody Simulator Example

Forebody simulators are designed to influence the air entering the inlet in the same manner as a complete aircraft forebody. Forebody simulator disadvantages include their limited useful range and the need for prior subscale wind tunnel tests to establish simulator design.

Freejet testing is also an alternative full scale inlet-engine test technique. The inlet-engine configuration is mounted downstream of a maneuverable freejet nozzle. Thus, the angle of attack and sideslip limitations of wind tunnels are avoided in freejet testing; however, forebody sizes are limited in this test technique, as well.

Forebody simulators can be substituted in this method of testing for large configurations. Because forebody simulators are used, simulating the proper distortion levels for a given flight condition requires flow matching conditions at a reference plane in front of the inlet to those obtained at the same reference plane in earlier

subscale inlet tests or in computational fluid dynamics (CFD) studies. This matching location is called the inlet reference plane (IRP) (Figure 13.).

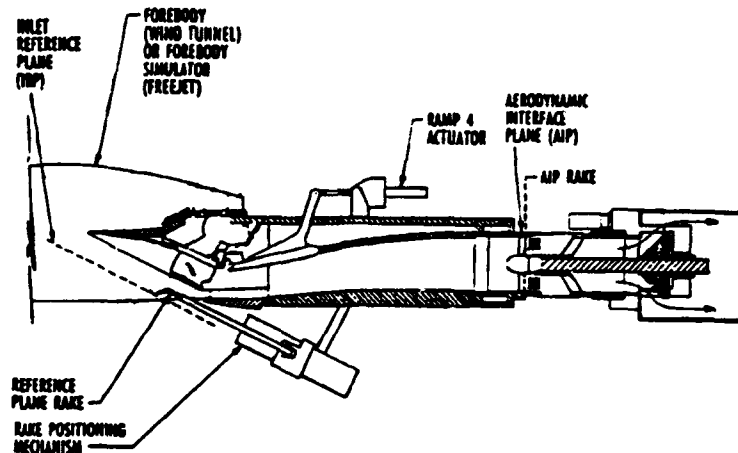


Figure 13. Inlet Reference Plane Location

Usually freejet nozzle position and Mach number are adjusted until IRP conditions match required conditions. Then, the appropriate data is recorded. Further details of the freejet test technique will be discussed in Chapter 2, as part of the description of the data used in this thesis.

1.4 Instrumentation and Data Reduction

Inlet test instrumentation requirements vary from program to program. Early attention to data recording and reducing techniques leads to larger benefits later in a development program. Because the subject of this analysis is inlet distortion, the primary focus will be the

instrumentation required to evaluate inlet distortion and the subsequent data reduction techniques required.

Determination of the aerodynamic interface plane (AIP) consistent for all phases of inlet testing is very important. AIP guidelines from Reference 8, are listed in Table 3.

Table 3.
AIP Placement Guidelines

1. The AIP should be located in a circular or annular section of the inlet duct.
2. The AIP should be located as close as practical to engine-face plane. The engine-face plane is defined by the leading edge of the most upstream engine strut, vane, or blade row.
3. The AIP should be located so that all engine airflow, and only the engine airflow, passes through it. The distance between the inlet auxiliary air systems and the AIP should be such that the effect of the auxiliary air systems on distortion is included in the measurements at the AIP.
4. The AIP location should be such that engine performance and stability are not measurably changed by interface instrumentation.

The number and location of probes at the AIP depends upon the accuracy of the pattern required, the complexity of data acquisition, and the rake-induced flow blockage. The obvious goal is to produce the most accurate pattern possible using the least costly instrumentation and minimal flow blockage.

The optimal distribution is the 40 probe configuration seen in Figure 14.

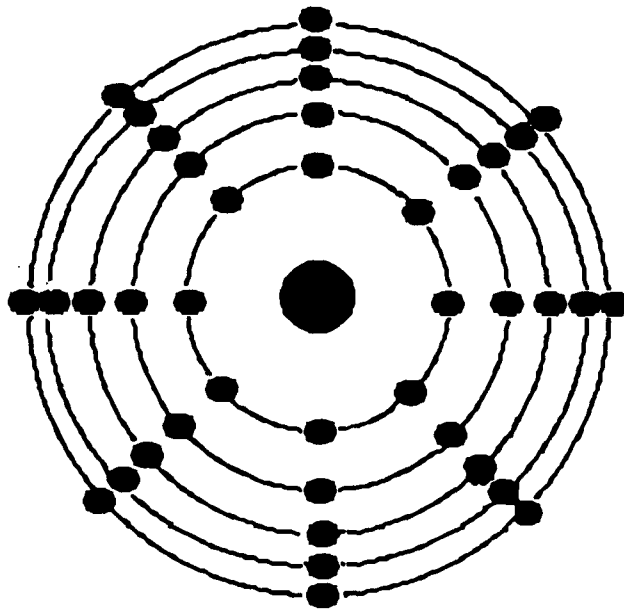


Figure 14. 40 Probe Rake Configuration

Past studies, such as Reference 9, have shown that 8 rakes of 5 probes (or rings) each is the minimum density required to attain an accurate distortion pattern. A minimum of 8 rakes are needed to accurately define circumferential distortion. The number of rings required may be more than 5 if the inlet produces distortion patterns with a strong radial content.

Probe placement may also depend upon the definition of total pressure recovery. As stated previously, pressure recovery is the ratio of engine face average total pressure to freestream total pressure. There must be a consistent definition of the term "average" throughout a test program when dealing with 40 distinct pressure measurements. Ideally, the definition should account for massflow, momentum and energy flux variations through the AIP. Several

definitions used in the past are flow-continuity, area-weighted, mass flow weighted, momentum-weighted, and entropy-derived averaging.⁷

The industry standard definition uses the area-weighted face averaging method. This means instrumented rings are placed at centers of equal area, and the following formula can be used to compute face average total pressure recovery:

$$\frac{P_{t2}}{P_{t0}} = \text{Recovery} = \frac{\sum_{i=1}^N \left(\frac{P_{t2}}{P_{t0}} \right)_i}{N} \quad (6)$$

where; N = the number of probes

This definition reduces the test instrumentation and processing requirements and simplifies the effort needed to define and evaluate distortion patterns. Reference 8 guidelines are based upon this definition.

Once the AIP rake characteristics are set, an accurate transducer/probe configuration must be established. The two requirements are (1) the transducer must have a nominally flat response to frequencies in excess of the highest frequency of interest, and (2) the probe must be smaller than the characteristic size of the eddy producing the highest frequencies of interest. If these two requirements are met, the transducer/probe configuration should be able to properly

sense airflow levels seen by the AIP. A more detailed discussion of transducer frequency response and probe size criteria can be found in Reference 7.

The remaining hardware needed to sense and record inlet test data depends upon the type of transducer selected. Generally, a data acquisition system will be set up as shown in Figure 15.

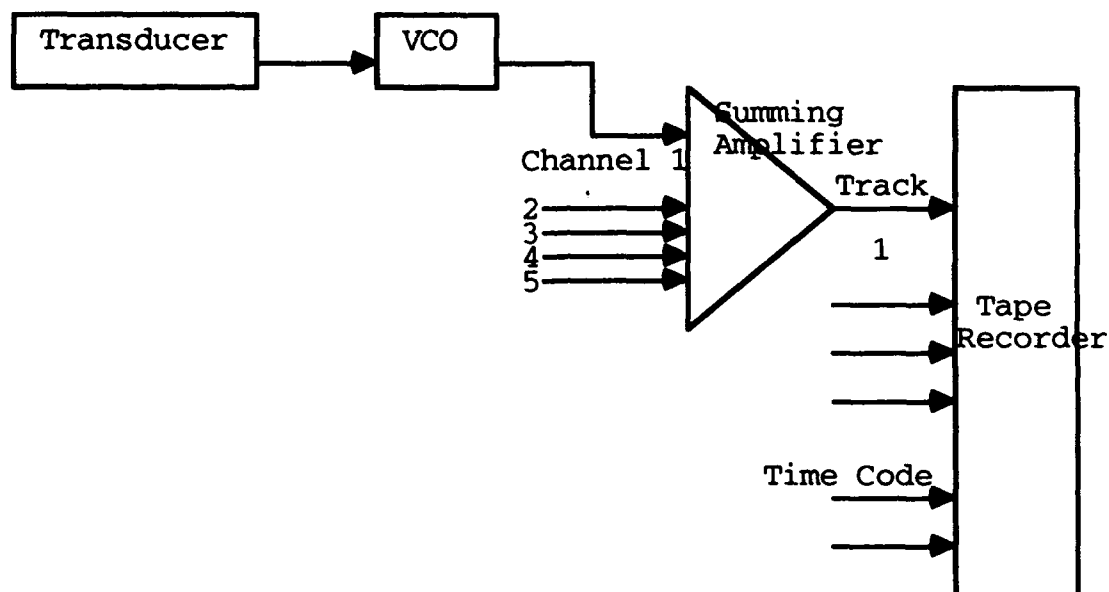


Figure 15. Data Acquisition System Set Up

Signals coming from a transducer are filtered if needed and then sent to a voltage controlled oscillator (VCO). The VCO output is a variable-frequency signal proportional to the transducer input signal. Each transducer has a corresponding VCO with a different output frequency. Data from several probes (VCO outputs) can then be added or multiplexed using a

summing amplifier (discriminator) and recorded on a single track of tape. Writing data from multiple probes onto several tracks of a magnetic tape reduces the instrumentation and memory size requirements of the entire system. Time codes and voice recordings are also written onto separate tracks to help in the data reduction process.

Data acquisition system accuracy is extremely important in order to establish accurate distortion levels. Small differences in pressure have significant effects on distortion levels. Inlet test conditions also have a large range of inlet pressure levels. 30 to 40 psi differences between the lowest and highest altitudes simulated make accuracy even more difficult to achieve. A two standard deviation error limit above or below the absolute pressure being measured is the set guideline. This equates to a $\pm 0.5\%$ limit on individual steady state pressure and a $\pm 2.0\%$ limit on dynamic pressures when engine stability is being evaluated.

The frequency response requirements of steady state and dynamic readings are different. To maintain data system accuracy, one of the methods used is to sense steady state (low frequency) and dynamic (high frequency) with separate probes located next to each other (Figure 16.).

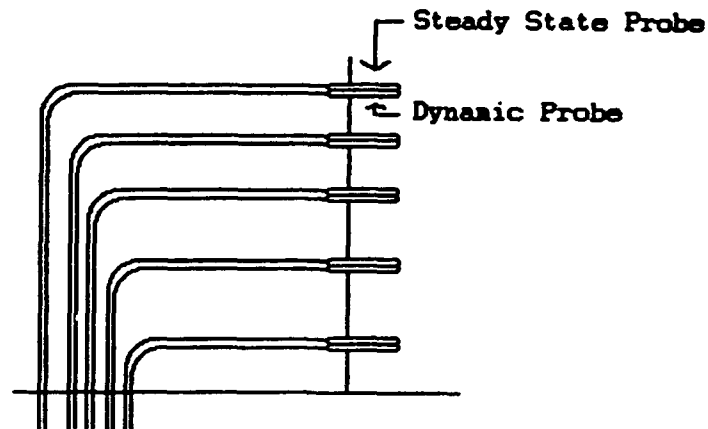


Figure 16. Dual-Probe Rake Configuration

The two components can be filtered separately and added later in the data reduction phase. This creates electrical signals with the full frequency content of the test signals and reduces the effort needed to reduce the enormous amount of data generated.

Filtering out extraneous high frequency noise and determining the frequencies critical to engine operability is also important during the data recording and editing phases. Data frequencies affecting engine operability vary from engine to engine and manufacturer to manufacturer. Frequencies outside the band of interest are normally filtered out to prevent extraneous noise, etc. from affecting distortion patterns. Thus, a "cut-off" frequency is usually defined to tell the filters how much frequency content should be recorded or edited.

The cut off frequency is usually pre-determined by the engine manufacturer and is usually a function of scale model size and engine RPM.

$$f = (\text{Scale Model Size}) * (\text{Engine Maximum RPM}) \quad (7)$$

As model sizes increase, lower cut-off frequencies are required. Power spectral density (PSD) plots provide information on the amount of energy present at each frequency. Frequency content of a filtered signal usually drops off shortly after the cut-off frequency as seen in Figure 17.

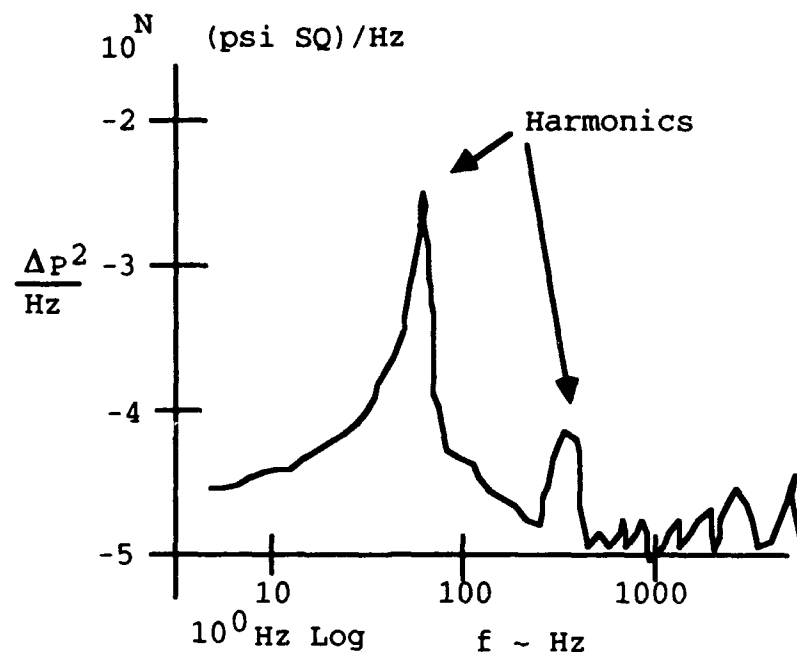


Figure 17. Example of Power Spectral Density Plot

PSD plots can also indicate physical flow characteristics such as shed vortices by showing high energy spikes in narrow frequency bands.

Data reduction can be performed concurrently with a test, after test completion, or a combination of both. It consists of three main tasks: identification of spurious signals from faulty transducers or signal conditioning, developing a method to handle the errant signals, and time editing of data.

There are several methods used to identify spurious signals. Shifts in ambient readings from test to test may indicate a faulty probe. Oscilloscopes or strip charts can be used to compare dynamic activities of channels during a test (Figure 18) or in the data reduction phase.



Good Probe



Bad Probe



Dead Probe

Figure 18. Example of Various Signal Types

This method is particularly effective if a probe fails for only a portion of the test period. Readings can be compared on adjacent probes, with too large a variation indicating bad data. Values can also be compared to the usable range of the transducers or the AIP average total pressure.

Once a channel fails, it is necessary to evaluate distortion patterns using channel substitution techniques on the bad probes. The method used must be consistent throughout a test program and if possible, the failure minimized or corrected during a test. Values substituted for faulty probes should be flagged in the resultant data.

If there is a large number of faulty steady state or dynamic probes, they should be replaced before the test is allowed to continue. The tolerance to the number of bad probes depends upon the objective of the test. Generally, adjacent probes that are faulty should be replaced. Reference 7 states that if "no more than five probes or more than 3 contiguous probes are bad, the distortion descriptors should be flagged."

If the number of faulty steady state probes is reasonable, there are several methods that can be used to compute substitute pressure values. If the faulty probe is not at the tip or hub, the four adjacent probe readings can be weight averaged to create a value. The average of two circumferentially adjacent probes is substituted for a faulty probe at the tip or hub. If one of the adjacent probes is

faulty, as well, the value from the next probe on the rake is substituted for both faulty probes.

Substitutions for faulty dynamic signals are more complicated. Creation of a time history from adjacent probes can be done using their dynamic total pressure histories. Calculations are then sent to a loop where the current faulty probe value is compared to the previous value calculated from the adjacent probe's time histories until the difference is within a set tolerance. An easier method is to "zero out" the dynamic signal while time editing the data, and use the steady state value as a total pressure value for the entire time slice.

Initial time history checks of selected parameters will determine the quality of data achieved during a test and the value of performing more analysis. The size of time segments required for future time editing can also be determined. Thirty to sixty seconds of run time are recommended for full scale tests. Unfortunately this large a time segment can lead to as many as 600,000 distinct distortion patterns in a digital editing session. Clearly, this enormous volume of data must be reduced to manageable levels.

Distortion interpretation techniques have been developed in the past using two goals: identification of inlet-engine compatibility characteristics and evaluation of engine operating conditions. The conservative approach commonly used is to select "worst case" or peak instantaneous

distortion patterns out of the many thousands of patterns generated. Then, engine stability criteria are applied to these cases. Determination of peak patterns is usually done using a set of mathematical formulas called distortion descriptors or indices, based on combinations of the 40 total pressure probe readings.

Universal distortion indices do not exist. Individual engine contractors have developed their own indices as a function of specific engine sensitivity. Usually the indices are generic enough to include weighting factors for each specific engine. Large index magnitudes indicate high distortion. How high is too high is a function of engine sensitivity. Two sets of distortion indices can be found in Appendix A. The 1419 indices have been developed by the Society of Automotive Engineers (SAE) as a set of indices that physically describe flow phenomena, while the K_{a2} index was developed by Pratt and Whitney to evaluate Pratt and Whitney engine operability. Both of these indices will be used in this thesis.

Computation of inlet distortion indices has been done in the past using analog distortion analyzers due to the large volumes of data involved. Analog editors are wired to compute the distortion descriptor of choice. Thus, continuous time traces of the indices can be recorded on the same analog tapes used to record the AIP pressures during a test. In post-test mode, analog distortion analyzers can be

designed with peak distortion detectors which flag maximum index levels and simultaneously instruct the analog-to-digital converters to freeze or digitize the 40 signals at the moment of peak detection.

Recent advances in sample rates and storage capacities of digital computers offer a cheaper alternative to analog editing. If a digital system is used, care must be taken to understand the uncertainties involved in recording the data digitally because these errors will be frozen in the digitized data for all time. It is also important to sample the data at a sufficient rate as it is digitized to accurately determine peak distortion events. The sampling rate should be able to provide information on the highest frequency of interest. Minimally, the sampling rate should be twice the maximum frequency; however, experience has shown that sampling rates of four to five times the maximum frequency are necessary if signal wave form is important.

1.5 Statistical Prediction Methods

Acquisition of dynamic data is an expensive proposition for any aircraft or missile program. Wind tunnel operational costs, model construction, instrumentation requirements, and data processing requirements can limit the size and scope of a test. In recent years, analytical substitutes have been investigated that synthesize dynamic distortion.

The analytical model must be capable of predicting peak distortion patterns accurately, economically, and with limited instrumentation requirements. The model should also be accurate within a wide range of turbulence levels. Various methods developed in recent years use either distortion parameters or inlet pressure statistical properties to predict maximum distortion levels. Distortion patterns have been generated using intensifications of steady state distortion patterns or random number processes.

King, Shuerman, and Muller (Reference 10) developed a method in which the 180° segment of the steady state map with the lowest average total pressure was defined. In this region, the steady state map was intensified by subtracting total pressure increments from steady state levels. The higher pressure 180° region was intensified by adding total pressure increments to steady state levels. Increments were computed using the root mean square (RMS) turbulence value for an individual probe summed with the 180° region's average RMS turbulence level.

$$P_{RMS} = \left[\lim_{T \rightarrow \infty} \frac{1}{T} \int_{-T/2}^{T/2} (P(t) - \bar{P})^2 dt \right]^{1/2} \quad (8)$$

where: t = Time
 $P(t)$ = Pressure signal during time Interval T
 \bar{P} = Average Pressure over time T

Reference 11 describes an alternate steady state intensification method using a sum of random isolated vortices where vortex strength is proportional to RMS turbulence level.

Past studies, including Reference 12, have shown that inlet total pressure fluctuations are random, normally distributed and stationary phenomena. Thus several random number statistical methods have been developed to predict distortion levels and patterns. The fundamental premise behind these methods divides dynamic total pressure into a steady state and fluctuating component with a zero mean value:

$$P_{t \text{ dyn}} = P_{t \text{ ss}} + P_{t \text{ f}} \quad (9)$$

where: $P_{t \text{ ss}}$ = steady state total pressure

$P_{t \text{ f}}$ = fluctuating or dynamic component
of total pressure

In terms of pressure recovery:

$$P_{t/P_{t0}})_i \text{ dyn} = P_{t/P_{t0}})_i \text{ ss} + \Delta P_{t \text{ RMS}/P_{t0}})_i * P_{t/P_{t0}})_i \text{ ss} * RN)_i \quad (10)$$

where: $P_{t/P_{t0}})_i \text{ ss}$ = steady state pressure reading
at probe i

$\Delta P_{t \text{ RMS}/P_{t0}})_i$ = RMS turbulence level at
probe i

$RN)_i$ = Random number

The steady state component is merely the individual steady state probe reading at the AIP. The dynamic component is represented by a random number generator with a normal distribution and the RMS turbulence value at each probe. (Figure 19.)

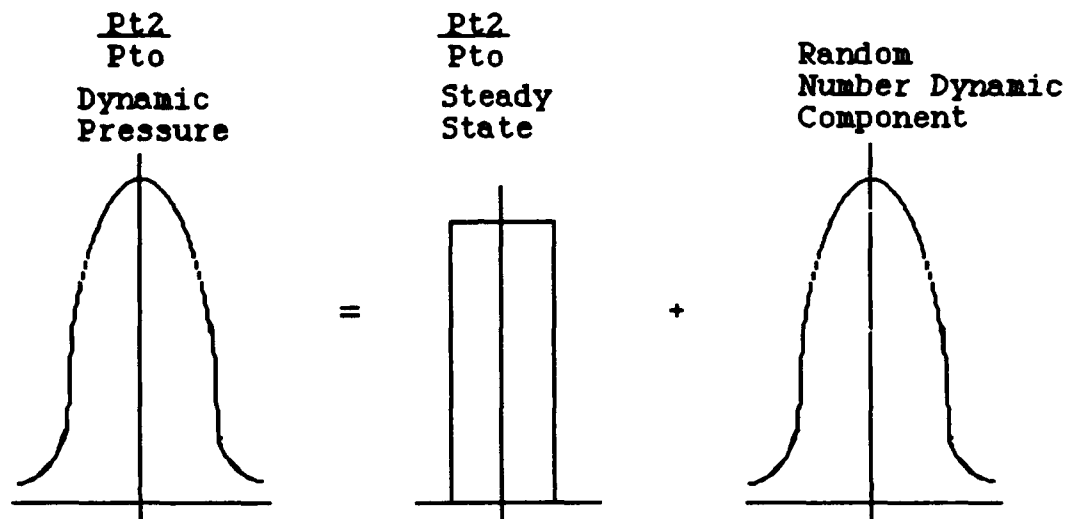


Figure 19. Dynamic Signal Representation

Thus, synthesized dynamic pressures can be generated multiple times to simulate multiple time slices in a complete time history. The synthesized pressures are then input into distortion index equations and peak distortion levels and maps are determined. References 5 and 12-15, provide descriptions of various efforts using this method. The following discussion will focus on Sedlock's method (Reference 15) because it will be used in this analysis.

Sedlock used the basic random number statistical technique with two additional refinements. Two digital filters were used to shape the power spectral density of the random numbers to approximate the power spectral density of the inlet pressure data. The Sedlock method also incorporated a map averaging process which creates six sets of random numbers each with a distinct peak distortion level and pattern. The dynamic total pressure recovery levels from each run are averaged together to create an "average" peak distortion pattern. The filters generally improved the peak distortion levels while the map averaging process improved peak distortion pattern matches with actual test data.

Most of the methods mentioned above also studied the possibility of using fewer than 40 probes to predict inlet distortion. The studies found that as few as four, eight or twelve turbulence measurements predicted distortion levels as well as forty probes. Unfortunately, as the number of probes decreased the match between predicted peak patterns and test data deteriorated.

These statistical techniques were developed for use in inlet preliminary design and development phases. Models could also be used for on-line prediction during tests based on limited instrumentation and thus provide space at the AIP for the measurement of other flow parameters. They can also provide insight into the type of inlet flow (random or non-

random) seen in test data distortion patterns as will be seen in the subsequent uncertainty analysis.

CHAPTER II

DATA BACKGROUND AND EVALUATION METHODS

2.1 ASTF Freejet Development Program

The development of a freejet test capability at Arnold Engineering Development Center (AEDC) was initiated in 1978. The development included the design of subsonic and supersonic nozzles accompanied by various support hardware for the Aeropropulsion Systems Test Facility (ASTF) C-2 test cell.¹⁶ The full-scale systems for the subsonic capability have been completed (Figure 20.) and an initial operating capability demonstrated.

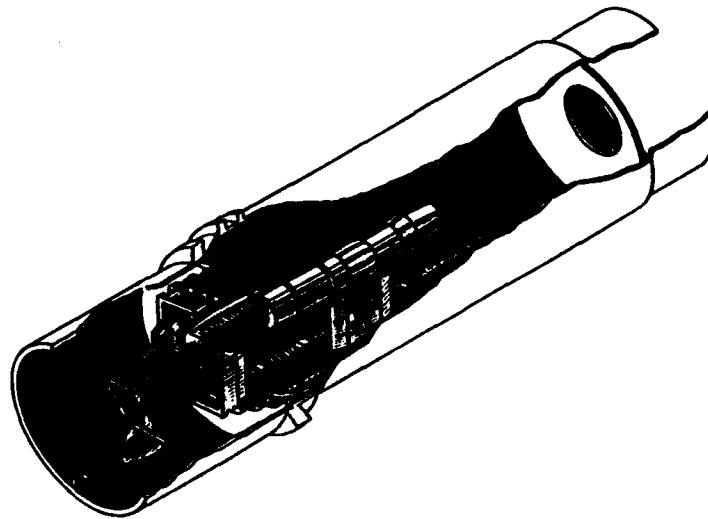


Figure 20. ASTF Freejet Set Up

The design of the full-scale components for a supersonic capability has also been completed.

A concurrent subscale freejet development program was also initiated in 1978 to address technology issues associated with the full scale program. The subscale efforts developed full scale hardware concepts and test techniques and validated the method for fighter aircraft inlet distortion evaluations. First, subsonic hardware concepts were evaluated through flow quality studies. This led to the development and evaluation of test techniques.

Test technique validation was based on the comparison of wind tunnel tests and subscale freejet tests using identical scale models of the U.S. Air Force F-16 and F-15 aircraft inlet/forebody systems. Steady state and dynamic total pressures were selected as measures of comparison. The wind tunnel test results were defined as the "industry standard."

The first tests in the validation program employed a 15% scale F-16 inlet model to establish the feasibility of the freejet concept up to a Mach number of 0.9 and an angle of attack of 30° .¹⁷ The favorable results obtained in the freejet tests of a fixed, chin-mounted inlet provided the impetus to proceed to a more comprehensive validation program.

A 16% scale model of the F-15 inlet was selected to represent a more complex, side-mounted, variable-geometry inlet system. The validation envelope was also expanded to

include both subsonic and supersonic conditions. The effort was initiated in 1986 with the design and fabrication of additional model and subscale freejet facility hardware.

In 1987, the ASTF Freejet Development Working Group comprised of representatives from the Aeronautical Systems Division (ASD) at Wright-Patterson Air Force Base and AEDC, was established to oversee the validation program. The working group developed the validation plan using a test matrix that addressed a wide range of Mach numbers and inlet positions for the F-15 (Figure 21.).

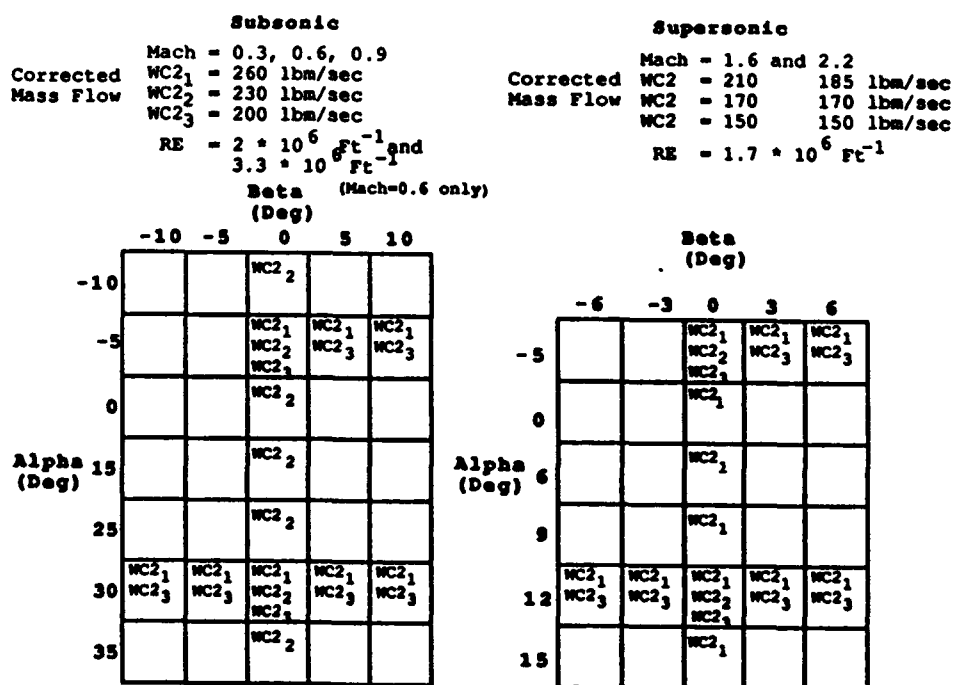


Figure 21. ASTF Freejet Development Program
F-15 Test Matrix

Additional work included extensive use of flow field measurements in establishing the simulation and the evaluation of a family of forebody simulators.

The baseline wind tunnel data was obtained in AEDC's 16T and 16S Propulsion Wind Tunnels (PWT). Each tunnel test section has a 16ft by 16ft cross section and a 40ft length. Subsonic testing was performed in the transonic tunnel, 16T, while supersonic testing was performed in the supersonic tunnel, 16S.

The subscale freejet experiments were conducted in R2A2, a small research tunnel at AEDC. The freejet model seen in Figure 22. from Reference 18, was a 15% scale model of the ASTF C-2 test cell.

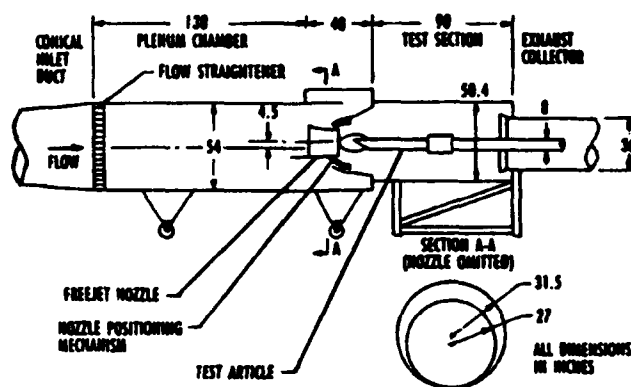


Figure 22. Subscale Freejet

The nozzle was mounted on an attitude positioning mechanism that provided remote control of nozzle orientations between -10° and $+31^\circ$ in pitch and $\pm 10^\circ$ in yaw. Extended pitch and

yaw envelopes were accomplished through offsets in test article pitch and yaw.

Five subscale freejet nozzles were fabricated during the development program (Figure 23.).

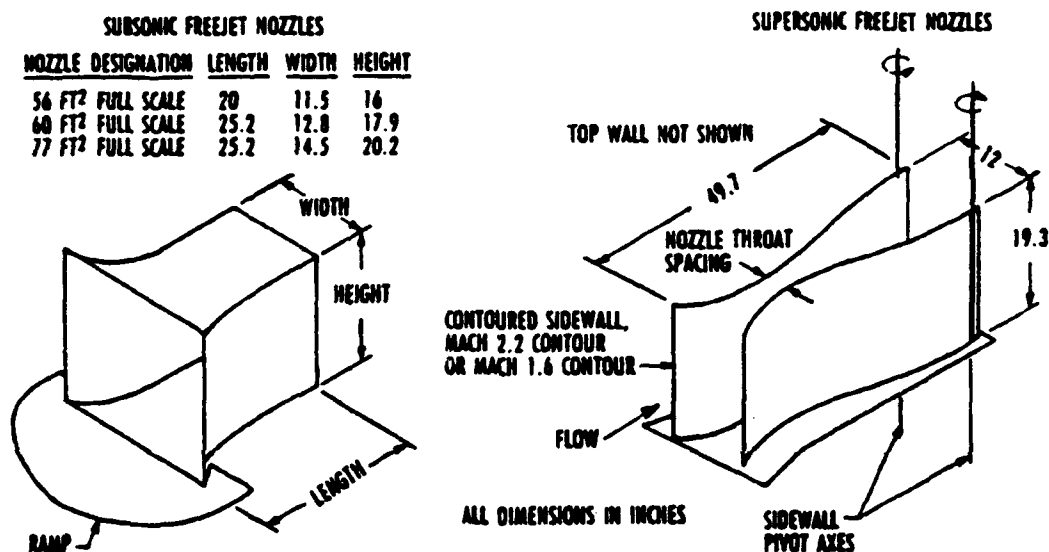


Figure 23. ASTF Subscale Freejet Nozzles

Two 16% scale model freejet nozzles simulating different full scale exit areas were used for subsonic F-15 testing. Mach numbers were varied by changing nozzle pressure ratio. Two 16% scale model freejet nozzles simulating Mach 1.6 and 2.2 conditions respectively were used in the supersonic portions of the test. Mach numbers were varied slightly off design levels by changing nozzle area ratio and nozzle pressure

ratio. Additional details on the freejet facility systems can be found in References 17 through 19.

The F-15 aircraft contains a pair of side-mounted two-dimensional external compression inlets (Figure 24.).

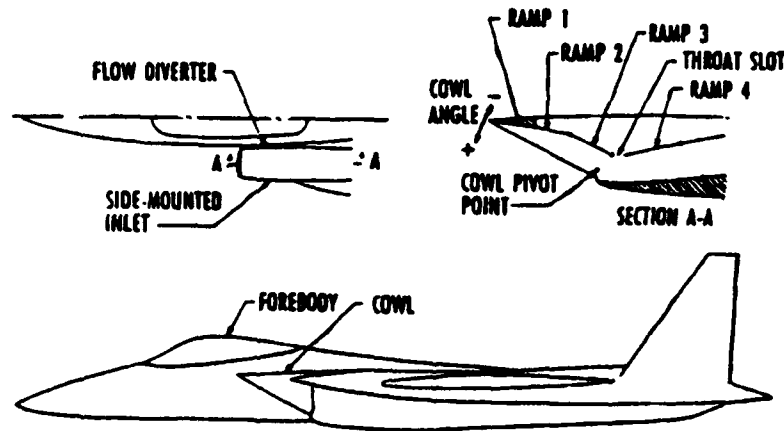


Figure 24. F-15 Aircraft

Three inlet ramps located ahead of a bypass air slot and one ramp behind the slot vary in position to optimize longitudinal stability, aircraft drag, and inlet-engine compatibility. Additional bleed air is extracted through porous holes in the inlet ramps.

The 16% scale model F-15 inlet model tested included the left inlet, a flow diverter, and a flow metering system (Figure 25.).

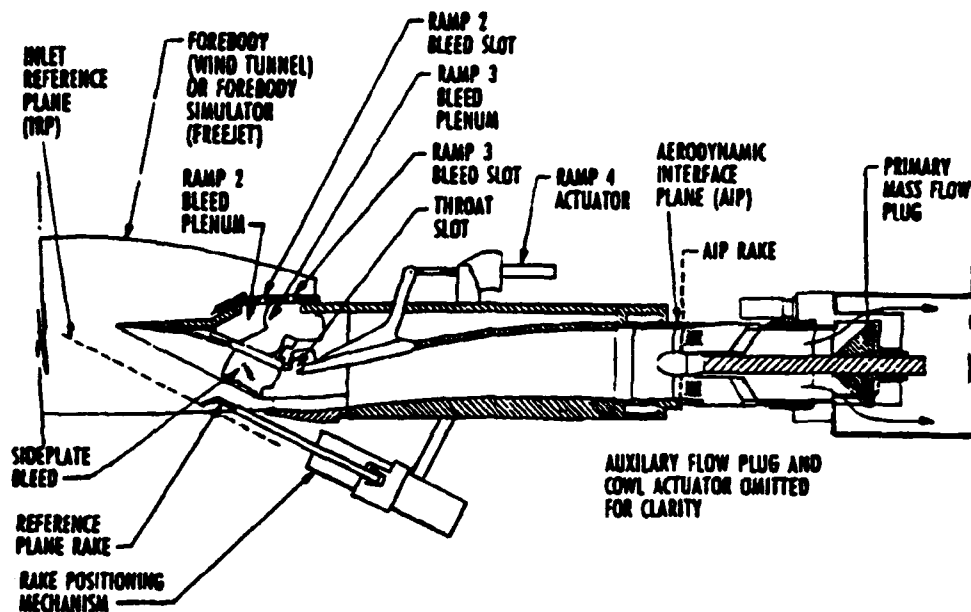


Figure 25. F-15 16% Scale Inlet Model

The lines of the aircraft were duplicated internally to the AIP and externally to a point aft of the inlet cowl lip. Inlet ramp positions and throat slot bleed rate were remotely varied to permit duplication of the airplane inlet schedules.

The complete F-15 forebody from nose to a station aft of the inlet was used in all wind tunnel tests. Subscale freejet tests used five forebody simulator designs with various design conditions (Figure 26.).

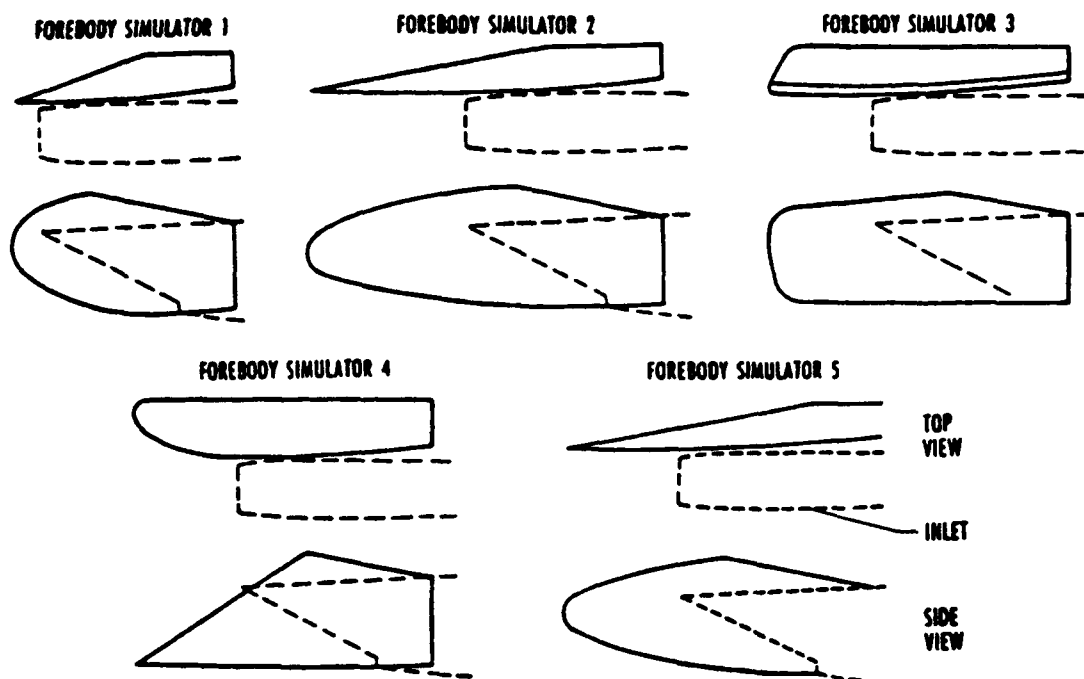


Figure 26. ASTF Freejet Forebody Simulators

Simulators 1 and 2 were developed previously for full scale F-15 inlet-engine wind tunnel tests. Forebody simulators 3, 4, and 5 were designed using a computational fluid dynamics code (CFD) called PARC3D.²⁰

Flow field measurements were obtained, in the wind tunnel tests and the subscale freejet tests, at the inlet reference plane (IRP) to relate AIP measurements and to control the experiments. Prior F-16 IRP measurements indicated freejet nozzle angle of attack conditions varied considerably from the angle of attacks simulated in the wind tunnel. IRP measurements were expanded during the F-15 tests with separate freejet tests that simulated families of freejet nozzle settings. Each grid of nozzle settings could

then be used to establish the exact freejet nozzle set point needed to simulate a specific wind tunnel test condition.

The inlet model instrumentation was identical in the wind tunnel and subscale freejet tests. Instrumentation included an IRP flow field rake, ramp pressure ports, and an AIP total pressure distortion rake. The AIP rake contained 40 dual total pressure probes to sense steady state and dynamic distortion levels (Figure 27.).

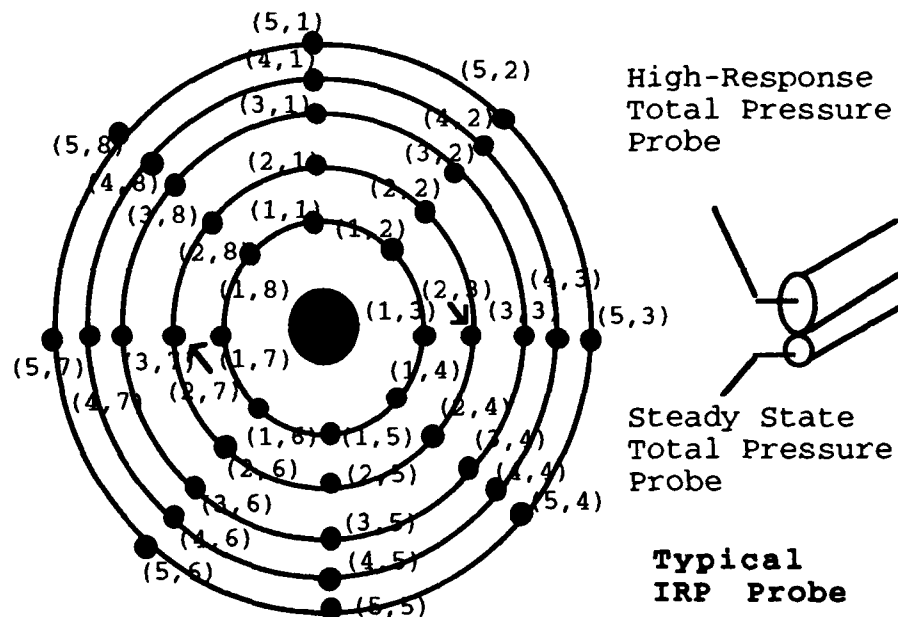


Figure 27. AIP Rake

The IRP rake was instrumented with three probes mounted laterally to span the width of the inlet (Figure 28.).

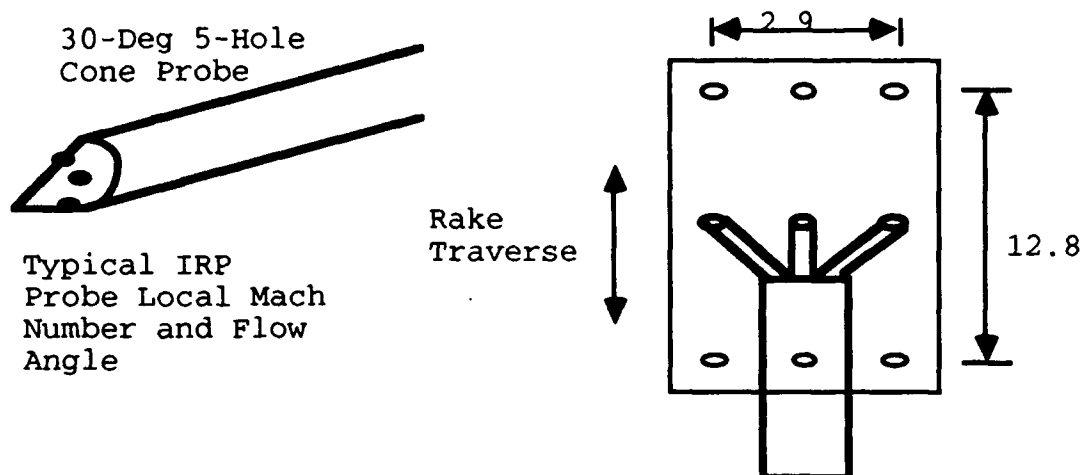


Figure 28. IRP Rake Set Up

The IRP flow field was surveyed taking readings every 1.6". The rake was then retracted and stored in a position below the inlet capture area and AIP measurements were taken. Steady state total pressures and 20 seconds of high response data at the AIP were recorded.

Test conditions, IRP flow field characteristics, flow rates, pressure distributions and inlet distortion were evaluated using steady state pressure and temperature measurements. Dynamic distortion parameters used to evaluate results were the RMS turbulence level, peak instantaneous distortion patterns, and the Pratt and Whitney K_{a2} distortion index. RMS turbulence levels were processed by AEDC. Peaks in dynamic distortion based on peak K_{a2} distortion index levels were performed by ASD using their Dynamic Data Editing and Computing (DYNADEC) system. The DYNADEC editing system will be described in Section 2.2.

Initial evaluations of wind tunnel-freejet comparisons were accomplished using four validation criteria established by the ASTF Freejet Working Group. The four measures of merit were: steady state face average total pressure recovery (P_{t2}/P_{t0}), face average RMS turbulence level, steady state probe-to-probe variation and dynamic probe-to-probe variation. Table 4 lists the four criteria and their respective measures of merit.

Table 4.
ASTF Freejet Validation Criteria

<u>Measures of Merit</u>	<u>Allowable Difference Between Freejet and Wind Tunnel</u>	
	<u>Steady State</u>	<u>Dynamic</u>
Total Pressure Recovery	1%	-
RMS Turbulence	-	1%
Probe-to-Probe Variation	2% RMSE	2% RMSE + Δ DYN

The steady state criteria required that the difference between the wind tunnel and subscale freejet recovery be less than 1%. Turbulence level differences between the two should also be less than 1%. Numerical probe-to-probe variation criteria were more difficult to evaluate.

The original steady state distortion pattern criteria called for steady state wind tunnel/subscale freejet comparisons to be within 2% root mean square error (RMSE).

This RMSE level had been achieved previously in matching distortion screens to wind tunnel turbulence levels. Due to concerns about the failure of this method to flag cases with large deviations and the possibility that the RMSE criterion was obsolete, a three tiered criterion was developed. The three tiers correspond to the mean, the mean plus one standard deviation, and the mean plus two standard deviations. Percentages in the three tiers were 1.35%, 2%, and 4%, respectively. This meant each of the 40 probe recovery levels in the wind tunnel and subscale freejet, at a select condition, were differenced. To meet the first tier, 50% of the differences must be within 1.35%. To meet the second tier, 68% of the differences must be within 2%. Last, 95% of the differences must be within 4%.

Dynamic criteria combined the three tiered steady state criteria with a dynamic adder (Δ DYN) to account for test and processing uncertainty. The dynamic adder was developed, using random number statistics and existing F-15 wind tunnel data, through a wide range of turbulence levels (Figure 29.).

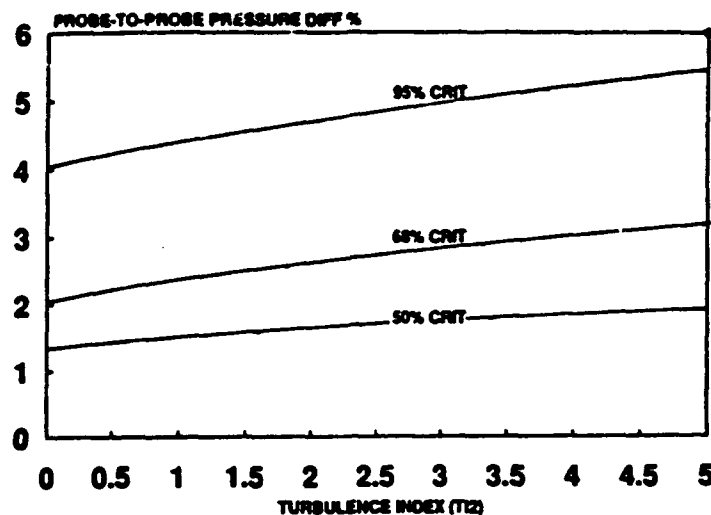


Figure 29. ASTF Freejet Dynamic Criteria

Dynamic pressures of wind tunnel/subscale freejet pairs were differenced and compared to the dynamic criteria at the respective turbulence levels. In Figure 29, 50% of the differences had to fall below the 50% curve. 68% of the differences had to fall below the 68% curve (one standard deviation) and 95% below the 95% curve (two standard deviations).

Initial evaluation of the wind tunnel and freejet pairs required that a point meet all three tier criteria to "pass." If one or two tiers "passed," the pass/fail judgement would be reviewed on a case by case basis. By March 1989, some pattern data was available for evaluation against the criteria. A majority of the subsonic cases met the recovery, turbulence and steady state criteria. There was; however, a high failure rate of wind tunnel/freejet pairs when the dynamic criteria were applied.

This high dynamic failure rate lead to a more detailed review of all of the points. Conclusions from this analysis

indicated that the four criteria did not adequately evaluate the wind tunnel/freejet pairs. No precedence existed for suitable dynamic probe-to-probe criteria, so the criteria created for this program were a first attempt. After considerable discussion among the Freejet Working Group members, the validation criteria evolved into an acceptance process as listed in Table 5.

Table 5.
Acceptance Process

1. Produce Steady State/Dynamic Total Pressure Maps
2. Apply Numerical Criteria
Freejet Validation Criteria
SAE AIR 1419 Indices
3. Review Total Pressure Maps for Pattern Similarities
Peaks and Valleys, Magnitudes, and Locations
Circumferential/Radial Extent
Steady State vs. Dynamic
Bad Probes and Uncertainty
4. Apply Previous Engine Experience
5. Review Multiple Peaks for Consistency of Patterns
6. Determine Acceptability Based on Numerical Criteria,
Judgement, and Experience

The acceptance process used the original criteria as a basis and added qualitative pattern evaluations and the application of previous experience of the ASTF Freejet Working Group members. Distortion pattern comparisons included considerations of high and low pressure locations and magnitudes, circumferential and radial extent, location of

faulty probes and multiple peak patterns to ensure that the entire time history was evaluated. A more detailed account of the acceptance process development can be found in Reference 21.

Final subsonic results after application of the acceptance process have not been completed to date, but will be completed in 1993. Supersonic wind tunnel/freejet pairs were also evaluated and several areas of concern arose. Supersonic tests were performed with three of the forebody simulators. Generally, recovery, turbulence and steady-state probe-to-probe criteria were met. The dynamic probe-to-probe criteria failed and pattern comparisons were not good. As a result, a majority of the supersonic points did not meet the acceptance process. The ASTF Freejet Working Group developed a plan to isolate the specific causes of the supersonic anomalies in an attempt to resolve them.

One possible explanation for these anomalies was aerodynamic interference originating from reflective shock waves in a high blockage freejet installation. Many of the more likely causes required additional testing to resolve; however, one of the low priority concerns that could be addressed immediately and that was much less costly than a test was an uncertainty analysis of the data measuring, recording and processing systems. AEDC representatives are currently investigating the data measuring and recording uncertainties. ASD took on the responsibility for

determining the data processing uncertainty analysis, which is the subject of this thesis.

2.2 DYNADEC Analog-Digital Computer Set up

In 1969, a joint effort between the ASD computer center and the Flight Dynamics Lab at Wright-Patterson Air Force Base was initiated to develop a hybrid editing system to screen inlet dynamic pressure distortion data. The resultant DYNADEC system utilized the capabilities of a hybrid computer to combine the speed of an analog computer with the precision and memory capabilities of a digital computer.²² This was a considerable advancement over the previous method of digitizing sort time ($< 1/2$ sec) segments of individual transducers, computing distortion parameters and then computing a peak distortion level and pattern. Recent advancements in digital computer capabilities have enabled many airframe and engine contractors to return to digital systems; however, analog systems remain a powerful tool to calculate a continuous solution of distortion index equations with massive quantities of data in an off-line mode.

A block diagram of the DYNADEC system is shown in Figure 30.

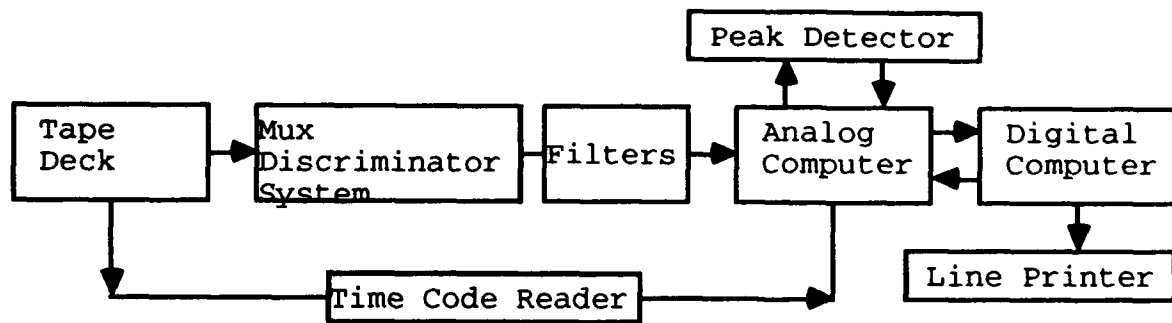


Figure 30. DYNADEC Equipment Set Up

The tape deck reads high response pressure transducer data from 14 track analog tapes at the designated tape speed. The signals are then demultiplexed or divided using discriminators at the frequencies they were recorded onto the tape, because data from several transducers are usually written onto one track. The individual probe dynamic signals are filtered using ac coupled filters to remove any steady state components or dc bias present on the tape. The filters also eliminate high frequency data above the selected cutoff frequency. The filtered data is then sent to the analog computer where the data is gain compensated to account for individual transducer response characteristics.

Each fluctuating component is added to its corresponding steady state value to form the actual dynamic total pressure signal. Steady state values are set in the digital computer which sends the values to the analog where they are added to the fluctuating signal. Fluctuating signals are multiplied by factors established during the wind tunnel and freejet

tests to convert the signals coming off the tape from volts to lb/in^2 (psi). Thus, the fluctuating component is properly scaled to steady state levels. A partial block diagram of the analog components in DYNADEC can be seen in Figure 31.

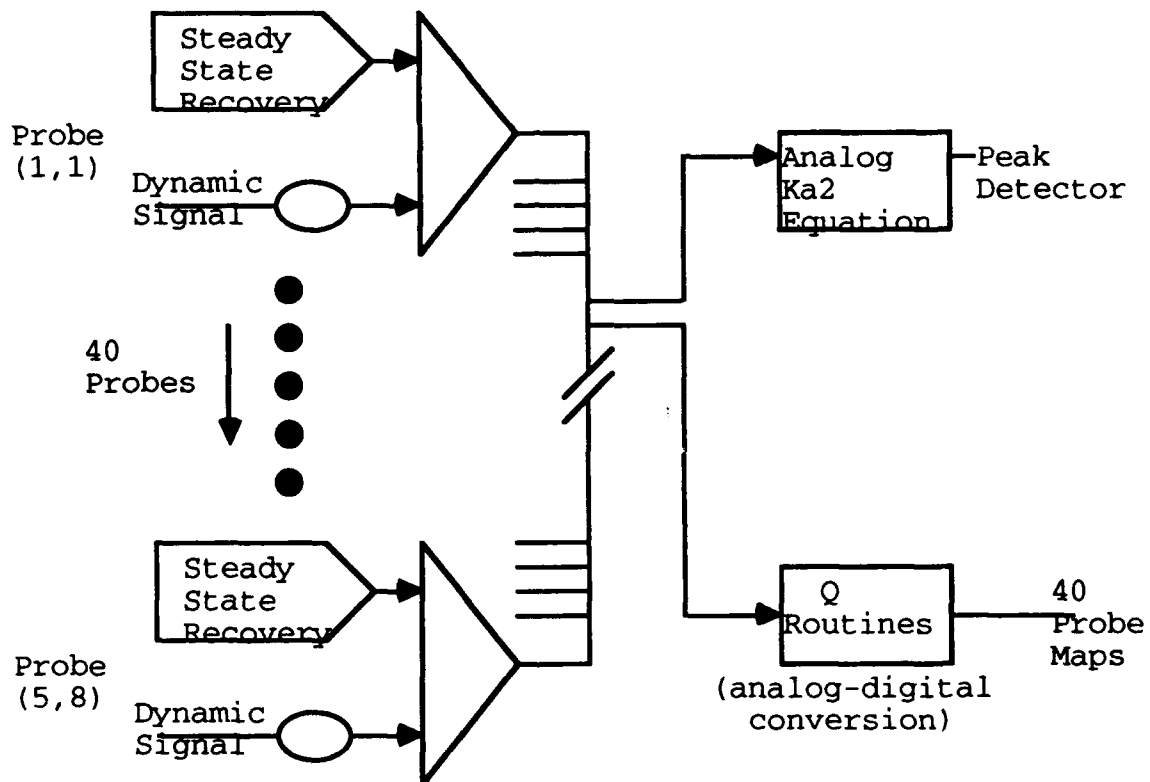


Figure 31. DYNADEC Analog Wiring

The total pressure signals are then sent to the engine distortion parameters wired in the analog computer. The distortion parameter is fed into the peak detector network. Peak values above a certain preset threshold are stored in the digital computer along with their associated time codes

and total pressures until a higher magnitude peak occurs or the time slice editing is complete (Figure 32.).

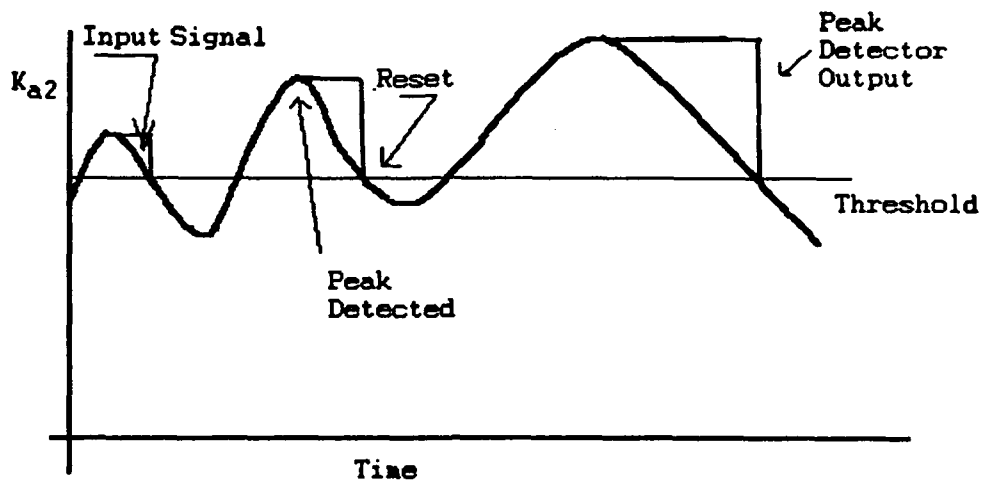


Figure 32. DYNADec Peak Detector Set Up

When the editing is completed, the compressor face maps of steady state values and the peak instantaneous distortion with associated test data are printed out. Example output can be seen in Figure 33.

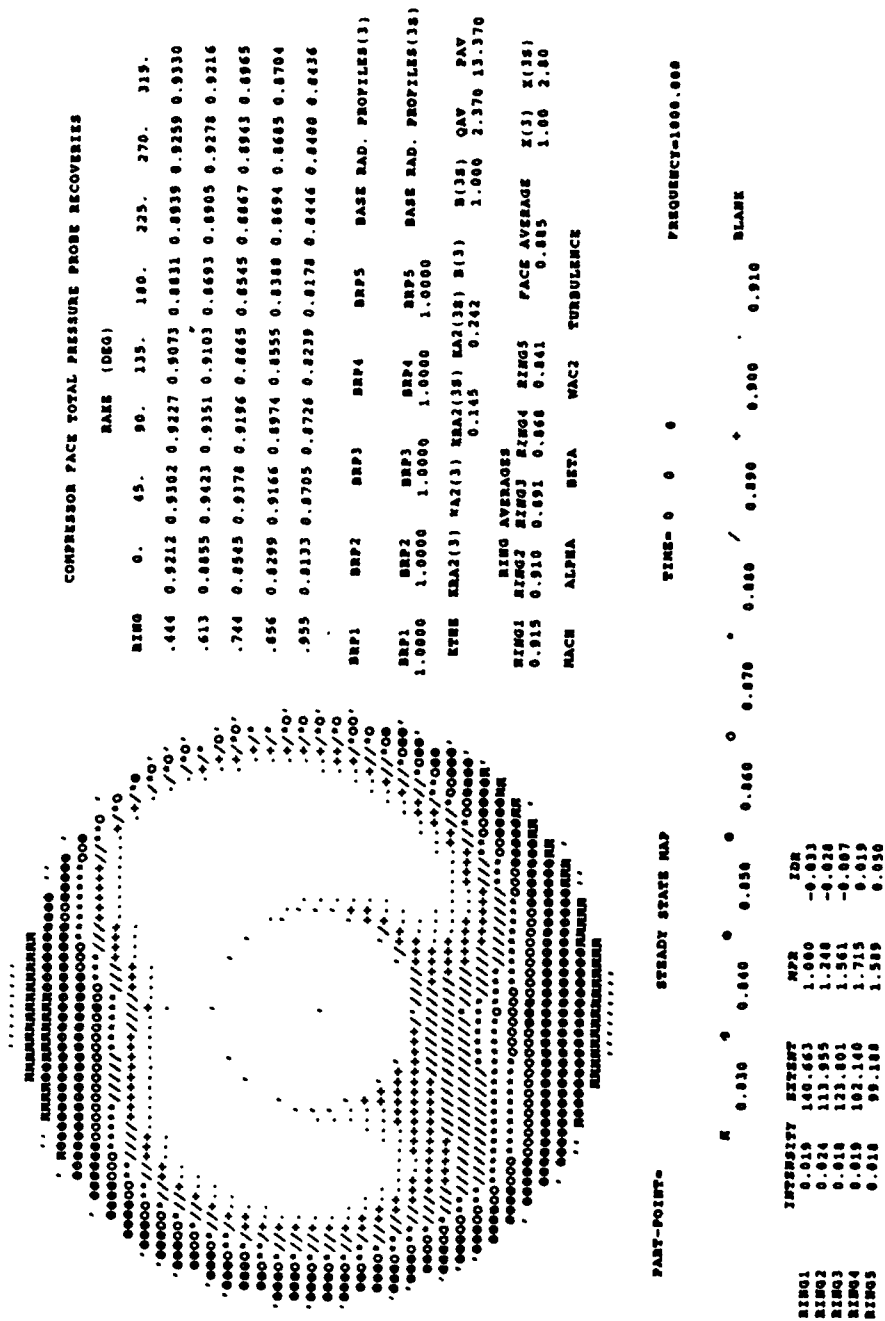


Figure 33. DYNADEC Example Output

Figure 33. (Continued)



Operation of the DYNADEC system is accomplished by two people due to system complexity. A project engineer from Wright-Patterson's computer center is responsible for running the hybrid computer during editing. He or she also programs the analog and logic patchboards, maintains the digital computer program and performs daily system checkouts. An engineer familiar with the test data determines which cases to screen, provides steady state and transducer calibration data and interprets results. He or she also runs the tape drive and time code machines during editing.

A more detailed account of DYNADEC set up as it pertains to editing the ASTF Freejet development data can be found in Appendix B.

2.3 Basic Uncertainty Methodology

Accurate measurements of any quantity will always contain some error. Errors induced by construction of "identical" measurement instruments, environmental variations, handling methods and errors inherent in the measurement instruments themselves must be identified and understood before the measurement takes place. Because of error, all that can be seen is the measured quantity and not the true value (Figure 34.).

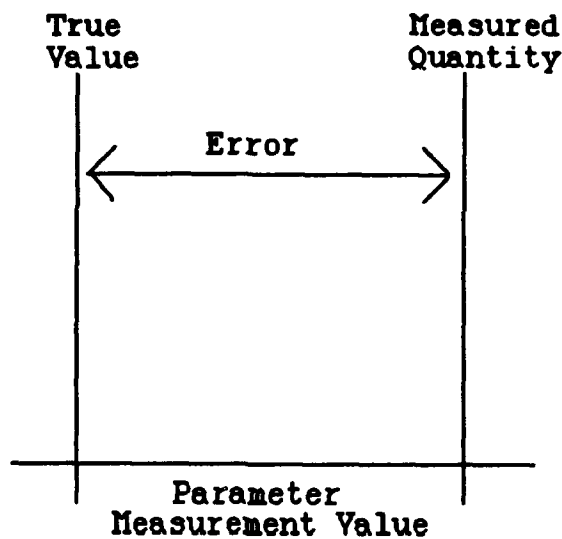


Figure 34. Bias Error

Thus, error magnitudes must be defined to ensure a useful measurement.

Uncertainty is used to quantify measurement error. Uncertainty is "the largest expected value of measurement error," and is divided into two quantities; a precision (or random) error and a bias (or fixed) error.²⁴ Accurate measurements should have small precision and bias errors (Figure 35.).

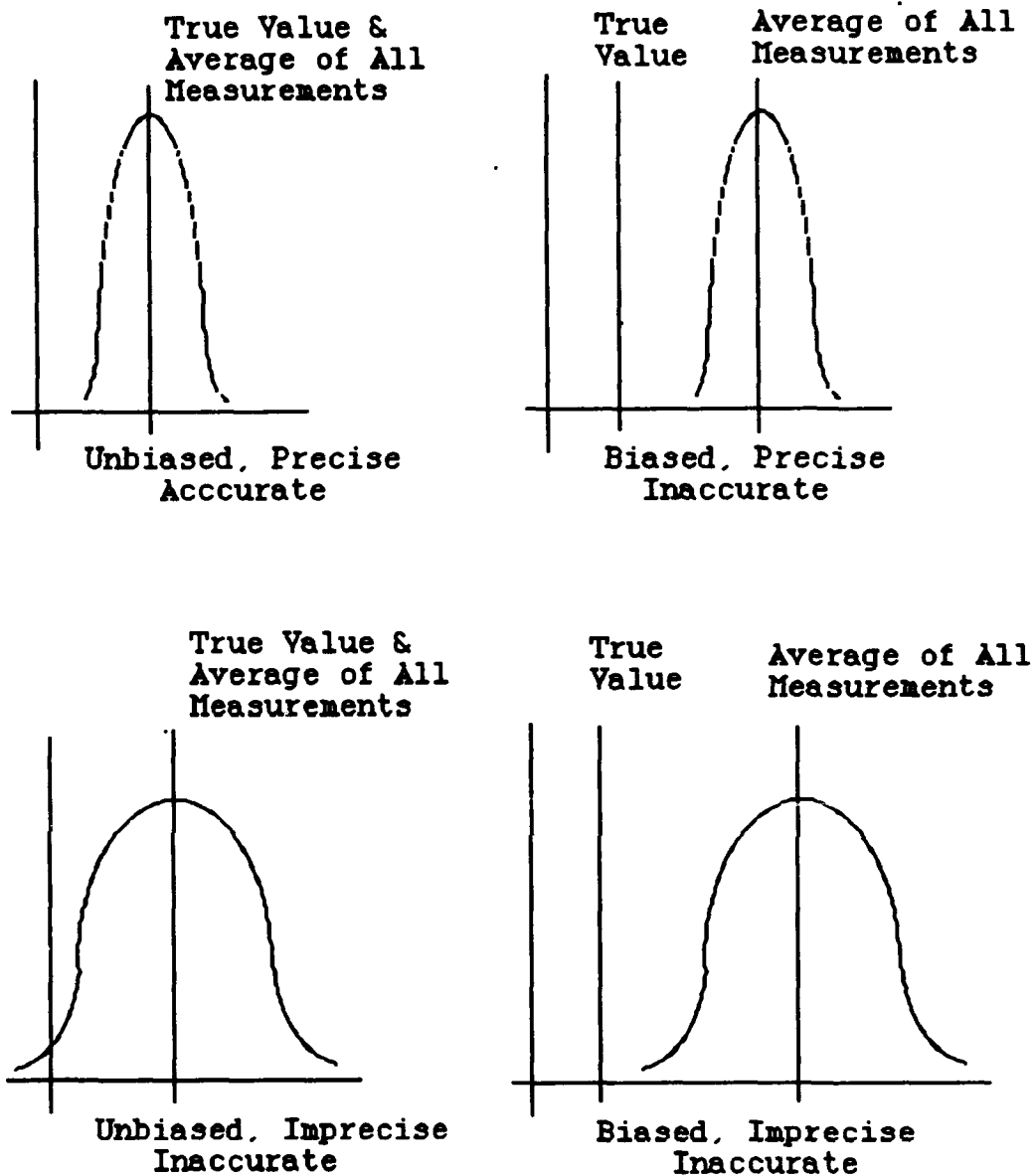


Figure 35. Measurement Error

Precision error is the magnitude variation seen, as a quantity is measured repeatedly under the same conditions. Precision errors tend to cause small measurement variations that are normally distributed around the average measurement (Figure 36.).

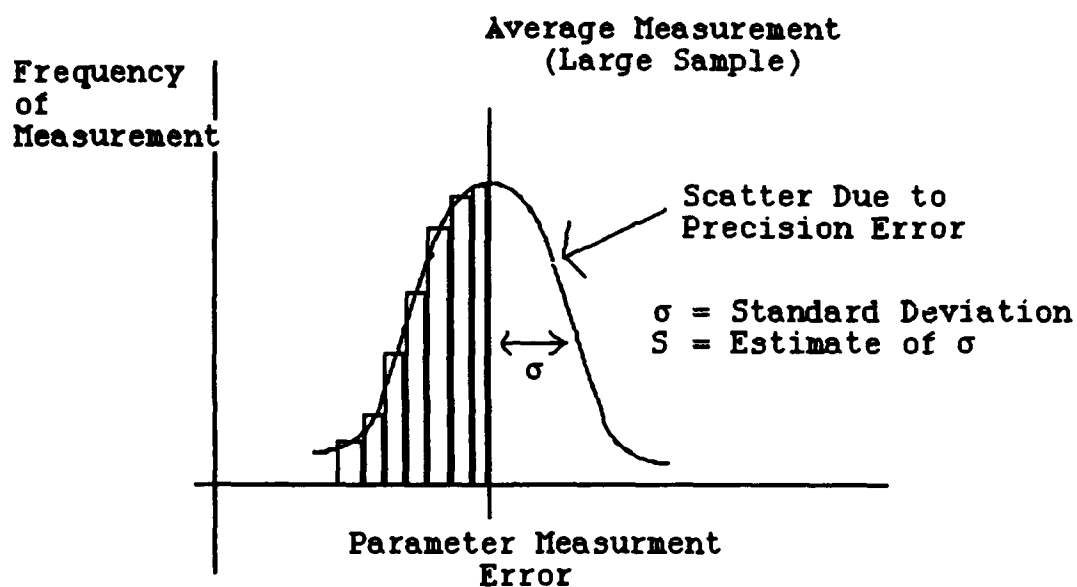


Figure 36. Precision Error

Normal distributions are characterized by the standard deviation, σ , which is usually estimated using the precision index, S .

σ (standard deviation) = S (precision index)

$$S = \frac{\sqrt{\sum_{i=1}^n (X_i - \bar{X})^2}}{n - 1} \quad (11)$$

where; n = # of measurements or samples

X_i = individual measurements

\bar{X} = average of all measurements

The quality of the precision index depends on the number of measurements used. Larger samples improve the estimation of the true standard deviation. The number of measurements is considered large if 30 or more measurements are taken. The basis of this lies in random number statistics. If large samples are used, the interval bounded by $\pm 2S$ will contain the true value 95% of the time. The boundaries actually vary as $t_{95}S$ where t_{95} is from Student "t" statistical tables.²⁴

Table 6.
Student "T" Values

Degrees of Freedom or Samples	<u>$t_{95\%}$</u>
1	12.706
2	4.3027
3	3.1825
4	2.7764
5	2.5706
6	2.4469
7	2.3646
8	2.3060
9	2.2622
10	2.2281
14	2.1448
18	2.1009
22	2.0739
26	2.0555
30	2.0423
34	2.0323
36	2.0281
40	2.0211

" t_{95} " approaches a value of 2 as the number of degrees of freedom or samples increases. At 30 or more samples, t_{95} is

close enough to the value of 2, that the engineering community uses 30 as the large sample standard. Small samples (< 30) require small sample statistical methods that are discussed in Appendix B of Reference 25.

Bias error is a constant or systematic error occurring throughout a test. Every measurement will have the same bias error magnitude, although bias errors may drift or change with test condition. In order to compute the magnitude of the bias error, the true value must be known. (Figure 37.).

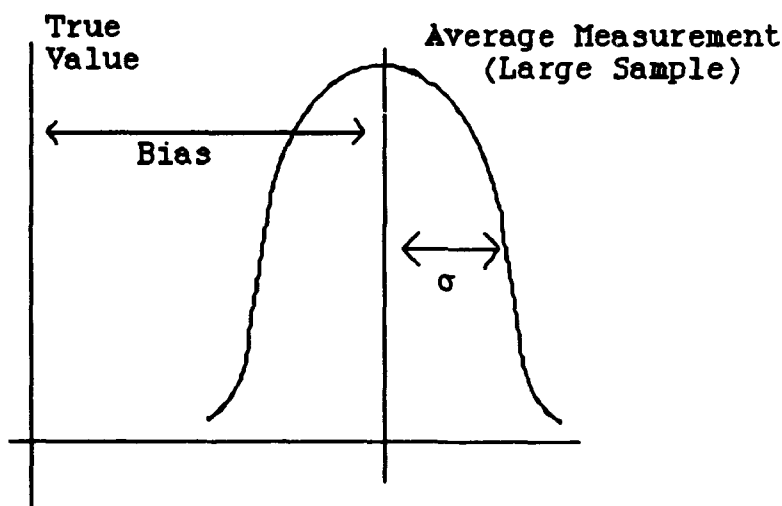


Figure 37. Bias Error Determination

Generally, the true value is not known and the bias error must be estimated using relevant data and engineering judgement.

Bias and precision errors can be further divided into four elemental errors; calibration, data acquisition, data

reduction and mathematical model errors. Calibration, data acquisition and data reduction errors are associated with the measured quantities. Mathematical model errors are induced by calculation procedures based upon measured parameters. This means that the individual component bias and precision errors must be added together in some fashion to form total system bias and system errors. Elemental errors are usually added taking the root-sum-square of all components:

$$B = \sqrt{\sum_{i=1}^n (B_i)^2} \quad (12)$$

$$S = \sqrt{\sum_{i=1}^n (S_i)^2} \quad (13)$$

Where: B_i = Individual Component
Bias Errors
 S_i = Individual Component
Precision Indices

Bias and precision errors are usually combined into one uncertainty parameter for simplicity and comparison. Two common definitions are additive uncertainty, U_{add} , and root-sum-squared uncertainty, U_{rss} .

$$U_{add} = B + 2S \quad (14)$$

$$U_{rss} = \sqrt{B^2 + (2S)^2} \quad (15)$$

where B = Bias error

S = Precision index

2 = 95% factor from Student "t" table

U_{add} or U_{rss} should give an estimate of the largest error expected in a measurement process. Thus, the interval of $\pm U$ should contain the true value (Figure 38.).

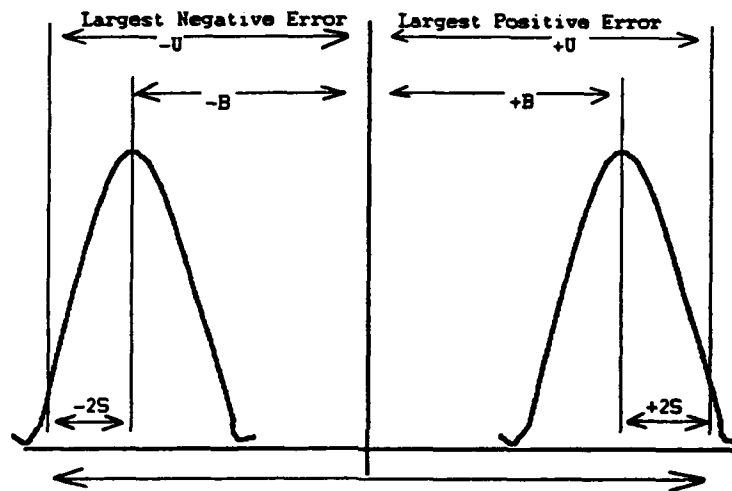


Figure 38. Uncertainty Interval about the Mean

Past Monte Carlo analysis on U_{add} and U_{rss} showed that U_{add} exhibited a coverage of the true value (or confidence level) of 99%, while U_{rss} had a confidence level of 95%.

It is important to use an accurate, precise method to evaluate uncertainty. Reference 25 lists the suggested method for determining in-flight thrust measurement uncertainty. A modified version of this method will be used to evaluate the ASTF Freejet Development data set with the

DYNADEC system. This analysis will be described in the next section.

2.4 Uncertainty Analysis Applied to Data Set

The uncertainty analysis procedure developed for the ASTF Freejet data required the determination of the appropriate level of analysis. The first step in the in-flight thrust measurement analysis in Table 7, states that all elemental errors for each measurement should be identified first.²⁵

Table 7.
Steps for Determining In-Flight Thrust Uncertainty

1. Identify all elemental errors for each measurement in the ground test facility and in-flight related to determining thrust
2. Preliminarily classify elemental error sources as bias or precision
3. Estimate the magnitude of each elemental error
4. For each flight test measurement process, make the final bias or precision classification
5. Combine elemental errors to define measurement bias and precision error components and tabulate elemental errors
6. Propagate measurement error components to calculated thrust
7. Calculate uncertainty limit from error components
8. Report results

When applied to DYNADEC, this would mean going through each individual amplifier, integrator, etc., and determining precision and bias errors for each. This method was not feasible due to the large amount of time and effort required.

The plan developed attempted to accurately quantify uncertainty at a reasonable level of detail.

Three DYNADEC component errors were known before this analysis. There is a 20- μ s time delay before the peak detector realizes a peak exists. The system must switch from track to store mode once a peak is detected. This results in an additional 75- μ s time delay before the data is stored and a $\pm 1\text{mv/s}$ error in changing modes. These three errors associated with the peak detector were considered the major contributors to overall system error, based upon the prior experience of the system operators.

The problem at this point was applying these errors to dynamic total pressure signals. The $\pm 1\text{mv/s}$ error in changing modes could be converted directly to psi/s because the dynamic signals coming off the tape were in volts and the conversion factor was known. It would appear that evaluating a time delay error in units of time would depend upon the wave form of the signal. A highly dynamic or turbulent signal may be affected more because of the higher signal amplitudes involved (Figure 39.).

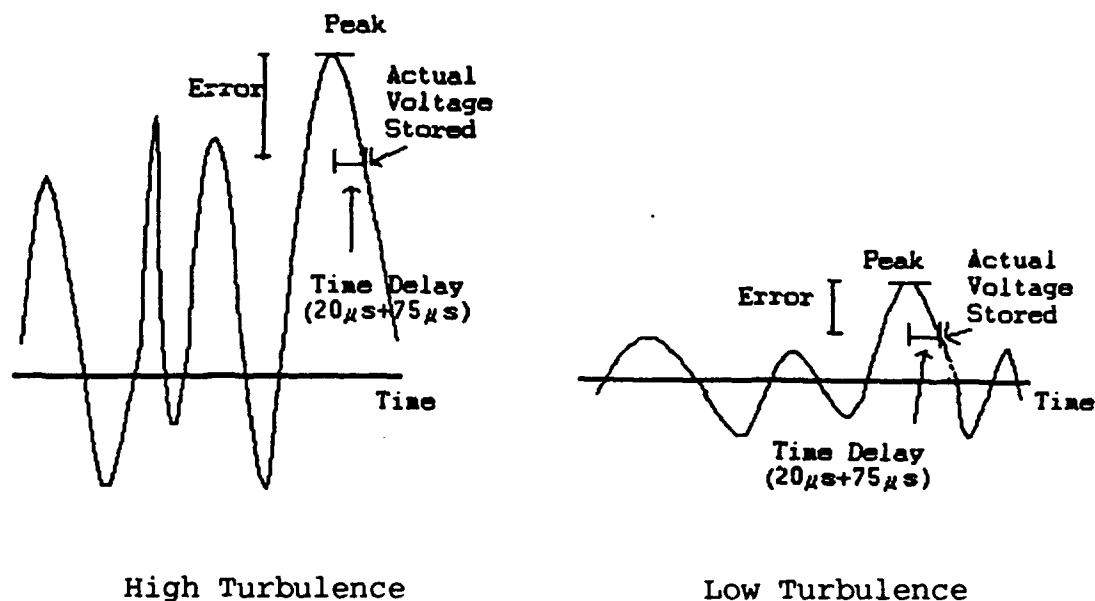


Figure 39. Amplitude Variation with Turbulence Level

Frequency content also has an effect. Lower frequency energies would be less affected by the time delay because the signal drop-offs occur in a longer time span. Thus, any uncertainty analysis methodology required consideration of the way uncertainty varied with turbulence level.

One method of converting the error in time to one in pressure units would be to create known sinusoidal signals and record them on an analog tape with a time code. When the tape was played, the known peak values and their associated time would be analyzed. The differences in peak magnitude from the true value would establish the true bias error. Turbulence effects could be evaluated by recording sinusoidal signals of varying frequency and amplitude on an analog tape and screening the resultant signals for peaks with known

amplitudes. Unfortunately, recording devices were not available to perform this method of evaluation.

An alternate method was to treat the entire DYNADEC system as a "black box" and compare values going into the system to values coming out. The three known error contributors could be evaluated by including them in an overall system precision error. Precision error could be evaluated using multiple runs of DYNADEC while reading off the same peak time slice. Static bias error could be evaluated using daily system checkouts where known input signals were compared to output signals. This method was applied in this analysis due to its feasibility.

The decision to use a "black box" approach eliminated the need to identify and classify elemental error sources. The next step was to propagate the errors to pertinent measured and calculated parameters. Looking at the amount of pressure and distortion index data available, it was decided that the uncertainty analysis would primarily focus on determination of the precision and bias errors for each of the 40 dynamic pressure recoveries and for the Pratt and Whitney K_{a2} index as a function of RMS turbulence level.

The next step was to establish a data matrix to work from. The following six points from the ASTF Freejet Development data set were selected.

Table 8.
Uncertainty Analysis Data Matrix

Wind Tunnel Run Number	Freejet Run Number	Mach	α	β	Wac2	RMS Turbulence	
						Wind Tunnel	Freejet
603.4	72.067	0.6	-10°	0°	226	1.31 %	1.62 %
563.4	14.148	0.3	30	-10	240	3.35	3.02
1170.1	59.022	2.2	-5	0	183	5.35	4.82

These six points were selected to cover a wide range of test conditions and turbulence levels. The wind tunnel and freejet points were selected in pairs simulating identical test conditions. The uncertainty analysis applied to a wind tunnel/freejet pair would also directly apply to the acceptance process comparison of the two test points. The six points selected will be referred to by their run numbers throughout the remainder of this thesis.

Each of the six points was set up on the DYNADEC system. The peak detector threshold was set and an initial screening of 20 sec of dynamic data ensued. If more than one peak was detected, the threshold was increased and another screening occurred. This process was repeated until the threshold was high enough to detect a single peak in the 20 sec of dynamic data.

Once the "peak" peak dynamic pattern was established, the pattern was screened 50 times to obtain a large sample (> 30). Screening generally occurred in groups of 10 runs on 5 different days. This enabled the analysis to account for

possible day to day changes in the system that would affect overall interpretation of the results. A run log of the analysis is listed in Table 9.

Table 9.
Uncertainty Analysis Run Log

Test																	
Point	February, 1992																
	3	4	5	6	7	8	9	10	11	12	13	14	15	16	17	18	
WT603.4																	
FJ72.067																10	
WT563.4		10	10							10						10	
FJ14.148			20	10	10			10									
WT1170.1										10						10	
FJ59.022								10		10						20	
												March, 1992					
	19	20	21	22	23	24	25	26	27	28	29	30	31	1	2	3	
WT603.4	10		10			10											
FJ72.067		16				15				11							
WT563.4			10														
FJ14.148																	
WT1170.1			10			11											
FJ59.022		10															
	4	5	6														
WT603.4		10	10														
FJ72.067																	
WT563.4																	
FJ14.148																	
WT1170.1			9														
FJ59.022																	

On days where more than 10 runs of the same points occurred, the runs were divided by running one group of 10 runs at the beginning of the day and a second set three to four hours

later. The entire data set was run over a 1-month period in the spring of 1992.

After screening the 6 "peak" peak patterns a total of 302 times, a method to reduce the amount of information in the runs was required. A four-level approach with increasing amounts of detailed analysis was developed and is listed in Table 10.

Table 10.
Analysis Plan

- | | |
|---------|--|
| Level 1 | <ol style="list-style-type: none"> 1) Group 6 runs and sort using spreadsheet <ol style="list-style-type: none"> a) analog, digital parameters b) ring, face averages c) 1419 indices 2) Compute distributions on analog, digital parameters and 6 sample probes per case noting noise errors (bi-polarity) and RMS turbulence levels |
| Level 2 | <ol style="list-style-type: none"> 1) Find mean (\bar{X}) and precision index (S) on analog, digital indices and 40 probes 2) Note $\bar{X} \pm 2S$ and outliers, see if indices outliers match runs with probe outliers 3) Note shift in parameters from analog to digital 4) Decide if outliers need to be eliminated and \bar{X} and S recalculated 5) Note RMS levels 6) See if bad probes (zeroed out) show normal distributions and little scatter if 1 of 6 distributions performed in Level 1 analysis 7) Note shapes of distributions, relatable to round-off error |
| Level 3 | <ol style="list-style-type: none"> 1) Compute distributions on all probes 2) Check if noise appears on probes with low RMS turbulence 3) Compute distributions on 1419 indices, ring average recoveries and face average recovery 4) Eliminate outliers from distributions and recompute \bar{X} and S as needed 5) Run Sedlock distortion prediction program to compare to \bar{X}'s of 40 probes on each case 6) Make comparative total pressure maps of Sedlock and \bar{X}'s of 40 probes for each of the 6 cases 7) Note run schedule and check to see if any noise occurs on specific days or is there any other pattern to it 8) Note any differences between FJ-WT, FJ-FJ, WT-WT comparisons. Any trends with RMS turbulence level? |

Table 10 (continued)

- | | |
|---------|--|
| Level 4 | <ol style="list-style-type: none">1) Find system bias errors using system static checks of parameters and 40 individual probes2) Add bias error to precision indexes to compute overall DYNADEC system error. |
|---------|--|

First, K_{a2} levels seen by the analog computer were recorded and sorted, so a distribution analysis could be done. The analog K_{θ} and K_{ra2} components of K_{a2} were also analyzed. K_{θ} is a measure of circumferential pressure defects. K_{ra2} is a measure of radial pressure defects. The analysis included looking for trends in the distributions (scatter, noise, etc) as a function of turbulence level.

The analysis actually dealt with two sets of K_{a2} indices. As seen previously in Figure 31., the peak detector reads a K_{a2} signal from one branch of the analog computer. Once the peak pattern is established, the 40 dynamic pressures are digitized through another branch of the system and a K_{a2} value based on these 40 pressures is also calculated. In this analysis, the term "analog K_{a2} " will refer to the K_{a2} seen by the peak detector while the term "digital K_{a2} " will refer to the K_{a2} calculated from the peak distortion pattern pressure recoveries. A similar distortion analysis was also performed on the digital K_{a2} values as part of the first level of evaluation.

Ring averages and dynamic face average total pressure recoveries were evaluated in the same manner. It was believed that ring and face average results could provide some insight into the K_{θ} and K_{ra2} components of the K_{a2} distortion index since K_{θ} and K_{ra2} are computed using those parameters. AIR 1419 indices were investigated as alternate distortion parameters. While the data was not screened using

these parameters, a qualitative distribution comparison between K_{a2} and the 1419 indices could give some prediction of future DYNADEC screening with the 1419 indices.

Second level analysis was a much more detailed procedure. The precision index, S , and mean, \bar{x} , were calculated for the analog indices, the digital indices and on each of the 40 probes for all six cases. $\bar{x} \pm 2S$ was computed to bound the scatter within the 95% (two standard deviation) range as discussed in the previous section. Data falling outside these bounds by more than one standard deviation was labeled an "outlier." Outliers skew mean and precision index magnitudes to inaccurate levels that may lead to an inaccurate interpretation of the results. K_{a2} 's of individual runs with one or two probe outliers were checked to see if the run with an individual probe outlier corresponded with a K_{a2} , K_0 , or K_{ra2} outlier.

Any shifts in K_{a2} , K_{ra2} , or K_0 levels from analog to digital values were noted in the 2nd level of analysis. Six probes from each run were randomly selected for initial distribution analysis. Gaussian (normal) behavior was checked. Distributions on bad probes, where the dynamic signal was "zeroed" out and a steady state recovery level substituted, were also checked to ensure that the dynamic signal was being suppressed properly.

The third level of analysis was the most detailed of the four. Distributions on each probe for each case were

computed. Any noise (bi-polarity) behavior was noted and its relation to RMS turbulence level on a probe and face average level was investigated. Noise behavior was also related to the run days to see if one day in particular, generated all of the errant cases. Ring average recovery, face average recoveries and 1419 index distributions were done for comparison with the K_{a2} distributions. Precision indices and means values were recomputed excluding outliers. Distributions on all probes and distortion indices were also recomputed, excluding outliers.

The Sedlock statistical distortion program described in the previous chapter, was used to test the random character of the data.¹⁵ It was hoped that, if a total pressure map of the means associated with the precision indices of the 40 probes, matched the Sedlock predicted peak distortion pattern, it could be said that the data was random in nature. This qualitative evaluation would justify the random number statistical analysis performed with the data. At higher RMS turbulence levels, this assumption was expected to break down as physical phenomena such as shed vortices drive the flow.

The 40 RMS turbulence levels and steady state total pressures from each of the six runs were used as input cases for the Sedlock program. The appropriate number of samples (random numbers) used to predict a peak pattern was not known ahead of time. Previous program users ran a case at the cutoff frequency of the test data for a 1 second duration.

Thus, a case with a cutoff frequency of 1000 Hz would be run for 1 second, six times employing the map averaging technique of the Sedlock Program.¹⁶ This run would then generate 6000 random numbers at each of the 40 probe locations.

It was unknown if 1 second was the appropriate time segment to use in the analysis. One might jump to the conclusion that if the analog data was screened for 20 seconds at a cutoff frequency of 1000 Hz using the DYNADEC system, the Sedlock program should also be run for 20 seconds. The computer run times needed to generate 20,000 random numbers, 6 times for each probe, were prohibitive; so the Sedlock analysis was started at the opposite end of the time scale, 1/2 second. Run times were increased until the average variation in the predicted peak distortion patterns were less than 1/2 % in recovery level from run to run and no overall significant pattern shifts were observed. These "converged" peak patterns were then compared to the mean values of the DYANDEC results of the same test point.

The final step in the third level of analysis was to observe any differences in the wind tunnel and freejet results. Comparisons among the three freejet cases were done as well as among the three wind tunnel cases. Trends with turbulence level were noted. Specific probes with a large amount of scatter (high precision index) were flagged if they were consistently imprecise across all of the six cases.

The fourth level of analysis involved determination of static data processing bias errors for each of the 40 probes involved in the ASTF Freejet Program data and for the K_{a2} , K_0 and K_{ra2} distortion parameters. Bias errors were calculated from daily DYNADEC system static checkouts and static checks performed before each data point was edited for peak dynamic patterns. The static checks involved sending known static signals through the DYNADEC system and observing how much the exiting signal magnitudes differed from the known input quantities. The known static signals are essentially 40 created steady state pressure recoveries listed in Table 11.

Table 11. Static Check Recovery Levels

PSSR	PSST	ZPSS
0.84000	16.80000	8.40000
0.86000	17.20000	8.60000
0.88000	17.60000	8.80000
0.90000	18.00000	9.00000
0.92000	18.40000	9.20000
0.94000	18.80000	9.40000
0.96000	19.20000	9.60000
0.98000	19.60000	9.80000
0.82000	16.40000	8.20000
0.84000	16.80000	8.40000
0.86000	17.20000	8.60000
0.88000	17.60000	8.80000
0.90000	18.00000	9.00000
0.92000	18.40000	9.20000
0.94000	18.80000	9.40000
0.96000	19.20000	9.60000
0.80000	16.00000	8.00000
0.82000	16.40000	8.20000
0.84000	16.80000	8.40000
0.86000	17.20000	8.60000
0.88000	17.60000	8.80000
0.90000	18.00000	9.00000
0.92000	18.40000	9.20000
0.94000	18.80000	9.40000
0.78000	15.60000	7.80000
0.80000	16.00000	8.00000
0.82000	16.40000	8.20000
0.84000	16.80000	8.40000
0.86000	17.20000	8.60000
0.88000	17.60000	8.80000
0.90000	18.00000	9.00000
0.92000	18.40000	9.20000
0.76000	15.20000	7.60000
0.78000	15.60000	7.80000
0.80000	16.00000	8.00000
0.82000	16.40000	8.20000
0.84000	16.80000	8.40000
0.86000	17.20000	8.60000
0.88000	17.60000	8.80000
0.90000	18.00000	9.00000
0.92000	18.40000	9.20000
0.94000	18.80000	9.40000
0.86000	17.20000	8.60000
0.88000	17.60000	8.80000
0.90000	18.00000	9.00000

The third column of numbers (zpss) in Table 11 are the 40 static signals actually sent through the system during static checks. Recovery levels (pssr) are scaled (psst, zpss) to allowable system voltage levels through the following formulas:

$$P_{t2}/P_{t0})_{ss} i * P_{av} * Z1 = \text{known signal used for system check} \quad (16)$$

where: P_{av} = Engine face average total pressure (P_{t2}) = 20 for static check
 $Z1$ = Scaling factor
= 0.5 for static check

The 40 known static signals were read at the two locations in the DYANDEC system in Figure 40.

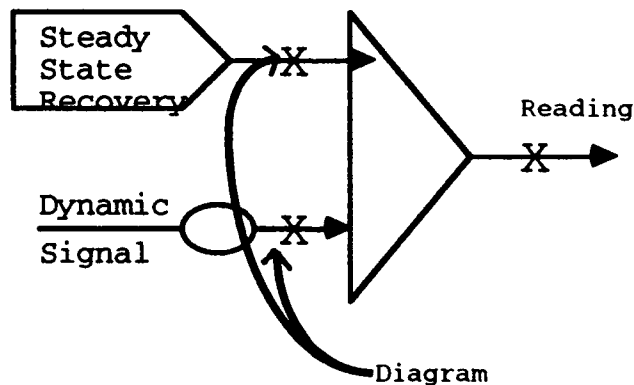


Figure 40. Probe Bias Error Signal Locations

The "reading" value is the scaled steady state signal after passing through an amplifier. The "diagram" value is the sum of the scaled steady state levels defined above for the

static check and the value seen in the dynamic branch. In normal operation, the dynamic signals off the analog tapes are travelling through this branch. For daily system checks, no dynamic signal exists, so the contribution from this branch to the 40 "diagram" levels is zero.

Table 12 is an example output from a daily static check.

Table 12. Daily Static Check Example Output

PAGE 1

COMPONENT	READING	DIAGRAM	EQUATION	ERROR	TOL=0.0010
1A001 SUM	-0.196	-0.197	-0.400	0.004	mm
1A005 SUM	-0.197	-0.198	-0.400	0.003	mm
1A006 L T/S	-0.196	-0.198	-0.400	0.004	mm
1A007 L	-0.196	-0.198	-0.400	0.004	mm
1A011 SUM	-0.195	-0.195	-0.400	0.003	mm
1A015 SUM	-0.196	-0.195	-0.400	0.003	mm
1A016 SUM	-0.195	-0.195	-0.400	0.003	mm
1A021 SUM	-0.196	-0.197	-0.400	0.003	mm
1A021 L	-0.196	-0.194	-0.400	0.006	mm
1A012 L	-0.197	-0.194	-0.400	0.003	mm
1A013 MUL	-0.197	-0.194	-0.400	0.003	mm
1A013 MUL	6.012	6.012	5.968	0.044	mm
1A013 MUL	1.002	1.001	1.024	-0.023	mm
1A031 SUM	-0.195	-0.195	-0.400	0.003	mm
1A031 L	-0.195	-0.194	-0.400	0.006	mm
PAGE 2					
1A025 SUM	-0.195	-0.199	-0.400	0.005	mm
1A026 L T/S	-0.197	-0.198	-0.400	0.003	mm
1A027 L	-0.196	-0.198	-0.400	0.004	mm
1A031 SUM	-0.197	-0.199	-0.400	0.004	mm
1A035 SUM	-0.197	-0.197	-0.400	0.003	mm
1A071 SUM	-0.196	-0.195	-0.400	0.003	mm
1A041 SUM	-0.196	-0.197	-0.400	0.003	mm
1A051 SUM	-0.197	-0.199	-0.400	0.003	mm
1A032 L	-0.197	-0.194	-0.400	0.003	mm
1A042 L	-0.195	-0.198	-0.400	0.005	mm
1A033 MUL	6.043	6.040	5.968	0.075	mm
1A043 MUL	6.043	6.040	5.968	0.075	mm
1A041 SUM	-0.195	-0.195	-0.400	0.003	mm
1A041 L	-0.195	-0.194	-0.400	0.006	mm
PAGE 3					
1A045 SUM	-0.197	-0.196	-0.400	0.004	mm
1A046 L T/S	-0.195	-0.198	-0.400	0.003	mm
1A047 L	-0.195	-0.198	-0.400	0.003	mm
1A055 SUM	-0.195	-0.196	-0.400	0.003	mm
1A056 L	-0.195	-0.196	-0.400	0.003	mm
1A061 SUM	-0.196	-0.196	-0.400	0.003	mm
1A065 SUM	-0.196	-0.197	-0.400	0.003	mm
1A075 SUM	-0.196	-0.197	-0.400	0.003	mm
1A062 L	-0.197	-0.194	-0.400	0.003	mm
1A072 L	-0.197	-0.194	-0.400	0.003	mm
1A063 MUL	6.000	6.006	5.968	0.032	mm
1A073 MUL	6.000	6.006	5.968	0.032	mm
1A051 SUM	-0.195	-0.195	-0.400	0.003	mm
1A051 L	-0.195	-0.194	-0.400	0.006	mm
PAGE 4					
1A081 SUM	-0.195	-0.195	-0.400	0.003	mm
1A085 SUM	-0.197	-0.198	-0.400	0.003	mm
1A111 SUM	-0.196	-0.196	-0.400	0.004	mm
1A112 L	-0.197	-0.196	-0.400	0.004	mm
1A115 SUM	-0.197	-0.197	-0.400	0.003	mm
1A116 L	-0.195	-0.196	-0.400	0.003	mm
1A131 SUM	-0.196	-0.197	-0.400	0.003	mm

Table 12. (Continued)

1A125	SUM	-9.198	-9.199	-9.200	0.002
2A102	L	-7.524	-7.508	-7.725	0.417
2A112	L	-2.062	-2.836	-3.200	0.364
2M103	MUL	5.656	5.659	5.968	-0.312
2M113	MUL	0.942	0.938	1.024	-0.046
2A072	L	-6.600	-6.593	-6.992	0.349
2A022	L	8.123	8.128	8.362	-0.239
PAGE 5					
2A001	SUM	-7.595	-7.595	-7.600	0.005
2A005	SUM	-7.797	-7.795	-7.800	0.005
2A062	L	-7.999	-7.999	-8.000	0.001
2A007	L	-8.199	-8.198	-8.200	0.002
2A011	SUM	-8.396	-8.397	-8.400	0.004
2A015	SUM	-8.601	-8.602	-8.600	-0.002
2A016	L	-8.797	-8.796	-8.800	0.004
2A021	SUM	-8.997	-8.996	-9.000	0.004
2A002	L	-7.738	-7.748	-7.725	-0.020
2A012	L	-3.378	-3.204	-3.200	-0.070
2M003	MUL	6.008	5.992	5.968	0.040
2M013	MUL	1.138	1.125	1.024	0.114
2A032	L	-7.132	-7.148	-6.992	-0.156
2A026	L 7/8	8.468	8.460	8.362	0.098
PAGE 6					
2A107	L	3.997	3.999	4.000	-0.003
1A106	L	6.617	6.615	6.610	-0.003
1A122	L	3.907	3.908	3.909	-0.002
1A126	L	6.471	6.471	6.473	-0.002
1A132	L	3.817	3.816	3.818	-0.002
1A131	SUM	6.328	6.326	6.327	0.002
1A136	L	3.725	3.725	3.727	-0.002
1A135	SUM	6.183	6.181	6.182	0.002
2A132	L	3.635	3.635	3.636	-0.001
2A131	SUM	6.039	6.035	6.036	0.004
1A076	L	8.783	8.781	8.780	0.003
2A001	SUM	-8.782	-8.784	-8.780	-0.004
2A084	SUM	-8.784	-8.784	-8.780	-0.004
PAGE 7					
2A097	L	-2.365	-2.360	-2.350	-0.015
3A012	L	-3.412	-3.370	-3.350	-0.042
3A022	L	-4.395	-4.350	-4.350	-0.045
3A032	L	-5.392	-5.350	-5.350	-0.042
3A042	L	-6.357	-6.280	-6.250	-0.067
3P024	L	-8.033	-8.033	-8.032	-0.001
3P025	L	-8.348	-8.340	-8.334	-0.006
3P026	L	-8.368	-8.361	-8.357	-0.004
3P027	L	-8.383	-8.384	-8.382	-0.003
3P030	L	-8.407	-8.407	-8.406	-0.001
3A065	SUM	1.820	1.810	1.802	0.018
PAGE 8					
3A052	L	-2.164	-2.310	-2.350	-0.054
3A072	L	-3.393	-3.380	-3.350	-0.043
3A106	L	-4.410	-4.350	-4.350	-0.060
3A122	L	-5.387	-5.360	-5.350	-0.037
3A132	L	-6.447	-6.420	-6.350	-0.087
3P045	L	-8.056	-8.056	-8.056	0.000
3P046	L	-8.325	-8.326	-8.322	-0.004
3P047	L	-8.346	-8.346	-8.343	-0.004
3P050	L	-8.303	-8.203	-8.202	-0.002
3P051	L	-8.178	-8.178	-8.176	-0.003
3A125	SUM	1.518	1.513	1.500	0.018

Table 12. (Continued)

PAGE 9				PAGE 10				PAGE 11			
COMPONENT	READING	DIAGRAM	EQUATION	COMPONENT	READING	DIAGRAM	EQUATION	COMPONENT	READING	DIAGRAM	EQUATION
2A036 L	-4.194	-4.160	-4.181	2A036 L	8.398	8.396	8.400	2A036 L	8.398	8.396	8.400
2A075 SUM	4.194	4.192	4.191	2A075 L	0.397	0.395	0.400	2A075 L	0.397	0.395	0.400
2A076 L	2.498	2.501	2.487	2A076 L	0.796	0.798	0.800	2A076 L	0.796	0.798	0.800
2A101 SUM	2.255	2.261	2.245	2A101 L	9.000	9.000	9.000	2A101 L	9.000	9.000	9.000
2A036 L	8.398	8.396	8.400	2A036 L	9.196	9.196	9.200	2A036 L	9.196	9.196	9.200
2A075 L	0.397	0.395	0.400	2A075 L	9.398	9.396	9.400	2A075 L	9.398	9.396	9.400
2A076 L	0.796	0.798	0.800	2A076 L	9.597	9.596	9.600	2A076 L	9.597	9.596	9.600
2A101 L	9.000	9.000	9.000	2A101 L	9.795	9.795	9.800	2A101 L	9.795	9.795	9.800
2A036 L	8.398	8.396	8.400	2A036 L	9.197	9.197	9.200	2A036 L	9.197	9.197	9.200
2A075 L	0.397	0.395	0.400	2A075 L	9.397	9.397	9.400	2A075 L	9.397	9.397	9.400
2A076 L	0.796	0.798	0.800	2A076 L	9.596	9.596	9.600	2A076 L	9.596	9.596	9.600
2A101 L	9.000	9.000	9.000	2A101 L	9.398	9.398	9.400	2A101 L	9.398	9.398	9.400
2A036 L	8.398	8.396	8.400	2A036 L	9.196	9.195	9.200	2A036 L	9.196	9.195	9.200
2A075 L	0.397	0.395	0.400	2A075 L	9.395	9.395	9.400	2A075 L	9.395	9.395	9.400
2A076 L	0.796	0.798	0.800	2A076 L	9.598	9.598	9.600	2A076 L	9.598	9.598	9.600
2A101 L	9.000	9.000	9.000	2A101 L	9.196	9.196	9.200	2A101 L	9.196	9.196	9.200
2A036 L	8.398	8.396	8.400	2A036 L	9.398	9.398	9.400	2A036 L	9.398	9.398	9.400
2A075 L	0.397	0.395	0.400	2A075 L	9.197	9.197	9.200	2A075 L	9.197	9.197	9.200
2A076 L	0.796	0.798	0.800	2A076 L	9.597	9.597	9.600	2A076 L	9.597	9.597	9.600
2A101 L	9.000	9.000	9.000	2A101 L	9.397	9.397	9.400	2A101 L	9.397	9.397	9.400

The leftmost column is the individual amplifier numbers within the DYNADEC system. "Reading" and "diagram" levels from each of the 40 probes are listed in the "Page 10" section of the table. The column labeled "equation" is the known input signal levels. Bias errors were computed by comparing differences between the known "equation" magnitudes and the "reading" and "diagram" levels:

$$\text{Bias error} = \max [(\text{"equation"} - \text{"reading"}), (\text{"equation"} - \text{"diagram"})] \quad (17)$$

This quantity is also calculated in the static check output and can be seen under the column labeled "error" in Table 12.

K_{a2} , K_0 , and K_{ra2} bias errors were determined in a similar manner. Readings from three amplifiers were used to calculate these bias errors. Readings from amplifier 65 (3A065) under the "Page 7" heading of Table 12 was used to calculate the K_{ra2} bias error. Amplifier 75 (2A075) under the "Page 9" heading of Table 12 was used to calculate the K_0 bias error. Readings from amplifier 76 (2A076) from the same page were used to calculate the K_{a2} bias error. The analog computer locations of their "diagram" and "reading" levels can be seen in Figure 41.

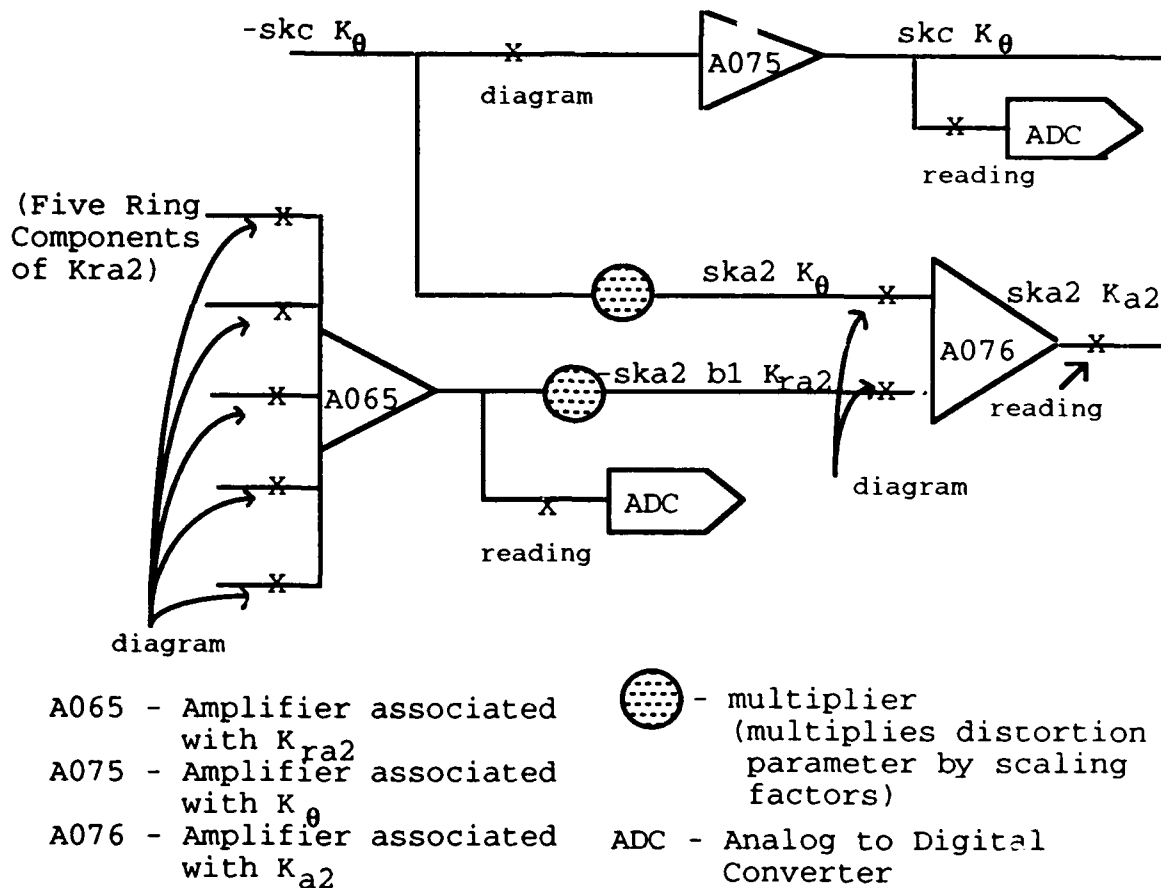


Figure 41. Distortion Parameter Bias Error Signal Locations

The "equation" values are the known K_{a2} , K_{θ} and K_{ra2} signals.

K_{a2} , K_{θ} and K_{ra2} bias errors are also computed using equation 17. It should be noted that the static check K_{a2} , K_{θ} and K_{ra2} levels are also scaled to fall within the voltage levels of the DYNADEC system.

$$\text{Actual } K_{a2} = K_{a2} \text{ reading from system} / ska2 \quad (18)$$

where: $ska2 = 4.0$

$$\text{Actual } K_0 = K_0 \text{ reading from system} / skc \quad (19)$$

where. $skc = 1.0$, scale factor

$$\text{Actual } K_{ra2} = K_{ra2} \text{ reading from system} / skra2 \quad (20)$$

where: $skra2 = 1.25$, scale factor

The 40 individual probe bias errors were also measured in the static checks done before each test point was edited. An example output from this static check can be seen in Table 13.

Table 13. Example Output from a Static Check Performed Before a Test Point is Edited

[illegible]

Table 13. (Continued)

Table 13. (Continued)

A DEGREES	SINE(A)	COSINE(A)
0.00	0.00000	1.00000
45.00	0.70711	0.70711
90.00	1.00000	0.00000
135.00	0.70711	-0.70711
180.00	0.00000	-1.00000
225.00	-0.70711	-0.70711
270.00	-1.00000	0.00000
315.00	-0.70711	0.70711
0.00	0.00000	1.00000
45.00	0.70711	0.70711
90.00	1.00000	0.00000
135.00	0.70711	-0.70711
180.00	0.00000	-1.00000
225.00	-0.70711	-0.70711
270.00	-1.00000	0.00000
315.00	-0.70711	0.70711

The known input signals are listed in the "zpss" (pressure, steady state) column. The analog reading is listed in the "dval" (digital value) column. Bias errors were computed by differencing the two columns.

$$\text{Bias error} = \text{zpss} - \text{dval} \quad (21)$$

These values are computed in the static checks and can be seen in the "diff" (difference) column of Table 11.

This version of the static checks is done to measure the difference between the steady state recoveries in the analog system and the known recoveries before each point. Figure 42 shows the analog locations where the signals.

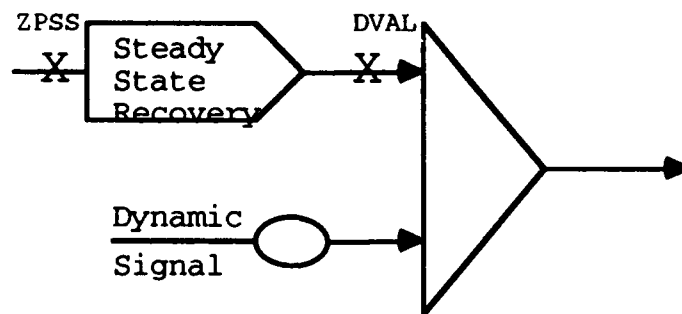


Figure 42. Probe Bias Error Signal Locations from Static Checks of Test Points

No dynamic signal exists in the dynamic branch for this static check, so the bias errors calculated essentially

become identical to the bias errors calculated in the daily system static checks:

$$\text{Bias error} = \text{"zpss"} - \text{"dval"} = \text{"equation"} - \text{"diagram"} \quad (22)$$

Thus, the overall static bias error will sum and average the two errors:

$$\text{Bias Error)}_{\text{probe}} = \frac{\sum_{i=1}^n (\text{zpss-dval}) + \sum_{i=1}^m (\text{equation-diagram})}{(n + m)} \quad (23)$$

where: $n = 156$

$m = 45$

45 daily initial static checks from June, 1991 to March 1992 were used to determine K_{a2} , K_{θ} , K_{ra2} and the 40 individual probe bias errors. Also used to compute the 40 individual probe bias errors, were the 156 static checks, done before each test point was edited. Results of this effort will be discussed in Chapter 3.

CHAPTER III

DISCUSSION OF RESULTS

3.1 Level 1 Analysis

Much of the work in the four levels of analysis centered around the use of spreadsheets and basic computer graphics to handle the large quantities of data involved. The spreadsheets of data will not be included in the data in the appendices because all of the data is shown in the probability distributions in Appendix B. The data in the appendices are the final distributions after the four levels of analysis were completed and outliers eliminated. This discussion presents results in the order that they were listed in the the Analysis Plan (Table 10).

All probe recovery, distortion index, and ring average data were placed in chronological order and then sorted for the probability distributions in the first level of analysis. Distributions for the analog and digital K_{a2} , K_{θ} and K_{ra2} indices and digital AIR 1419 indices can be seen in Appendix B. Six sample probes of each case were selected at random for a cursory look at any noise or outliers present in the data.

The majority of the effort in the first level of analysis was performed in more detail in the second and third

levels of analysis and those results will be discussed. What was important to note at this point, was that the digital K_{a2} , K_θ and K_{ra2} distributions of the six cases exhibited slightly larger scatter bands than their respective analog component distributions. This was expected because the analog K_{a2} , K_θ and K_{ra2} levels are based upon one analog-to-digital (a-d) conversion of one reading in the analog system. The digital values were based upon forty a-d conversions of the forty dynamic total pressures. This approach introduced forty individual a-d conversion precision errors into one distortion index value. The analog levels contained one analog-to-digital conversion error in one distortion index value.

Level 1 analysis of the $M=0.6$ freejet case, FJ72.067, showed bi-polar distributions of the analog and digital distortion indices. This indicated noise was present in the DYNADEC system or on the analog data tape. Further investigation of total pressure recovery distributions of this point indicated that four of the six probes analyzed had bi-polar characteristics with several unique runs falling well outside the $\pm 2S$ range of the mean (outliers) (Figure 43.)

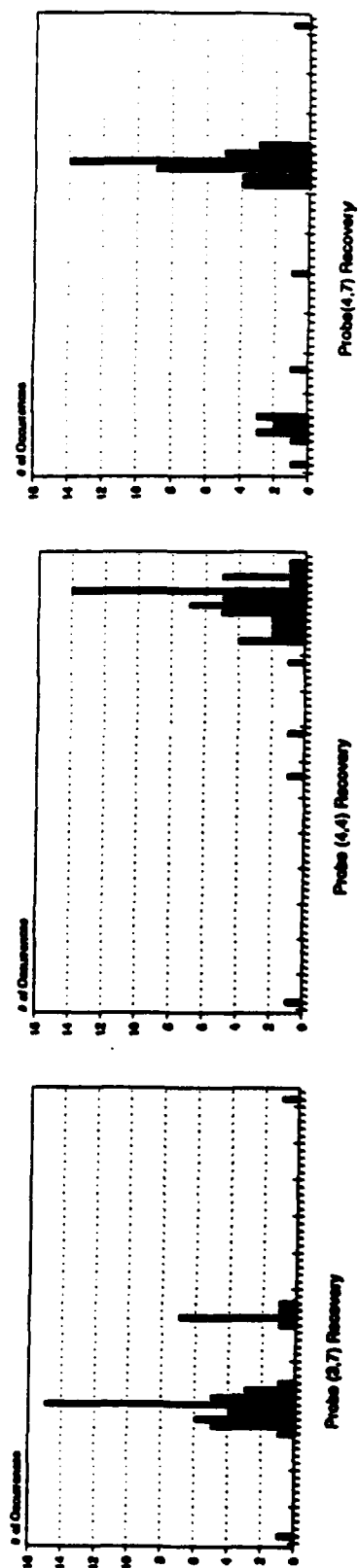
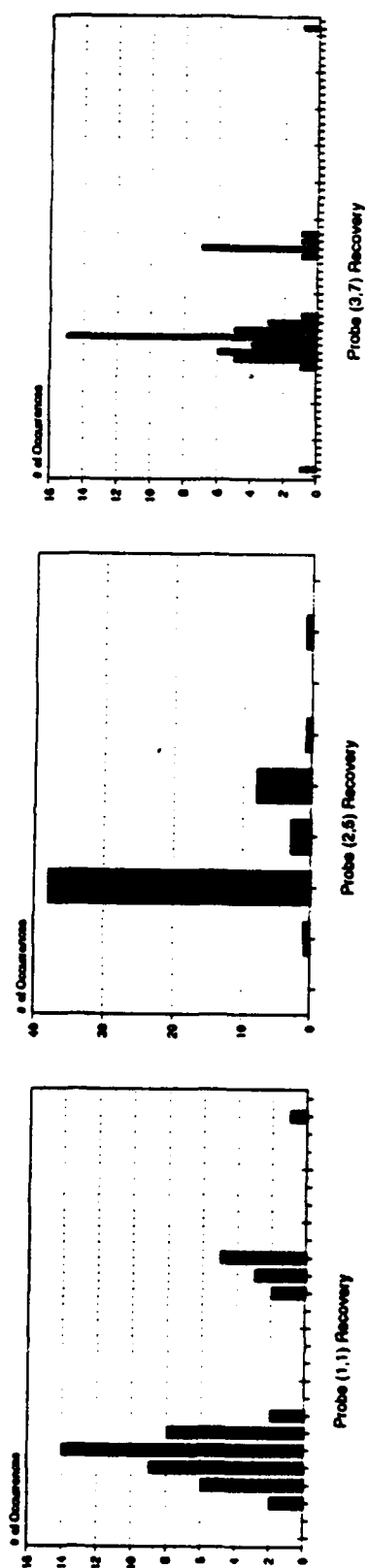


Figure 43. FJ72.067 Six Probe Distributions

Preliminary analysis of the five remaining cases showed that outliers were present in some runs, but bi-polar behavior in the recovery distributions was not present (Figure 44.).

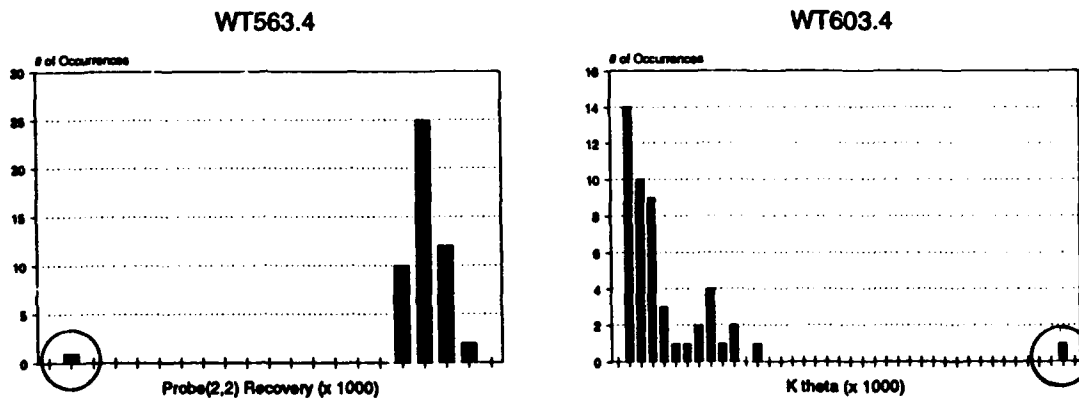


Figure 44. Level 1 Analysis Example Outlier Cases

This implied that the noise in the FJ72.067 data was on the tape, but a more detailed analysis was needed at this point to more fully understand the problem.

AIR 1419 indices were also investigated. Distributions on these parameters in Appendix B showed that the AIR 1419 index components seemed to exhibit less scatter than the Pratt and Whitney indices of the same point; however the AIR 1419 components are usually combined in some fashion like the method in Appendix A to form a " K_{a2} -like" index. Since no index existed for this database, a more appropriate

comparison would be the AIR 1419 index components and the ring average recovery distributions, since K_{ra2} is a function of the ring averages. In affect ring average recovery is a component of K_{a2} just as Radial and Circumferential Intensity, MPR and Extent are components of the AIR 1419 distortion index.

This comparison seemed to indicate that the AIR 1419 components exhibited less scatter in their distributions than the ring average recoveries; however two observations make this conclusion less definite. First, were the scales of the AIR 1419 components and ring average recovery distributions comparable? It probably would have been more accurate to compare the two data sets on a non-dimensionalized basis, for instance as a percentage of an average recovery and average AIR 1419 component. Due to time constraints and the amount of work involved in non-dimensionalizing data for 180 distribution plots, this was not done.

The second concern was that the resultant peaks were a function of peak analog K_{a2} and not AIR 1419 indices. While the ring average recoveries and AIR 1419 index components were both a function of the 40 digitized recoveries, it would have been more appropriate to screen the data with the AIR 1419 indices and then perform the comparison. The DYNADEC system was wired for AIR 1419 indices at the time of this analysis, so a re-screening of the data could not be done.

3.2 Level 2 Analysis

The first step in the second level of analysis was the determination of a preliminary mean (\bar{x}) and precision index (S) for each of the forty probes and the analog and digital distortion indices. Table 14 shows the results of this effort.

**Table 14. Preliminary Means and
Precision Indices for Six Test Points**

Probe	FJ72.067		WT603.4		FJ14.148	
	\bar{x}'	+2S/ \bar{x}	\bar{x}'	+2S/ \bar{x}	\bar{x}'	+2S/ \bar{x}
(1,1)	1.0323	1.0216	1.0493	0.2735	1.0976	0.1451
(1,2)	1.0378	2.1407	1.0474	1.0703	1.0148	0.9218
(1,3)	1.0454	1.5694	1.0505	0.2444	0.9890	0.1555
(1,4)	1.0722	1.6862	1.0517	0.3380	0.9921	0.1803
(1,5)	1.0336	1.7946	1.0510	0.2252	0.9862	0.1191
(1,6)	1.0160	1.3053	1.0424	0.2094	0.9849	0.1386
(1,7)	1.0420	0.9748	1.0651	0.3664	1.0718	0.1130
(1,8)	1.0214	1.6904	1.0352	0.2025	1.0941	0.1258
(2,1)	1.0072	1.8175	1.0343	0.3590	1.0590	0.1924
(2,2)	1.0525	1.2778	1.0500	0.1996	1.0817	0.1515
(2,3)	1.0447	0.9249	1.0494	0.2665	1.0156	0.1421
(2,4)	1.0505	1.7238	1.0510	0.2636	1.0008	0.1379
(2,5)	1.0048	0.2157	1.0251	0.2345	0.9884	0.2135
(2,6)	0.9940	2.0750	1.0236	0.2941	0.9804	0.1526
(2,7)	0.9831	1.4459	1.0370	0.3230	0.9811	0.1444
(2,8)	0.9707	2.3391	0.9455	2.9537	1.0111	0.5139
(3,1)	0.9695	2.8914	0.9731	0.2144	0.9867	0.2237
(3,2)	1.0721	3.4707	1.0362	0.2559	1.1073	0.1773
(3,3)	1.0225	0.7588	1.0298	0.2826	1.0536	0.1012
(3,4)	1.0428	1.7420	1.0192	0.2598	0.9533	0.1572
(3,5)	0.9775	0.2588	0.9767	0.2433	0.9841	0.2163
(3,6)	0.9873	0.9339	1.0215	0.0945	0.9830	0.1375
(3,7)	0.9768	1.7788	1.0187	0.2156	1.0035	0.2160
(3,8)	0.9564	2.0214	0.9312	0.2387	1.0098	0.0893
(4,1)	0.9316	2.8252	0.9371	0.2631	0.9674	0.1984
(4,2)	1.0697	4.0929	1.0171	0.3048	1.0725	0.2374
(4,3)	1.0002	1.3844	0.9992	0.3359	1.0261	0.3230
(4,4)	1.0140	1.9087	0.9436	0.3668	0.9785	0.3057
(4,5)	0.9728	0.6758	0.9581	0.2662	0.9668	0.2872
(4,6)	1.0266	1.5686	1.0114	0.3709	0.9963	0.2546
(4,7)	0.9968	2.9454	0.9916	0.3470	0.9231	0.3686
(4,8)	0.9465	1.8709	0.9144	0.2094	0.9571	0.1558
(5,1)	0.8983	0.4239	0.9127	0.2115	0.9547	0.1467
(5,2)	0.9914	2.0270	0.9719	0.2620	0.9972	0.1600
(5,3)	0.9355	3.0378	0.9691	0.4185	1.0170	0.2384
(5,4)	0.9213	2.5248	0.9021	0.2467	0.9476	0.1723
(5,5)	0.9615	0.9565	0.9638	0.3597	0.9282	0.2236
(5,6)	1.0025	1.6271	1.0012	0.2543	0.9483	0.1073
(5,7)	0.9949	3.3808	0.9819	0.2386	0.9626	0.2372
(5,8)	0.9231	2.2222	0.9101	0.3279	0.9269	0.1828
Ave		1.7850		0.3603		0.2116

Table 14. (Continued)

Probe	WT563.4		FJ59.022		WT1170.1	
	\bar{x}'	$+2S/\bar{x}$	\bar{x}'	$+2S/\bar{x}$	\bar{x}'	$+2S/\bar{x}$
(1,1)	1.0506	0.3653	0.7667	0.4015	0.9445	0.1742
(1,2)	1.0304	0.6017	0.6835	0.5487	0.9451	0.5831
(1,3)	1.0214	0.4742	0.7882	0.2921	0.9373	0.0876
(1,4)	0.9959	0.6291	0.8774	0.2653	0.9817	0.1781
(1,5)	0.9580	0.4141	0.8936	0.1443	1.0392	0.1188
(1,6)	0.9772	0.3896	1.0059	0.3799	1.0153	0.1100
(1,7)	1.0197	0.5786	0.9974	0.3185	0.9453	0.1918
(1,8)	1.0512	0.3384	0.9011	0.2986	0.9110	0.1614
(2,1)	0.9967	0.5344	0.9318	0.3066	0.9348	0.1268
(2,2)	1.0549	0.5228	0.8606	0.2911	1.0093	0.0823
(2,3)	1.0674	0.4011	0.7874	0.2429	1.0230	0.1944
(2,4)	1.0342	0.5510	1.1605	0.1609	1.0674	0.1303
(2,5)	0.9664	0.8500	1.0904	0.3371	1.0754	0.1305
(2,6)	1.0029	0.1992	1.0861	0.3109	1.0157	0.0706
(2,7)	1.0330	0.3630	1.0117	0.2344	0.9518	0.1916
(2,8)	1.0293	0.4820	0.9046	0.5848	0.9309	0.7890
(3,1)	0.9657	0.5041	1.0032	0.2308	0.9547	0.1046
(3,2)	1.0801	0.8697	1.0365	0.1828	1.0227	0.0705
(3,3)	1.0612	0.7389	1.0665	0.3843	1.0897	0.1893
(3,4)	1.0405	1.1043	1.0683	0.3734	1.0983	0.1103
(3,5)	0.9531	0.4440	1.2008	0.2783	1.0554	0.0719
(3,6)	1.0019	0.3447	1.0445	0.2610	1.0137	0.1943
(3,7)	1.0039	0.3287	1.0092	0.2494	0.9612	0.1453
(3,8)	1.0132	0.9616	0.9149	0.1906	0.9485	0.1283
(4,1)	0.9483	0.1616	0.9840	0.2535	0.9671	0.0864
(4,2)	1.0360	0.6172	1.0854	0.1442	1.0293	0.1942
(4,3)	1.0448	0.8280	1.1458	0.4344	1.0994	0.1695
(4,4)	0.9926	0.6942	1.0725	0.0470	1.0918	0.1242
(4,5)	0.9434	0.7908	1.1570	0.2928	1.0598	0.0649
(4,6)	0.9965	0.2564	1.0435	0.2421	1.0073	0.1710
(4,7)	1.0046	0.2731	1.0219	0.2075	0.9614	0.3009
(4,8)	0.9908	0.6873	0.9286	0.1428	0.9423	0.0976
(5,1)	0.9270	0.2689	1.0070	0.1437	0.9644	0.0684
(5,2)	0.9774	0.2319	1.0915	0.3352	0.9799	0.0464
(5,3)	1.0184	0.6891	1.0998	0.3344	1.0673	0.1771
(5,4)	0.9396	0.1914	1.1502	0.2617	1.0502	0.1211
(5,5)	0.9100	1.0177	1.1318	0.2914	1.0298	0.1700
(5,6)	0.9617	0.7102	1.0785	0.1486	0.9876	0.1495
(5,7)	0.9473	0.3062	0.9722	0.0530	0.9615	0.0930
(5,8)	0.9530	0.3950	0.9397	0.0642	0.9291	0.0756
Ave		0.5277		0.2666		0.1611

Table 14. (Continued)

		FJ72.067		WT603.4		FJ14.148	
Probe		\bar{x}'	$+2S/\bar{x}$	\bar{x}'	$+2S/\bar{x}$	\bar{x}'	$+2S/\bar{x}$
Analog	K theta	0.5128	4.5358	0.2933	1.7358	0.7282	0.5326
	K ra2	0.3359	12.5506	0.3133	2.7098	0.5036	1.8508
	Ka2	0.1440	8.4508	0.1124	1.6169	0.1944	1.1297
Digital	K theta	0.5338	6.0640	0.3006	12.2254	0.7301	0.6127
	K ra2	0.3357	21.3682	0.3521	5.4714	0.6089	2.4424
	Ka2	0.1466	9.2543	0.1224	2.7474	0.2156	1.3392

		WT563.4		FJ59.022		WT1170.1	
Probe		\bar{x}'	$+2S/\bar{x}$	\bar{x}'	$+2S/\bar{x}$	\bar{x}'	$+2S/\bar{x}$
Analog	K theta	0.4716	0.8768	2.4292	0.9586	1.4735	0.1295
	K ra2	0.6128	3.4624	2.9347	0.5594	1.1162	0.7545
	Ka2	0.1828	2.2871	3.7609	0.5560	1.4753	0.6236
Digital	K theta	0.4812	2.6444	2.5838	0.7899	1.4619	1.0482
	K ra2	0.6708	2.2365	3.0459	0.4250	1.1700	0.9341
	Ka2	0.1955	1.5423	3.9134	0.4250	1.5367	0.8852

The table lists the quantity $\pm 2S/\bar{x}$ rather than $\pm S$, to observe how large the quantity $\pm 2S$ is in relation to the mean. The idea behind the use of $\pm 2S$ was the fact that the acceptance process associated with this data set was based upon the $\pm 2S$ range discussed in Chapter 2, and $\pm 2S$ is the industry standard evaluation level. These values should be considered a conservative estimation of the precision indices because they include the outliers that will be eliminated in the third level of analysis. It also should be noted that the means (\bar{x}) of the forty probes were non-dimensionalized in Table 14 by the face average recovery of each case. The distortion indices were non-dimensionalized by the average of the indices of all 6 test points.

$$\left| \bar{x}'_{Ka2}, \bar{x}'_{K\theta}, \bar{x}'_{Kra2} \right| = \frac{\bar{x}_K \big|_{\text{test point}}}{\sum_{n=1}^6 \bar{x}_{K_n}} \quad (24)$$

\bar{x}_K = Mean Distortion Parameter
for a test point
(\bar{x} of K_{a2} , K_{θ} , or K_{ra2})

$\sum_{n=1}^6 \bar{x}_K$ = Sum of means of a distortion
parameter of each test point
(for K_{a2} , this sum is \bar{x}_{Ka2} 's
of WT603.4, FJ72.067, WT563.4
FJ14.148, WT1170.1, and FJ59.022)

Results in Table 14 showed that the noise present in the distributions of FJ72.067 were also present in the precision

indices. $\pm 2S/\bar{x}$ values from K_{a2} , K_0 , and K_{ra2} were affected much more than the individual probe $\pm 2S/\bar{x}$ quantities. This may be due to the fact that the distortion indices are a function of forty probes of data read from an analog tape. The digital precision indices from FJ72.067 were larger than the analog magnitudes. This provided further evidence that the analog-to-digital conversion of forty probes introduced additional error in the digital distortion parameters.

Another method used to analyze the resultant means and precision indices of the distortion parameters was to observe how the analog and digital levels of the same test point differed. Digital K_0 readings had slightly higher magnitudes. The $\Delta(D-A)/\text{Digital}$ parameter in Table 15. is a measure of the difference between the digital and analog levels with respect to the digital readings:

Table 15.
Analog and Digital K_θ Levels for Six Test Points

	FJ	WT	FJ	WT	FJ	WT
	72.067	603.4	14.148	563.4	59.022	1170.1
RMS % Turbulence	1.62	1.31	3.02	3.35	4.85	5.35
Analog K_θ	0.5128	0.2933	0.7282	0.4716	2.4292	1.4735
Digital K_θ	0.5338	0.3006	0.7301	0.4812	2.5838	1.4619
$\Delta (D-A)$	-0.021	-0.0073	-0.0019	-0.0096	-0.1546	0.011
$\frac{\Delta (D-A)}{\text{Digital}}$	3.934	2.428	0.260	1.995	5.983	0.793

$$\frac{\Delta (D-A)}{\text{Digital}} = \frac{\text{Digital Reading} - \text{Analog Reading}}{\text{Digital Reading}} \quad (25)$$

The differences were reasonable with the exception of the 6% difference in K_θ levels from freejet point FJ59.022. These parameters were also plotted to observe any trends with RMS turbulence level (Figure 45.).

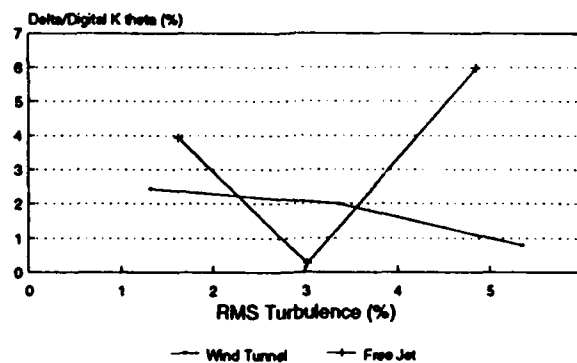


Figure 45. K_θ Digital-Analog Difference Vs. RMS Turbulence Level

As a whole, there did not appear to be any trends with RMS turbulence. The two data sets were divided into freejet and wind tunnel results. The freejet data curve was inconclusive. The wind tunnel differences appeared to decrease as a percentage of digital K_0 with increasing RMS turbulence level.

K_{ra2} and K_{a2} analog to digital magnitude shifts were also analyzed (Tables 16 and 17).

Table 16.
 K_{ra2} Analog and Digital Magnitude Comparison,
 With Outliers

	FJ	WT	FJ	WT	FJ	WT
	72.067	603.4	14.148	563.4	59.022	1170.1
RMS %	1.62	1.31	3.02	3.35	4.85	5.35
Turbulence						
Analog K_{ra2}	0.3359	0.3113	0.5036	0.6128	2.9347	1.1162
Digital K_{ra2}	0.3357	0.3521	0.6089	0.6708	3.0459	1.17
$\Delta (D-A)$	0.0002	-0.0388	-0.1053	-0.058	-0.1112	0.0538
$\frac{\Delta (D-A)}{\text{Digital}}$	0.060	11.020	17.293	8.646	3.651	4.598

Table 17.
K_{a2} Analog and Digital Magnitude Comparison,
With Outliers

	FJ	WT	FJ	WT	FJ	WT
	72.067	603.4	14.148	563.4	59.022	1170.1
RMS % Turbulence	1.62	1.31	3.02	3.35	4.85	5.35
Analog K _{a2}	0.1440	0.1124	0.1944	0.1828	3.7609	1.4753
Digital K _{a2}	0.1466	0.1224	0.2156	0.1955	3.9134	1.5367
$\Delta (D-A)$	-0.0026	-0.01	-0.0212	-0.0127	-0.1525	-0.0614
$\Delta (D-A)$ <u>Digital</u>	1.774	8.170	9.833	6.496	3.897	3.996

In each case, digital magnitudes were higher than analog magnitudes. K_{ra2} and K_{a2} differences were much larger as a percentage of digital components than the differences seen in the K₀ results. This may be due the fact that the K₀ equation is a function of the forty individual probe readings and the K_{ra2} equation is a function of the five ring average recoveries (see Appendix A). An error in one of the forty a-d converters producing the digital K₀ level will not have as great an effect as an error in one of the five ring average signals used to compute K_{ra2}.

The digital-analog differences as a percentage of digital K_{ra2} and K_{a2} were also plotted (Figures 46 and 47).

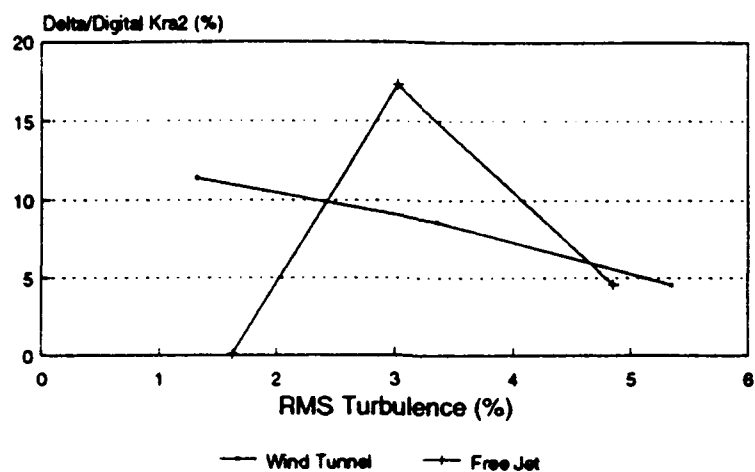


Figure 46. K_{ra2} Digital-Analog Difference Vs. RMS Turbulence Level

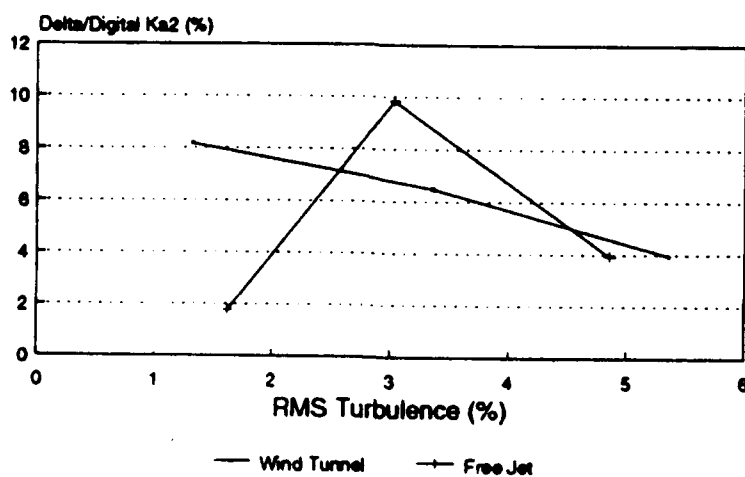


Figure 47. K_{a2} Digital-Analog Difference Vs. RMS Turbulence Level

Once again, the data as a whole and the freejet data by itself was inconclusive. Wind tunnel differences decreased with increasing RMS turbulence level. Final judgements on these results were not made until outliers in the data were removed in the third level of analysis.

The next step was to identify outliers outside the $x \pm 2S$ range in the distributions. Generally, if a single reading was more than $\pm 3S$ away from the mean value, it was considered an outlier. Unique readings closer to the mean than $\pm 3S$ were retained for further inspection in the third level of analysis.

Because of the bi-polar characteristics of the FJ72.067 results, outliers and noise runs were retained for the remainder of the analysis. The $M=0.6$ wind tunnel point paired with FJ72.067, WT603.4 contained some outliers that were visually obvious, but noise was not observed (Figure 48.).

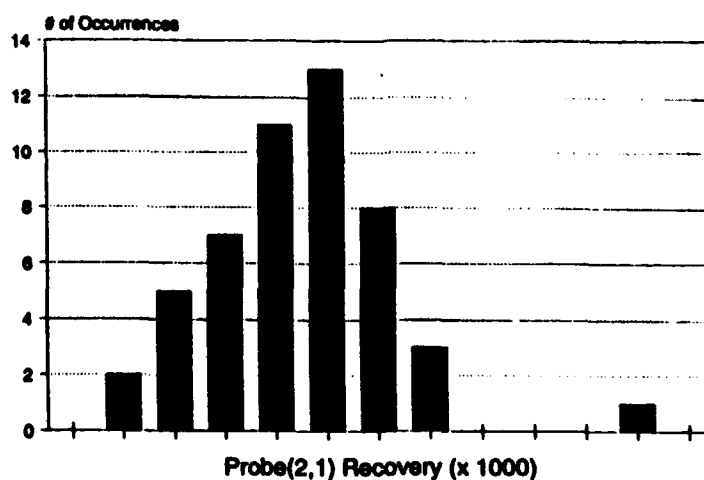


Figure 48. WT603.4 Outlier

Distributions of the M=0.3 wind tunnel point, WT563.4 (Figure 49.), indicated that one run of the 50 edited consistently produced the outliers seen in the distributions.

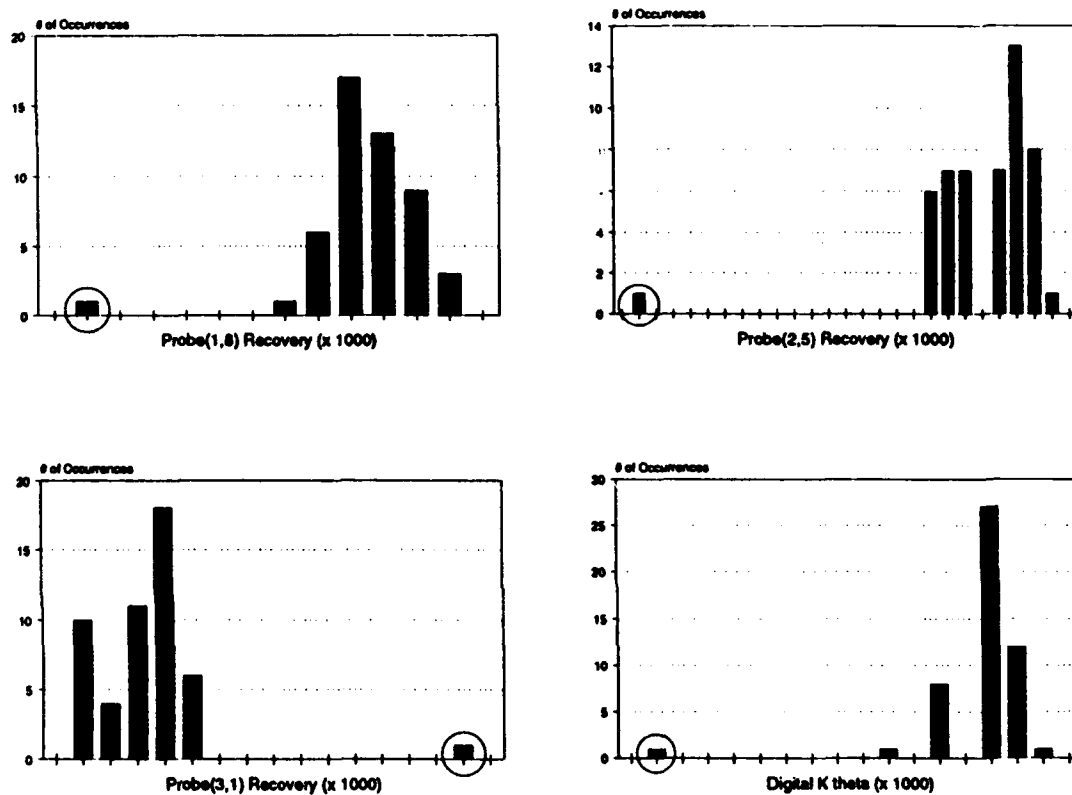


Figure 49. WT563.4 Outliers

This particular run was the first, chronologically, out of the 50 runs. This meant that if the first run produced outliers on the remaining probe distributions done in the third level of the analysis, data from this run should be eliminated from the analysis entirely.

Outliers in the initial distributions of the three remaining test points, FJ14.148, FJ59.022, and WT1170.1 were not as obvious and required distributions on all of the forty probes before any conclusions could be made.

Faulty probe distributions were also investigated to monitor the analog computer's ability to zero out the incoming dynamic signal. Table 18 lists the faulty probes for each of the six test points.

Table 18.
Faulty Probe Log

<u>FJ72.067</u>	<u>WT603.4</u>	<u>FJ14.148</u>	<u>WT563.4</u>	<u>FJ59.022</u>	<u>WT1170.1</u>
(2,5)	None	(1,7)	None	(4,4)	(5,2)
(3,5)		(2,8)		(5,7)	
(4,5)		(4,8)		(5,8)	

where (i,j)= (ring, rake) position

The only faulty probe selected in the initial distributions of the Level 1 analysis was the probe on ring 2, rake 5 of FJ72.067 as shown in Figure 50.

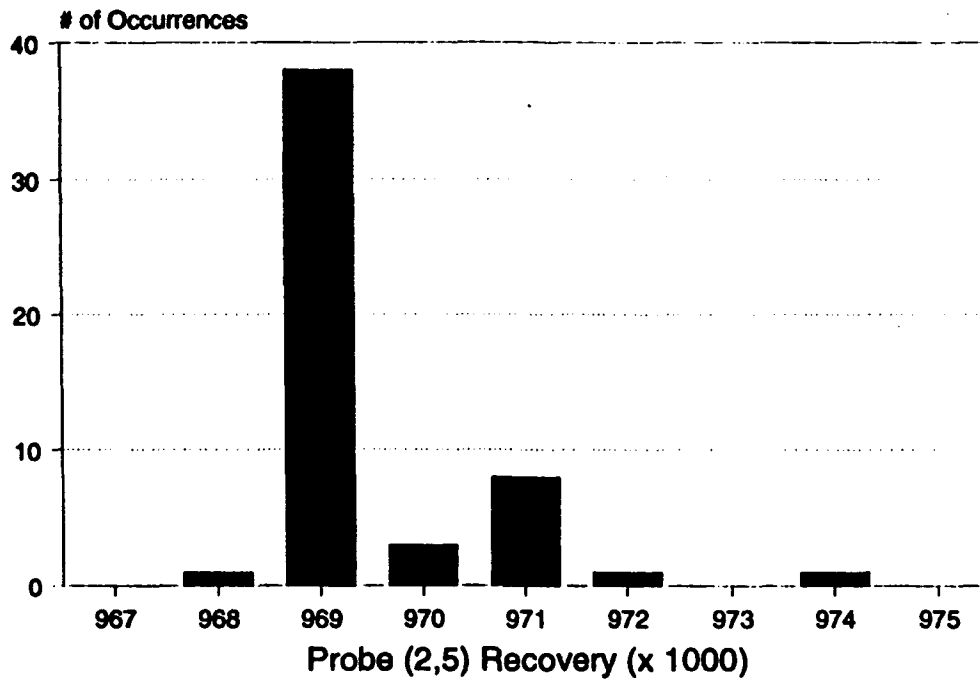


Figure 50. FJ72.067 Faulty Probe Distribution Example

The distribution on this probe indicated that the system was "zeroing" out the dynamic signal in a precise and accurate manner. Further study of the other faulty probes was accomplished in the third level of analysis.

The last area of concern in the second level of analysis was the shape of the distributions. Distortion parameters and probe distributions in Appendix B show that precision increases (less scatter) with increasing RMS turbulence level. This is probably due to the fact that high turbulence signals have large amplitudes, thus the DYNADEC peak detector can more easily discern a definite peak from signal and system noise sources which should have magnitudes less than 1 % RMS levels.

3.3 Level 3 Analysis

The third level of analysis was initiated with the computation of distributions of ring average recoveries, AIR 1419 indices, and each of the 40 probes. Before returning to concerns raised in the second level of analysis, outliers were eliminated. Table 19 lists the outliers eliminated by parameter and case number.

Table 19 Outliers Eliminated

1) FJ72.067	None	
2) WT603.4	Digital K ₀	Case 11,42
	K _{ra2}	Case 11,42
	K _{a2}	Case 11,42
	Probe (1,2)	Case 42,43,49
	Probes (1,3), (1,4), (1,8), (2,1), (2,3), (2,6), (3,2), (4,3), (4,4), (4,5), (4,6), (5,8)	Case 9
	Probe (2,8)	Case 11,32,42
	Probe (4,7)	Case 9,49
	Ring Average Ring 2	Case 42
	AIR 1419 Intensity	
	Ring 2	Case 42
	MPR Ring 1	Case 9,10
	MPR Ring 4	Case 9
	MPR Ring 5	Case 9
	IDR Ring 2	Case 11,42
3) FJ14.148	Probe (1,2)	Case 8,32
	Probe (3,1)	Case 50
4) WT563.4	All Indexes, Probes, Ring Averages AIR 1419 Indices	Case 1
5) FJ59.022	Analog K ₀	Case 3,17
	Analog K _{ra2}	Case 3,17
	Analog K _{a2}	Case 3,17
	Probes (2,8)	Case 43
6) WT1170.1	Digital K ₀	Case 48
	Digital K _{ra2}	Case 48
	Digital K _{a2}	Case 48
	Probe (1,2)	Case 45,48

Case numbers are the order in which the individual runs occurred. Case 1 was the first run of the first day editing was performed on that particular test point. Case 50 was the last run on the last day editing was performed on a test point.

Several outlier patterns emerged from the data in Table 19 and Table 9, the run log of this analysis. The M=0.6 wind tunnel case, WT603.4, had many unique probe readings outside the $\pm 2S$ range of the mean. Most of the outliers occurred in Case 9, run on the first day editing this point, and Case 42, run on the last day editing this point. Less than half of the 40 probe distributions were affected, so data from Case 9 and Case 42 was not eliminated in the distributions where no outliers were present.

Level 2 preliminary results from the M=0.3 wind tunnel case, WT563.4, indicated that the first run of the first day (Case 1) produced all of the outliers for this test point. Distributions on all probes, AIR 1419 indices and ring averages showed that approximately 75 % of the distributions contained one outlier from Case 1. Since the majority of the data was affected, all recoveries, distortion indices and ring averages from Case 1 of WT563.4 were eliminated from the remainder of this analysis.

Distributions of the remaining wind tunnel point, WT1170.1, and two of the freejet points, FJ14.148 and FJ59.022, contained few outliers. What outliers did exist

did not exhibit trends over the data set of the particular point. What was interesting to observe in the two $M=2.2$ test points, WT1170.1 and FJ59.022, was that outliers on the K_{a2} , K_θ and K_{ra2} distributions existed while the individual probes on these cases were not outliers themselves. This is due to the fact that a majority of readings may fall to one side of the mean, but remain within the $\pm 2S$ range of the mean. This drives the K_{a2} , K_θ and K_{ra2} levels to extreme highs or lows (outliers).

Distributions on the sixth test point, FJ72.067, showed that a majority of the probes and distortion parameters had the bi-polar (noise) characteristic seen in the second level of analysis. Outliers were retained in this case to observe any relationships they may have had with the noise.

Several other factors affected the selection of outliers. Outliers from each of the six cases were checked against one another to see if they occurred on the same day, on the same probe, or exclusively in the wind tunnel or freejet data sets. Probe (1,2) seemed to have slightly more scatter than most of the other probe distributions, but no other trends were seen in the data. Outliers occurred at random, on different days, and throughout both data sets.

Outliers on the five test points were eliminated and distributions, means, and precision indices were recomputed. The resultant distributions can be seen in Appendix B. The new means and precision indices are listed in Table 20.

**Table 20. Means and Precision
Indices for Six Test Points**

Probe	FJ72.067		WT603.4		FJ14.148	
	\bar{x}'	$+2S/\bar{x}$	\bar{x}'	$+2S/\bar{x}$	\bar{x}'	$+2S/\bar{x}$
(1,1)	1.0323	1.0216	1.0493	0.2735	1.0976	0.1451
(1,2)	1.0378	2.1407	1.0484	1.0703	1.0155	0.9218
(1,3)	1.0454	1.5694	1.0503	0.2444	0.9890	0.1555
(1,4)	1.0722	1.6862	1.0515	0.3380	0.9921	0.1803
(1,5)	1.0336	1.7946	1.0509	0.2252	0.9862	0.1191
(1,6)	1.0160	1.3053	1.0423	0.2094	0.9849	0.1386
(1,7)	1.0420	0.9748	1.0651	0.3664	1.0717	0.1130
(1,8)	1.0214	1.6904	1.0350	0.2025	1.0941	0.1258
(2,1)	1.0072	1.8175	1.0341	0.3590	1.0590	0.1924
(2,2)	1.0525	1.2778	1.0499	0.1996	1.0817	0.1515
(2,3)	1.0447	0.9949	1.0492	0.2665	1.0156	0.1421
(2,4)	1.0505	1.7238	1.0509	0.2636	1.0007	0.1379
(2,5)	1.0048	0.2157	1.0250	0.2345	0.9884	0.2135
(2,6)	0.9940	2.0750	1.0234	0.2941	0.9804	0.1526
(2,7)	0.9831	1.4459	1.0369	0.3230	0.9810	0.1444
(2,8)	0.9707	2.3391	0.9484	2.9537	1.0111	0.5139
(3,1)	0.9695	2.8914	0.9730	0.2144	0.9865	0.2237
(3,2)	1.0721	3.4707	1.0361	0.2559	1.1072	0.1773
(3,3)	1.0225	0.7588	1.0297	0.2826	1.0536	0.1012
(3,4)	1.0428	1.7420	1.0191	0.2598	0.9533	0.1572
(3,5)	0.9775	0.2588	0.9766	0.2433	0.9841	0.2163
(3,6)	0.9873	0.9339	1.0214	0.0945	0.9830	0.1375
(3,7)	0.9768	1.7788	1.0186	0.2156	1.0035	0.2160
(3,8)	0.9564	2.0214	0.9311	0.2387	1.0098	0.0893
(4,1)	0.9316	2.8252	0.9370	0.2631	0.9673	0.1984
(4,2)	1.0697	4.0929	1.0170	0.3048	1.0725	0.2374
(4,3)	1.0002	1.3844	0.9990	0.3359	1.0261	0.3230
(4,4)	1.0140	1.9087	0.9433	0.3668	0.9784	0.3057
(4,5)	0.9728	0.6758	0.9580	0.2662	0.9668	0.2872
(4,6)	1.0266	1.5686	1.0112	0.3709	0.9963	0.2546
(4,7)	0.9968	2.9454	0.9916	0.3470	0.9231	0.3686
(4,8)	0.9465	1.8709	0.9143	0.2094	0.9571	0.1558
(5,1)	0.8983	0.4239	0.9126	0.2115	0.9547	0.1467
(5,2)	0.9914	2.0270	0.9718	0.2620	0.9972	0.1600
(5,3)	0.9355	3.0378	0.9690	0.4185	1.0170	0.2384
(5,4)	0.9213	2.5248	0.9021	0.2467	0.9476	0.1723
(5,5)	0.9615	0.9565	0.9637	0.3597	0.9282	0.2236
(5,6)	1.0025	1.6271	1.0012	0.2543	0.9483	0.1073
(5,7)	0.9949	3.3808	0.9818	0.2386	0.9626	0.2372
(5,8)	0.9231	2.2222	0.9101	0.3279	0.9269	0.1828
Ave		1.7850		0.3603		0.2116

Table 20. (Continued)

Probe	WT563.4		FJ59.022		WT1170.1	
	\bar{x}'	$+2S/\bar{x}$	\bar{x}'	$+2S/\bar{x}$	\bar{x}'	$+2S/\bar{x}$
(1,1)	1.0504	0.3653	0.7667	0.4015	0.9445	0.1742
(1,2)	1.0301	0.6017	0.6835	0.5487	0.9456	0.5831
(1,3)	1.0211	0.4742	0.7882	0.2921	0.9373	0.0876
(1,4)	0.9955	0.6291	0.8774	0.2653	0.9817	0.1781
(1,5)	0.9582	0.4141	0.8936	0.1443	1.0392	0.1188
(1,6)	0.9774	0.3896	1.0059	0.3799	1.0153	0.1100
(1,7)	1.0198	0.5786	0.9974	0.3185	0.9453	0.1918
(1,8)	1.0513	0.3384	0.9011	0.2986	0.9110	0.1614
(2,1)	0.9963	0.5344	0.9318	0.3066	0.9348	0.1268
(2,2)	1.0552	0.5228	0.8606	0.2911	1.0093	0.0823
(2,3)	1.0675	0.4011	0.7874	0.2429	1.0230	0.1944
(2,4)	1.0346	0.5510	1.1605	0.1609	1.0674	0.1303
(2,5)	0.9668	0.8500	1.0904	0.3371	1.0754	0.1305
(2,6)	1.0029	0.1992	1.0861	0.3109	1.0157	0.0706
(2,7)	1.0331	0.3630	1.0117	0.2344	0.9518	0.1916
(2,8)	1.0291	0.4820	0.9047	0.5848	0.9309	0.7890
(3,1)	0.9653	0.5041	1.0032	0.2308	0.9547	0.1046
(3,2)	1.0807	0.8697	1.0365	0.1828	1.0227	0.0705
(3,3)	1.0616	0.7389	1.0665	0.3843	1.0897	0.1893
(3,4)	1.0412	1.1043	1.0683	0.3734	1.0983	0.1103
(3,5)	0.9529	0.4440	1.2008	0.2783	1.0554	0.0719
(3,6)	1.0016	0.3447	1.0445	0.2610	1.0137	0.1943
(3,7)	1.0040	0.3287	1.0091	0.2494	0.9612	0.1453
(3,8)	1.0125	0.9616	0.9149	0.1906	0.9485	0.1283
(4,1)	0.9482	0.1616	0.9840	0.2536	0.9671	0.0864
(4,2)	1.0363	0.6172	1.0854	0.1442	1.0293	0.1942
(4,3)	1.0453	0.8280	1.1457	0.4344	1.0994	0.1695
(4,4)	0.9930	0.6942	1.0725	0.0470	1.0918	0.1242
(4,5)	0.9428	0.7908	1.1570	0.2928	1.0598	0.0649
(4,6)	0.9964	0.2564	1.0435	0.2421	1.0073	0.1710
(4,7)	1.0045	0.2731	1.0219	0.2075	0.9613	0.3009
(4,8)	0.9903	0.6873	0.9286	0.1428	0.9423	0.0976
(5,1)	0.9270	0.2689	1.0070	0.1437	0.9644	0.0684
(5,2)	0.9773	0.2319	1.0915	0.3352	0.9799	0.0464
(5,3)	1.0187	0.6891	1.0998	0.3344	1.0673	0.1771
(5,4)	0.9396	0.1914	1.1502	0.2617	1.0502	0.1211
(5,5)	0.9093	1.0177	1.1318	0.2914	1.0298	0.1700
(5,6)	0.9621	0.7102	1.0785	0.1486	0.9876	0.1495
(5,7)	0.9472	0.3062	0.9722	0.0530	0.9615	0.0930
(5,8)	0.9527	0.3950	0.9397	0.0642	0.9291	0.0756
Ave		0.5277		0.2666		0.1611

Table 20. (Continued)

		FJ72.067		WT603.4		FJ14.148	
Probe		\bar{x}'	$+2S/\bar{x}$	\bar{x}'	$+2S/\bar{x}$	\bar{x}'	$+2S/\bar{x}$
Analog	K theta	0.5129	4.5358	0.2934	1.7358	0.7284	0.5326
	K ra2	0.3360	12.5506	0.3133	2.7098	0.5036	1.8508
	Ka2	0.1440	8.4508	0.1124	1.6169	0.1944	1.1297
Digital	K theta	0.5340	6.0640	0.2979	6.2757	0.7304	0.6127
	K ra2	0.3357	21.3682	0.3536	3.6851	0.6089	2.4424
	Ka2	0.1466	9.2543	0.1224	2.3987	0.2156	1.3392

		WT563.4		FJ59.022		WT1170.1	
Probe		\bar{x}'	$+2S/\bar{x}$	\bar{x}'	$+2S/\bar{x}$	\bar{x}'	$+2S/\bar{x}$
Analog	K theta	0.4718	0.8846	2.4286	0.7641	1.4740	0.1295
	K ra2	0.6130	3.4773	2.9335	0.3971	1.1162	0.7545
	Ka2	0.1829	2.2946	3.7600	0.3908	1.4756	0.6236
Digital	K theta	0.4822	1.0804	2.5847	0.7899	1.4618	0.9036
	K ra2	0.6706	2.1911	3.0460	0.4250	1.1696	0.7992
	Ka2	0.1956	1.5150	3.9141	0.4250	1.5364	0.7015

Results were excellent. Excluding FJ72.067, probe precision indices ($\pm 2S/\bar{x}$) were well below 1 %. The precision indices of K_{a2} , K_θ and K_{ra2} were generally less than 3 %. Even though noise was present in the FJ72.067 results, probe precision indices were quite good (< 4 %) for the noise levels seen.

Digital K_{a2} , K_θ and K_{ra2} precision indices from WT603.4 exceeded 2.3 %. This may be due to the low face average RMS turbulence level (1.31 %). Part of the acceptance process applied to the two data sets established 1 % face average RMS turbulence level as a lower bound on data that could be screened accurately on the DYNADEC system. Probe signals with lower RMS turbulence levels may blend with the DYNADEC system noise levels of the same energy content and produce errant data. The 1.31 % RMS turbulence level may have approached this limit and some greater amount of scatter was to be expected.

Concerns raised in the second level of analysis were re-addressed at this point. After the outliers were eliminated, the magnitude shift from analog K_{a2} , K_θ and K_{ra2} values to digital values remained. Digital magnitudes generally remained higher than analog magnitudes as seen Tables 21 through 23.

Table 21.
K_θ Analog and Digital Magnitude Comparison,
Outliers Eliminated

	FJ	WT	FJ	WT	FJ	WT
RMS %	72.067	603.4	14.148	563.4	59.022	1170.1
Turbulence	1.62	1.31	3.02	3.35	4.85	5.35
Analog K _θ	0.5129	0.2934	0.7284	0.4718	2.4286	1.4740
Digital K _θ	0.5340	0.2979	0.7304	0.4822	2.5847	1.4618
Δ (D-A)	-0.0211	-0.0045	-0.002	-0.0104	-0.1561	0.0122
<u>Δ (D-A)</u> <u>Digital</u>	3.951	1.511	0.274	2.157	6.039	0.835

Table 22.
K_{ra2} Analog and Digital Magnitude Comparison,
Outliers Eliminated

	FJ	WT	FJ	WT	FJ	WT
RMS %	72.067	603.4	14.148	563.4	59.022	1170.1
Turbulence	1.62	1.31	3.02	3.35	4.85	5.35
Analog K _{ra2}	0.3360	0.3133	0.5036	0.6130	2.9335	1.1162
Digital K _{ra2}	0.3357	0.3536	0.6089	0.6706	3.0460	1.1696
Δ (D-A)	0.0003	-0.0403	-0.1053	-0.0576	-0.1125	0.0534
<u>Δ (D-A)</u> <u>Digital</u>	0.089	11.397	17.293	8.589	3.693	4.566

Table 23.
K_{a2} Analog and Digital Magnitude Comparison,
Outliers Eliminated

	FJ	WT	FJ	WT	FJ	WT
	72.067	603.4	14.148	563.4	59.022	1170.1
RMS %	1.62	1.31	3.02	3.35	4.85	5.35
Turbulence						
Analog K _{a2}	0.1440	0.1124	0.1944	0.1829	3.76	1.4756
Digital K _{a2}	0.1466	0.1224	0.2156	0.1956	3.9141	1.5364
$\Delta(D-A)$	-0.0026	-0.01	-0.0212	-0.0127	-0.1541	-0.0608
$\frac{\Delta(D-A)}{\text{Digital}}$	1.774	8.170	9.833	6.493	3.937	3.957

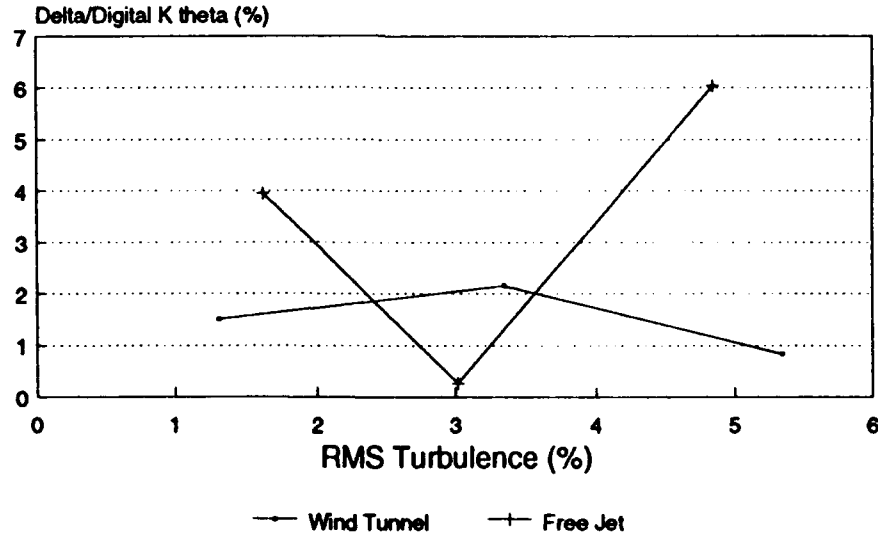


Figure 51. K_θ Digital-Analog Difference Vs. RMS
Turbulence Level, Outliers Eliminated

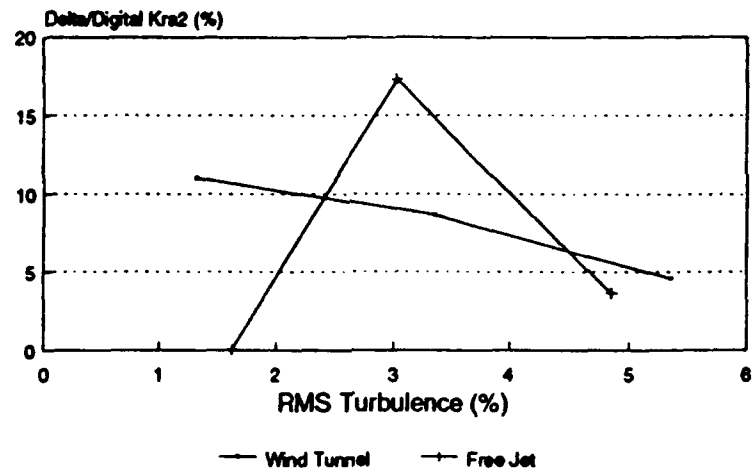


Figure 52. Kra2 Digital-Analog Difference Vs. RMS Turbulence Level, Outliers Eliminated

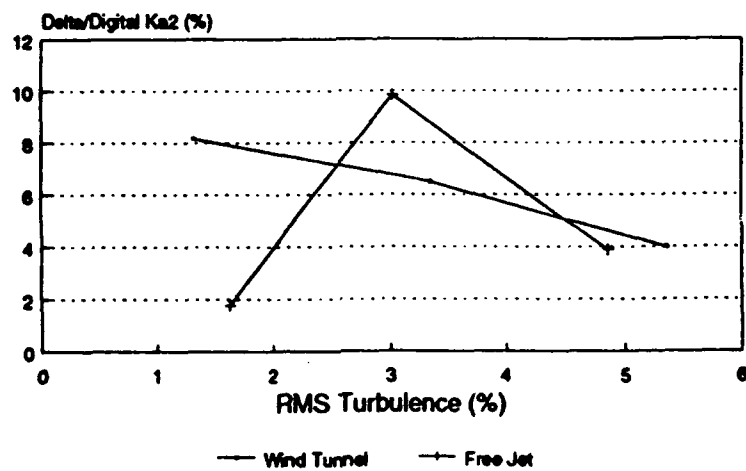


Figure 53. Ka2 Digital-Analog Difference Vs. RMS Turbulence Level, Outliers Eliminated

The differences between the analog and digital readings as a percentage of the digital readings decreased after the outliers were eliminated, but only by a very small amount. Trends remained the same. Figures 51-53 show the wind tunnel analog-digital differences continued to decrease with increasing RMS turbulence level and freejet data continued to exhibit no conclusive trend. Based on these results, it would be beneficial to analyze more wind tunnel and freejet points in a similar manner, at various RMS turbulence levels to confirm the trend seen in the wind tunnel data.

Observations on the remaining faulty probe distributions could also be made at this point. Distributions of FJ72.067 faulty probes did not exhibit the bi-polar noise characteristics of the working probes, as shown in Figure 54.

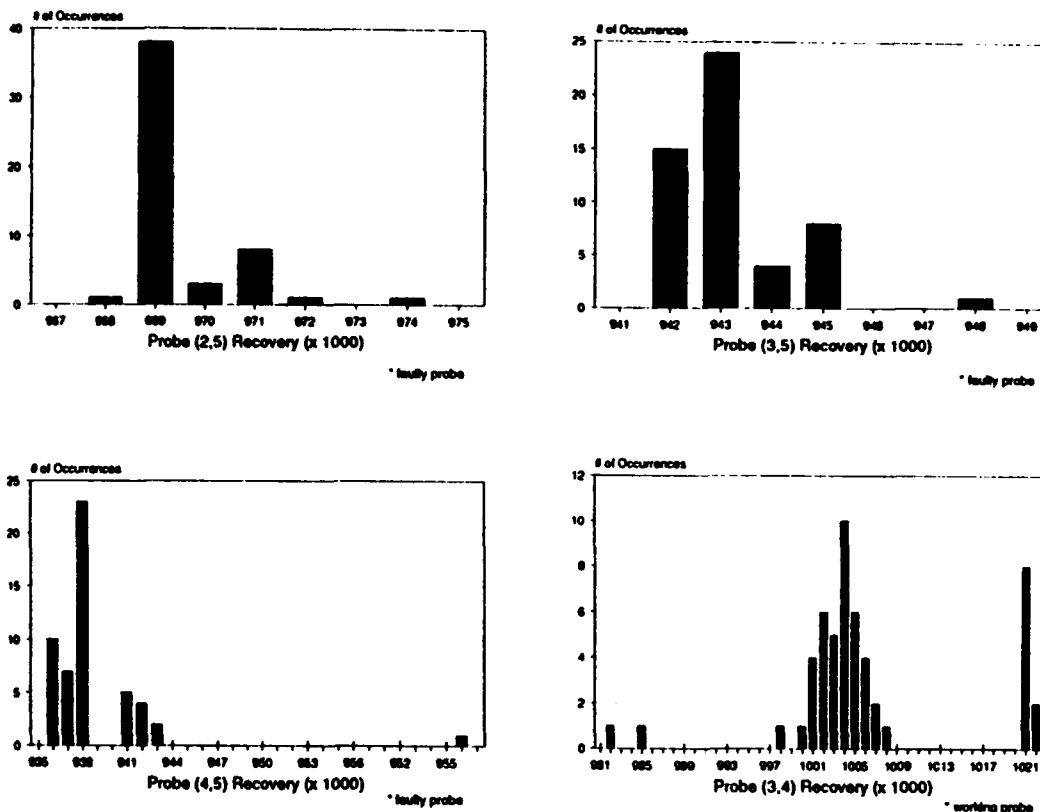


Figure 54. FJ72.067 Faulty Probe Distributions

It was thought that this case would test the ability of the system to zero out the dynamic signal due to the noise involved. Fortunately, the DYNADEC system performed well in this case. These results seemed to indicate that noise on the other probes was not in the DYNADEC system, but could be a characteristic of the peak selected or tape noise.

Distributions on the three remaining test points with faulty probes can be seen in Figures 55. through 57.

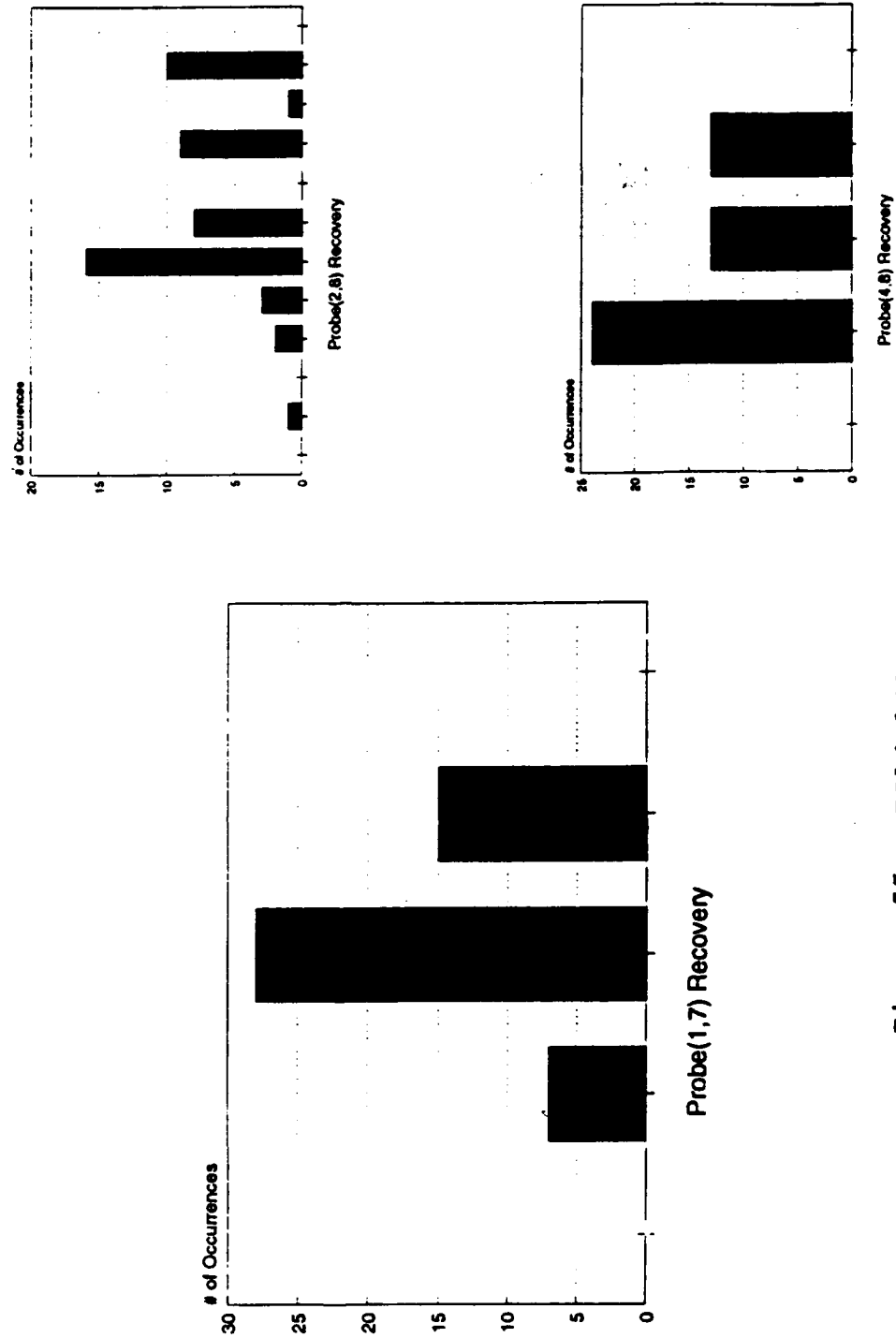


Figure 55. FJ14.148 Faulty Probe Distributions

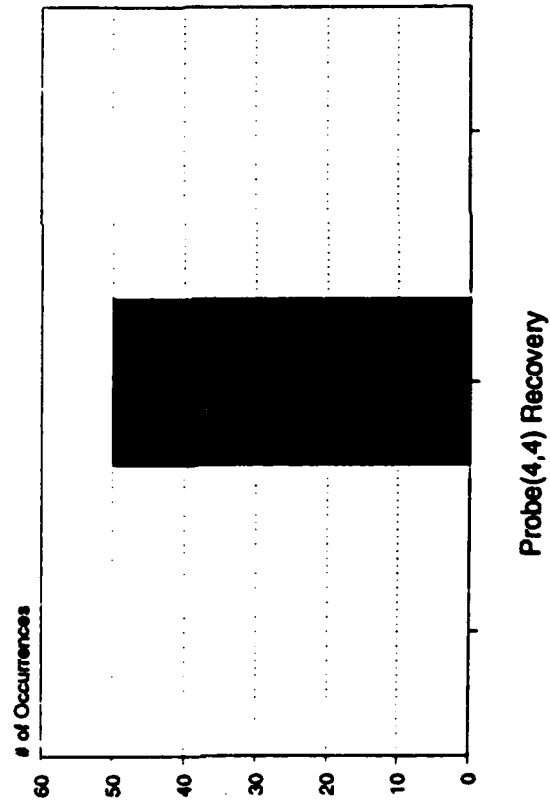
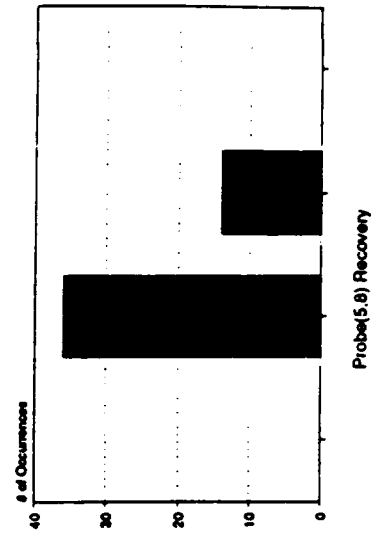
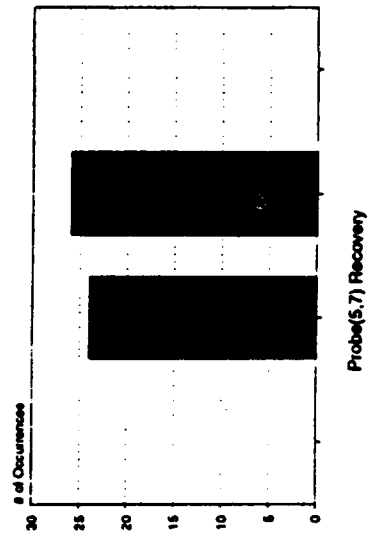
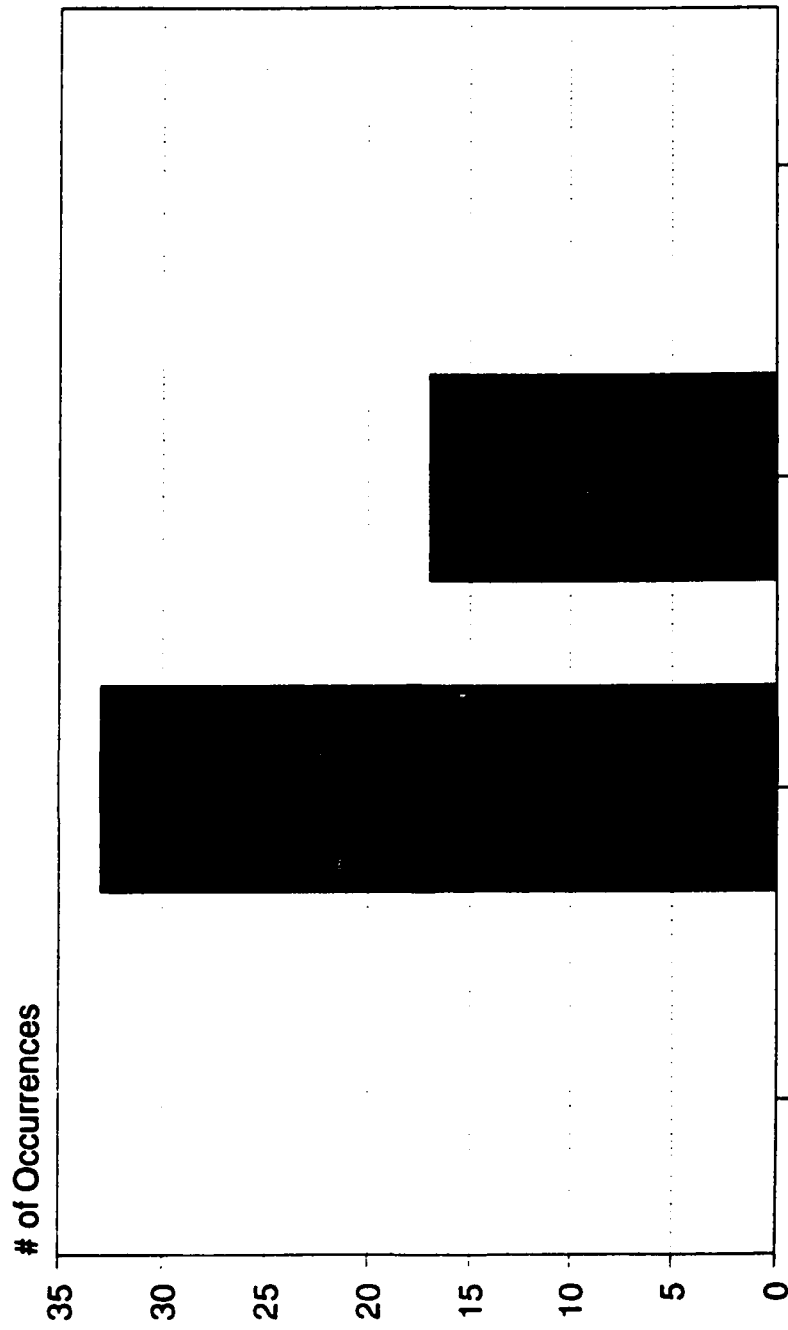


Figure 56. FJ59.022 Faulty Probe Distributions



Probe(5,2) Recovery

Figure 57. WT1170.1 Faulty Probe Distributions

Results were well within acceptable levels. Probe (2,8) from FJ14.148 exhibited some scatter, but this was probably not due to a problem in "zeroing" out the dynamic signal for this test point. Distributions on probe (2,8) from the other five cases show that this probe has more scatter than the adjacent probes. This characteristic appears in its precision indices, as well, as shown in Table 24.

Table 24.
Probe (2,8) Precision Indices

Test Point	Precision Index (%)
FJ72.067	1.00956
WT603.4	2.339063
FJ14.148	0.513871
WT563.4	0.464335
FJ59.022	0.788979
WT1170.1	0.527298

These magnitudes were higher than the adjacent probes, but were still fairly small.

The last item of concern left from the second level of analysis was the shapes of the distributions. After distributions on all of the probes were completed, it became apparent that data scatter decreased as face average RMS turbulence level increased (Figure 58.).

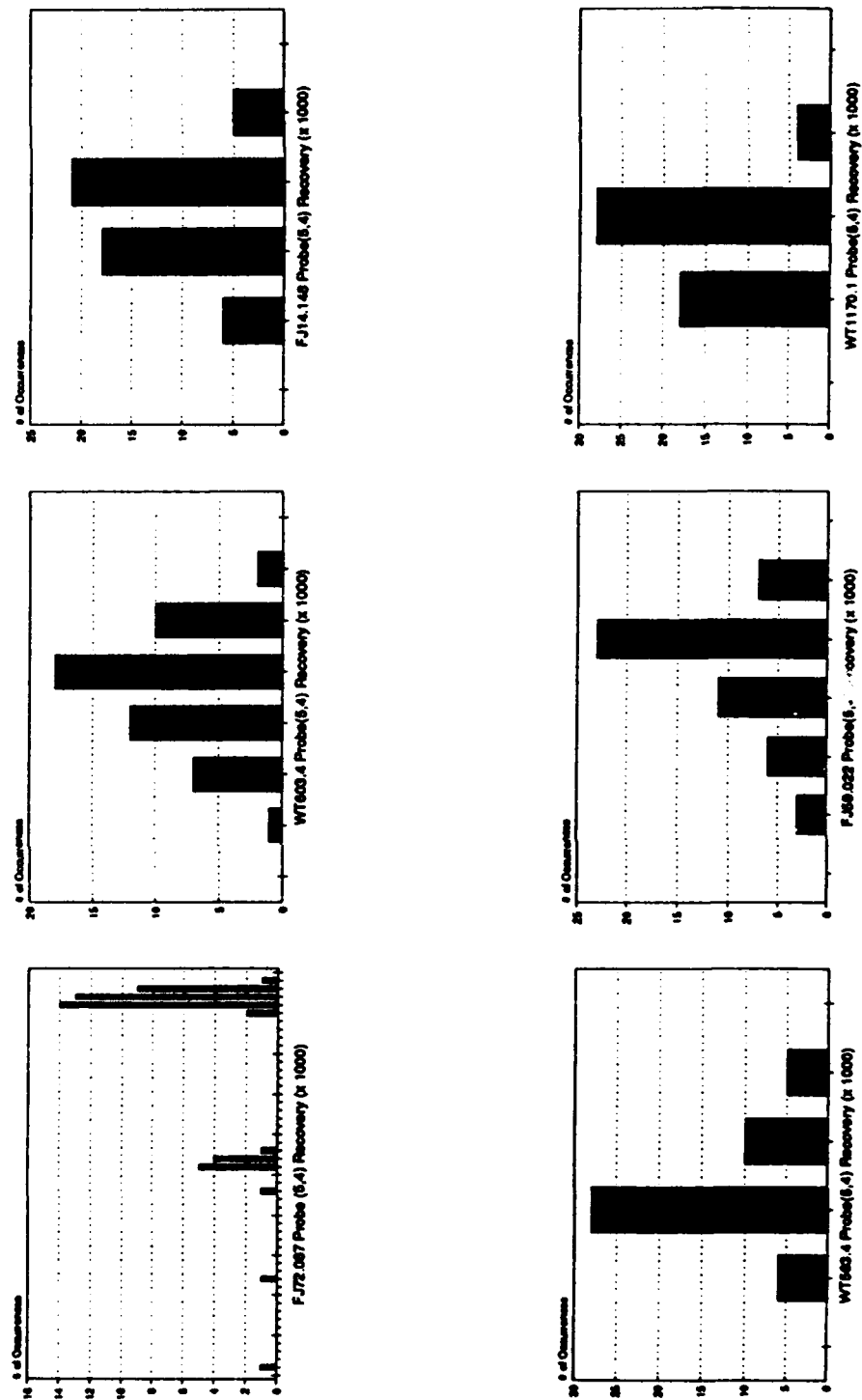


Figure 58. Probe (5,4) Distributions from Six Test Cases

This supported the idea that the DYNADEC system was more precise at higher RMS turbulence levels ($> 3 \%$) where peak amplitudes are considerably higher than any noise present.

The random nature of inlet dynamic data lead to the application of the random number statistical analysis performed on the data to this point. The Sedlock distortion prediction program was used at this point to ensure that the six cases selected were random in nature. If the Sedlock program, with its random number prediction technique produced, a peak dynamic pattern similar to a peak dynamic pattern consisting of the means (\bar{x}) of the 40 probes, the data exhibited random number tendencies and the analysis done to this point was valid. It was already known that FJ72.067 was exhibiting non-random (bi-polar) characteristics, but Sedlock program analysis was performed on this case to see how much the noise affected the peak pattern. The Sedlock program inputs are listed in Table 25.

Table 25.
Sedlock Program Inputs

- 40 steady state total pressure recoveries
- q/P_{t2} , dynamic pressure head (for K_{a2} computation)
- P_{t2} , the engine face average total pressure
- scaling factors as a function of airflow (for K_{a2} computation)
- rate (at least 4 times cutoff frequency of 1000 Hz)

This information was required on each of the six test points to run the Sedlock program.

The program was run interactively. Initial runs simulated a 1/2 second time slice at the test cutoff frequency of 1000 Hz. Faulty probe RMS levels were computed by weight-averaging adjacent probes based upon their distances. Butterworth filters were turned off because the analysis in Reference 16. showed that the filters did not improve results significantly. The map averaging technique was retained because Reference 16 results indicated that visible improvements in pattern matches were possible. Six peak dynamic maps were averaged to make the "Sedlock predicted" dynamic pattern. This meant six different sets of random numbers were generated for each run.

As discussed in Chapter 2, the proper number of samples required to produce a sufficiently accurate normal distribution of random numbers and synthesize an accurate peak dynamic pattern from the Sedlock program was unknown. Each test point used the same set of random numbers by inputting identical "seeds" into the random number generator. As the sample times increased from 1/2 second to 4 seconds, the random number generator would occasionally generate 0 as a random number. This produced a "divide by zero" error and was corrected by changing the seed input.

Initial runs simulated a 1/2 second time slice using 4050 samples. The number, 4050, came from a recommendation in Reference 15 that stated that the number of samples should be at least 8 times the cutoff frequency per second of data

to properly capture a sinusoidal wave form. Thus, a 1/2 second run generated 4050 random numbers at each of the 40 probes, six times for each of the six dynamic patterns. The six patterns were then averaged to make the "Sedlock predicted" peak dynamic pattern. The analysis was halted at 4 second time slices when run times (2 1/2 hours per run) became prohibitive and the program results seemed to "converge" to a distinct peak pattern for each of the six cases.

"Convergence" was defined as a combination of how the 40 probe recoveries fluctuated from run to run and how much the overall pattern changed from run to run as run times increased. The parameter used to compare fluctuations was the average of the 40 probe differences between the current run and the previous run (usually with a 1 second shorter run time):

$$\Delta = \frac{\sum_{i=1}^{40} \text{abs} \left[\frac{P_{t2}}{P_{to}} \right)_{i \text{ current run}} - \frac{P_{t2}}{P_{to}} \right)_{i \text{ run time 1 sec shorter}}}{40} \quad (26)$$

This parameter was tracked noting RMS turbulence level and run times. Results can be seen in Figure 59.

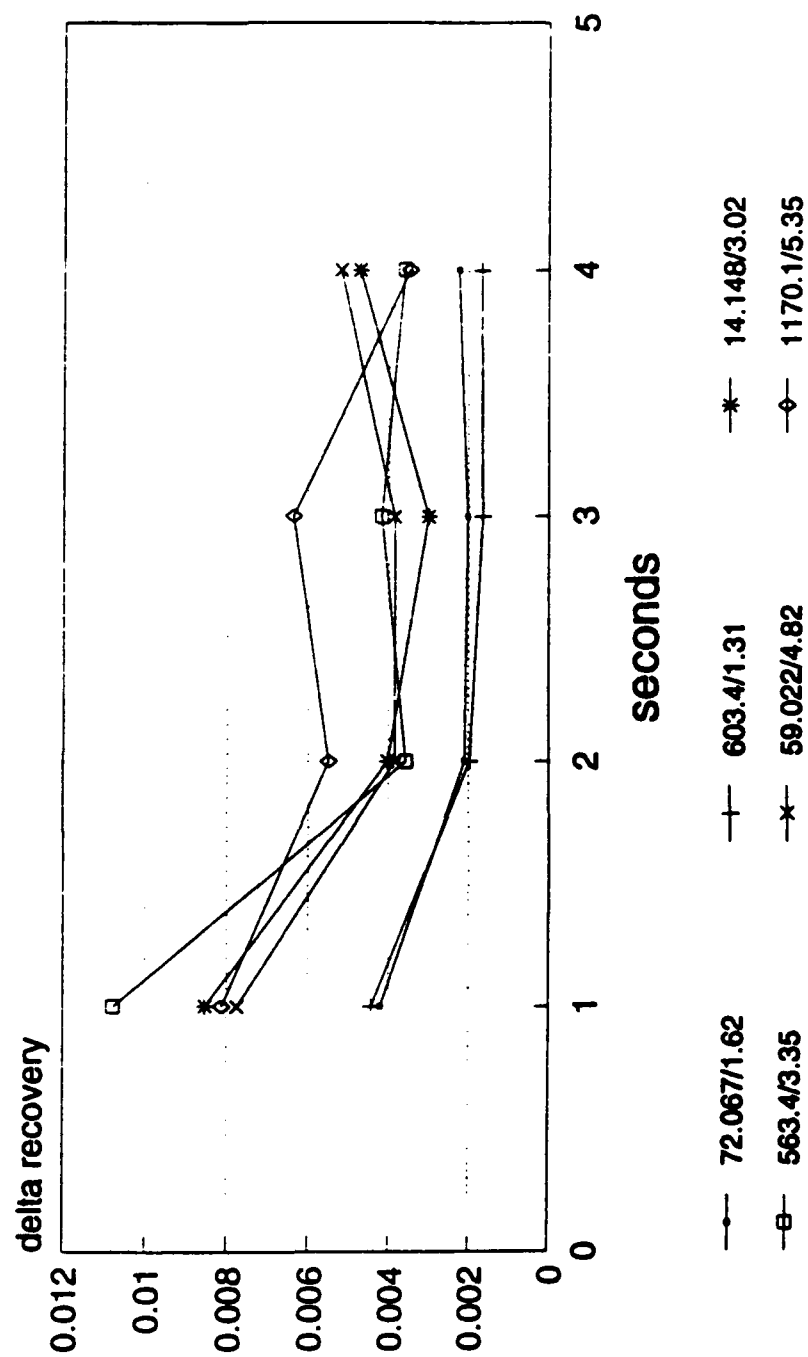


Figure 59. Sedlock Program Delta Recovery Vs. Run Time

After 1 to 2 seconds of run time for all six cases, changes in probe peak dynamic level were small. It was thought that the high RMS turbulence test points would take longer to "converge" due to the high individual probe RMS levels. The higher turbulence test points did produce higher magnitude Δ 's at 1 second, but seemed to converge just as quickly as the low turbulence runs. A possible sinusoidal characteristic was seen in the high turbulence runs (Figure 59.) implying some type of instability of the random number statistical model in the program. This is not surprising considering that peak dynamic patterns of high turbulence cases have some non-random phenomenon (shed vortices, etc.) driving the flow. More analysis could be done in the future in this area involving longer run times; however, the trade-off between the increasing run times and the amount of information gained should be weighed before further analysis is initiated.

Peak maps from all of the cases were compared to overall pattern changes with simulated time slices. These can be seen in Figures 60. through 71.

Freejet Point 72.067
Sedlock Predicted
4050 Samples

Freejet Point 72.067
Sedlock Predicted
8050 Samples

Level Recovery, $\frac{P_{t2}}{P_{t0}}$
F High
E
D
C
B
A

$\Delta = .009$ (.9%)

1 Low

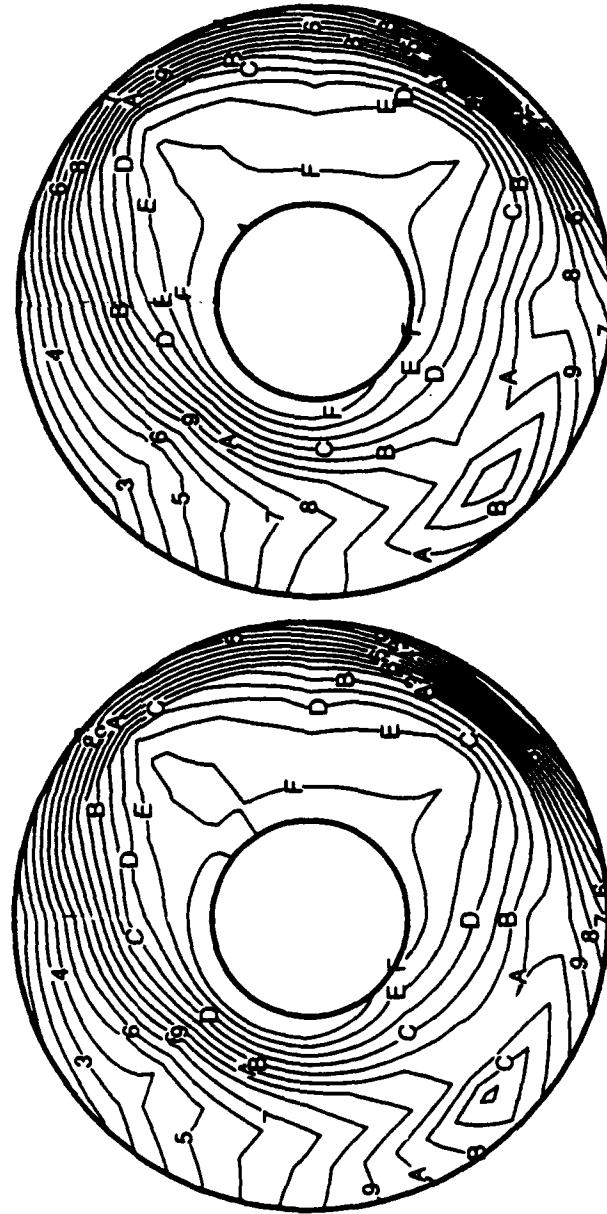


Figure 60. FJ72.067 Sedlock Predicted
Peak Distortion Pattern Evolution
with Number of Samples, 4050 & 8050
Samples

Freejet Point 72.067
Sedlock Predicted
16100 Samples

Freejet Point 72.067
Sedlock Predicted
24150 Samples

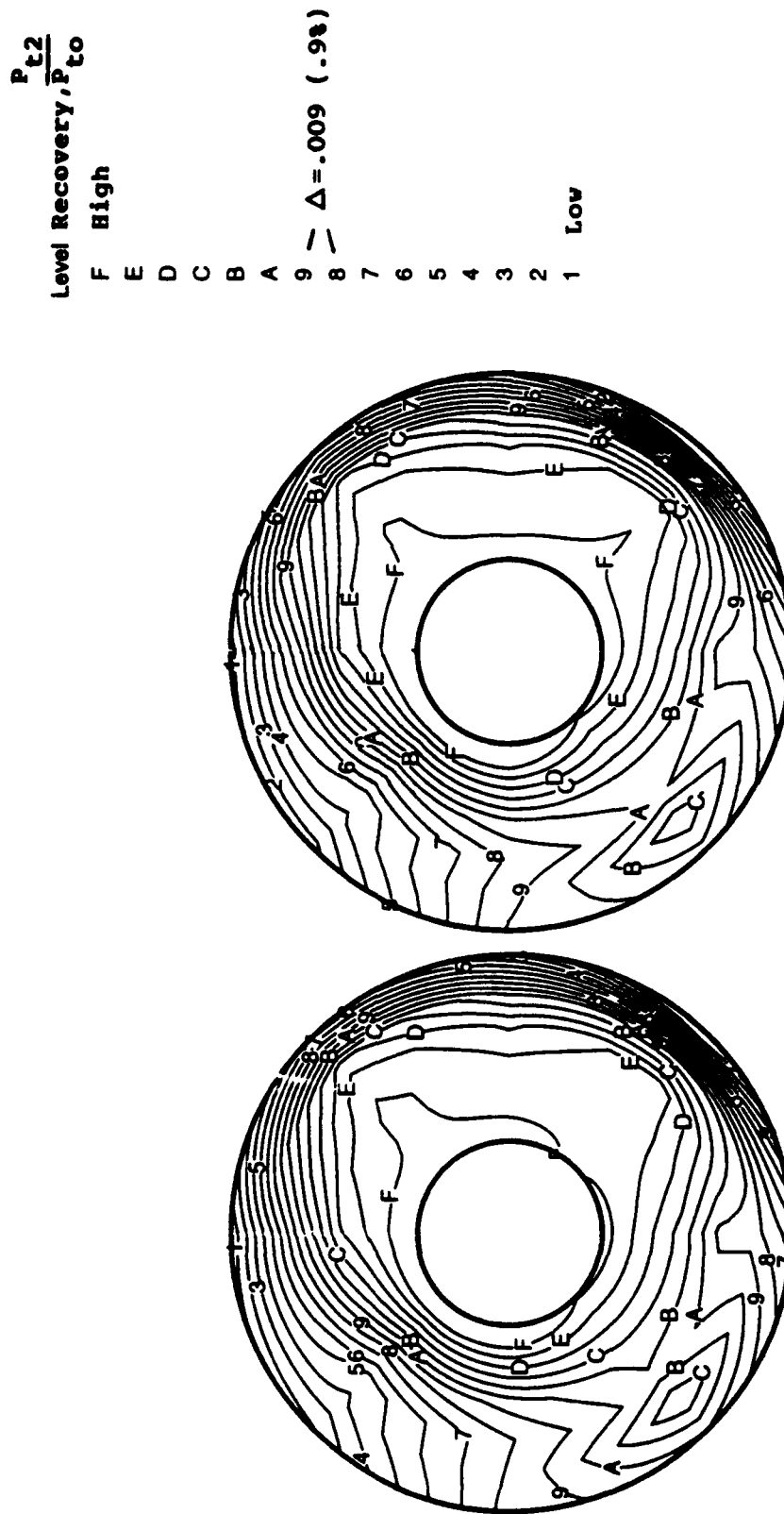


Figure 61. FJ72.067 Sedlock Predicted
Peak Distortion Pattern Evolution
with Number of Samples, 16100 & 24150
Samples

Wind Tunnel Run 603.4
Sedlock Predicted
4050 Samples

Wind Tunnel Run 603.4
Sedlock Predicted
8050 Samples

Level Recovery, $\frac{P_{t2}}{P_{t0}}$

F High

E

D

C

B

A

9

8

7

6

5

4

3

2

1 Low

$\Delta = .009 \text{ (}.9\%)$

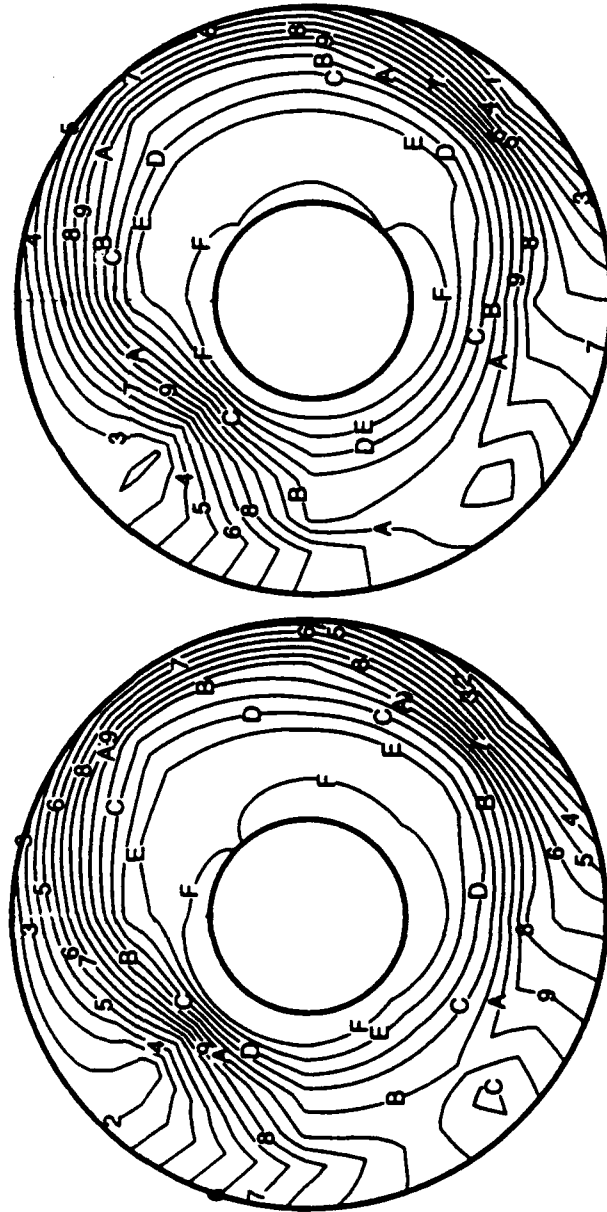


Figure 62. WT603.4 Sedlock Predicted Peak Distortion Pattern Evolution with Number of Samples, 4050 & 8050 Samples

Wind Tunnel Run 603.4
Sedlock Predicted
16100 Samples

Wind Tunnel Run 603.4
Sedlock Predicted
24150 Samples

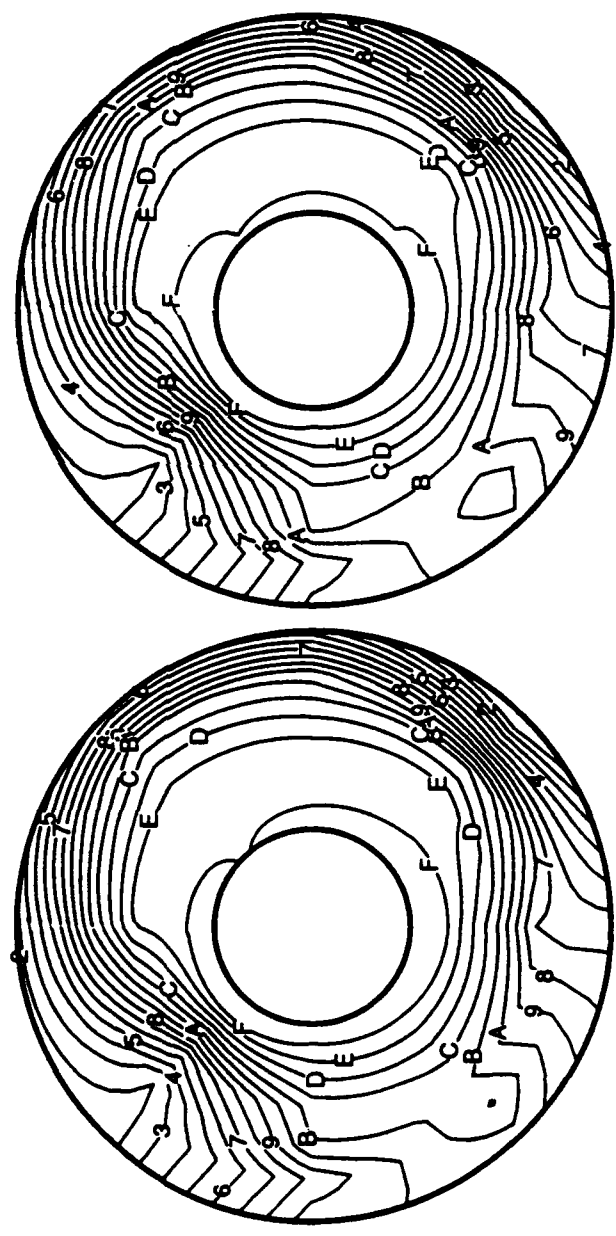
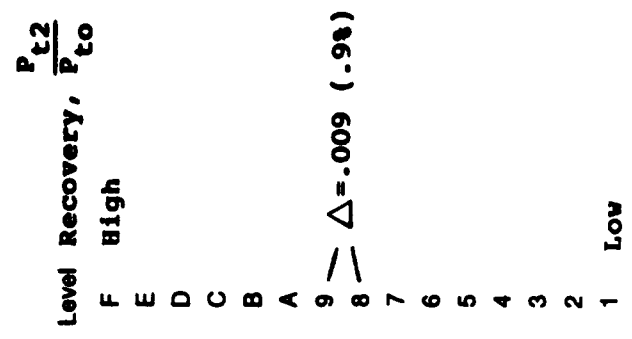


Figure 63. WT603.4 Sedlock Predicted Peak Distortion Pattern Evolution with Number of Samples, 16100 & 24150 Samples

Freejet Point 14.148
Sedlock Predicted
4050 Samples

Freejet Point 14.148
Sedlock Predicted
8050 Samples

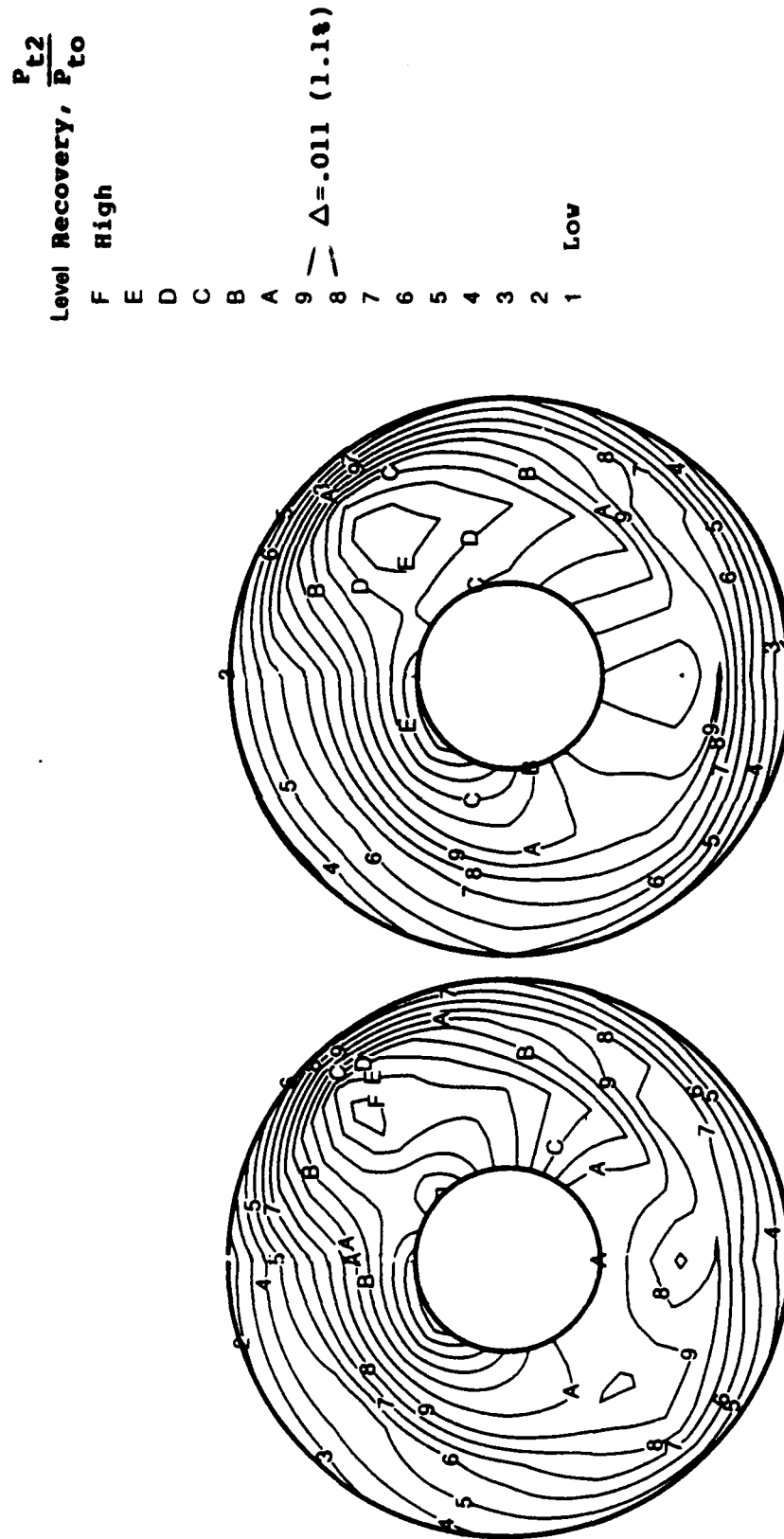


Figure 64. FJ14.148 Sedlock Predicted Peak Distortion Pattern Evolution with Number of Samples, 4050 & 8050 Samples

Freejet Point 14.148
Sedlock Predicted
16100 Samples

Freejet Point 14.148
Sedlock Predicted
24150 Samples

Level Recovery, $\frac{P_{t2}}{P_{t0}}$
F High
E
D
C
B
A
9
8
7
6
5
4
3
2
1 Low
 $\Delta = .011 (1.1\%)$

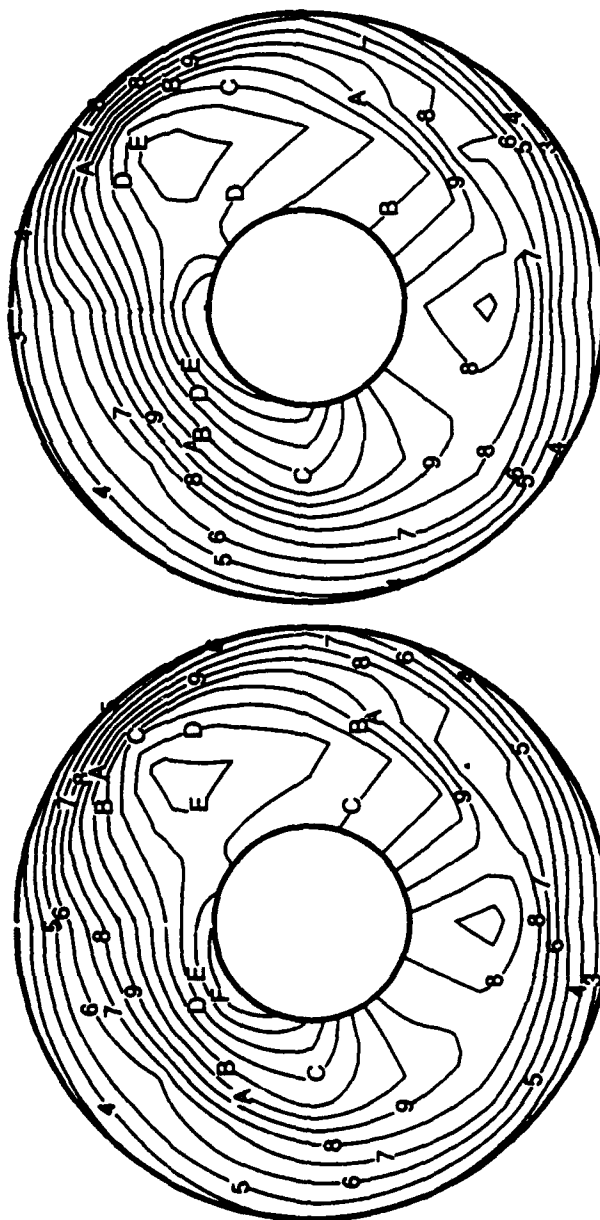


Figure 65. FJ14.148 Sedlock Predicted Peak Distortion Pattern Evolution with Number of Samples, 16100 & 24150 Samples

Wind Tunnel Run 563.4
Sedlock Predicted
4050 Samples

Wind Tunnel Run 563.4
Sedlock Predicted
8050 Samples

Level Recovery, $\frac{P_{t2}}{P_{t0}}$

F High

E

D

C

B

A

9

8

7

6

5

4

3

2

1 Low

$\Delta = .011 (1.1\%)$

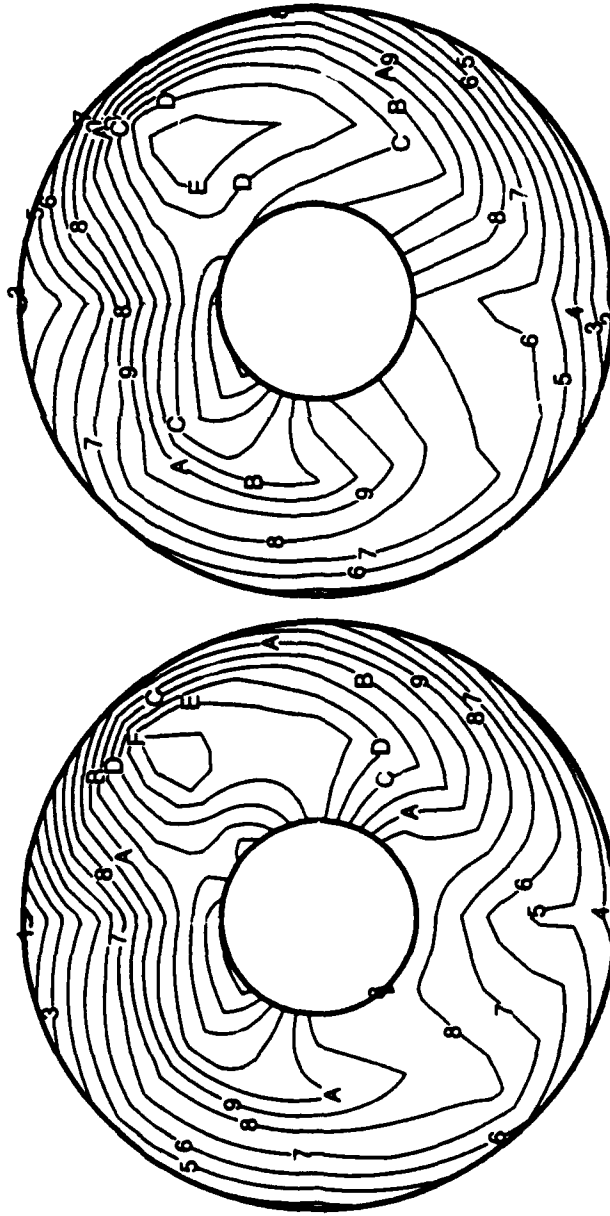


Figure 66. WT563.4 Sedlock Predicted Peak Distortion Pattern Evolution with Number of Samples, 4050 & 8050 Samples

Wind Tunnel Run 563.4
Sedlock Predicted
16100 Samples

Wind Tunnel Run 563.4
Sedlock Predicted
24150 Samples

Level Recovery, $\frac{P_{t2}}{P_{t0}}$

F High

E

D

C

B

A

9

8

7

6

5

4

3

2

1 Low

$\Delta = -0.011 (1.1\%)$

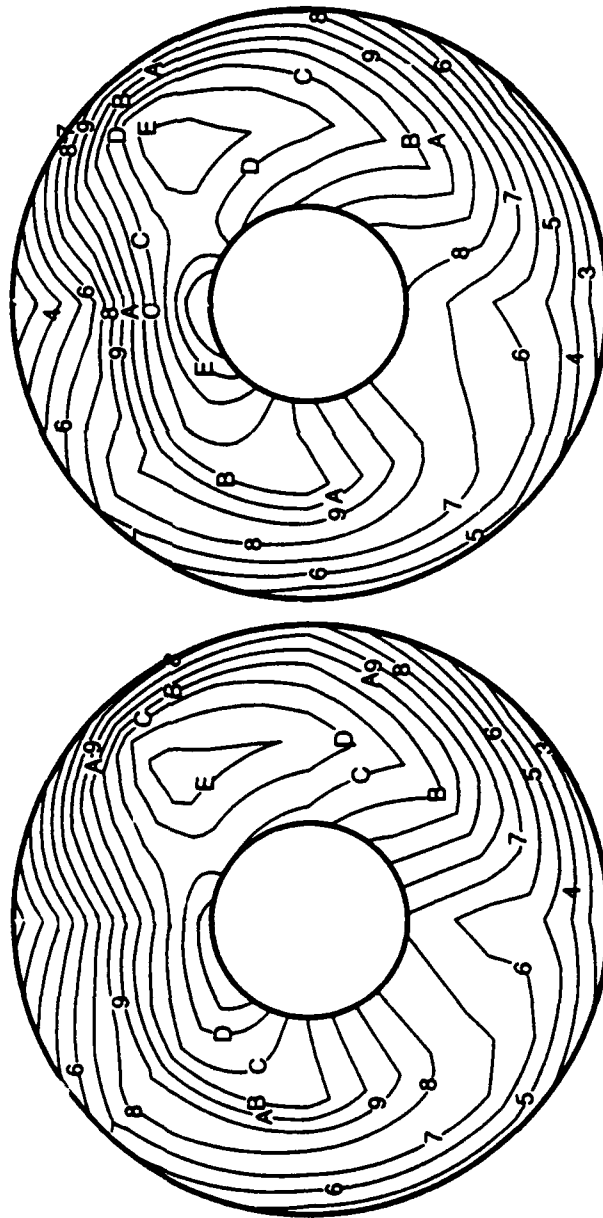


Figure 67. WT563.4 Sedlock Predicted Peak Distortion Pattern Evolution with Number of Samples, 16100 & 24150 Samples

Freejet Point 59.022
Sedlock Predicted
4050 Samples

Freejet Point 59.022
Sedlock Predicted
8050 Samples

$\frac{P_{t2}}{P_{t0}}$
Level Recovery, $\frac{P_{t2}}{P_{t0}}$
F High
E
D
C
B
A
9
8
7
6
5
4
3
2
1 Low
 $\Delta = .011 (1.1\%)$

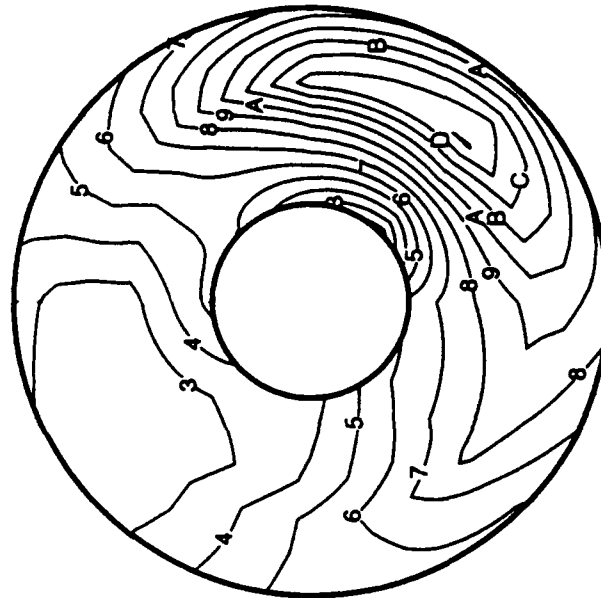


Figure 68. FJ59.022 Sedlock Predicted Peak Distortion Pattern Evolution with Number of Samples, 4050 & 8050 Samples

Freejet Point 59.022
Sedlock Predicted
16100 Samples

Freejet Point 59.022
Sedlock Predicted
24150 Samples

Level Recovery, $\frac{P_{t2}}{P_{t0}}$

F High

E

D

C

B

A

9

8

7

6

5

4

3

2

1 Low

$\Delta = .011 (1.1\%)$

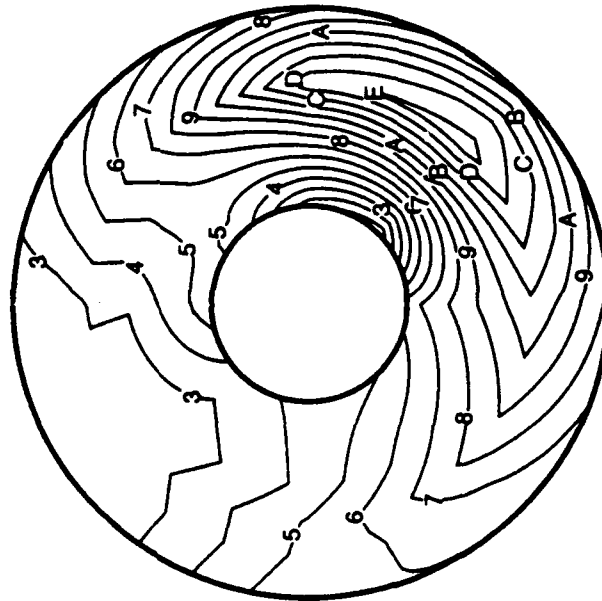


Figure 69. FJ59.022 Sedlock Predicted Peak Distortion Pattern Evolution with Number of Samples, 16100 & 24150 Samples

Wind Tunnel Run 1170.1

Sedlock Predicted
4050 Samples

Wind Tunnel Run 1170.1

Sedlock Predicted
8050 Samples

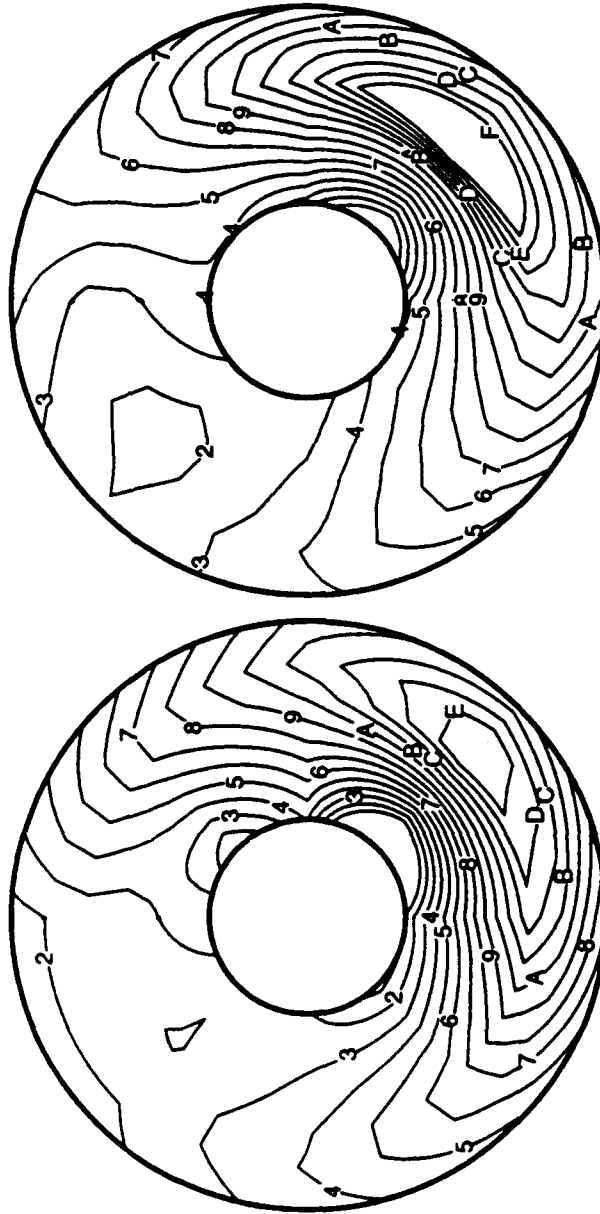
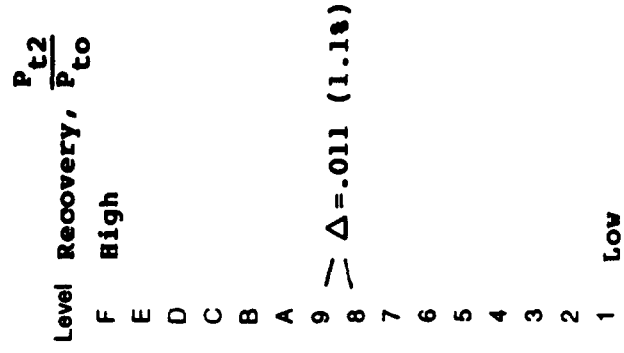


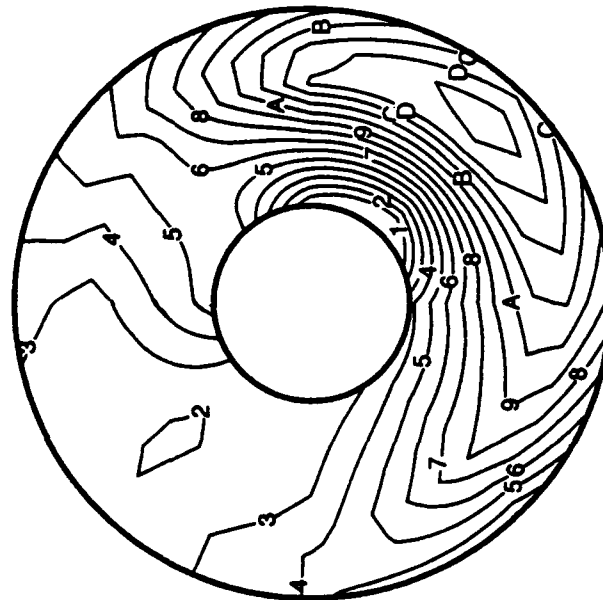
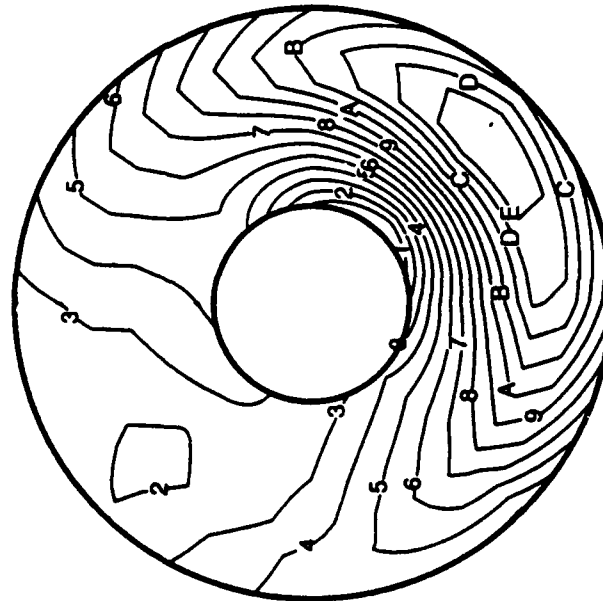
Figure 70. Wt1170.1 Sedlock Predicted
Peak Distortion Pattern Evolution
with Number of Samples, 4050 & 8050
Samples

Wind Tunnel Run 1170.1

Sedlock Predicted
16100 Samples

Wind Tunnel Run 1170.1

Sedlock Predicted
24150 Samples



Level Recovery, $\frac{P_{t2}}{P_{t0}}$

F High

E

D

C

B

A

9

8

7

6

5

4

3

2

1 Low

$\Delta = -.011 (1.1\%)$

Figure 71. Wt1170.1 Sedlock Predicted Peak Distortion Pattern Evolution with Number of Samples, 16100 & 24150 Samples

Table 26 lists the run times, numbers of samples per second and number of random numbers generated for one peak map and the total number of random numbers generated for a six peak average map.

Table 26.
Sedlock Program Run Times Simulated

Run Time	# Samples Per Case	One Map	Total
1/2 second	8050	4050	24300
1	8050	8050	48600
2	8050	16100	96600
3	8050	24150	144900
4	8050	32200	193200

Visible pattern changes occurred with 2 second or smaller run times just as the Δ parameter predicted.

The 4 second run patterns were compared to the means (\bar{x}) of the six DYNADEC runs. Results can be seen in Figures 72. through 77.

Freejet Point 72.067
50 Repeat Runs
Mean Recovery Levels

Freejet Point 72.067
Sedlock Predicted
32200 Samples

Level Recovery, $\frac{P_{t2}}{P_{t0}}$
F High
E
D
C
B
A
9
8
7
6
5
4
3
2
1 Low
 $\Delta = .009 \text{ (0.9\%)}$

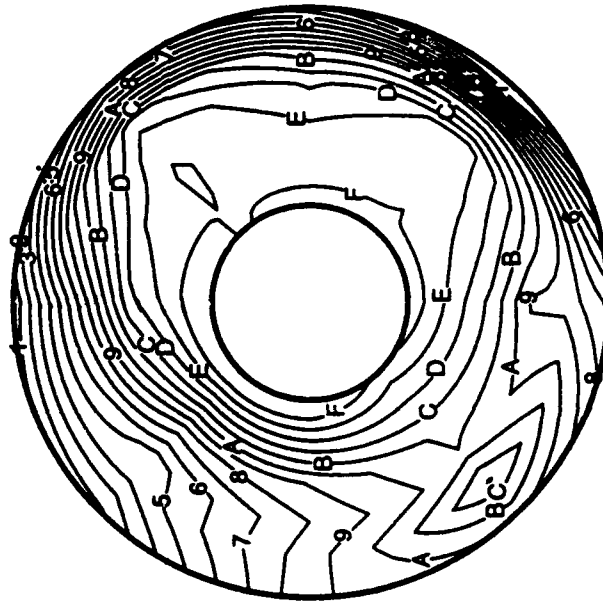
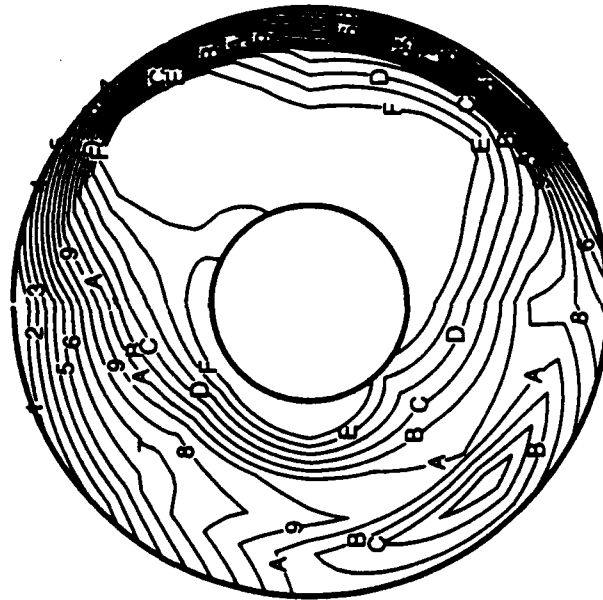


Figure 72. FJ72.067 Sedlock Predicted Peak Distortion Pattern at 4 sec Time Slice Vs. DYNADEC "Mean" Peak Distortion Pattern

Wind Tunnel Run 603.4
50 Repeat Runs
Mean Recovery Levels

Wind Tunnel Run 603.4
Sedlock Predicted
32200 Samples

Level Recovery, $\frac{P_{t2}}{P_{t0}}$

F High

E

D

C

B

A

9

8

7

6

5

4

3

2

1 Low

$\Delta = .009 \text{ (0.9\%)}$

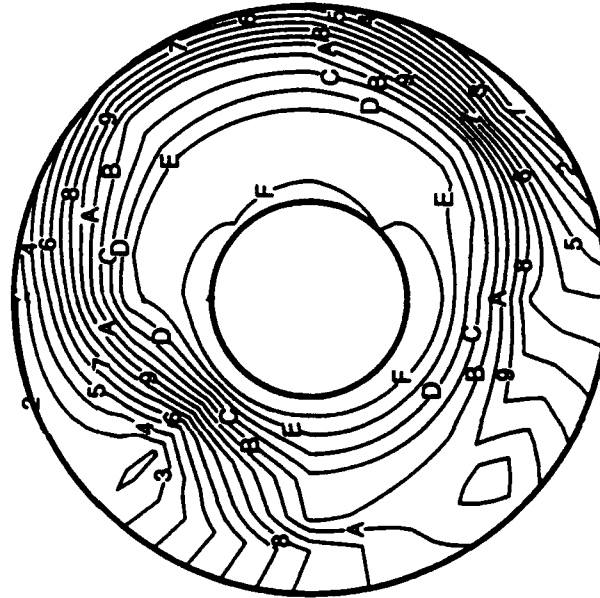


Figure 73. WT603.4 Sedlock Predicted Peak Distortion Pattern at 4 sec Time Slice Vs. DYNADEC "Mean" Peak Distortion Pattern

Freejet Point 14.148
50 Repeat Runs
Mean Recovery Levels

Freejet Point 14.148
Sedlock Predicted
32200 Samples

Level Recovery, $\frac{P_{t2}}{P_{t0}}$
F High
E
D
C
B
A
9
8
7
6
5
4
3
2
1 Low
 $\Delta = .011 (1.1\%)$

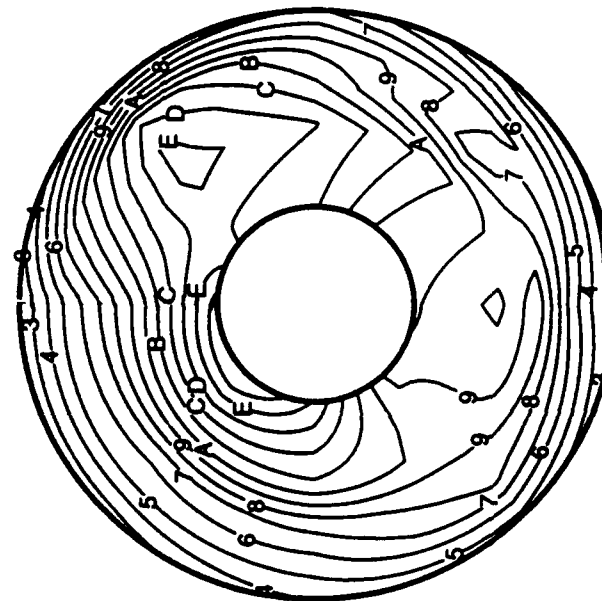


Figure 74. FJ14.148 Sedlock Predicted Peak Distortion Pattern at 4 sec Time Slice Vs. DYNADEC "Mean" Peak Distortion Pattern

Wind Tunnel Run 563.4
50 Repeat Runs
Mean Recovery Level

Wind Tunnel Run 563.4
Sedlock Predicted
32200 Samples

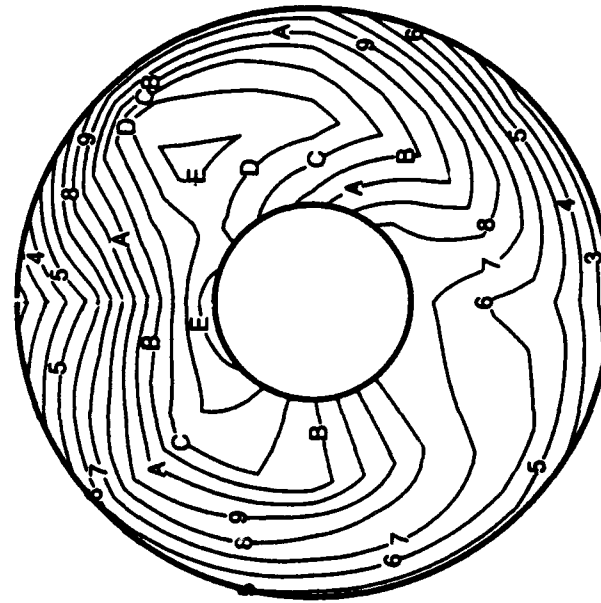
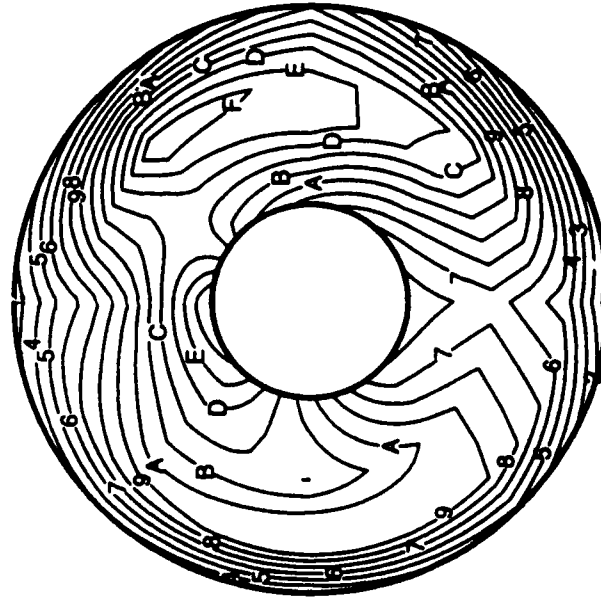
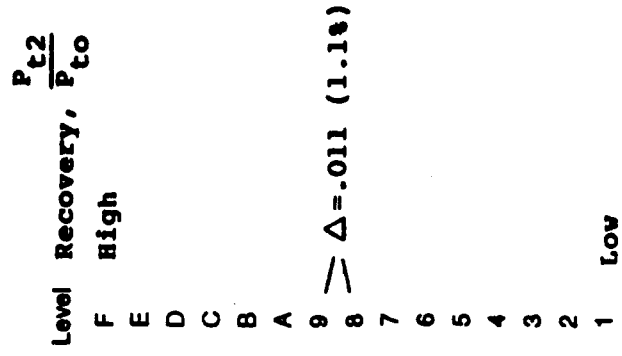


Figure 75. WT563.4 Sedlock Predicted Peak Distortion Pattern at 4 sec Time Slice Vs. DYNADEC "Mean" Peak Distortion Pattern

Freejet Point 59.022
50 Repeat Runs
Mean Recovery Levels

Freejet Point 59.022
Sedlock Predicted
32200 Samples

Level Recovery, $\frac{P_{t2}}{P_{t0}}$
F High
E
D
C
B
A
9
8
7
6
5
4
3
2
1 Low
— $\Delta = .011 (1.1\%)$

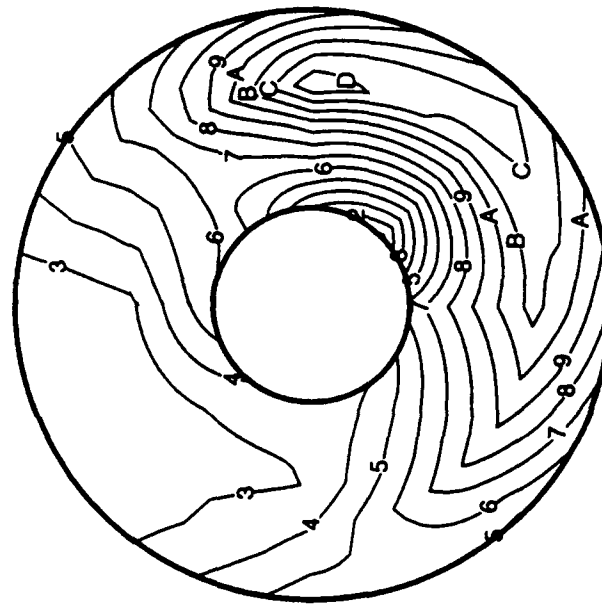
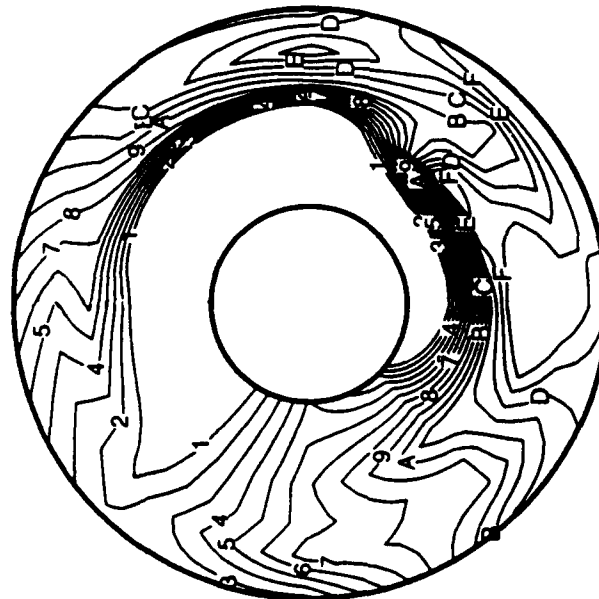


Figure 76. FJ59.022 Sedlock Predicted Peak Distortion Pattern at 4 sec Time Slice Vs. DYNADEC "Mean" Peak Distortion Pattern

Wind Tunnel Run 1170.1
50 Repeat Runs
Mean Recovery Levels

Wind Tunnel Run 1170.1
Sedlock Predicted
32200 Samples

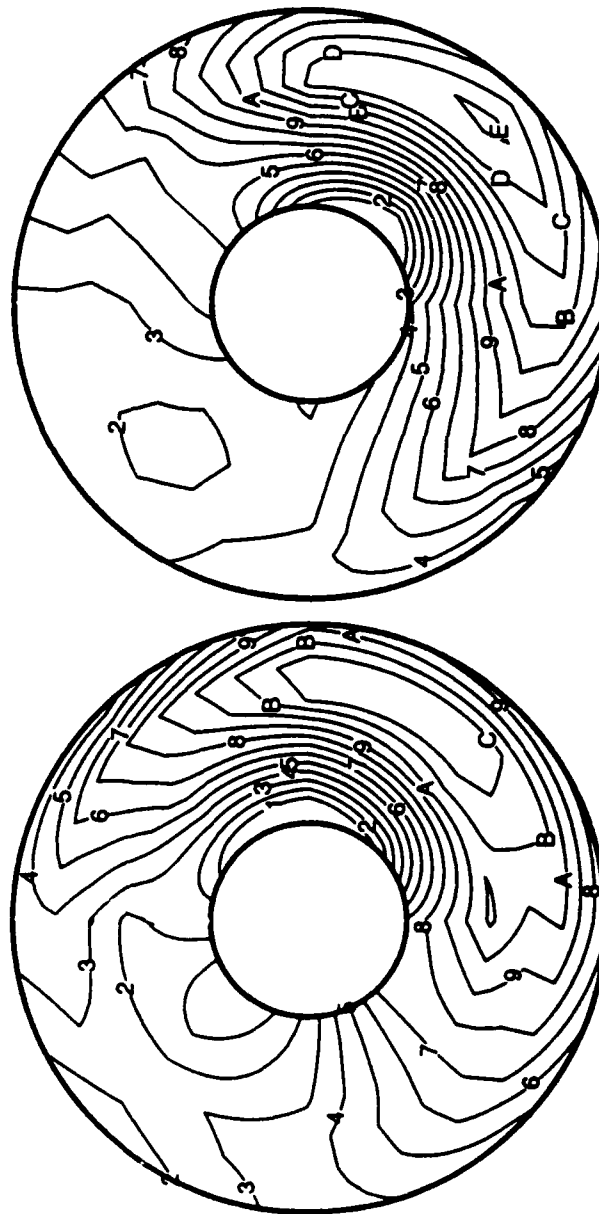
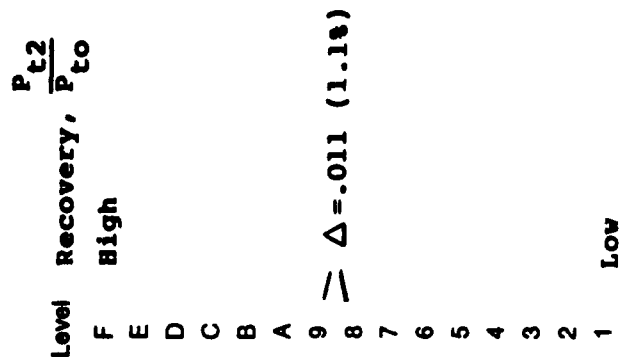


Figure 77. WT1170.1 Sedlock Predicted Peak Distortion Pattern at 4 sec Time Slice Vs. DYNADEC "Mean" Peak Distortion Pattern

Sedlock predicted pattern shapes of FJ72.067, FJ14.1489 and the three wind tunnel points matched DYNADEC "mean" peak distortion pattern shapes very well. The Sedlock predicted pattern of FJ59.022 did not. This indicates a non-random phenomenon is physically driving the flow in the subscale freejet at this condition. This is further substantiated by comparing the FJ59.022 results with the WT1170.1 results. The peak patterns of WT1170.1 and FJ59.022 should match because they simulated identical test conditions. The DYNADEC "mean" peak patterns do not match; however, the Sedlock predicted patterns matched fairly well. This indicates the $M=2.2$, 5.35 % turbulence case in the wind tunnel is producing random (normally distributed) turbulence. The subscale freejet data did not. The pair of points, obviously did not pass the acceptance process. The majority of the supersonic results were similar to this pair. This dissimilarity was what initiated this analysis.

A surprising observation about the Sedlock runs of the six test points was that the FJ72.067 results were so good even with 2 - 3 % noise on some of the probes. This implies that individual probes with bi-polar characteristics of 2 - 3 % can still produce accurate DYNADEC peak patterns. Comparisons of the DYNADEC and Sedlock patterns of FJ72.067 and its corresponding wind tunnel point, WT603.4, produced results that were similar to that of the $M = 2.2$ pair. The

Sedlock patterns of the two points matched more closely than their DYNADEC patterns.

These results, at such a low turbulence level where random number approximation predictions should match well, could lead one to question DYNADEC system performance. However, this conclusion does not take into account the limitations of the prediction method. As already discussed, patterns from high turbulence cases will not necessarily match the patterns synthesized from the random number statistics in the Sedlock program. The Sedlock program also uses only 40 steady state recoveries and the 40 probe RMS turbulence levels averaged over the entire test point pressure data. DYNADEC uses a continuous recording of the 40 individual dynamic probe readings from a test. The third pair of wind tunnel-freejet test points in this analysis, FJ14.148 and WT563.4, also refute this conclusion. Sedlock patterns do not match as well. This point also failed the Freejet Development Program's acceptance process.

This was believed to be the limit of useful information available in the Sedlock-DYNADEC comparison, so the noise from FJ72.067 was addressed at this point. There were three remaining options to investigate before drawing conclusions about this point. First the run schedule was examined case by case (Table 27).

Table 27.
FJ72.067 Run Schedule

Date	Case	Noise/ Outlier	Date	Case	Noise/ Outlier
2/18/92	1		2/24/92	27	
	2	Outlier		28	
	3	Outlier		29	Noise
	4	Outlier		30	
	5			31	
	6			32	Noise
	7			33	Noise
	8			34	Noise
	9	Noise		35	Noise
	10			36	Noise
2/20/92	11		2/28/92	37	Noise
	12			38	
	13			39	Noise
	14			40	
	15			41	
	16			42	
	17			43	
	18			44	
	19			45	
	20			46	
	21			47	
	22			48	
	23			49	Noise
	24			50	
	25			51	
	26			52	

A distinct pattern was found. With the exception of Case 49, all of the runs producing the second "clump" of data in the distributions were from two days; the first day and the third day. This implies that something was wrong with the DYNADEC system on those two days. However, several other cases were run on those two days and did not exhibit noise problems. This indicates that the problem was on the tape or was a characteristic of the peak selected.

Tape noise could be identified by connecting an oscilloscope to the output K_{a2} signal the peak detector was editing. A sketch of what was observed cannot be shown here because no recording device was available. Visual observation of the K_{a2} signal and several individual probes showed no evidence of specific harmonics that stood out above the normal PSD levels of the data. Significant spectral content above the 1000 Hz cut off frequency was present up to 1200 Hz where the signal dropped off significantly, as expected. It would have been more helpful to record the PSD's on paper to determine if the sampling rate of the PSD observed was adequate to draw these conclusions.

Strip charts on the K_{a2} parameter, peak detector and the forty probes were also observed (Figure 78.).

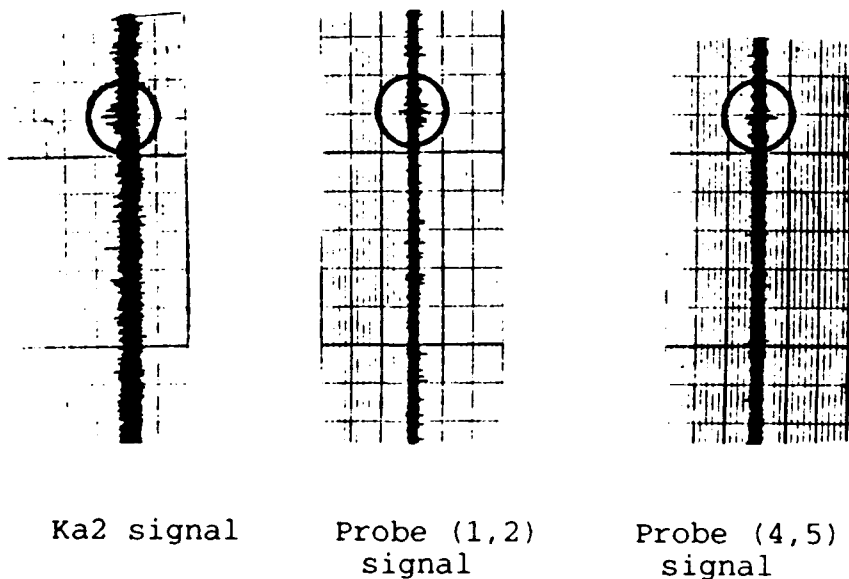


Figure 78. FJ72.067 Strip Charts

Strip chart pen response was much less than the frequency of the data, but some useful information was still possible. The FJ72.067 "peak peak pattern" occurred in a time slice with a number of large peaks. It is possible that in a region of highly concentrated peaks, the peak detector may have difficulty discerning a single peak, especially if peaks occur in a time that is less than the peak detector's time delay error.

The last subject addressed in the 2nd level of analysis was the comparison of precision indices of the freejet and wind tunnel data. This was accomplished using the $+2S/x$ plots in Figures 79. through 81.

COMPRESSOR MAP - 2S/mean (%)

WIND TUNNEL RUN 603.4

Mach = 0.6
 Alpha = -10
 Beta = 0
 WAC2 = 226 lb/sec
 RMS Turb = 1.31 %

FREEJET POINT 72.067

RMS Turb = 1.62 %

Level 2S/Σ (%)

7	3.000
6	2.500
5	2.000
4	1.500
3	1.000
2	0.500
1	0.000

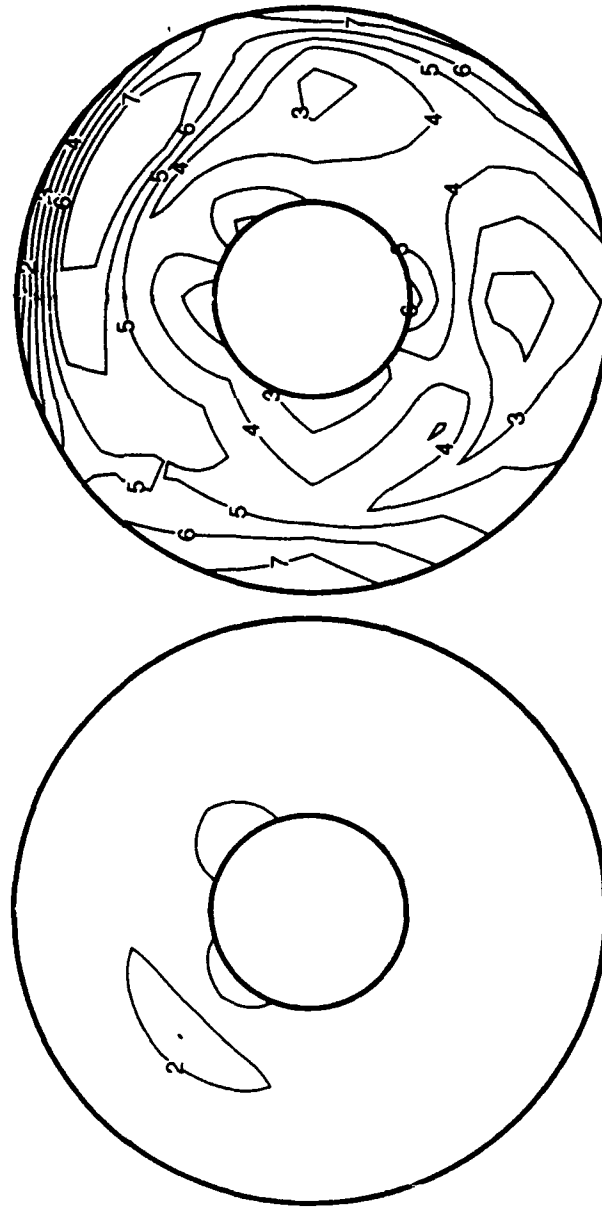


Figure 79. FJ72.067 and WT603.4 Forty Probe Precision Index Maps

COMPRESSOR MAP - 2S/mean (%)

WIND TUNNEL RUN 563.4

FREEJET POINT 14.148

Mach = 0.3

Alpha = 30

Beta = 10

WAC2 = 240 lb/sec

RMS Turb = 3.35 %

RMS Turb = 3.02 %

Level	2S/ \bar{x} (%)
7	3.000
6	2.500
5	2.000
4	1.500
3	1.000
2	0.500
1	0.000

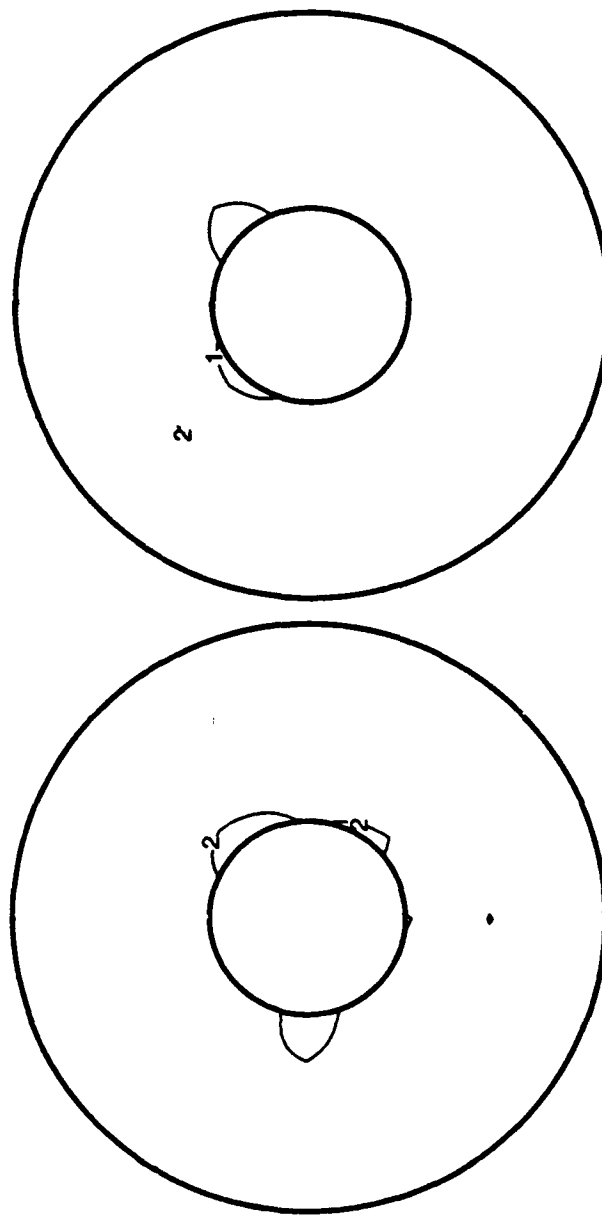


Figure 80. FJ14.148 and WT563.4 Forty Probe Precision Index Maps

COMPRESSOR MAP - 2S/mean (%)

WIND TUNNEL RUN 1170.1

FREEJET POINT 59.022

Mach = 2.2

Alpha = -5

Beta = 0

WAC2 = 183 lb/sec

RMS Turb = 5.35 %

RMS Turb = 4.82 %

Level 2s/Σ (%)

7	3.000
6	2.500
5	2.000
4	1.500
3	1.000
2	0.500
1	0.000

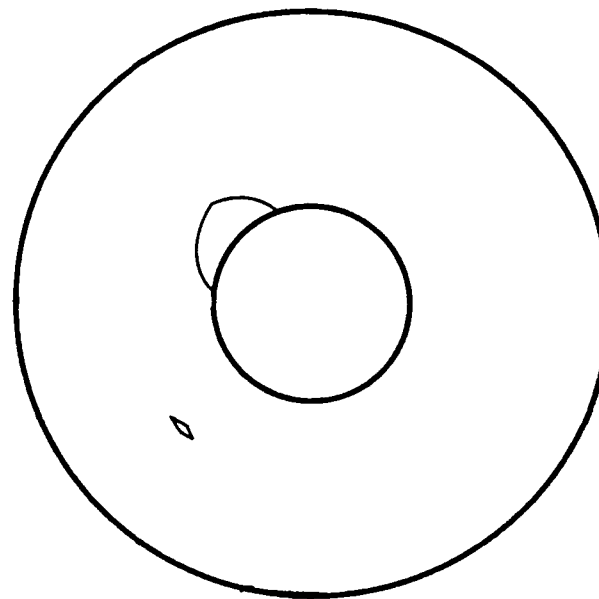
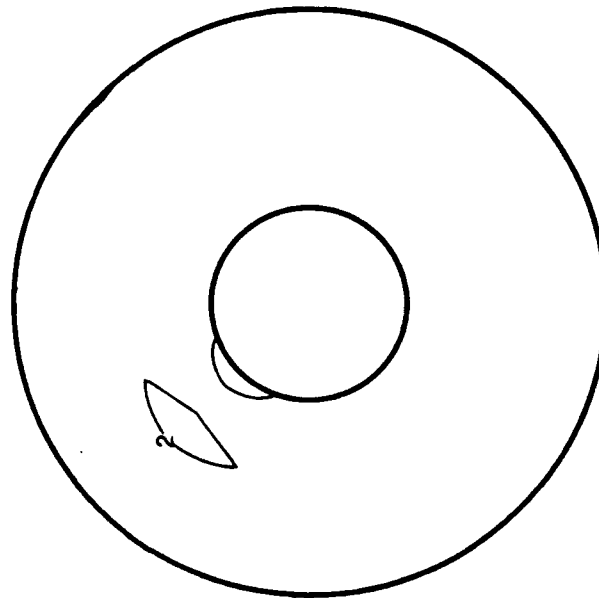


Figure 81. FJ59.022 and WT1170.1 Forty Probe Precision Index Maps

The first observation made is that the precision indices were very low. With the exception of the noise in FJ72.067, the indices were so low that no trends in individual data sets or with RMS turbulence level were possible. The only possible trend was a "high" precision index on distinct probes around the engine face hub and one additional probe at the "eleven o'clock" position. The precision indices of these probes were in the 0.5% to 1% range and not of significant concern because they were so small.

Comparison of the wind tunnel and freejet distortion parameters were also investigated.

Table 28.
Wind Tunnel and Freejet Distortion Indices

	FJ72.067	FJ14.148	FJ59.022	WT603.4	WT563.4	WT1170.1
Analog	2S/ \bar{x} '	2S/ \bar{x} '	2S/ \bar{x} '	2S/ \bar{x} '	2S/ \bar{x} '	2S/ \bar{x} '
K $_{\theta}$	4.5358	0.5326	0.7641	1.7358	0.8846	0.1295
K $_{ra2}$	12.5506	1.8508	0.3971	2.7098	3.4773	0.7545
K $_{a2}$	8.4508	1.1297	0.3908	1.6169	2.2946	0.6236
Digital						
K $_{\theta}$	6.064	0.6127	0.7899	6.2757	1.0804	0.9036
K $_{ra2}$	21.3685	2.4424	0.425	3.6851	2.1911	0.7992
K $_{a2}$	9.2543	1.3392	0.425	2.3987	1.515	0.7015

Table 28. results indicate low turbulence runs had larger precision indices than the four higher turbulence points. Precision indices of K $_{a2}$, K $_{\theta}$ and K $_{ra2}$ tended to decrease in magnitude with increasing RMS turbulence level when

consideration was given to round off error. The difference between a 0.764% precision index and a 0.533% precision index was not that much in a complex hybrid computer system like DYNADEC.

This completed the study of precision errors on the six data points. The final step in the analysis was the determination of a bias error for each of the 40 probes and the distortion parameters.

3.4 Level 4 Analysis

45 daily system static checks and 156 static checks performed prior to editing were compiled from data editing sessions between June 20, 1991 and March 6, 1992. While precision index data was recorded in a one month period in February, 1992, it was thought that use of a broader set of bias error data would show system variations from day to day operations over a time period of 9 months. Use of a broader data set also increased the number of samples used to compute the bias errors and hopefully made more accurate results.

The large amount of data involved was grouped in a spreadsheet according to type of static check. Runs were placed in chronological order by day and by time of day to see if any daily, weekly, or monthly trends were present. The spreadsheets are listed in Appendix C.

The first area of concern before the actual bias errors were computed was a system problem that occurred between

December 17, 1991 and February 3, 1992. The DYNADEC system was not "zero'ing" out faulty probe dynamic signals as well as in the past. Normally, the system prints out a "dynamic" faulty probe total pressure recovery equal to the steady state probe recovery $\pm 0.3\%$ - $\pm 0.4\%$ recovery. For instance, a faulty probe location with a steady state recovery of 0.9862 will usually have a dynamic recovery of 0.9862 ± 0.003 to ± 0.004 . The additional ± 0.003 error was due to analog system variations from run to run and was within tolerance limits.

In the December 1991 to February 1992 time frame, the DYNADEC system was producing "dynamic" faulty probe recoveries between 0.5% and 1% (± 0.005 - ± 0.01) off of the steady state recoveries. This was not in the acceptable range of system variations when compared to the normal range of between 0% and 0.5% (± 0.000 - ± 0.005) and the compressor face pattern quality was not good. Thus, test point editing results during this time period were thrown out.

The engineer responsible for the daily DYNADEC system operation continued to attempt to resolve the errors during this time period. Unfortunately, other programs had access to the analog computer side of the DYNADEC system and no daily problems were recorded. Daily system corrections such as equipment replacements were not recorded, so by February, when pattern quality "miraculously" improved and the zeroed probe dynamic recoveries were somewhat closer to the tolerance limits, very little additional information was

known about what had gone wrong. A log of daily system modifications and replacements was initiated at this point to prevent further unknown variations from occurring.

What was established during this time period was that the system error added on to the steady state recovery faulty probes increased in magnitude with the number of peaks detected and recorded by the peak detector. The errors seemed to increase as longer editing time slices were used, as well. The only method found to alleviate this problem was to increase the peak detector threshold to a level where three to five dynamic peaks were detected to reduce the number of dynamic patterns stored in the system per run. Once three to five peak times were known in the initial run of a point, each individual peak was recorded in separate editing runs over a short time frame. This was a "brute force" method, but was the only solution found that lowered the system errors on the faulty probes to tolerable levels.

Static bias errors were recorded during this time period and included in this analysis to see if further indications of what was wrong existed. The average bias error was computed for each of the 40 probes for the July 1991 static checks: the 12/91 - 2/3/92 time period, and the 2/4/92 - 3/6/92 time period. These values can be seen in Table 29.

Table 29.
DYNADEC System Bias Errors

					7/91	12/91-	2/4/92
	7/91 Error	12/91-2/3/92	2/4/92 on		Error	2/3/92	on
Probe	Used	Not Used	Used		Used	Not Used	Used
(1,1)	0.0019	0.0026	0.0026	K the	0.11	0.0197	0.0128
(1,2)	0.0024	0.0018	0.0021	K ra2	0.044	-0.0105	0.0036
(1,3)	0.0023	0.0029	0.0026	K a2	0.059	0.0418	0.0053
(1,4)	0.0019	0.0024	0.0022				
(1,5)	0.0024	0.0034	0.0031				
(1,6)	0.0021	0.0029	0.0025				
(1,7)	0.0017	0.0030	0.0029				
(1,8)	0.0021	0.0034	0.0028				
(2,1)	0.0022	0.0026	0.0028				
(2,2)	0.0020	0.0028	0.0025				
(2,3)	0.0020	0.0002	0.0017				
(2,4)	0.0022	0.0027	0.0025				
(2,5)	0.0020	0.0026	0.0021				
(2,6)	0.0016	0.0030	0.0032				
(2,7)	0.0027	0.0023	0.0023				
(2,8)	0.0017	0.0022	0.0020				
(3,1)	0.0010	0.0038	0.0038				
(3,2)	0.0013	0.0034	0.0033				
(3,3)	0.0020	0.0026	0.0028				
(3,4)	0.0018	0.0029	0.0028				
(3,5)	0.0013	0.0028	0.0028				
(3,6)	0.0010	0.0036	0.0036				
(3,7)	0.0012	0.0022	0.0020				
(3,8)	0.0013	0.0013	0.0016				
(4,1)	0.0014	0.0024	0.0025				
(4,2)	0.0011	0.0012	0.0011				
(4,3)	0.0013	0.0023	0.0025				
(4,4)	0.0011	0.0016	0.0020				
(4,5)	0.0013	0.0026	0.0023				
(4,6)	0.0010	0.0019	0.0017				
(4,7)	0.0017	0.0020	0.0019				
(4,8)	0.0020	0.0012	0.0012				
(5,1)	0.0019	0.0036	0.0029				
(5,2)	0.0023	0.0046	0.0052				
(5,3)	0.0028	0.0023	0.0025				
(5,4)	0.0016	0.0026	0.0031				
(5,5)	0.0018	0.0042	0.0035				
(5,6)	0.0005	0.0008	0.0014				
(5,7)	0.0007	0.0050	0.0045				
(5,8)	0.0004	0.0040	0.0044				
Avg	0.0017	0.0027	0.0026				

Table 29. (Continued)

Bias Error Used	Bias Error Not Used
(% Recovery)	(% Recovery)
0.0003	0.0003
0.0003	0.0002
0.0003	0.0004
0.0003	0.0003
0.0004	0.0004
0.0003	0.0004
0.0003	0.0004
0.0003	0.0004
0.0003	0.0003
0.0003	0.0004
0.0002	0.0003
0.0003	0.0003
0.0003	0.0003
0.0003	0.0004
0.0003	0.0003
0.0002	0.0003
0.0004	0.0005
0.0003	0.0004
0.0003	0.0003
0.0003	0.0004
0.0003	0.0004
0.0003	0.0005
0.0002	0.0003
0.0002	0.0002
0.0003	0.0003
0.0002	0.0002
0.0003	0.0003
0.0002	0.0002
0.0003	0.0004
0.0002	0.0003
0.0002	0.0003
0.0002	0.0002
0.0003	0.0005
0.0006	0.0006
0.0004	0.0003
0.0004	0.0004
0.0004	0.0006
0.0002	0.0001
0.0004	0.0007
0.0004	0.0005
0.0003	0.0004

The 12/91 - 2/92 time period shows a slightly higher 40 probe average bias error. Individual probe bias errors seem to be higher as well. However, these final results were scaled to system voltage levels. It was more appropriate to perform the actual comparisons in units of total pressure recovery in the same manner as the precision indices. Table 29. also lists the results in % recovery units.

Bias errors from the 12/91 - 2/92 time frame continued to be higher in % recovery units; however, the magnitudes of these errors (or the lack thereof) was key to their interpretation. The bias error magnitudes in % recovery units are on average 0.035%. This was well below the run to-run-system variations when the same peak was edited. Typical system variations were in the range of 0.2% to 0.3% recovery. These levels are also considerably lower than the precision indices (0.5% - 1%) recovery. Based on these comparisons, the static bias errors during this time period when the system was not "zeroing" out the faulty probes correctly could be considered negligible.

Once again, these bias errors are static bias errors. The recording equipment was not available to evaluate the peak detector time delay errors and so the error was grouped as a precision error as discussed in Chapter 2. Other methods of evaluating the peak detector were not considered because of the highly dynamic nature of that branch of the DYNADEC system.

The last task of the analysis was to combine the precision indices and bias errors into overall DYNADEC system errors. A magnitude comparison of the two components revealed that the bias errors were so small compared to the precision indices that the bias error contribution was classified as negligible and the overall DYNADEC system errors were taken as the precision errors listed in Tables 20 and 28.

CHAPTER IV

CONCLUSIONS AND RECOMMENDATIONS

The following conclusions and recommendations are made, based on the results of the uncertainty analysis:

1. Precision errors for each of the forty probes and the K_{a2} , K_{θ} , and K_{ra2} distortion parameters were computed. Magnitudes were so low ($< 1\%$) in five of the six cases, that any point to point variations could not be discerned. What variations existed were attributed to basic system operation variations.
2. The data showed no precision index magnitude trends as a function of RMS turbulence levels. Some of the larger precision indices ($\pm 2S/\bar{x}$) levels seen (0.5%- 1%) were concentrated about the engine face hub and at the "eleven o'clock" position on the engine face.
3. Scatter in the probability distributions decreased with increasing turbulence level. This is probably due to DYNADEC recognizing higher amplitude signals better than signals that blend with system or signal noise.
4. The narrow scatter band exhibited by the distributions on the faulty probe recoveries show that DYNADEC was able to eliminate the dynamic signal of the faulty probes well.

5. Any trends with Mach number, angle-of-attack, angle-of-sideslip, airflow, or any other test condition were not investigated because trends in the dynamic data based on these quantities were highly configuration dependent. The appropriate quantity to monitor was the amount of signal energy through Power Spectral Density (PSD) plots and RMS turbulence levels. These parameters are generic enough to allow the conclusions presented here to be applied to any data set edited by the DYNADEC system.
6. Precision indices for the lowest turbulence freejet test point, FJ72.067, were in the 2 - 3 % range. This is still a reasonable level compared to uncertainty levels seen in flight test data.
7. Based upon analysis of the days the noise occurred, the strip charts of Ka2 and probe signals, the observed PSD frequency content and the faulty probe distributions, it was concluded that the noise was a characteristic of the tape or a close succession of peaks on the tape. Further analysis on this point should involve editing and interpreting another peak in the time history of this point. The time involved in recording and analyzing another 50 repeat runs of the same peak was time prohibitive at this point. However, the results of another peak would more firmly establish the causes of the noise here.

8. The probe means (\bar{x}) calculated for FJ72.067 matched the Sedlock predicted pattern, indicating that random number statistics were still applicable with 2 - 3 % system noise.
9. Results from the Sedlock program on four of the other five test points matched their respective "mean" peak distortion patterns well, both in magnitude level and in visual comparison. The exception was FJ59.022, the M=2.2 freejet case, where a physical phenomena is more than likely driving the flow to non-random distortion levels.
10. Sedlock results of wind tunnel and freejet points at the same condition matched one another better than the respective DYNADEC peak patterns. This is due to the limitations of the Sedlock random number statistical model and the test data itself. It is not a DYNADEC system error.
11. Precision errors ($\pm 2S/\bar{x}$) and scatter on the K_{a2} , K_0 and K_{ra2} distortion indices generally decreased in magnitude with increasing RMS turbulence level. This is probably due to the fact that high turbulence data has much higher amplitude dynamic signals which help set it apart from lower amplitude noise.
12. The magnitude shift from analog to digital distortion parameters decreased as a percentage of the digital components with RMS turbulence level for the three wind

tunnel points. No pattern was seen in the Freejet data. More repeat points at various turbulence levels are required before a definite trend should be concluded.

13. AIR 1419 index component distributions exhibited less scatter than their respective ring average recovery distributions; however, no firm conclusion could be made about these results because the data was not screened on the AIR 1419 parameters and the distribution scales of recovery and AIR 1419 components were not necessarily the same. A comparison of the distributions as a percentage of their mean levels would be more appropriate.
14. Static bias errors on the forty probes were much less than the run to run system variations. Static bias errors were slightly higher during the time period when the DYNADEC system was not eliminating the faulty probe dynamic signals well. The solution found, that running short editing times with high peak detector thresholds, should be considered interim at best and monitored closely in future editing sessions.
15. It would be helpful, with future data sets edited on the DYNADEC system, to perform an analysis similar to this one on a smaller scale. Thus, initial behavior of the data set with the system is gained.

16. The impending conversion to an all-digital DYNADEC system calls for a repeat analysis using the six test points used here. A comparison between the two systems will be extremely useful and new system accuracy can be established immediately.

APPENDIX A

PRATT AND WHITNEY AND AIR 1419 DISTORTION PARAMETERS

Pratt and Whitney's K_{a2} Distortion Index was developed to measure the effect of inlet distortion on the operability of all Pratt and Whitney engines. K_{a2} is divided into two components that are representative of pressure variations in the radial direction of the engine face (radial distortion) and in the circumferential direction of the engine face (circumferential distortion):

$$K_{a2} = K_{\theta} + b K_{ra2} \quad (27)$$

where: K_{θ} = Fan Circumferential

Distortion Factor

K_{ra2} = Fan Radial Distortion

Factor

b = Radial Distortion

Weighting Factor (Function

of Engine and Engine Airflow)

The 'b-factor' varies as a function of a specific engine's sensitivity to radial distortion and engine airflow.

The K_{θ} formula is listed below:

$$K_{\theta} = \frac{\sum_{ring=1}^J \left[\left(\frac{A_n}{n^2} \right)_{\max ring} \right] * \frac{1}{D_{ring}}}{\left(\frac{q}{P_t} \right)_{Ref} \sum_{ring=1}^J \frac{1}{D_{ring}}} \quad (28)$$

Where: J = Number of Rings (probes per leg)

D = Ring Diameter

$(q/P_t)_{ref}$ = Engine Face Dynamic Pressure Head,
Function of Engine Airflow

$$A_n = \sqrt{a_n^2 + b_n^2}, \quad n = 1, 2, 3, 4 \quad (29)$$

where:

$$a_n = \frac{\Delta\theta}{180} \sum_{k=1}^K \frac{\frac{P_{t2}}{P_{to}}(k\Delta\theta)}{\frac{P_{t2}}{P_{to}}} \cos(k\Delta\theta)$$

$$b_n = \frac{\Delta\theta}{180} \sum_{k=1}^K \frac{\frac{P_{t2}}{P_{to}}(k\Delta\theta)}{\frac{P_{t2}}{P_{to}}} \sin(k\Delta\theta)$$

$$\frac{P_{t2}}{P_{t0}} (k\Delta\theta) = \text{Local Total Pressure Recovery at angle, } k\Delta\theta$$

$$\frac{\overline{P_{t2}}}{P_{t0}} = \text{Face Average Total Pressure Recovery}$$

$$\left(\frac{A_n}{n^2} \right)_{\max} = \text{Maximum Value for Four Fourier Coefficients Calculated; Normally } n = 1$$

K = Number of Rake Legs

$\Delta\theta$ = Angular Distance Between Rake Legs

The K_{ra2} formula is listed below:

$$K_{ra2} = \frac{\sum_{\text{ring}=1}^J \left(\frac{\Delta P_{t2}}{\overline{P_{t2}}} \right)_{\text{ring}} * \frac{1}{D_{\text{ring}}}^{2.8}}{\left(\frac{q}{P_t} \right)_{\text{Ref}} \sum_{\text{ring}=1}^J \frac{1}{D_{\text{ring}}}^{2.8}} \quad (30)$$

$$\text{where: } \left(\frac{\Delta P_{t2}}{\overline{P_{t2}}} \right)_{\text{ring}} = \left| \frac{P_{t2}^*/P_{t0}}{\overline{P_{t2}}/P_{t0}} - \frac{P_{t2 \text{ base}}^*}{\overline{P_{t2}}} \right| \frac{\overline{P_{t2}}}{P_{t2 \text{ base}}^*}$$

$$\frac{P_{t2 \text{ base}}^*}{\overline{P_{t2}}} = \text{Reference Radial Profile, function of } \left(\frac{q}{P_t} \right)_{\text{ref}}$$

P_{t0} = Freestream Total Pressure

K_{a2} levels of concern vary with engine and engine airflow. and are determined in ground testing.

The AIR 1419 distortion parameters were created by the Society of Automotive Engineers and are named for the report describing them (Reference 7). The indices are composed of four parts: circumferential intensity, extent, multiple-per-rev and radial intensity. Circumferential intensity ($\Delta P_{C/P}$) is a measure of the magnitude of the low pressure defect, by ring, with respect to the ring average total pressure recovery.

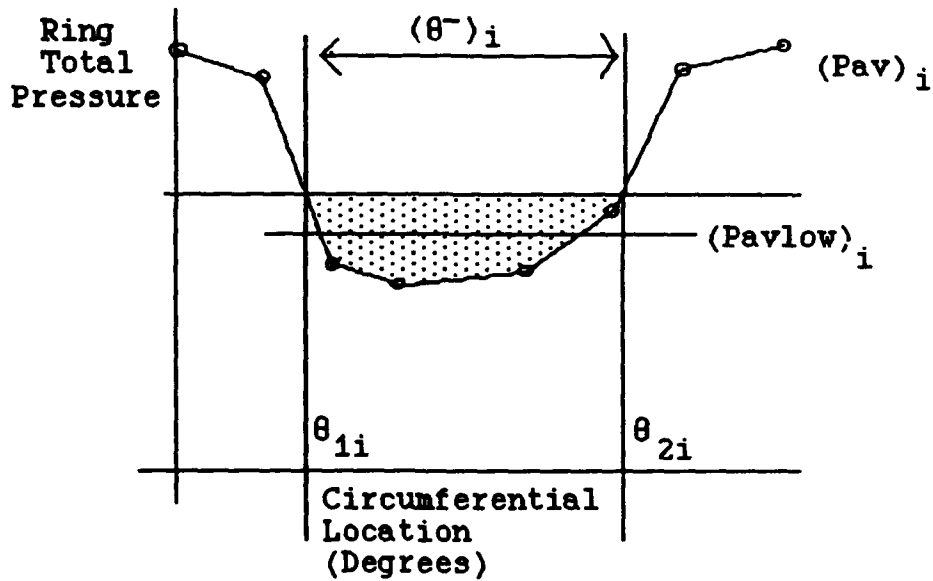


Figure 82. Circumferential Intensity Definition

$$\left\{ \frac{\Delta P_c}{P} \right\}_i = \frac{(P_{av})_i - (P_{avlow})_i}{(P_{av})_i} \quad (31)$$

where: $(P_{av})_i$ = Ring Average Total
Pressure Recovery

$(P_{avlow})_i$ = Low Pressure Region
Average Total Pressure
Recovery

Patterns with more than one low pressure region on a ring sum the individual regions $(\Delta P_c/P)_i$ levels if the regions are less than 25° apart, designating an equivalent 1-per-revolution low pressure region. If the low pressure regions are greater than 25° apart, the $\Delta P_c/P$ value associated with the maximum $(\Delta P_c/P)_i \theta_{ik}$ level is taken as the value for that ring.

Extent is the measure of the angular length of the low pressure region by ring:

$$\text{Extent} = (\theta^-)_i = \theta_{2i} - \theta_{1i} \quad (32)$$

Extent is portrayed graphically in Figure 82 above. Multiple low pressure regions are evaluated in the same manner as intensity. Extents are summed if low pressure regions are less than 25° apart. The θ_i from the maximum $(\Delta P_c/P)_i \theta_{ik}$ is used if the low pressure regions are more than 25° apart.

Multiple-Per-Revolution (MPR) is a measure of the "effective" number of low pressure regions for each ring by relating the sum of the low pressure regions on a ring to the maximum low pressure region:

$$\text{Multiple-Per-Rev (MPR)}_i = \frac{\sum_{k=1}^Q \left(\frac{\Delta P_c}{P} \right)_{ik} \theta_{ik}^-}{\max \left[\left(\frac{\Delta P_c}{P} \right)_{ik} \theta_{ik}^- \right]} \quad (33)$$

where: $\left(\frac{\Delta P_c}{P} \right)_{ik}$ = the k^{th} low pressure region of ring i

θ_{ik}^- = corresponding extent of ring i

Q = total number of low pressure regions on ring i

Radial Intensity measures the difference between ring average pressure and face average pressure:

$$\left(\frac{\Delta P_r}{P} \right)_i = \frac{(P_{fav}) - (P_{av})_i}{(P_{fav})} = \text{IDR}_i \quad (34)$$

where: $(P_{fav})_i$ = Face Average Total
Pressure Recovery

$(P_{av})_i$ = Ring Average Total
Pressure Recovery

The four 1419 index components are usually combined in a form related to the loss of compressor surge pressure ratio. The resultant formula is usually a function of the specific engine of interest, but an example from Reference 7 is seen below:

$$\Delta PRS = \sum_{i=1}^J \left[KC_i \left(\frac{\Delta P_c}{P} \right)_i + KR_i \left(\frac{\Delta P_r}{P} \right)_i + C_i \right] * 100 \quad (35)$$

where: ΔPRS = Loss in Surge Pressure Ratio
Due to Distortion

J = Number of Instrumentation Rings

KC_i = Circumferential Distortion
Sensitivity (function of engine)

KR_i = Radial Distortion
Sensitivity (function of engine)

$\left(\frac{\Delta P_c}{P} \right)_i$ = Circumferential Intensity

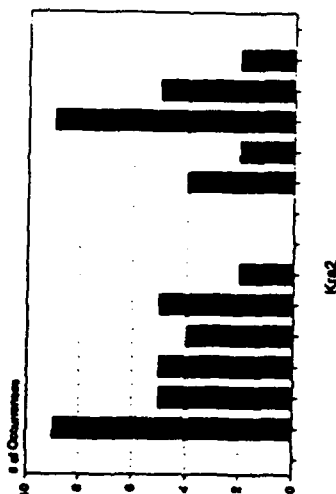
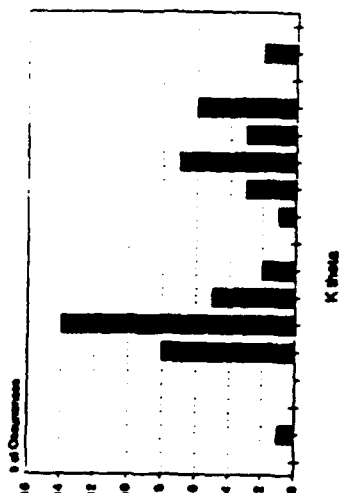
$\left(\frac{\Delta P_r}{P} \right)_i$ = Radial Intensity

C_i = Offset Term (can be function
of MPR and Extent)

AIR 1419 distortion parameters are much more physically descriptive of the airflow than Pratt and Whitney K_{a2}

distortion index. More information on the 1419 indices can be found in Reference 7.

APPENDIX B PRECISION INDEX DATA



FJ72.067 Analog Parameter Distributions



Figure 83. FJ72.067 Analog Parameter Distributions

FJ72.067 Digital Parameter Distributions

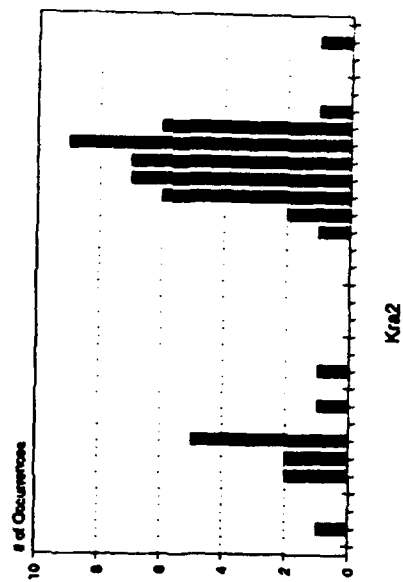
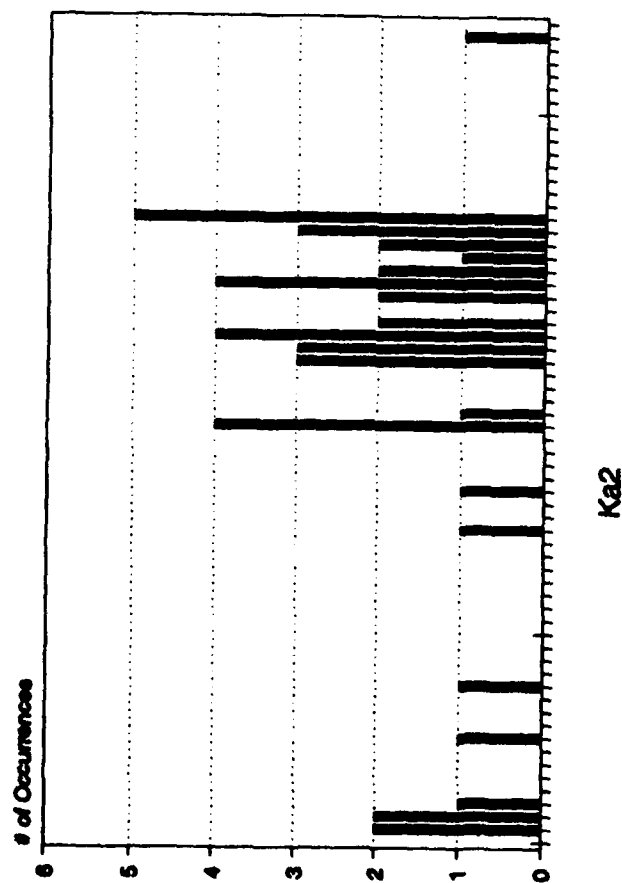
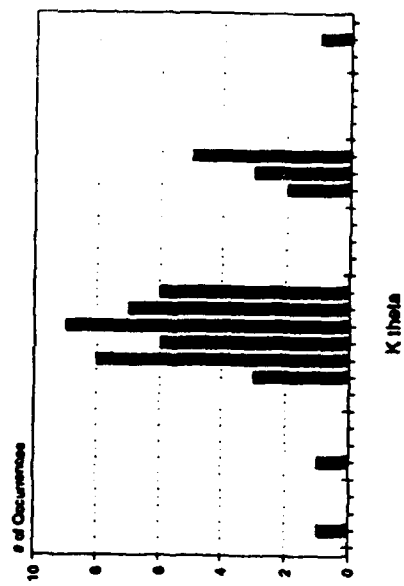


Figure 84. FJ72.067 Digital Parameter Distributions

FJ72.067 Dynamic Ring & Face Average Recovery (P_{12}/P_{10}) Distributions

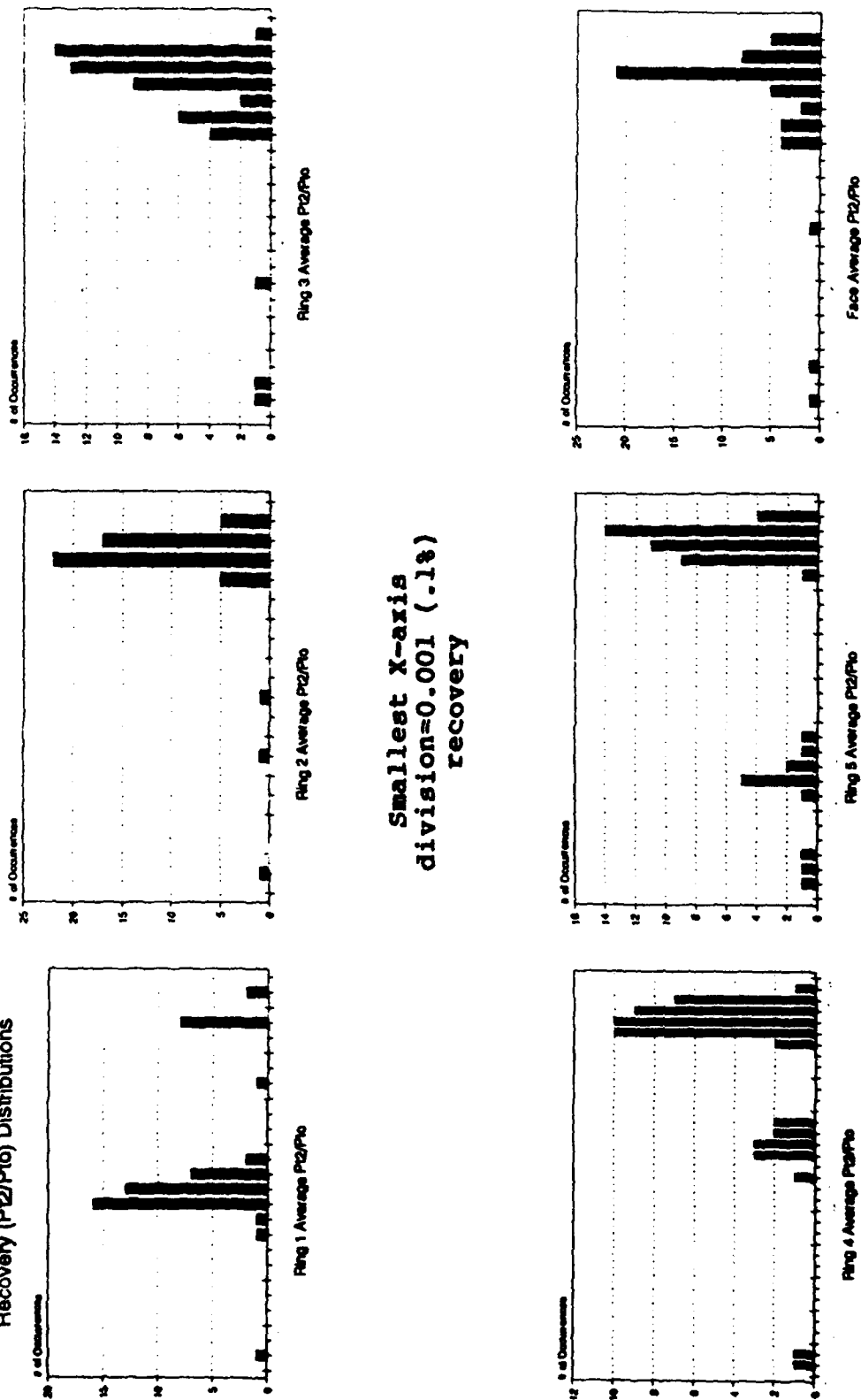
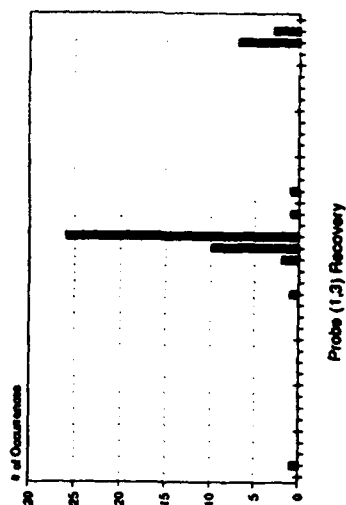
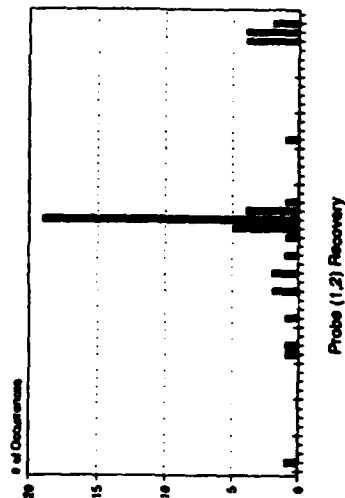
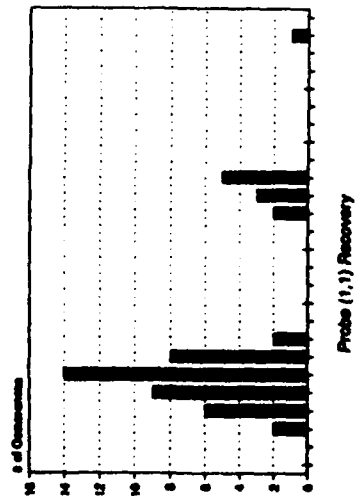


Figure 85. FJ72.067 Dynamic Ring and Face Average Recovery Distributions

FJ72.067 Probe Recovery Distributions



Smallest X-axis
division=0.001 (.1%)
recovery

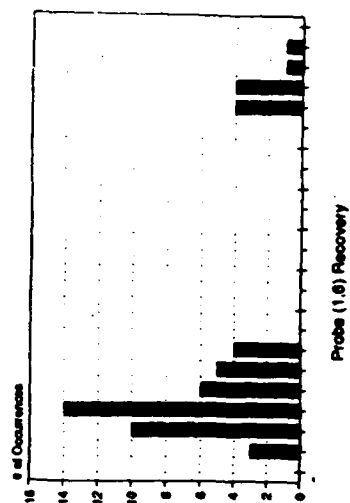
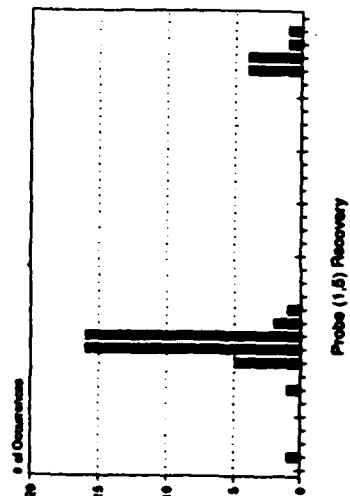
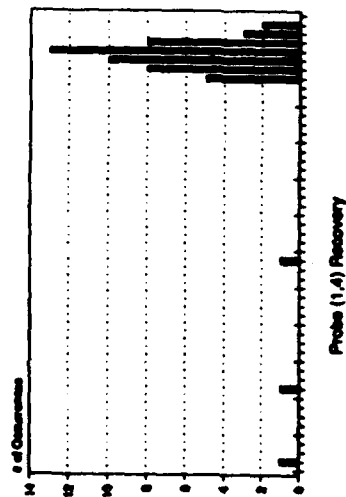


Figure 86. FJ72.067 Probe Recovery Distributions

Figure 86. (Continued)

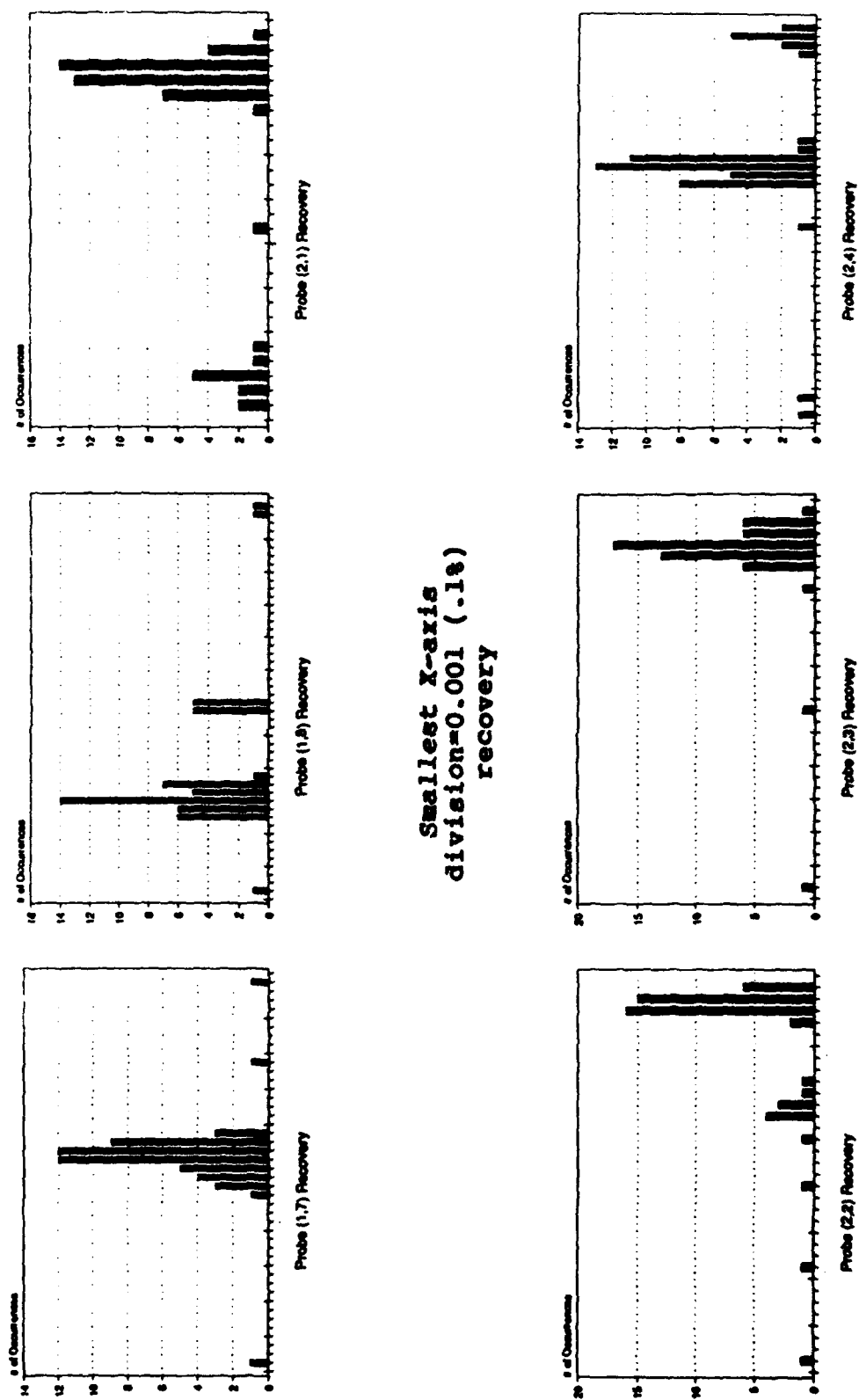
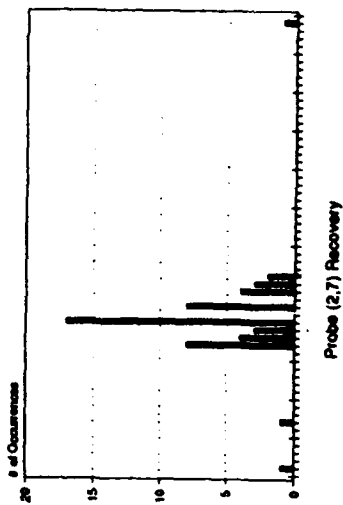
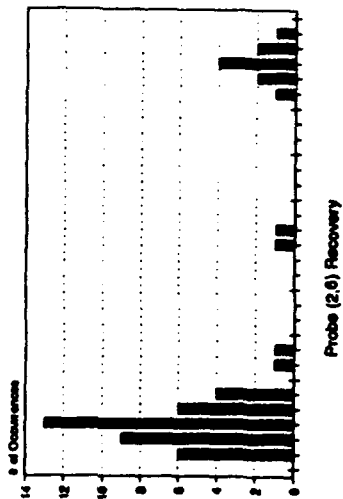
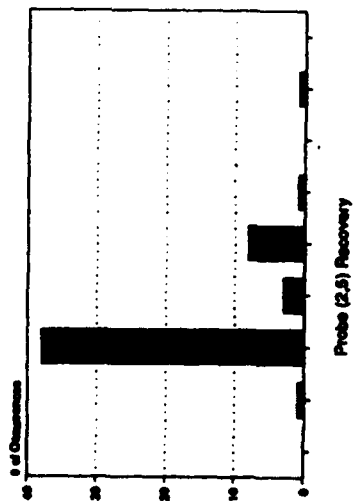


Figure 86. (Continued)



Smallest X-axis
division=0.001 (.1%)
recovery

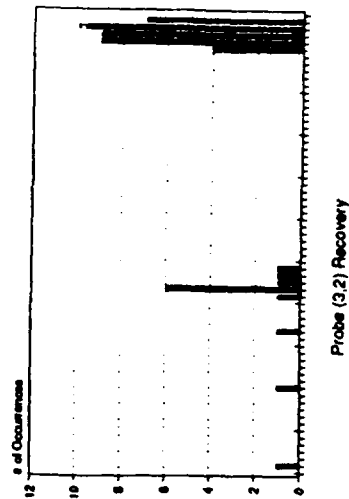
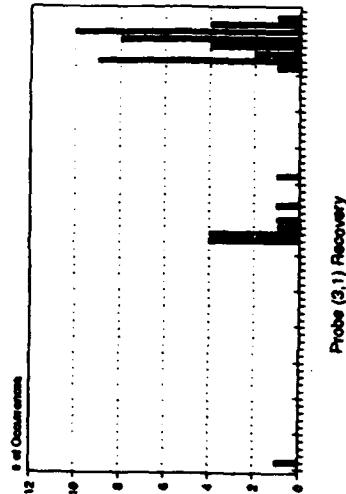
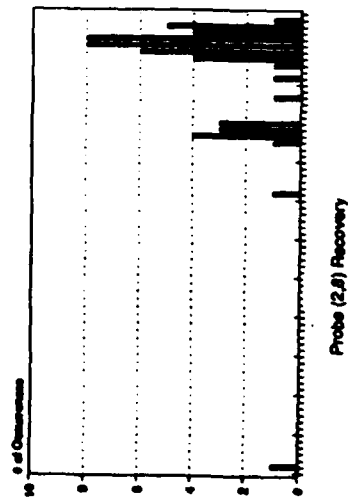
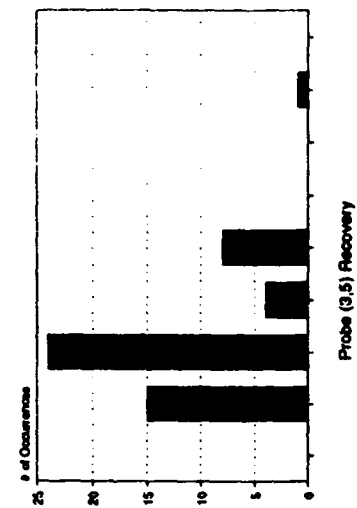
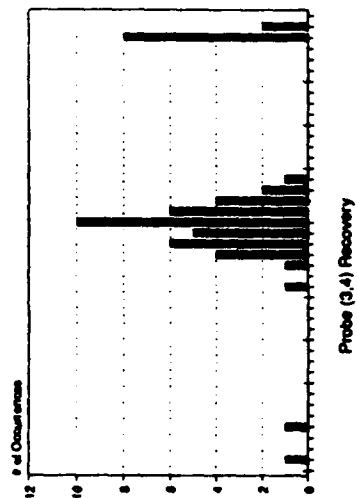
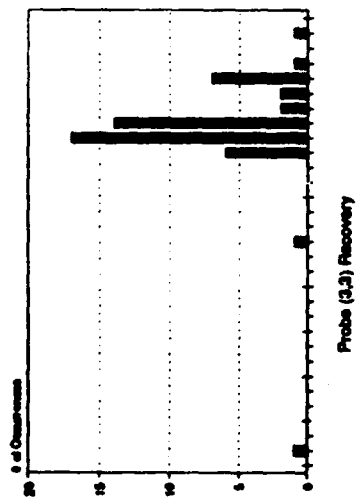


Figure 86. (Continued)



Smallest X-axis
division=0.001 (.1%)
recovery

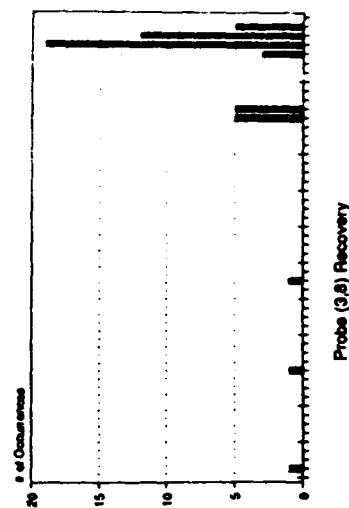
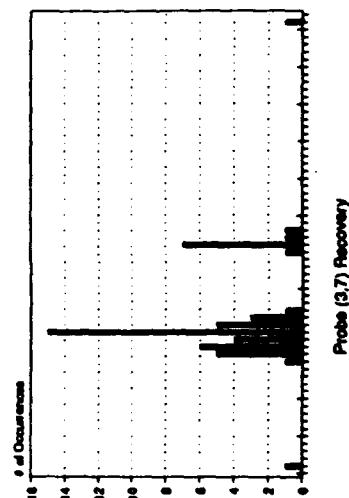
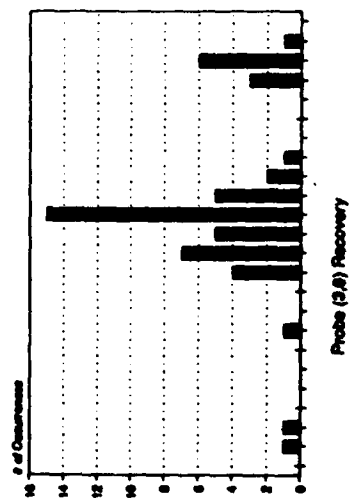
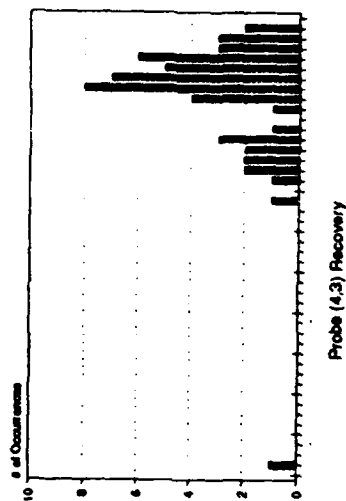
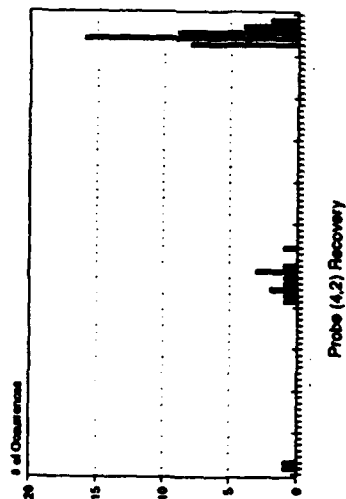
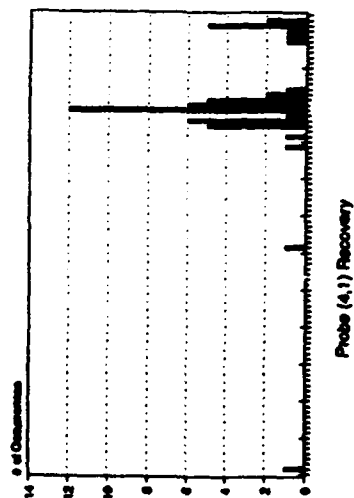


Figure 86. (Continued)



Smallest X-axis
division=0.001 (.18)
recovery

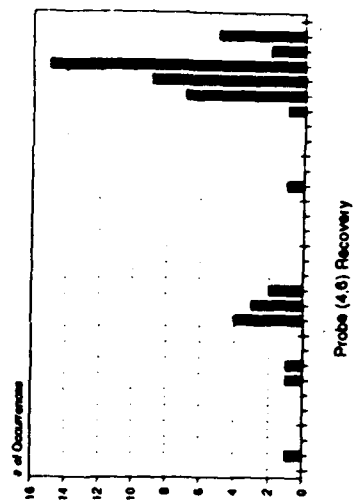
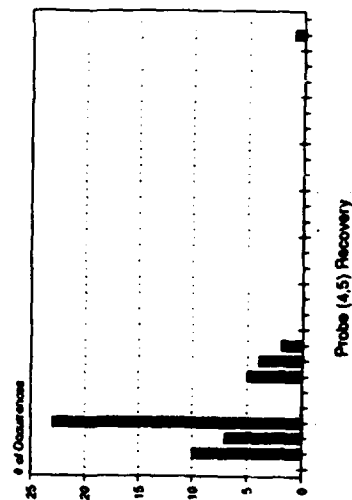
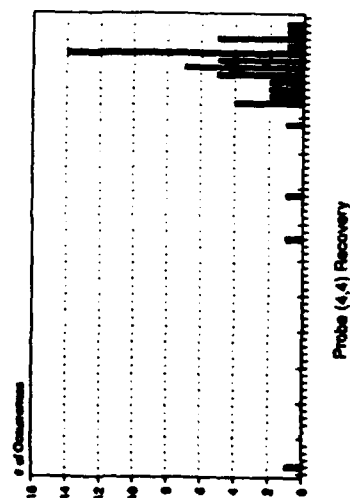
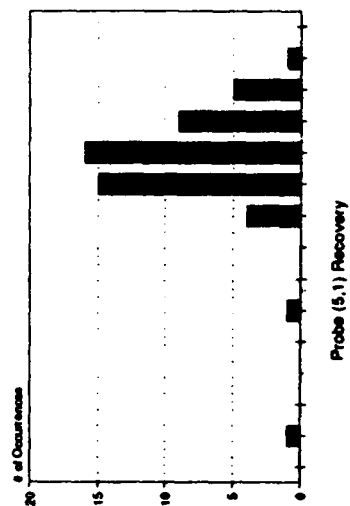
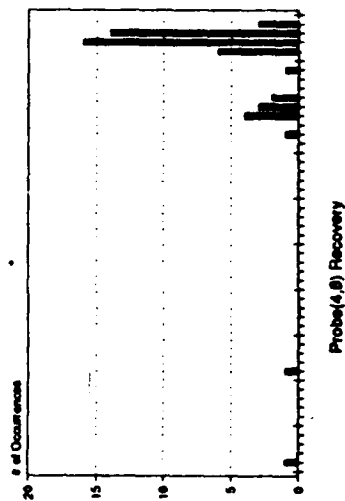
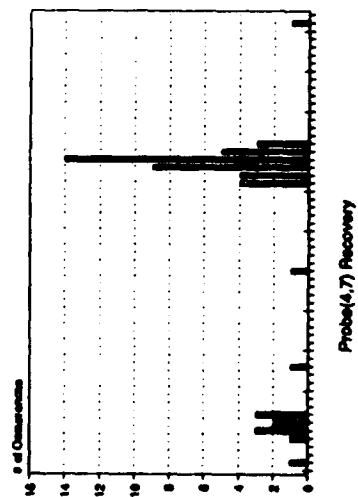


Figure 86. (Continued)



Smallest X-axis
division=0.001 (.1%)
recovery

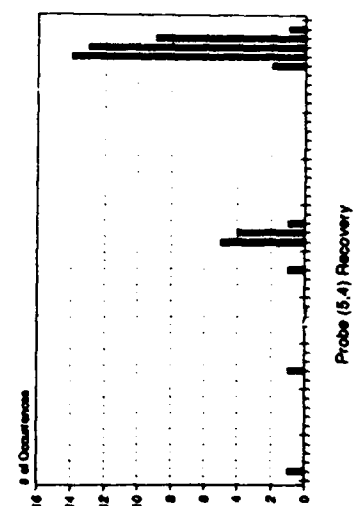
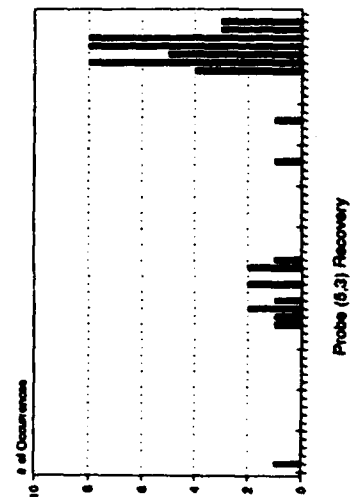
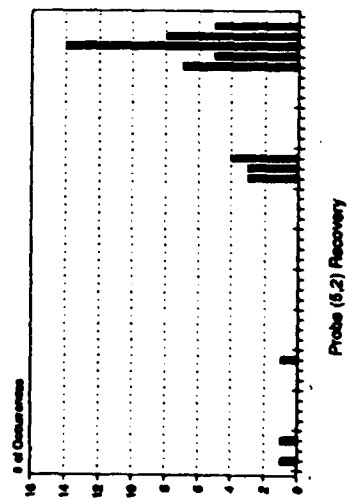
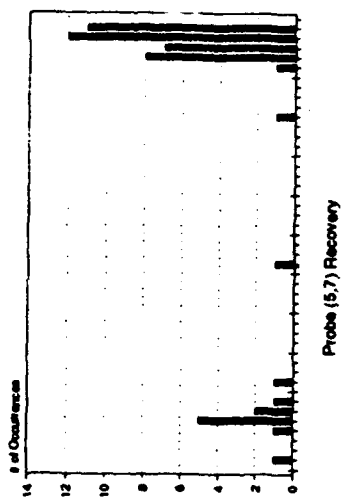
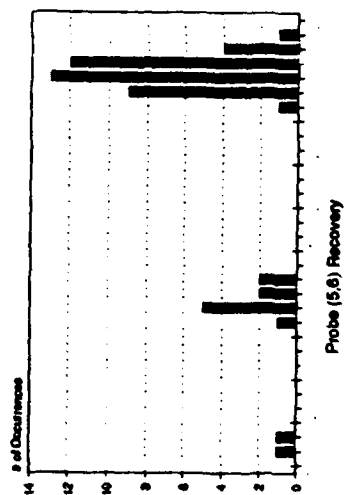
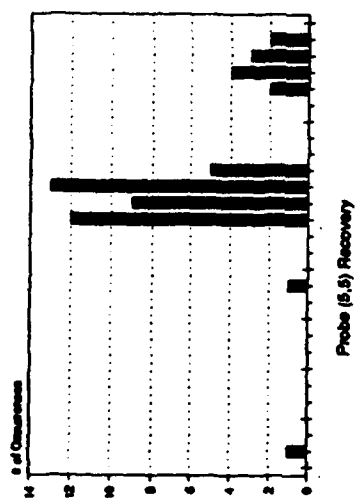
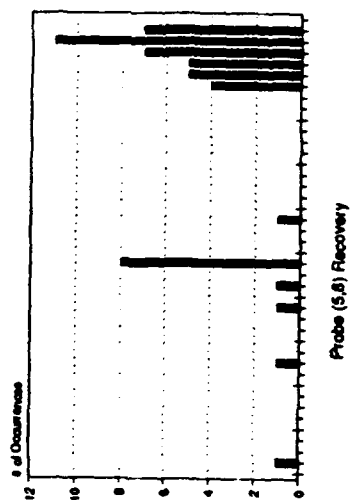


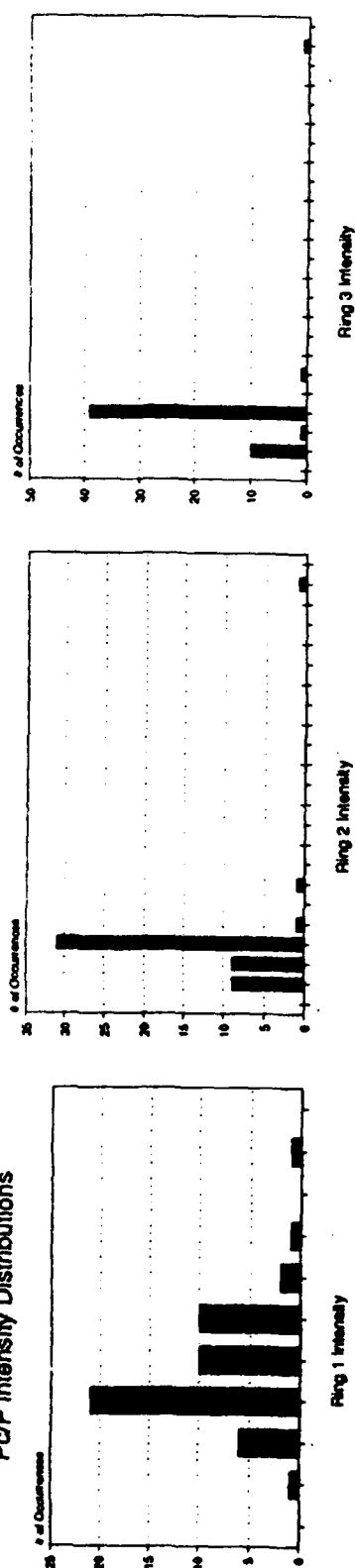
Figure 86. (Continued)



Smallest X-axis
division=0.001 (.1%)
recovery



FJ72.067 1419 Index
Pc/P Intensity Distributions



FJ72.067 Dynamic 1419 Indices Multiple Per Rev Distributions

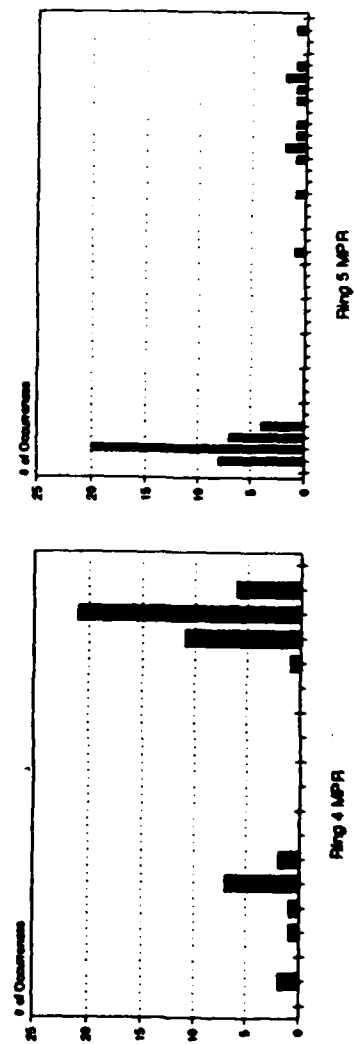
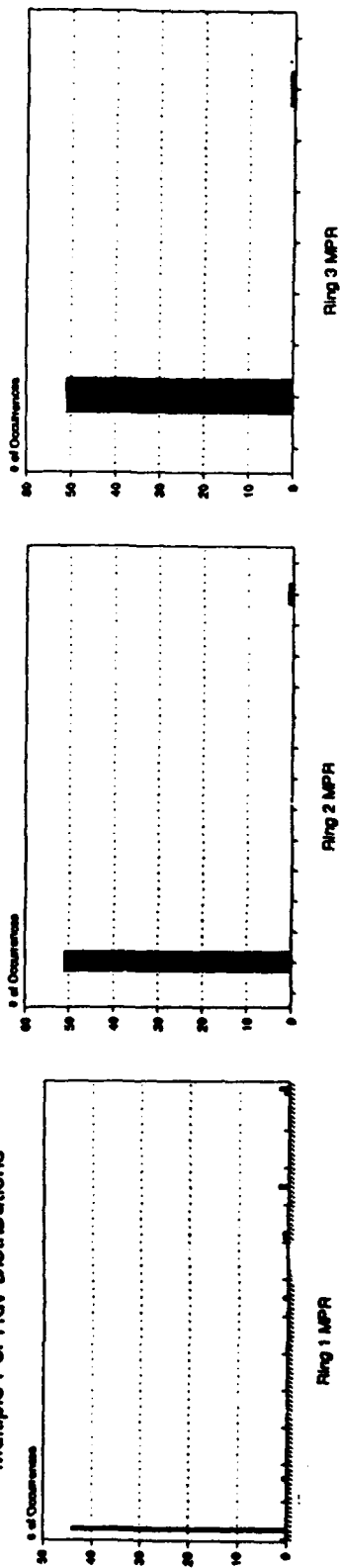


Figure 88. FJ72.067 MPR Distributions

FJ72.067 1419 Index
Extent Distributions

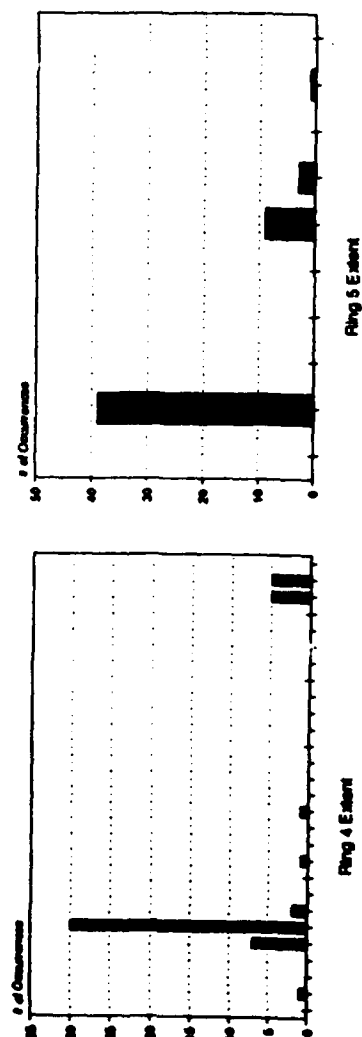
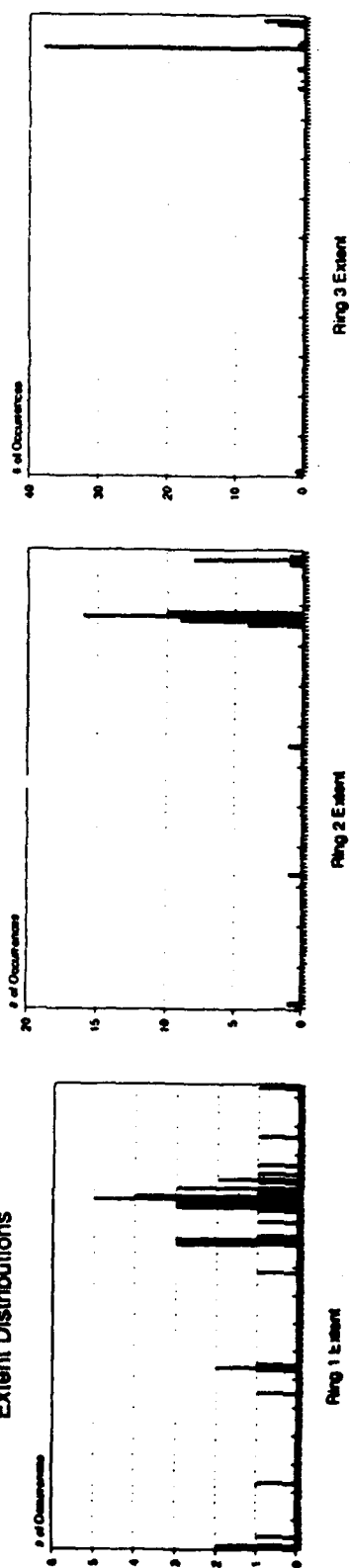


Figure 89. FJ72.067 Extent
Distributions

FJ72.067 1419 Index
Pr/P (IDR) Distributions

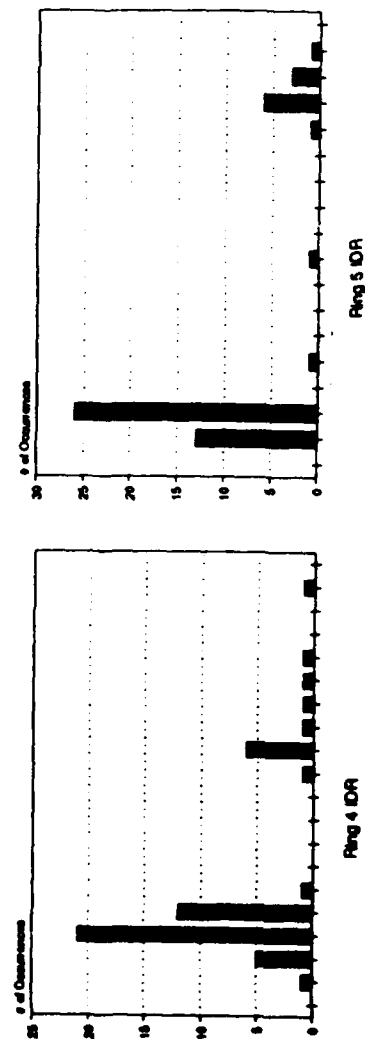
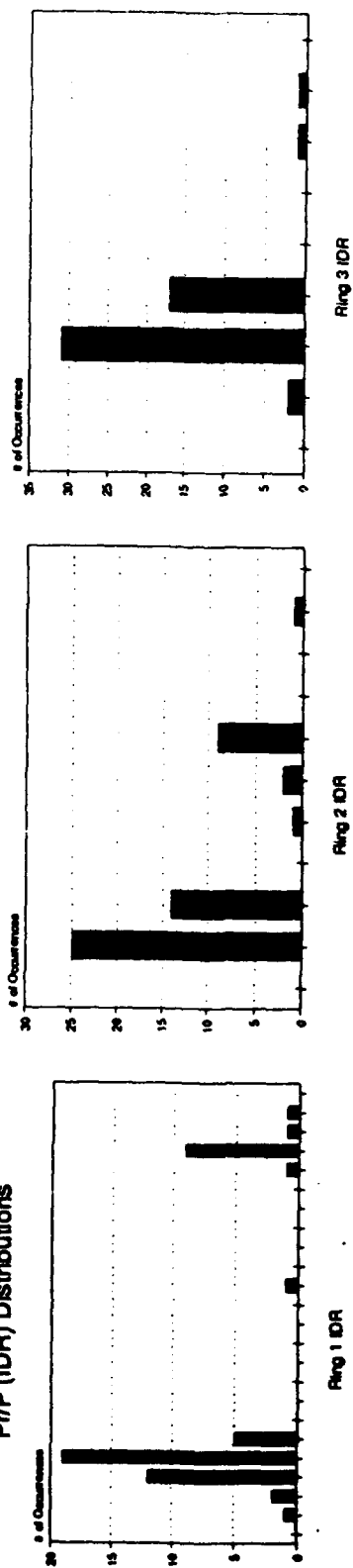


Figure 90. FJ72.067 Δ Pr/P, IDR Distributions

WT603.4 Analog Parameter Distributions

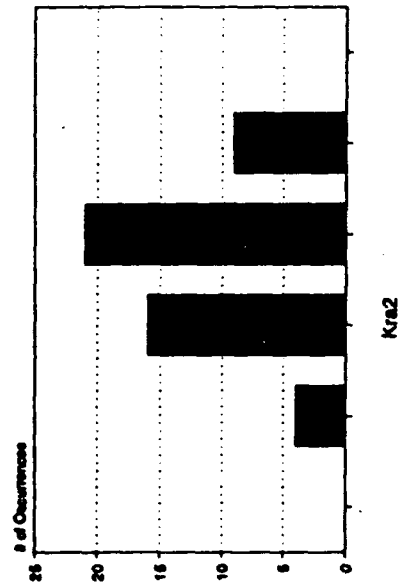
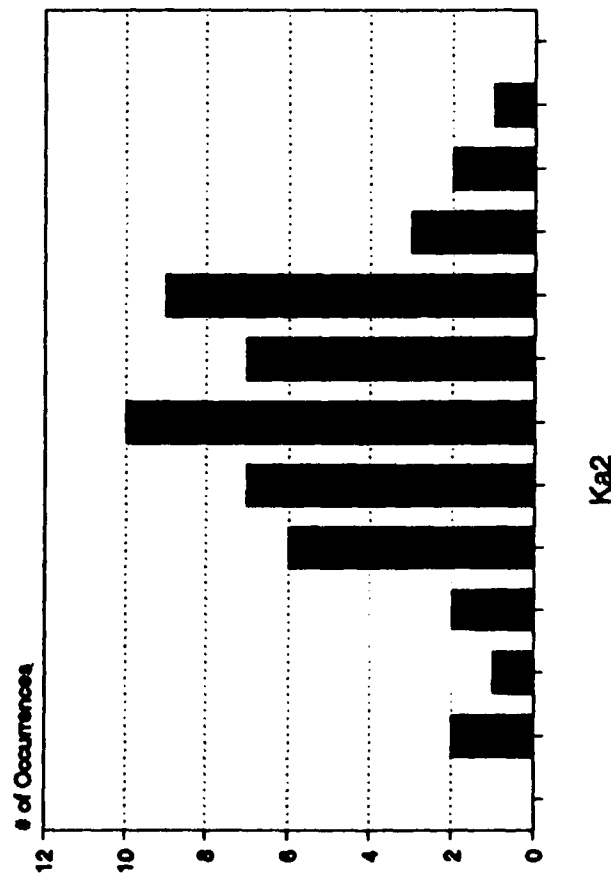


Figure 91. WT603.4 Analog Parameter Distributions

WT603.4 Digital Parameter Distributions

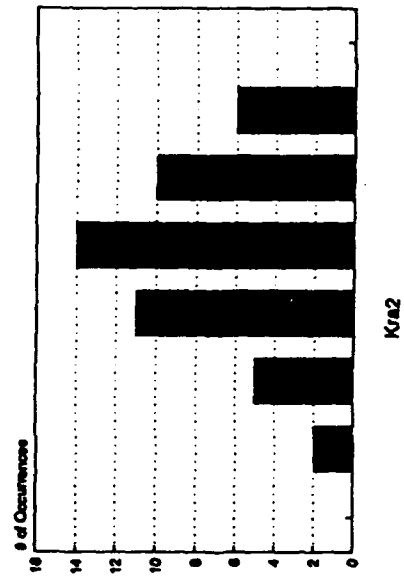
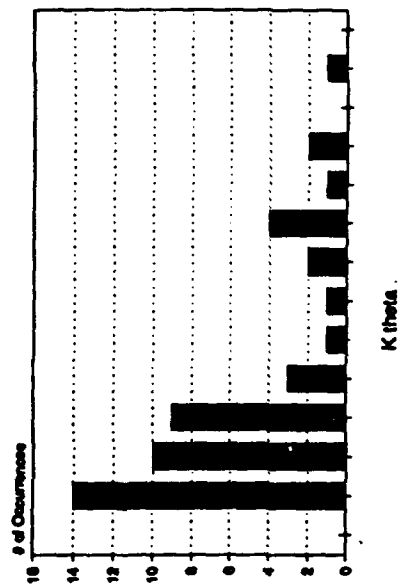
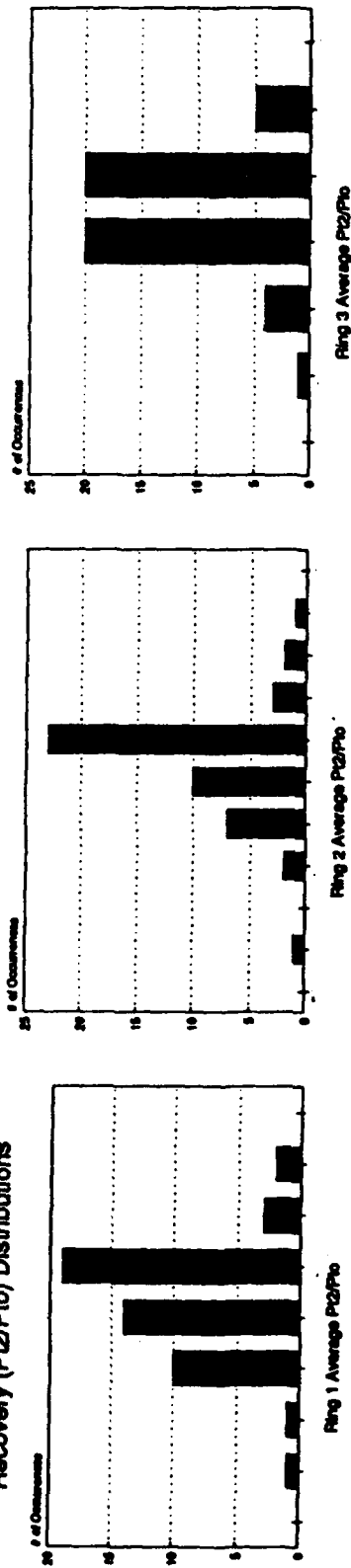


Figure 92. WT603.4 Digital Parameter Distributions

WT603.4 Dynamic Ring & Face Average
Recovery (P2/P10) Distributions



Smallest X-axis
division=0.001 (.1%)
recovery

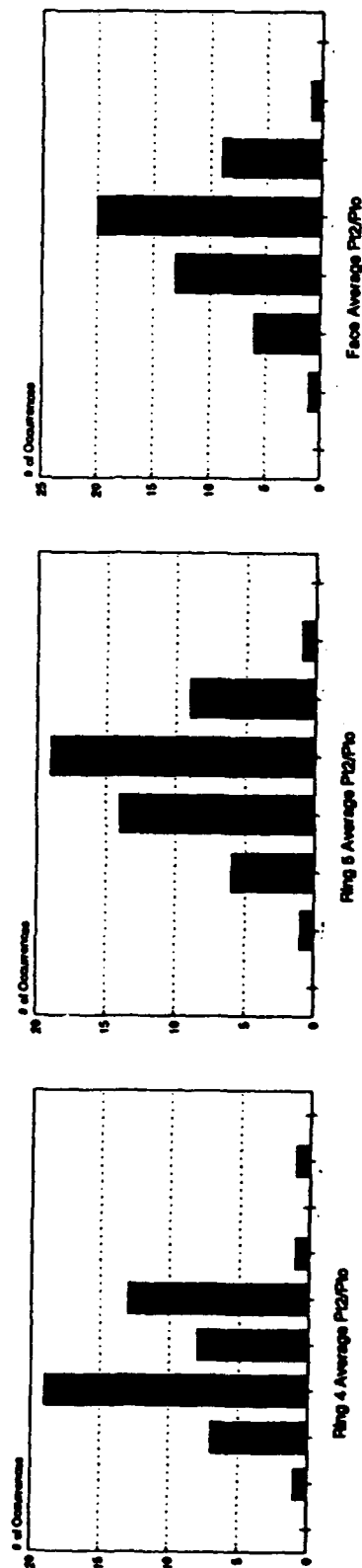
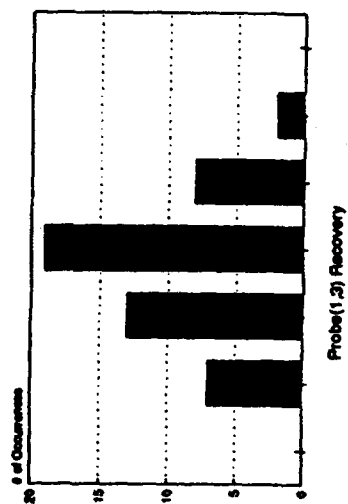
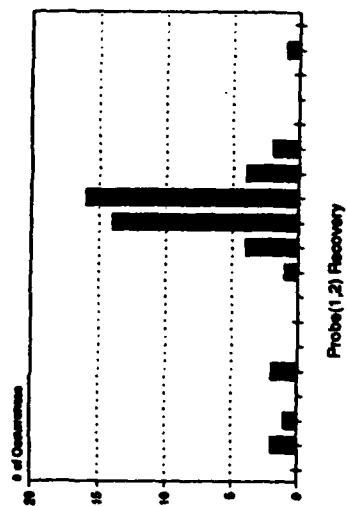


Figure 93. WT603.4 Dynamic Ring and
Face Average Recovery Distributions

Prob(1,1) Recovery	p of Consensus
0	14.5
2	12.5
4	10.5
6	9.5
8	8.5
10	7.5
12	6.5
14	5.5
16	4.5



**Smallest X-axis
division=0.001 (.1%)
recovery**

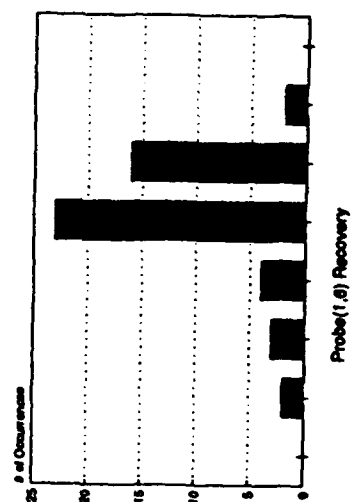
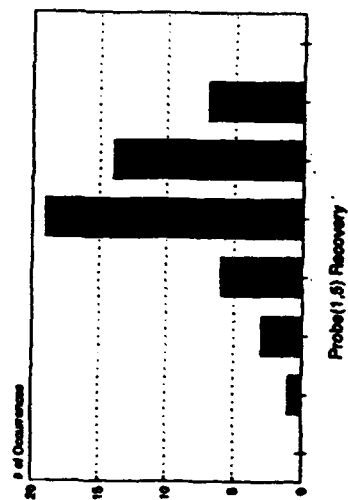
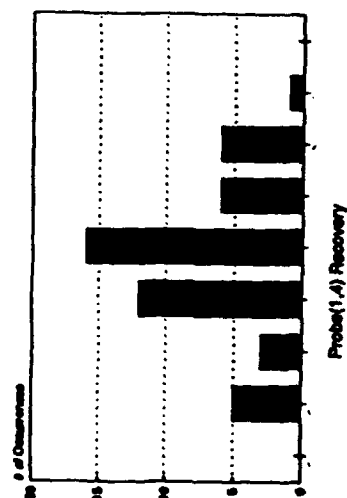
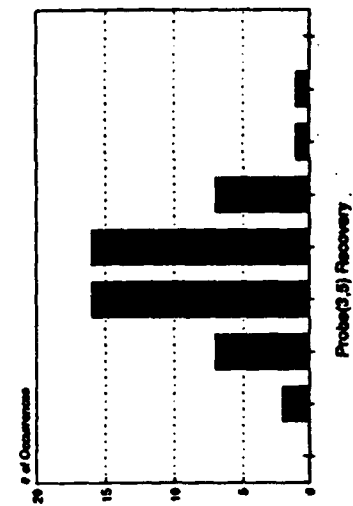
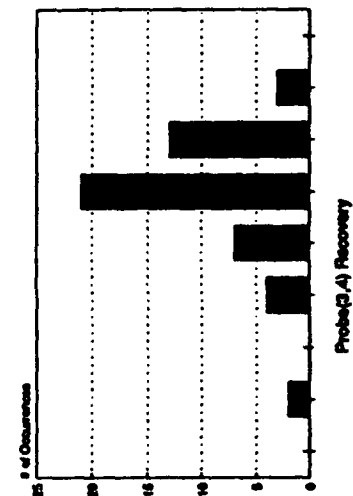
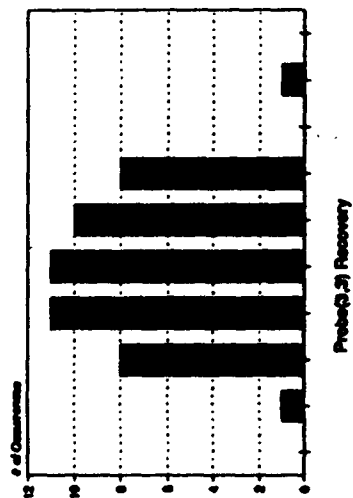


Figure 94. WT603.4 Probe Recovery Distributions

Figure 94. (Continued)



Smallest X-axis
division=0.001 (.1%)
recovery

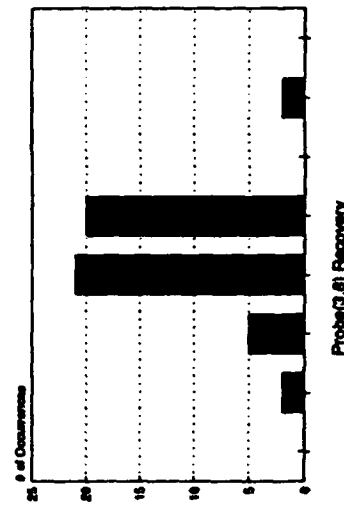
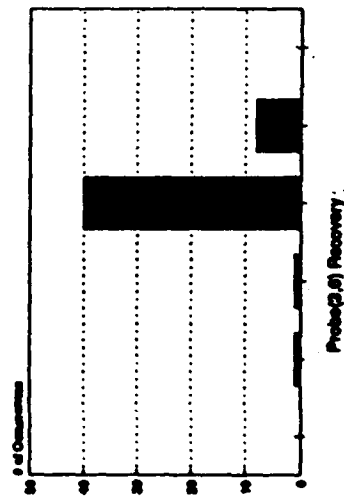
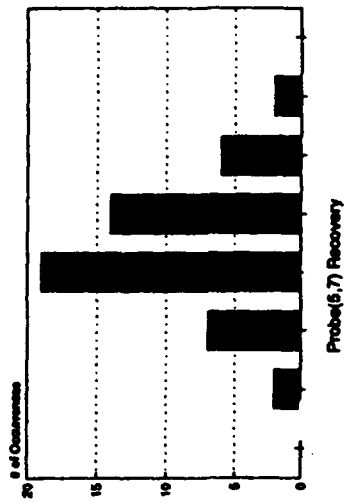
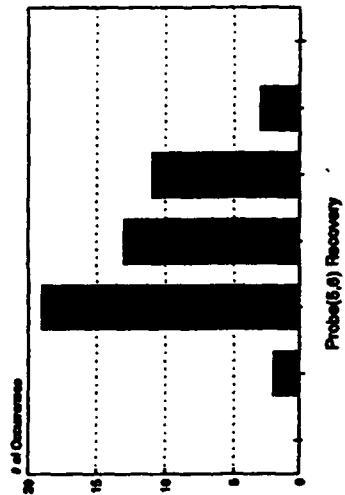
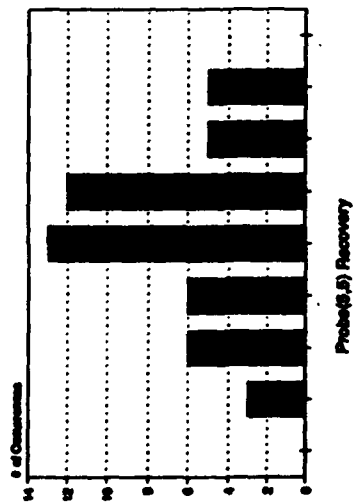
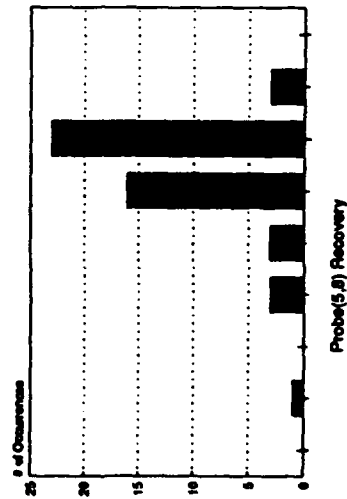


Figure 94. (Continued)



Smallest X-axis
division=0.001 (.1%)
recovery



WT603.4 1419 Indices
PcP Intensity Distributions

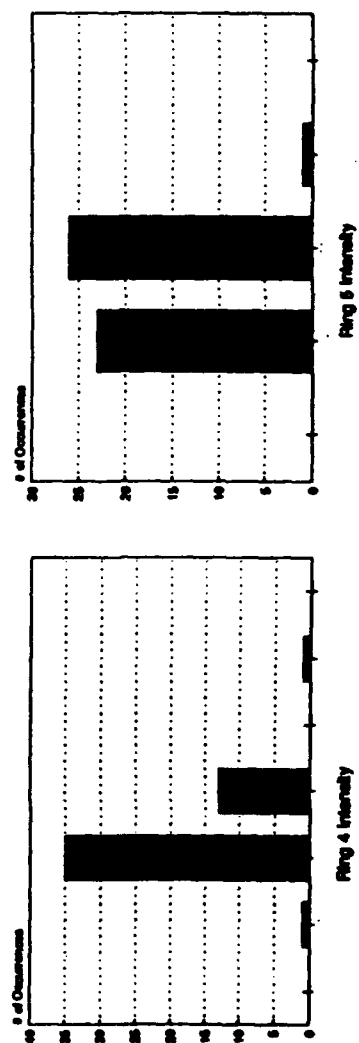
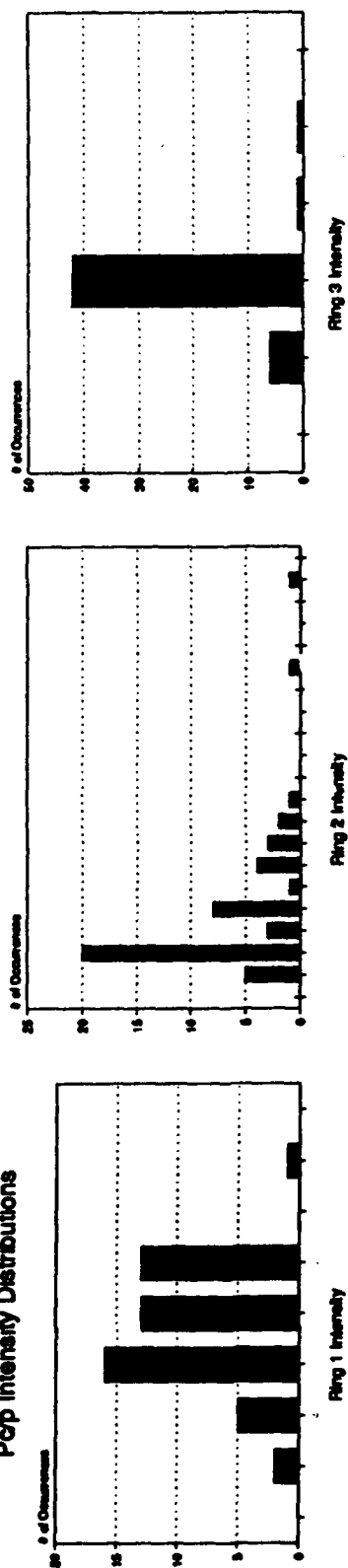


Figure 95. WT603.4 Δ Pc/P, Intensity Distributions

Figure 1 consists of three histograms arranged horizontally, each showing the distribution of the number of occurrences (Y-axis, 0 to 25) for a specific MPR (X-axis). The histograms are labeled 'Ring 1 MPR', 'Ring 2 MPR', and 'Ring 3 MPR' from left to right.

- Ring 1 MPR:** The distribution is highly skewed towards 0 occurrences, with a peak at 0 (approximately 22 occurrences). There are smaller peaks at 1 (approximately 5 occurrences) and 2 (approximately 3 occurrences).
- Ring 2 MPR:** The distribution is more spread out, with a peak at 2 occurrences (approximately 22 occurrences). Other significant peaks are at 1 (approximately 18 occurrences) and 3 (approximately 15 occurrences).
- Ring 3 MPR:** The distribution is also spread out, with a peak at 2 occurrences (approximately 22 occurrences). Other significant peaks are at 1 (approximately 18 occurrences) and 3 (approximately 15 occurrences).

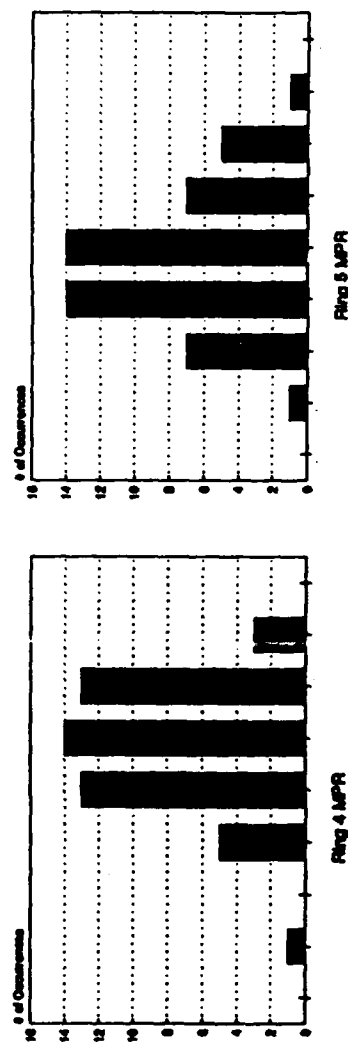


Figure 96. WT603.4 MPR Distributions

WT603.4 1419 Indices Extent Distributions

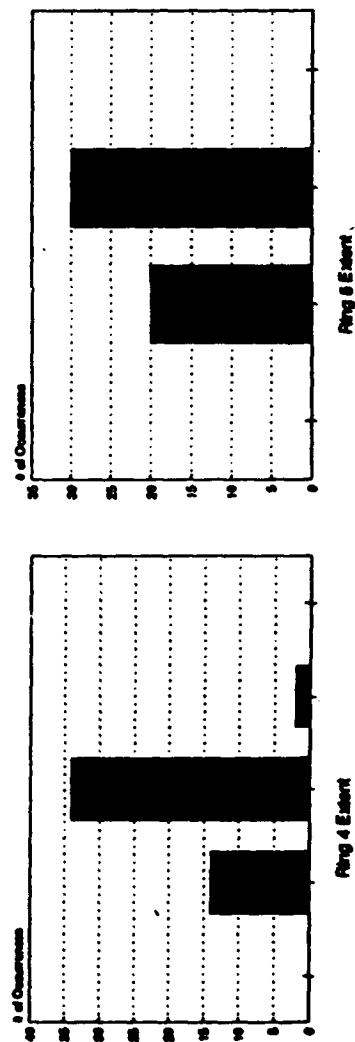
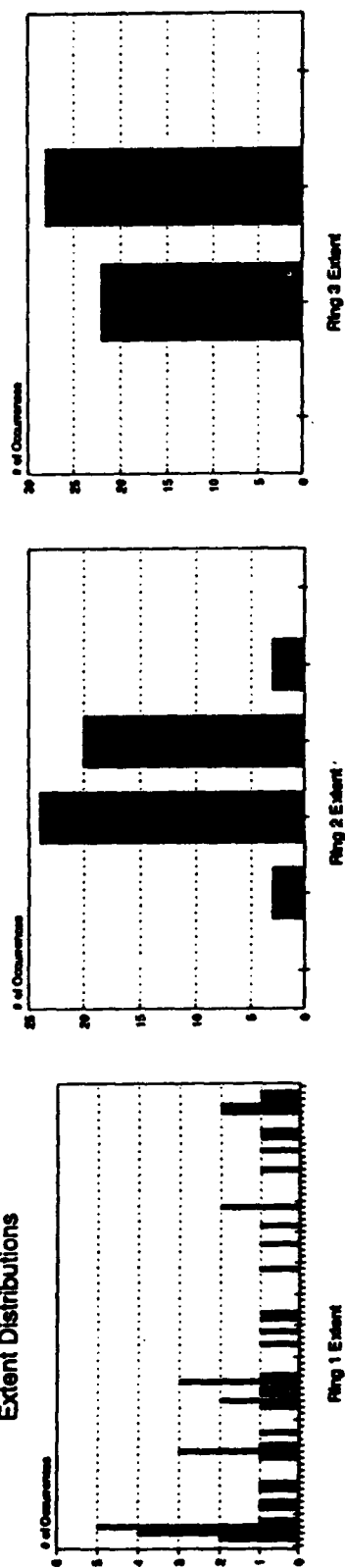


Figure 97. WT603.4 Extent Distributions

WT603.4 1419 Indice
Pr/P (IDR) Distributions

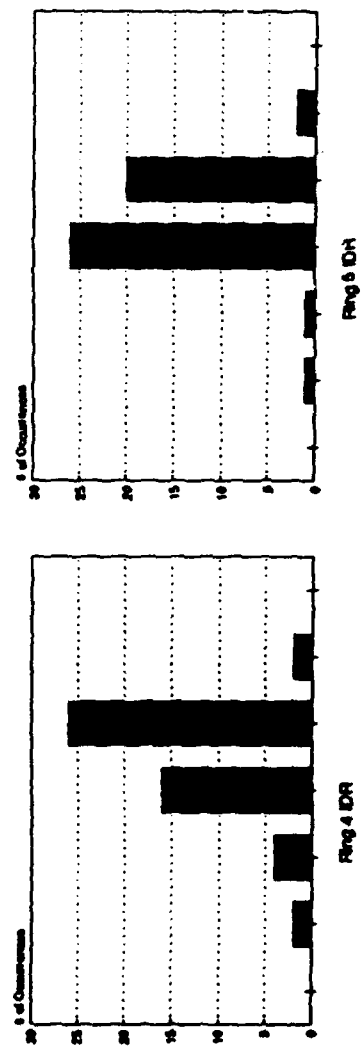
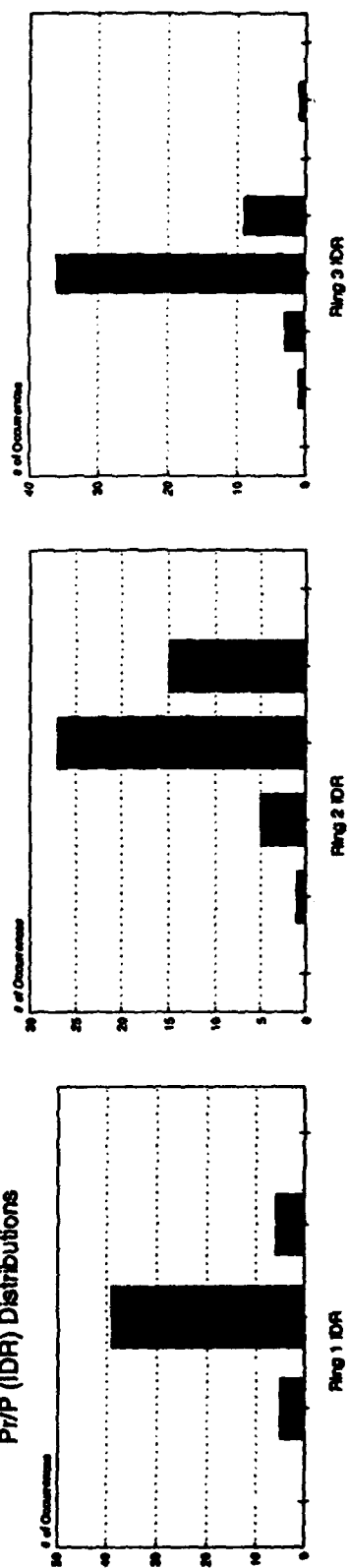


Figure 98. WT603.4 Δ Pr/P, IDR
Distributions

FJ14.148 Analog Parameter Distributions

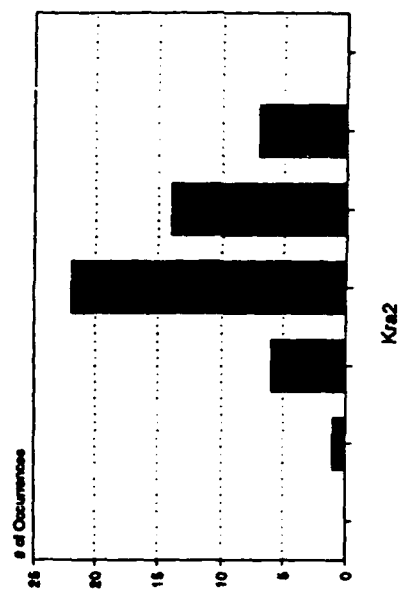
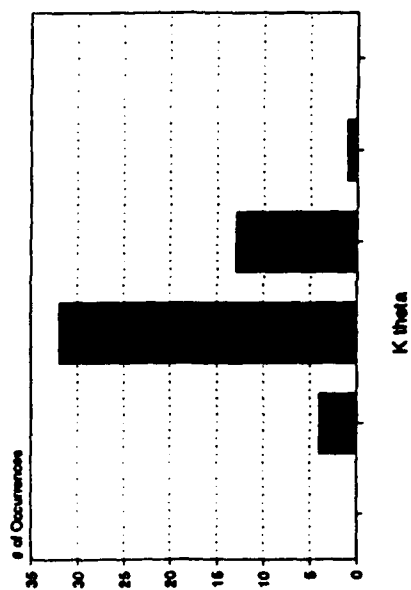
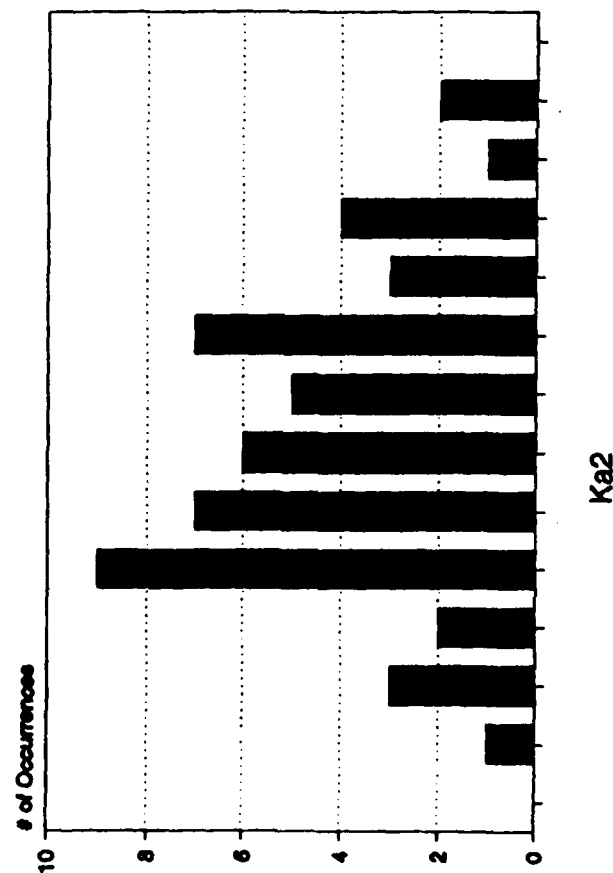


Figure 99. FJ14.148 Analog Parameter Distributions

FJ14.148 Digital Parameter Distributions

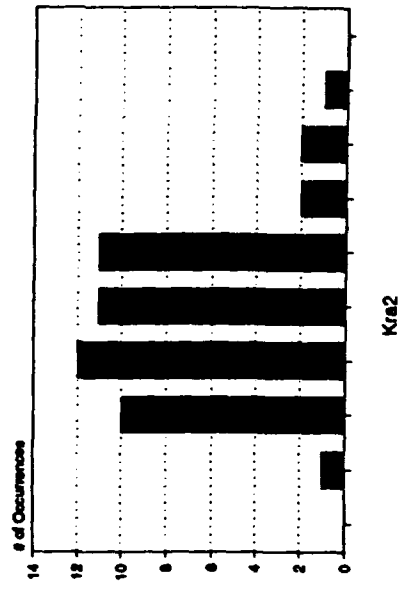
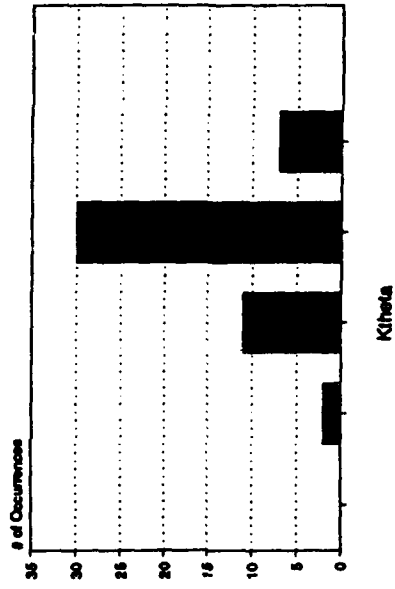
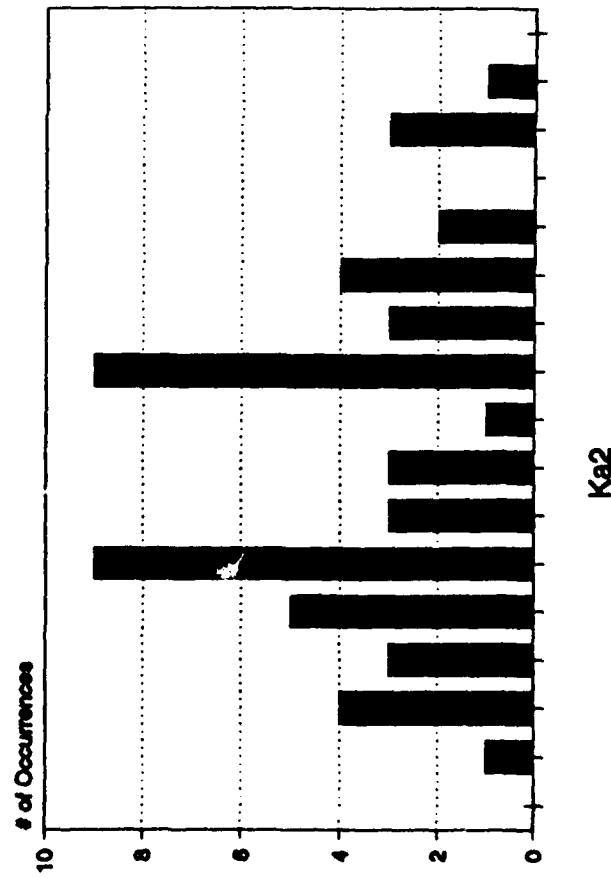


Figure 100. FJ14.148 Digital Parameter Distributions

FJ14.148 Dynamic Ring & Face Average Recovery (P_{12}/P_{10}) Distributions

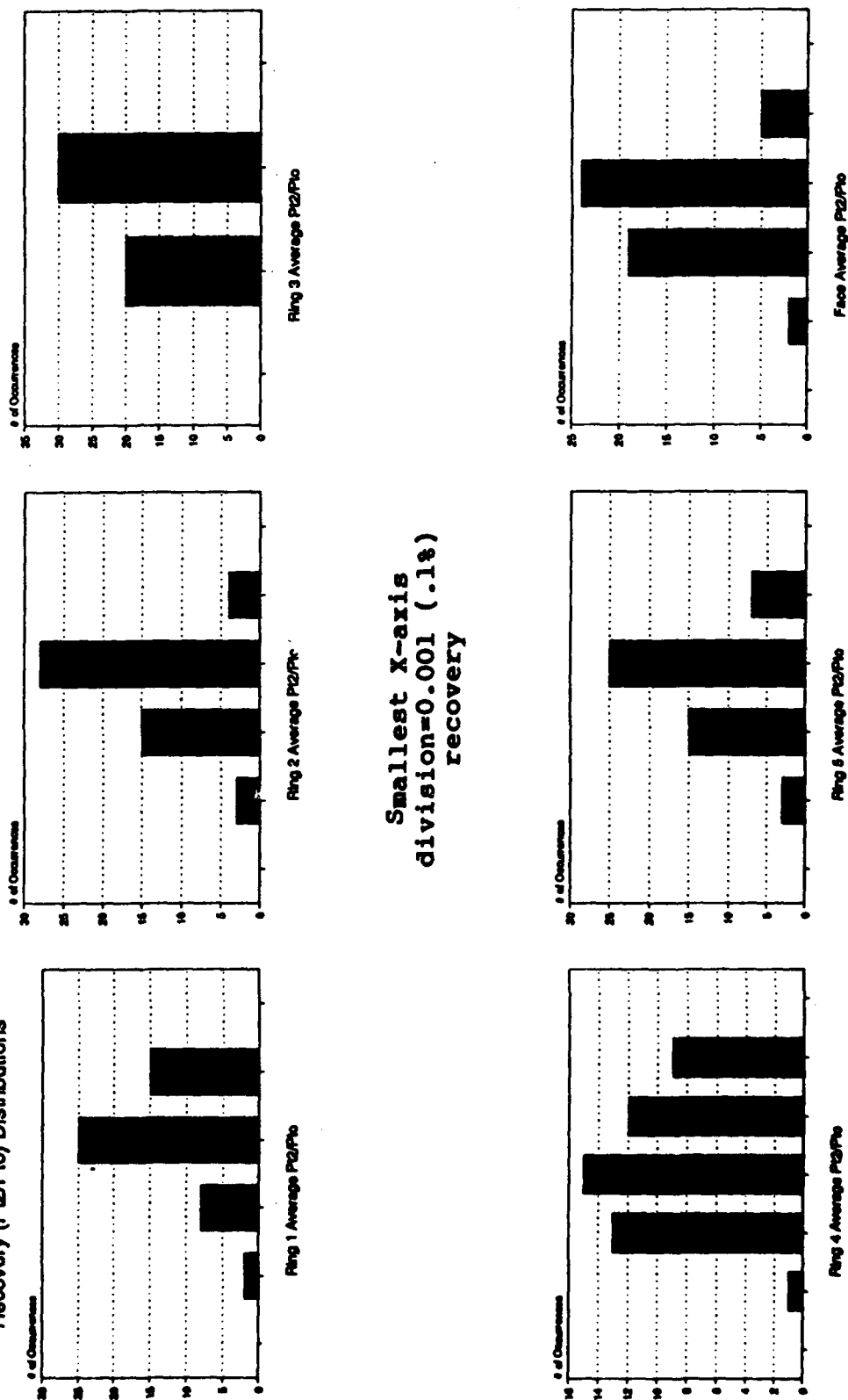


Figure 101. FJ14.148 Dynamic Ring and Face Average Recovery Distributions

FJ14.148 Probe Recovery Distributions

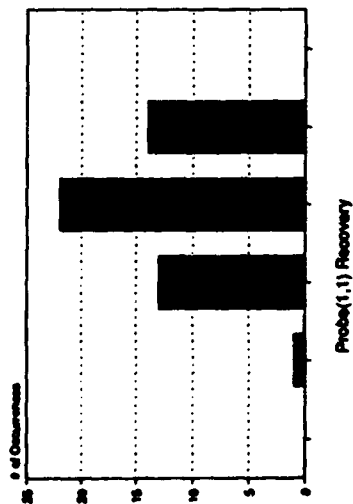
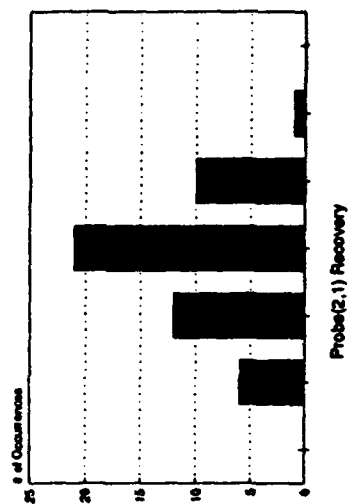
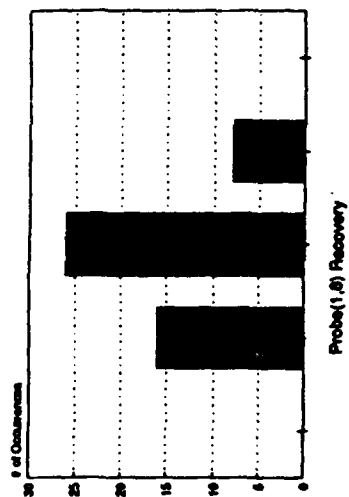
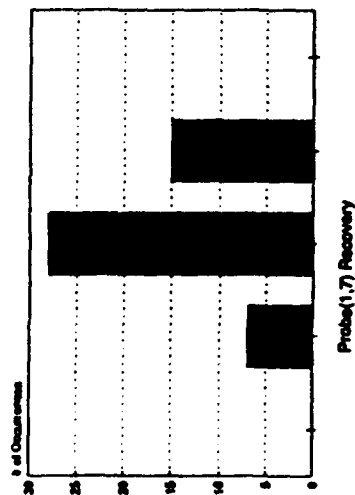


Figure 102. (Continued)



Smallest X-axis
division=0.001 (.1%)
recovery

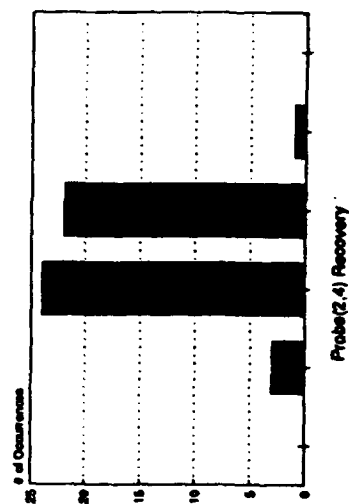
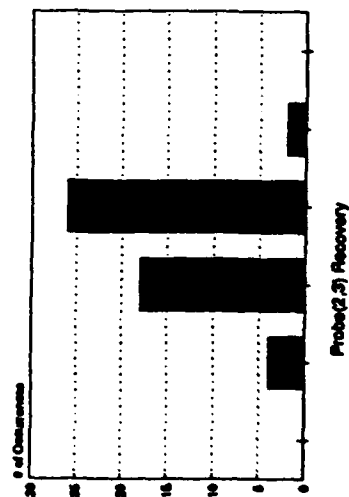
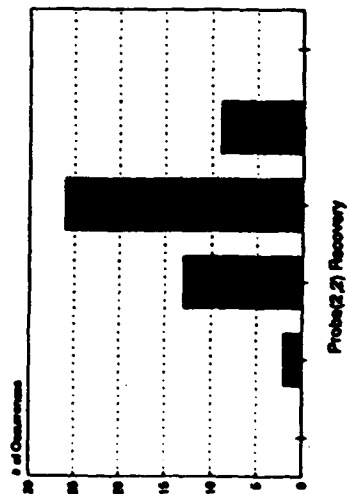
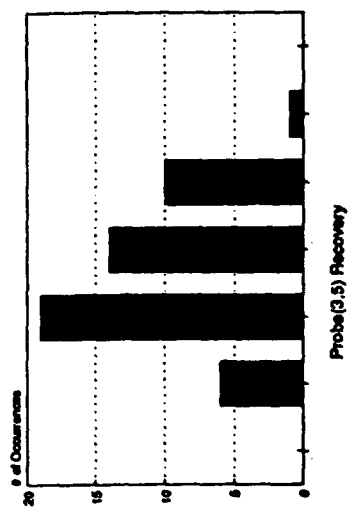
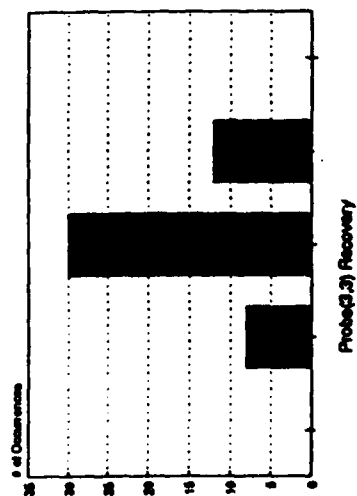


Figure 102. (Continued)



Smallest X-axis
division=0.001 (.1%)
recovery

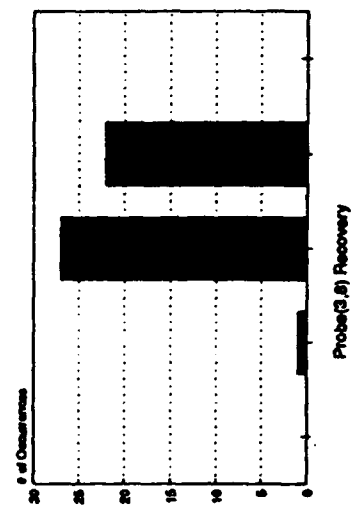
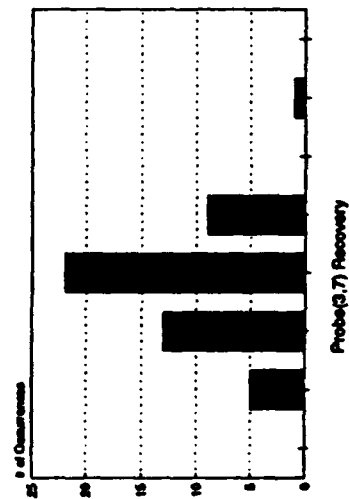
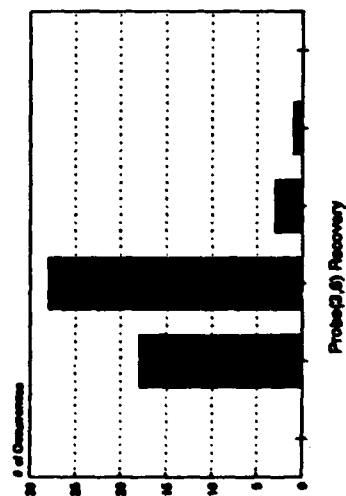
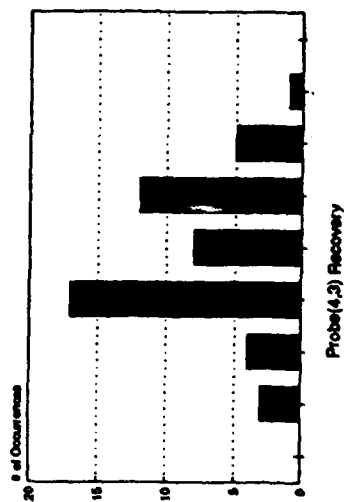
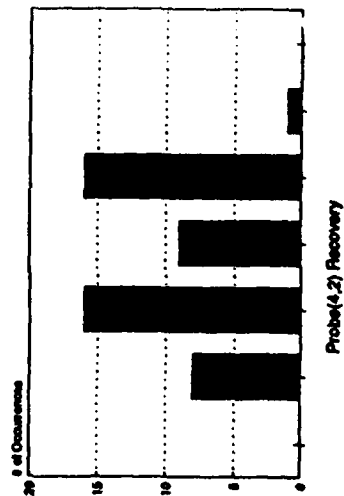
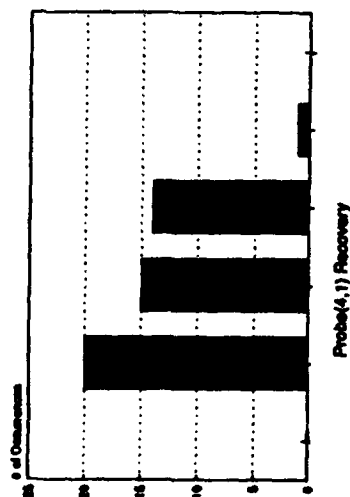


Figure 102. (Continued)



Smallest X-axis
division=0.001 (.1%)
recovery

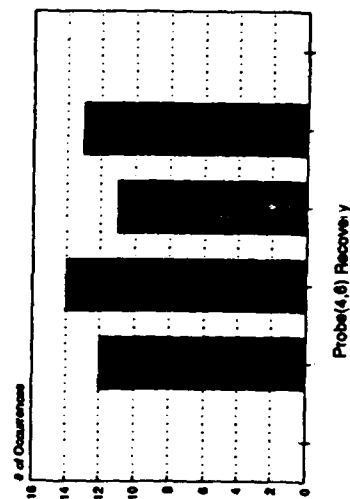
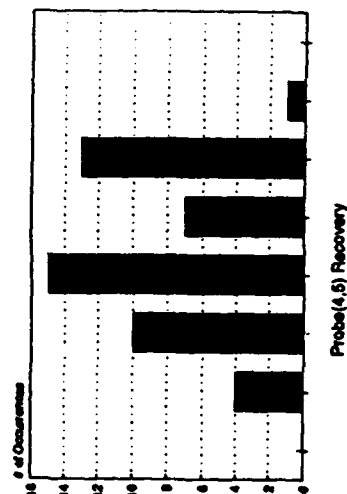
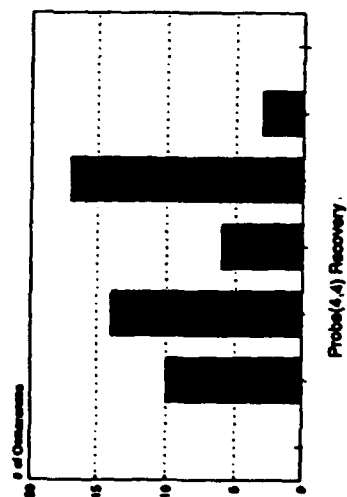
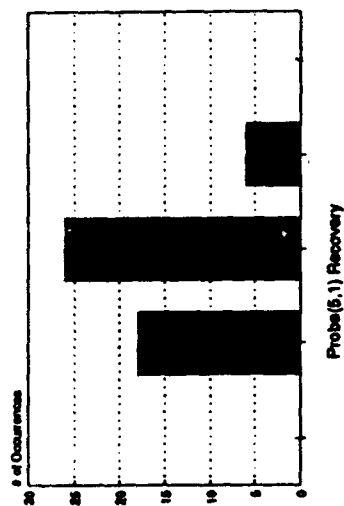
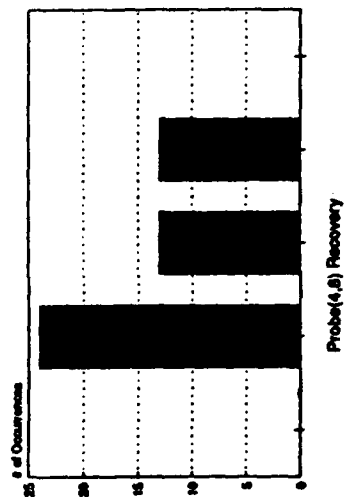
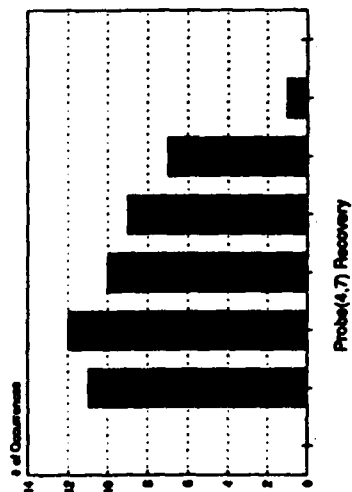


Figure 102. (Continued)



Smallest X-axis
division=0.001 (.1%)
recovery

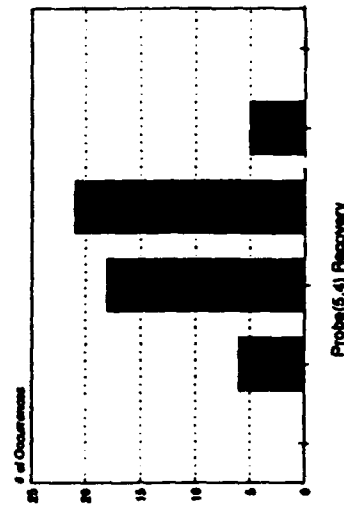
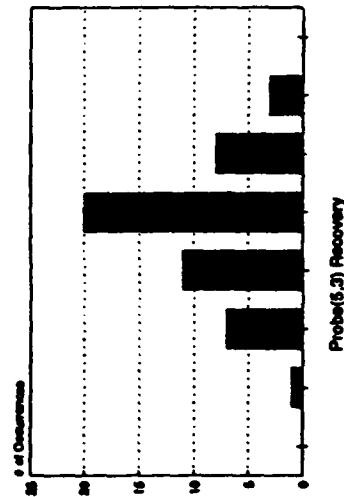
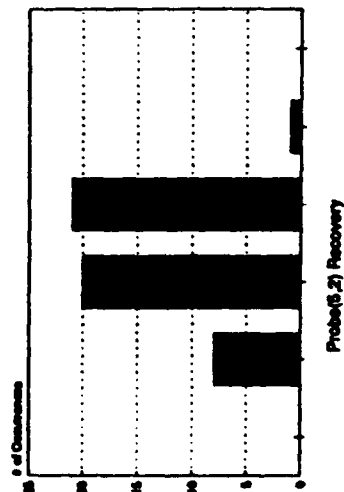
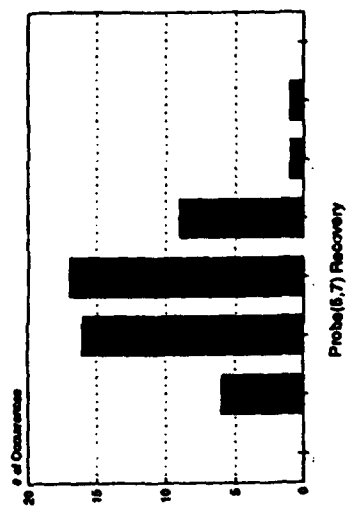
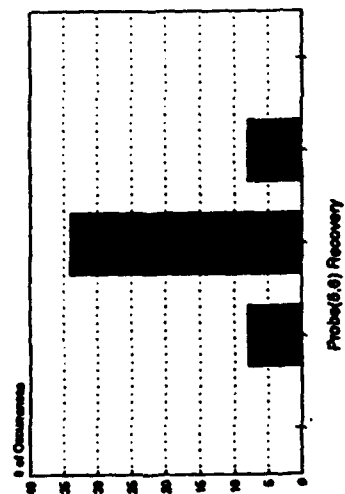
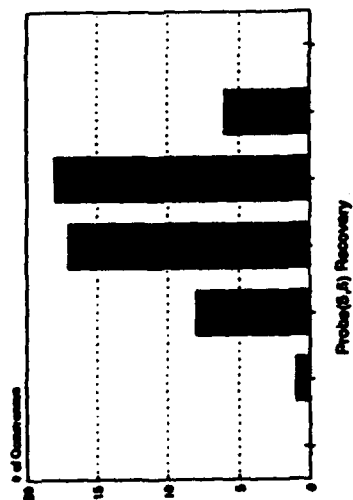
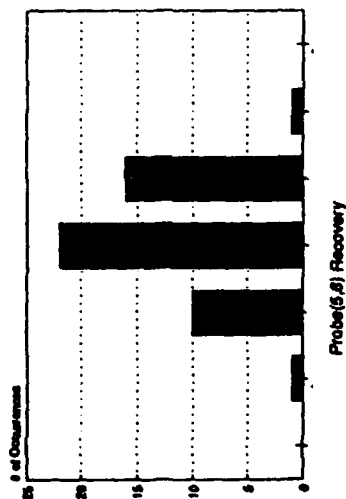


Figure 102. (Continued)



Smallest X-axis
division=0.001 (.1%)
recovery



FJ14.148 1419 Indices Pc/p Intensity Distributions

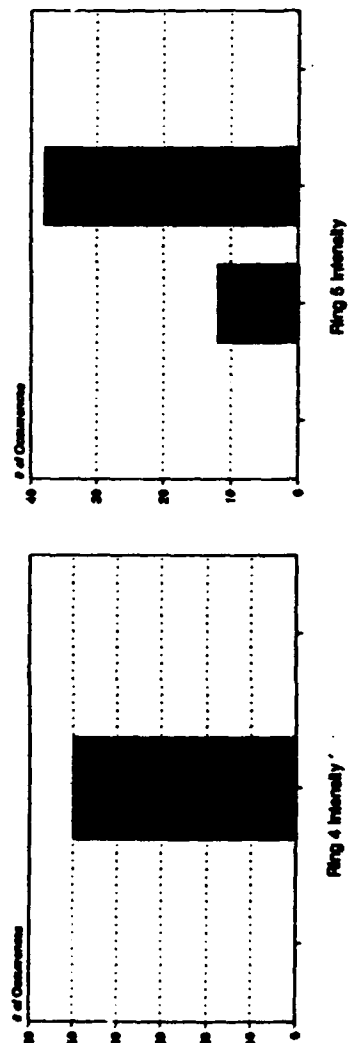
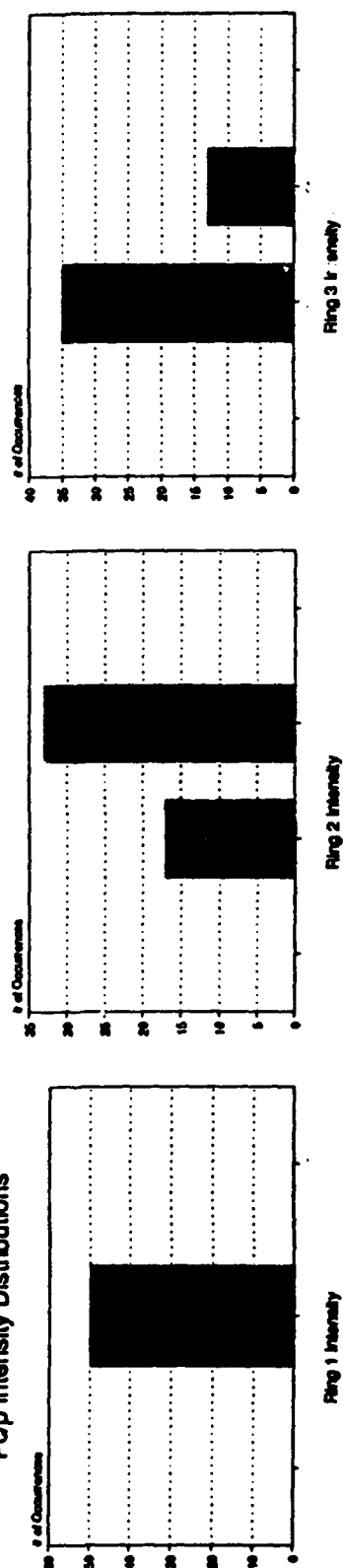


Figure 103. FJ14.148 Δ Pc/P, Intensity Distributions

FJ14.148 1419 Indices
Multiple Per Rev (MPR) Distributions

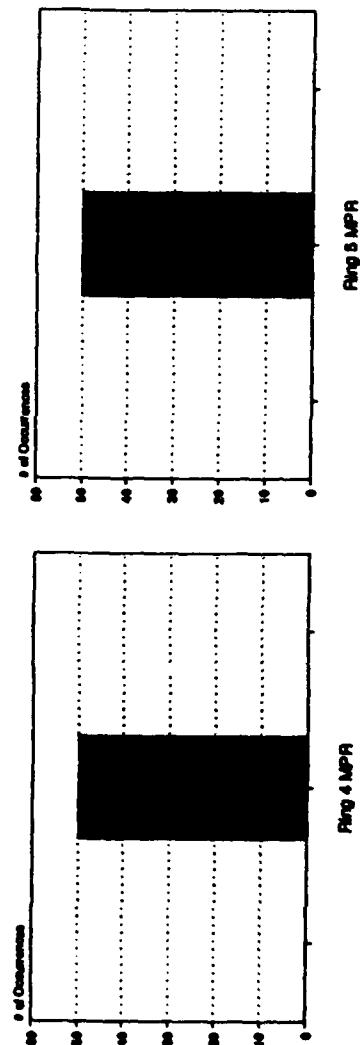
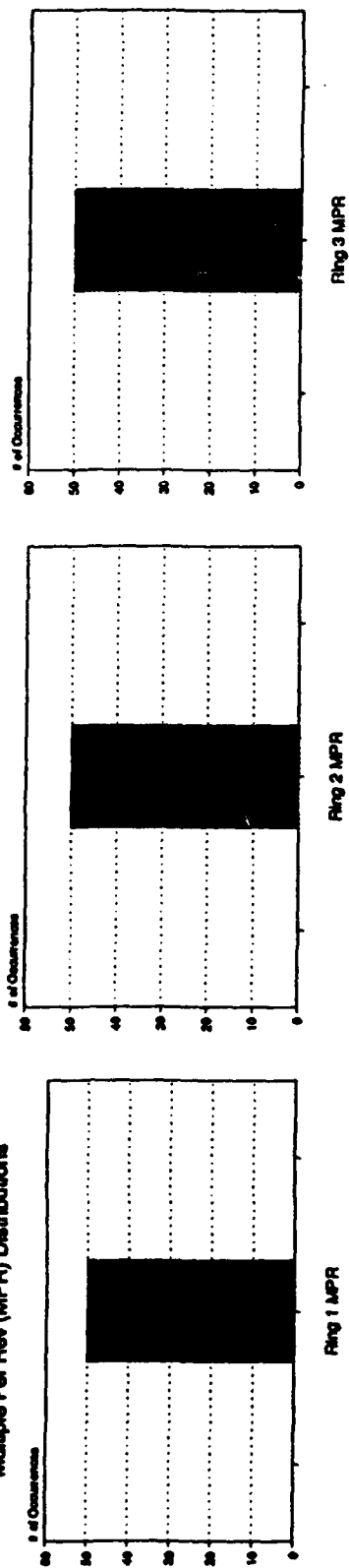


Figure 104. FJ14.148 MPR
Distributions

FJ14.148 1419 Indices
Extent Distributions

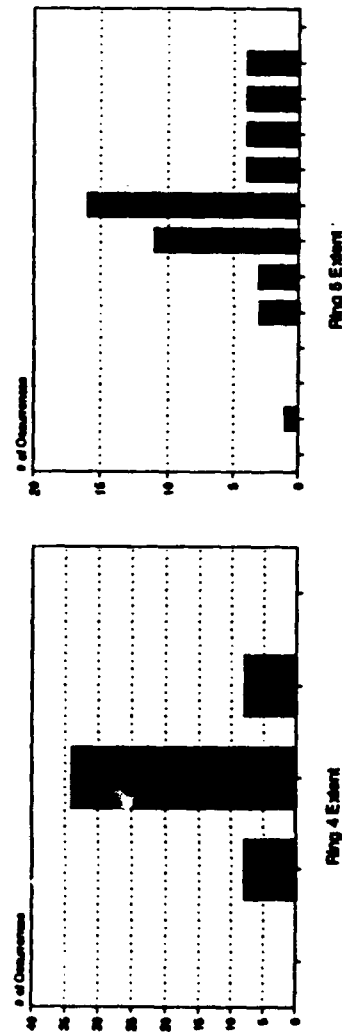
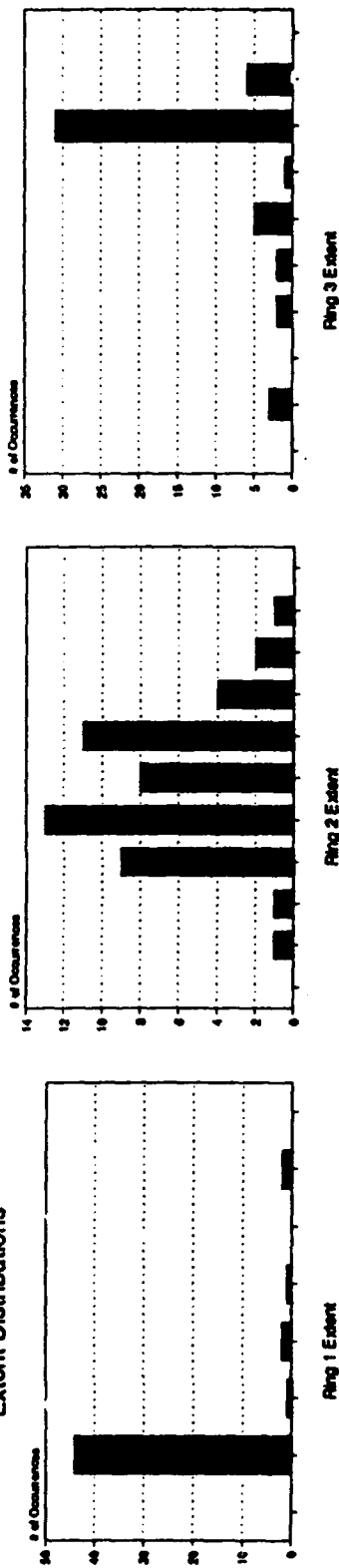


Figure 105. FJ14.148 Extent
Distributions

FJ14.148 1419 Index
P/P (IDR) Distributions

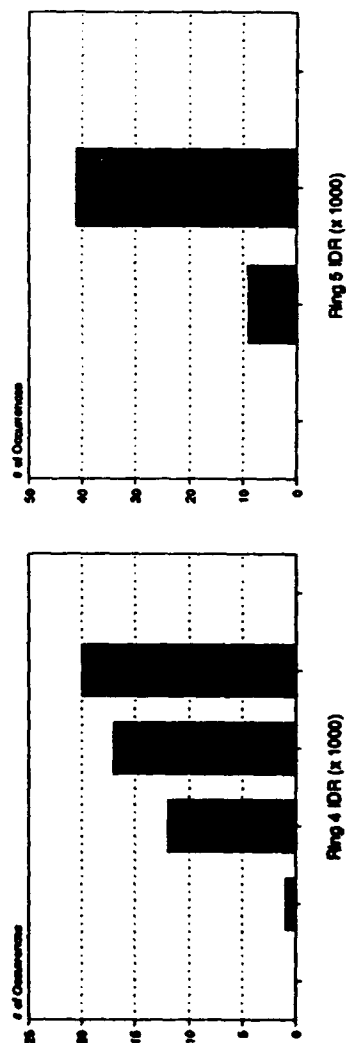
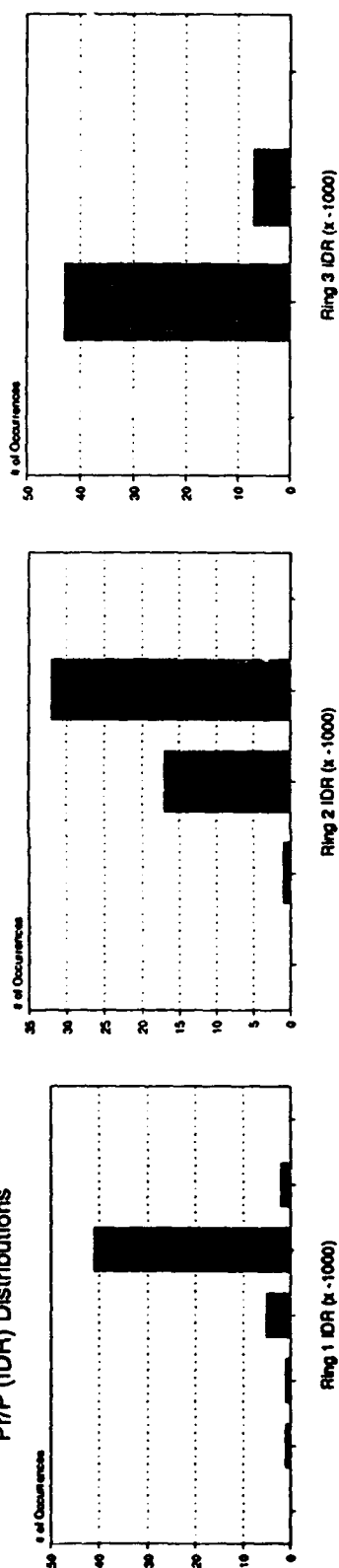


Figure 106. FJ14.148 Δ Pr/P, IDR
Distributions

WT563.4 Analog Parameter Distributions

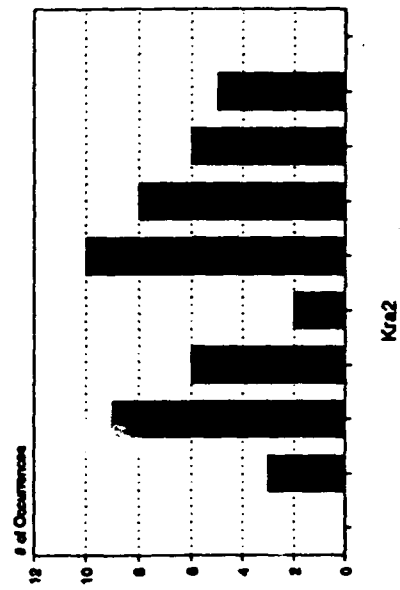
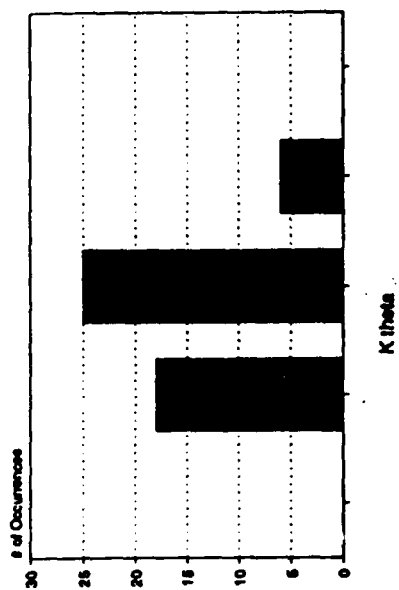
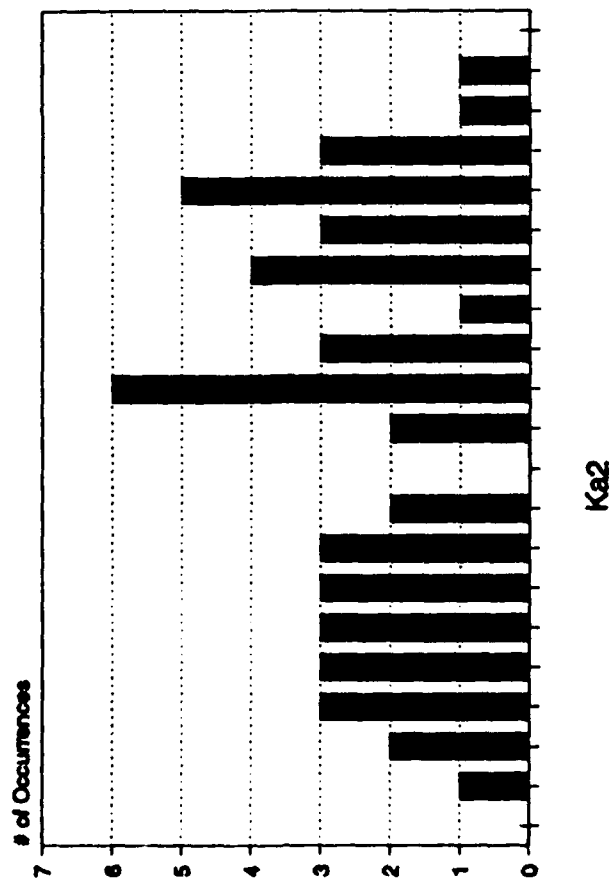


Figure 107. WT563.4 Analog Parameter Distributions

WT563.4 Digital Parameter Distributions

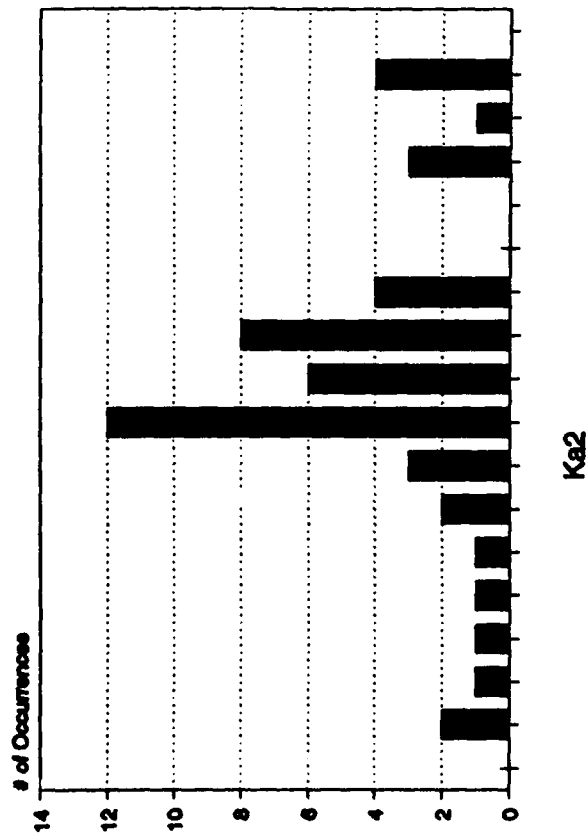
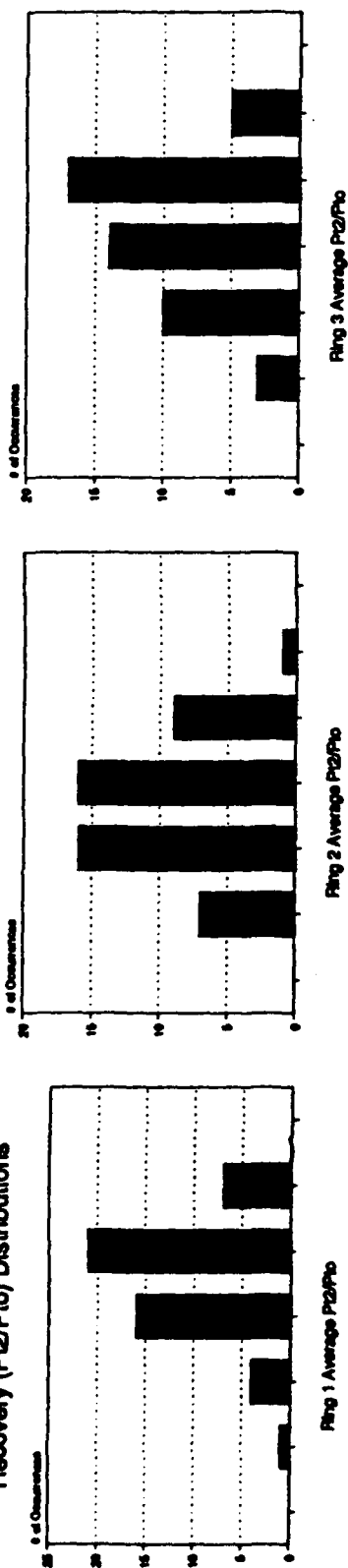


Figure 108. WT563.4 Digital Parameter Distributions

WT563.4 Dynamic Ring & Face Average
Recovery (P12/P10) Distributions



Smallest X-axis
division=0.001 (.1%)
recovery

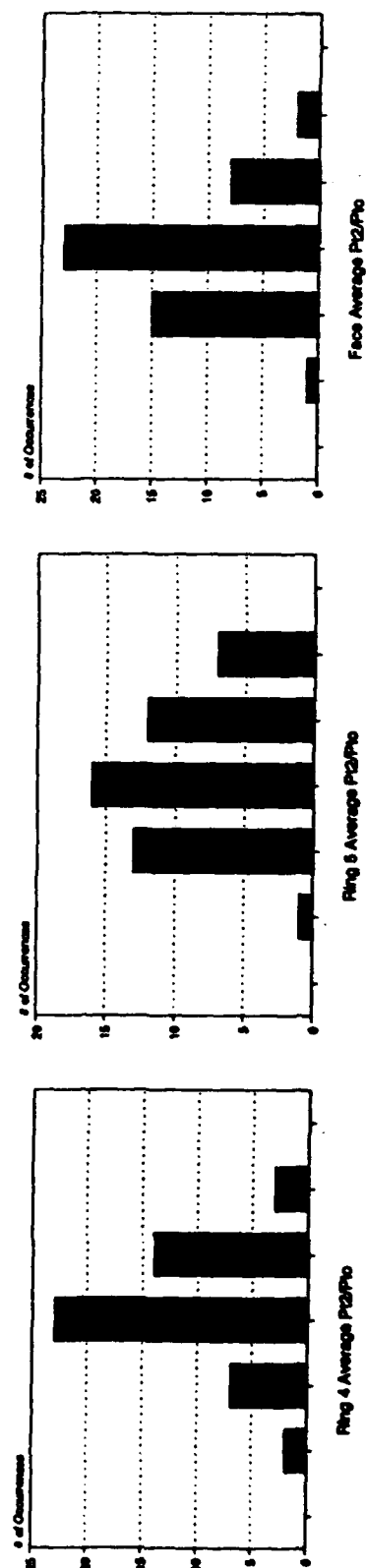
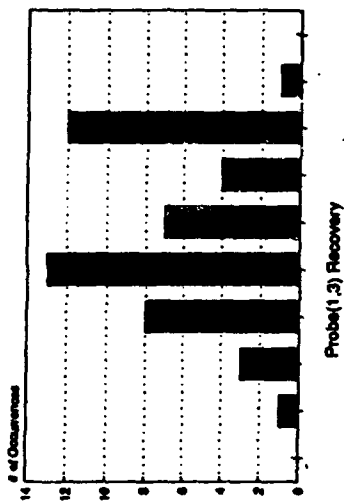
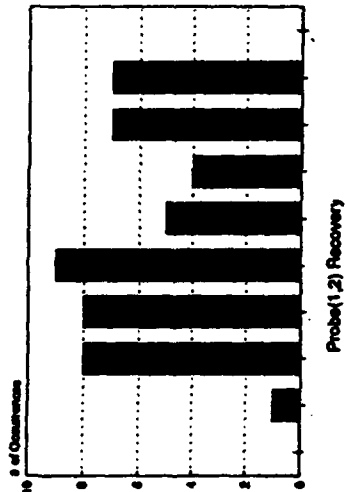
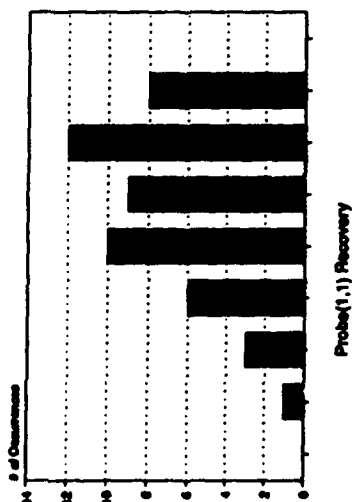


Figure 109. WT563.4 Dynamic Ring and
Face Average Recovery Distributions

WT563.4 Probe Recovery Distributions



Smallest X-axis
division=0.001 (.1%)
recovery

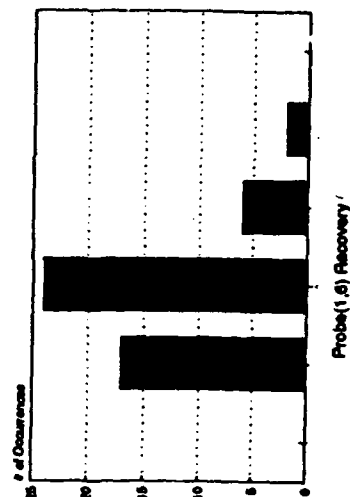
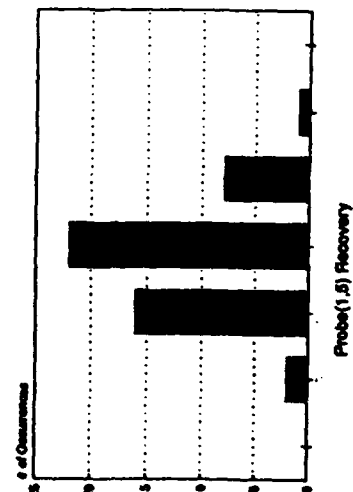
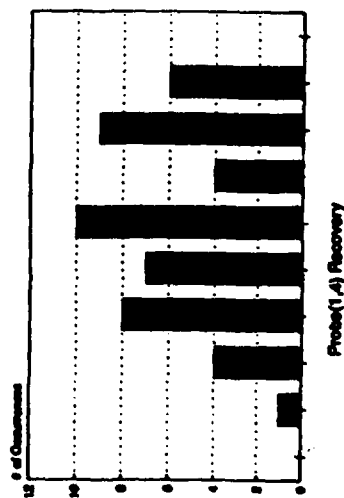
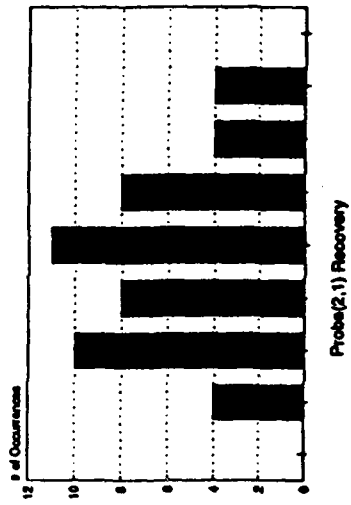
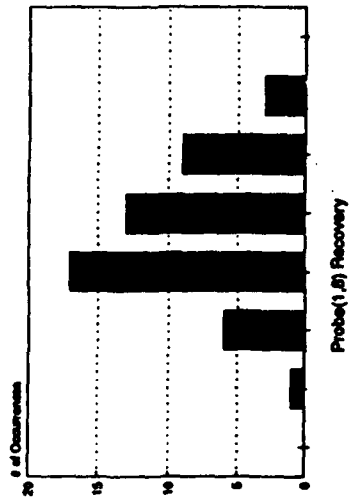
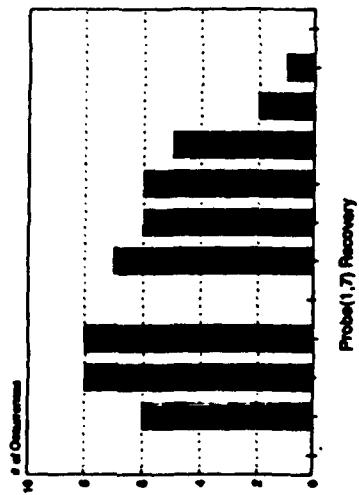


Figure 110. WT563.4 Probe Recovery Distributions

Figure 110. (Continued)



Smallest X-axis
division=0.001 (.1%)
recovery

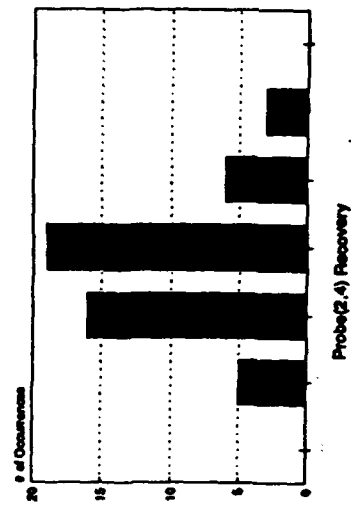
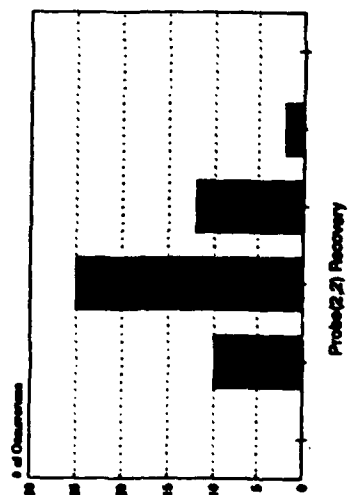
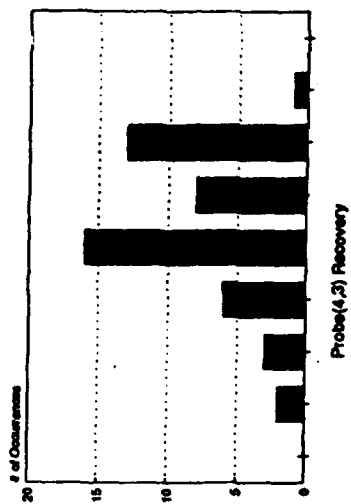
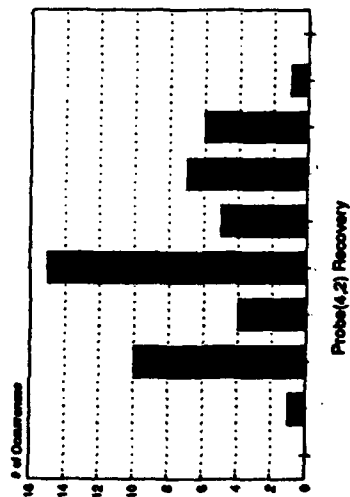
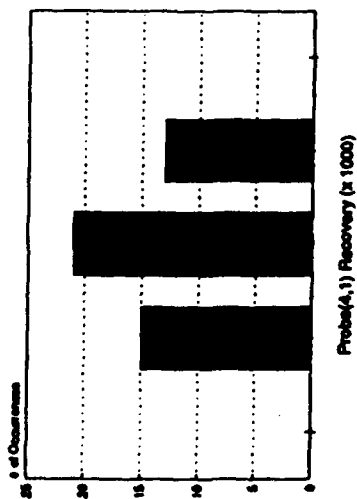


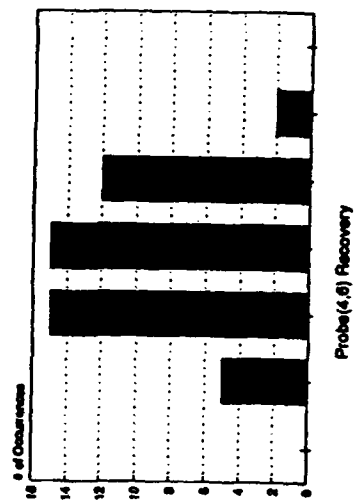
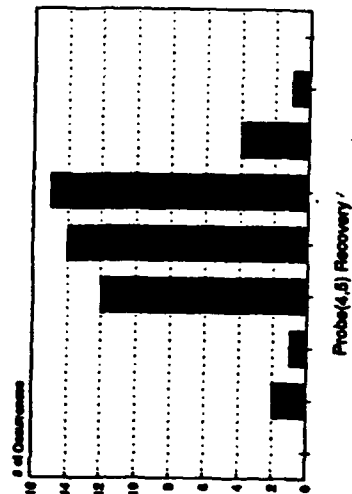
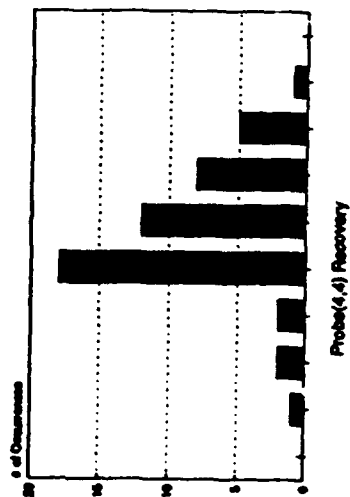
Figure 110. (Continued)



Figure 110. (Continued)



Smallest X-axis
division=0.001 (.1%)
recovery



WT563.4 1419 Indices
Pc/P Intensity Distributions

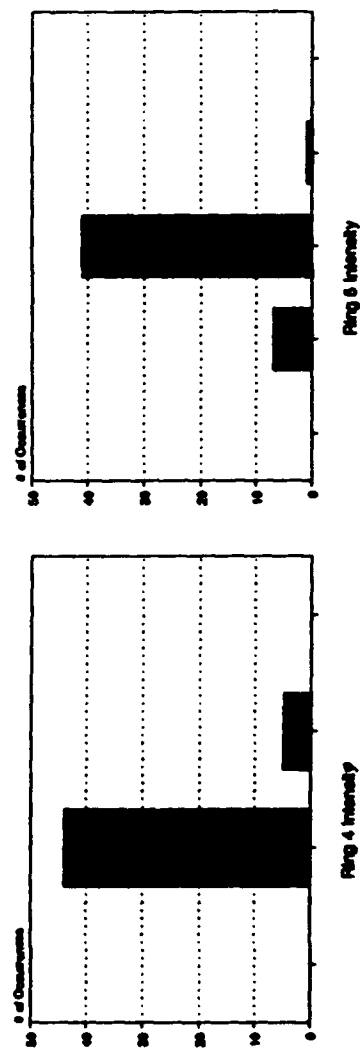
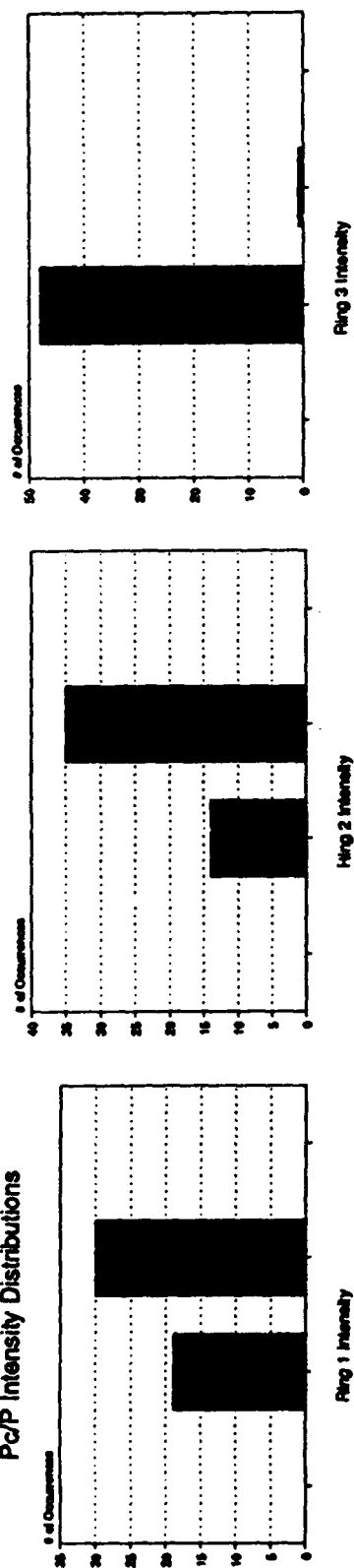


Figure 111. WT563.4 Δ Pc/P, Intensity Distributions

WT563.4 Dynamic 1419 Indices
Multiple Per Rev Distributions

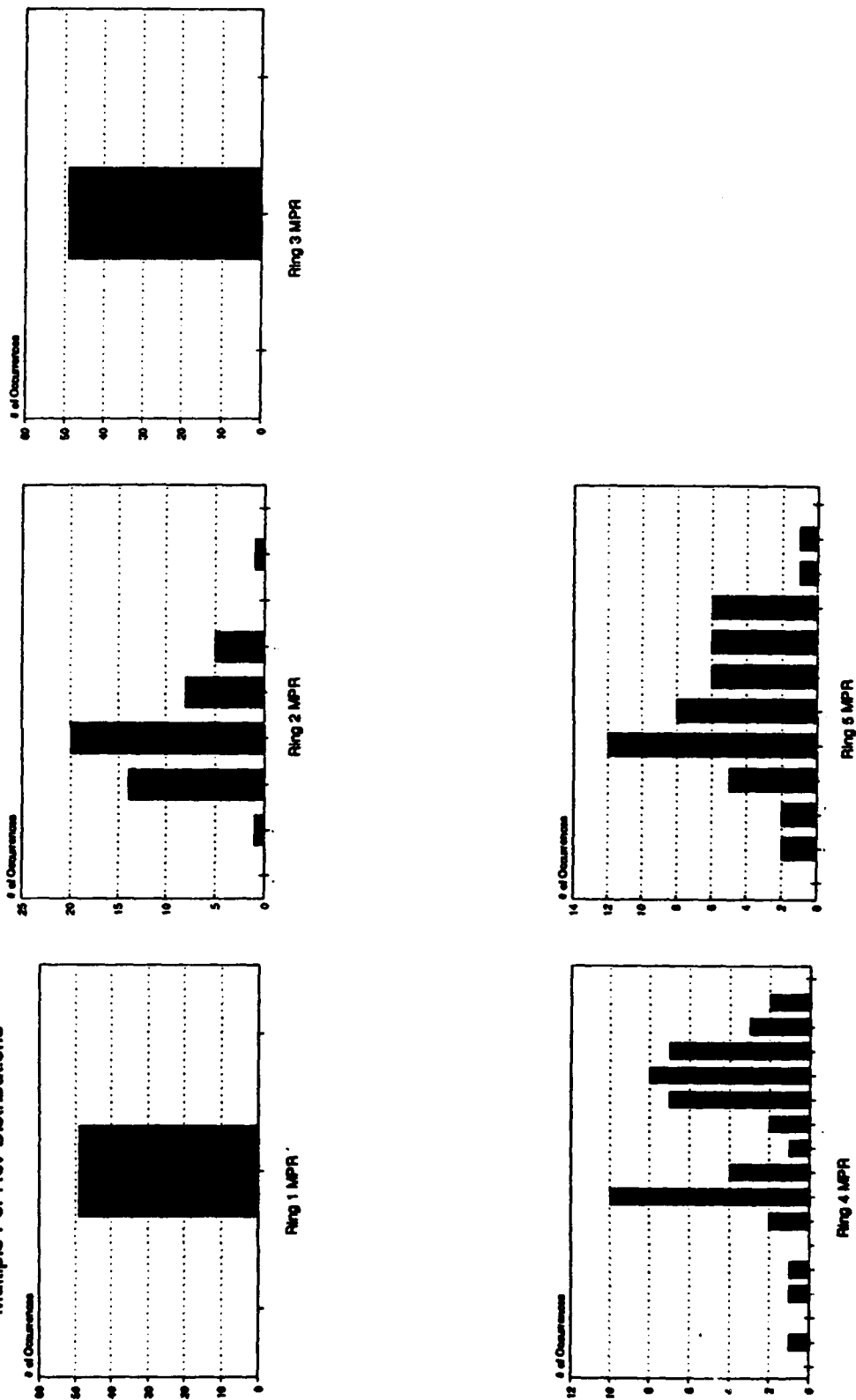
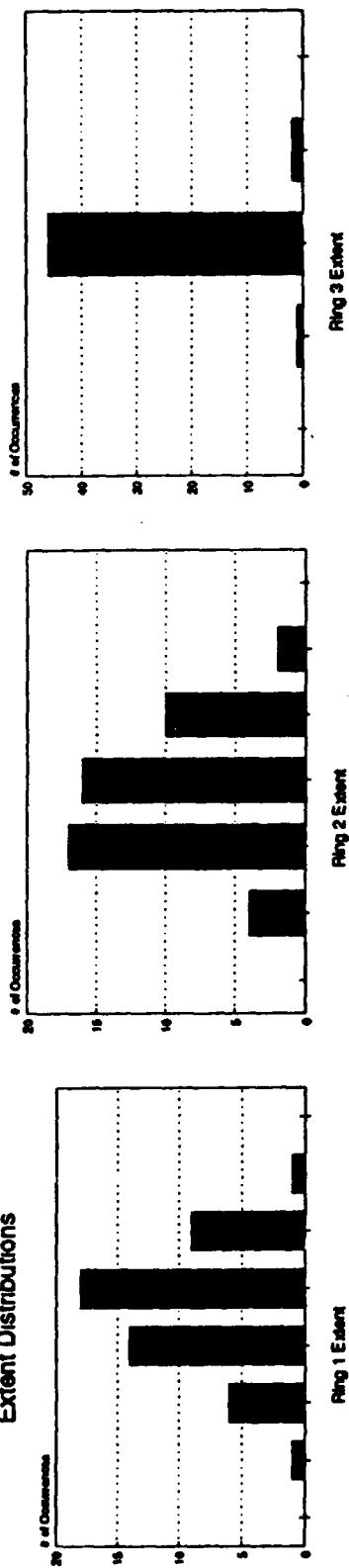


Figure 112. WT563.4 MPR Distributions

WT563.4 1419 Indices
Extent Distributions



WT563.4 1419 Indices
Pr/P (IDR) Distributions

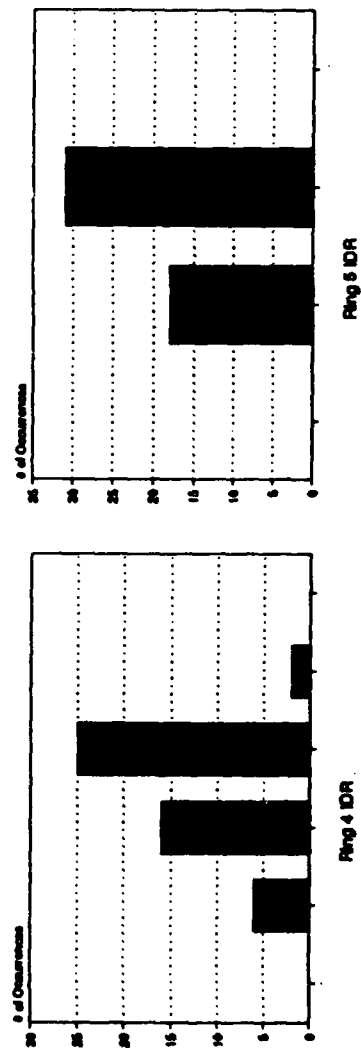
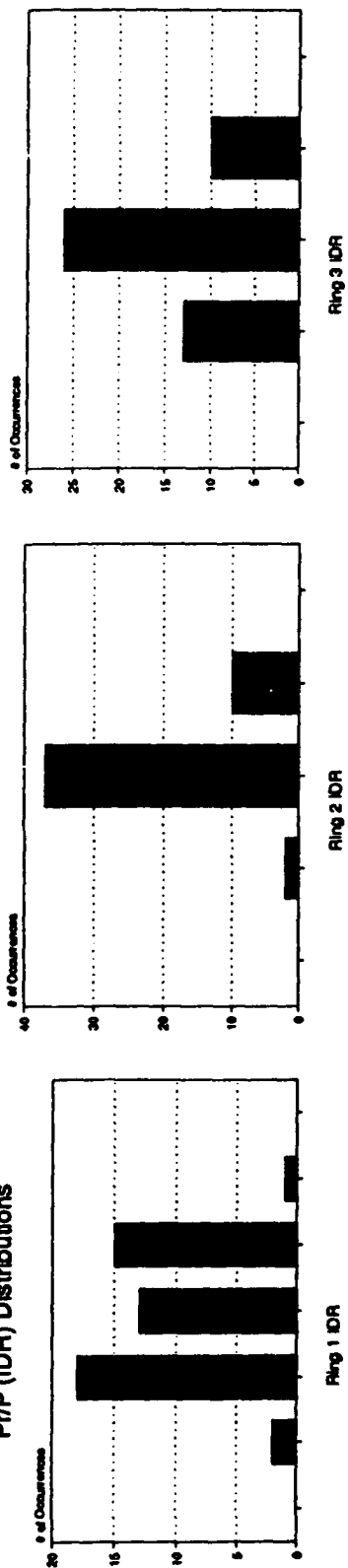


Figure 114. WT563.4 Δ Pr/P, IDR
Distributions

FJ59.022 Analog Parameter Distributions

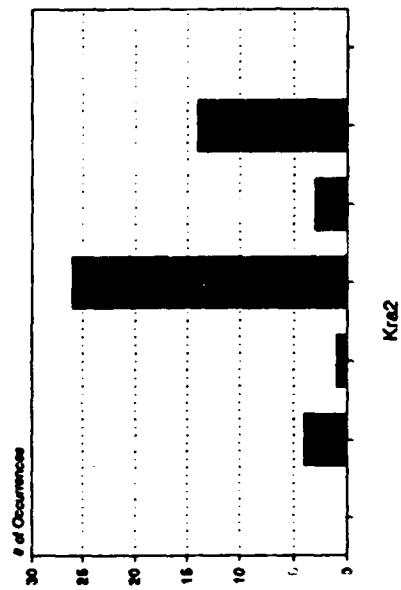
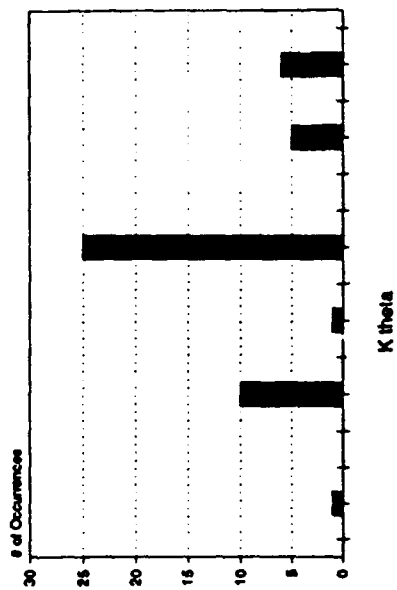
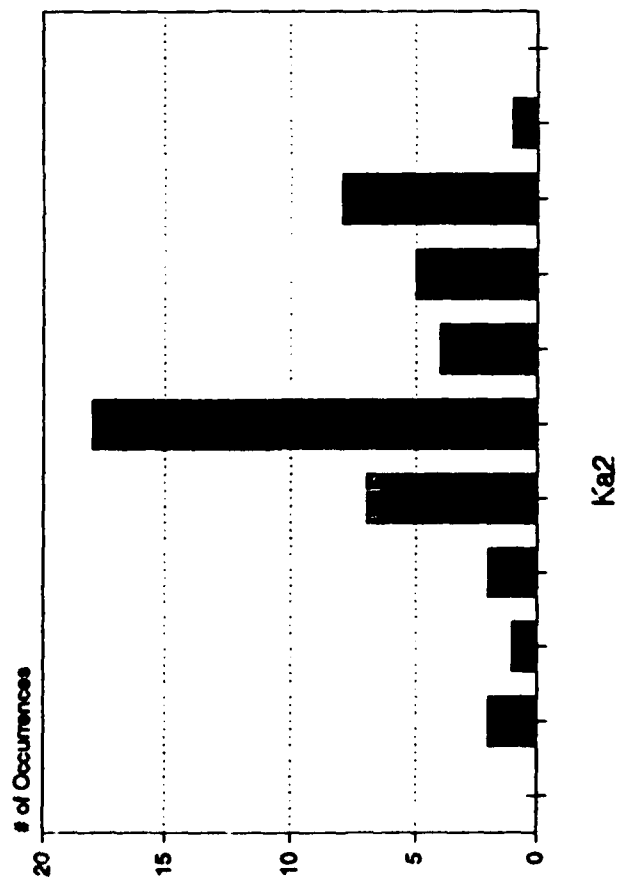


Figure 115. FJ59.022 Analog Parameter Distributions

FJ59.022 Digital Parameter Distributions

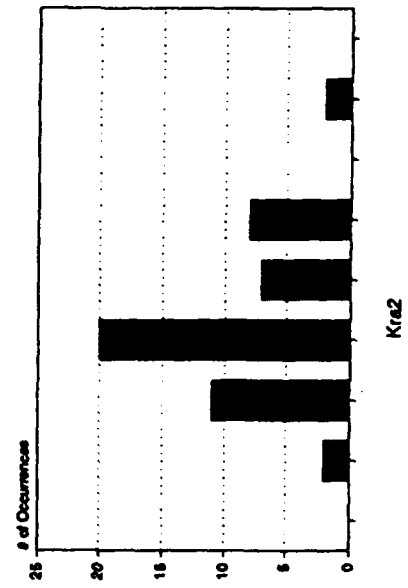
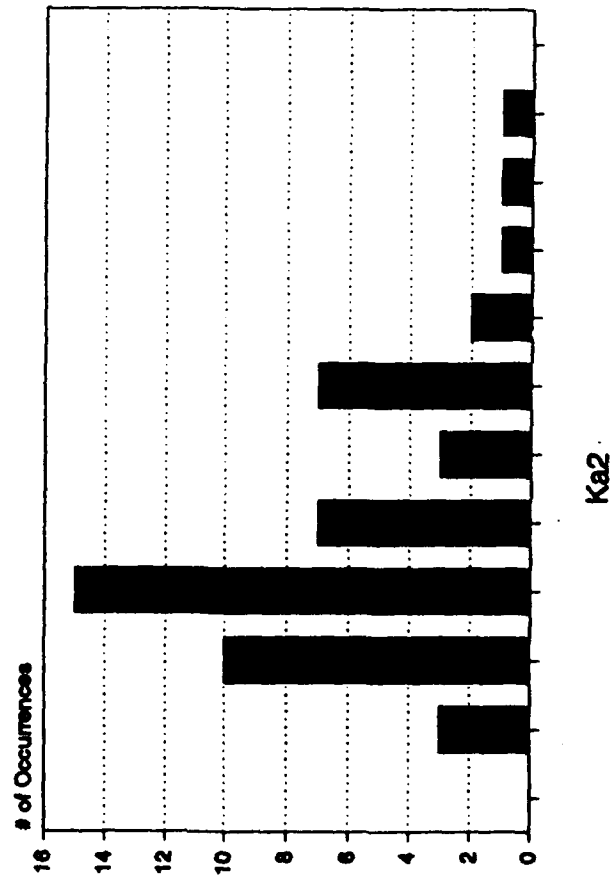
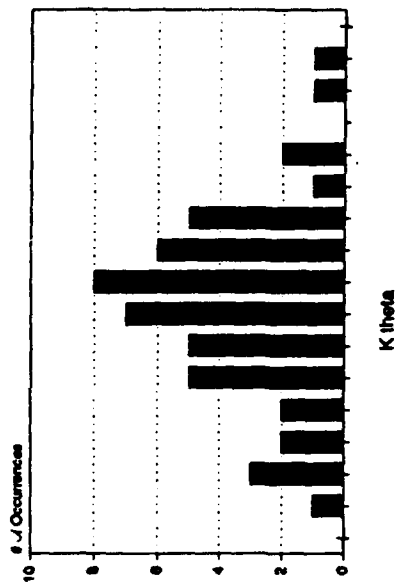
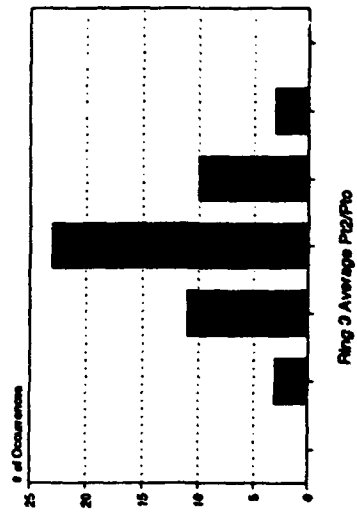
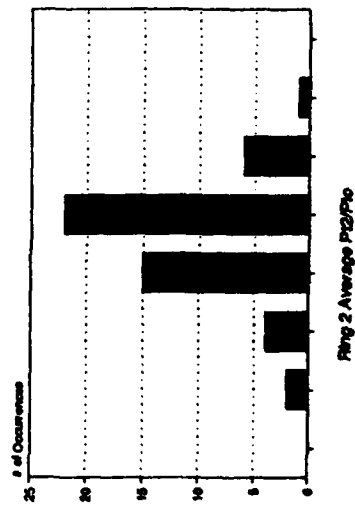
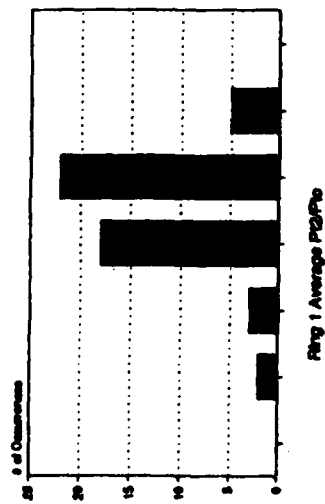


Figure 116. FJ59.022 Digital Parameter Distributions

FJ59.022 Dynamic Ring & Face Average Recovery (P_{12}/P_{10}) Distributions



Smallest X-axis
division=0.001 (.1%)
recovery

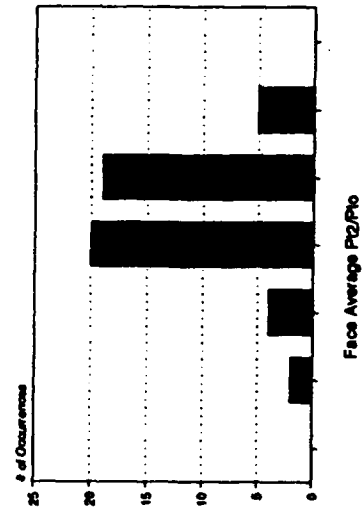
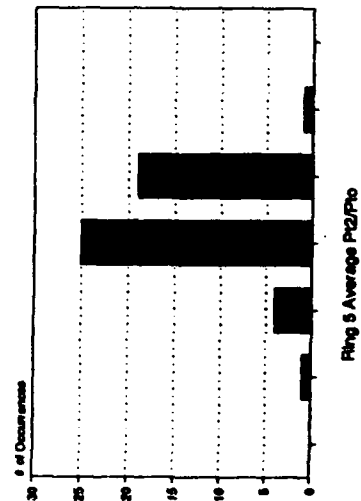
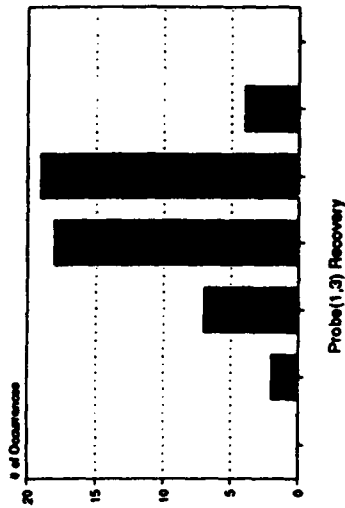
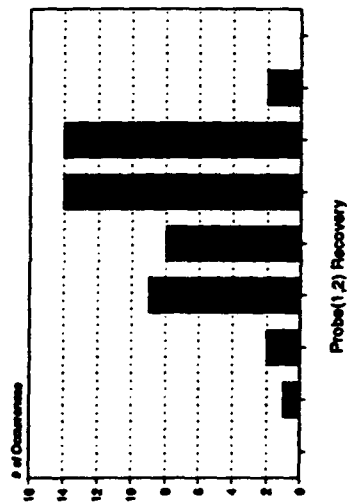
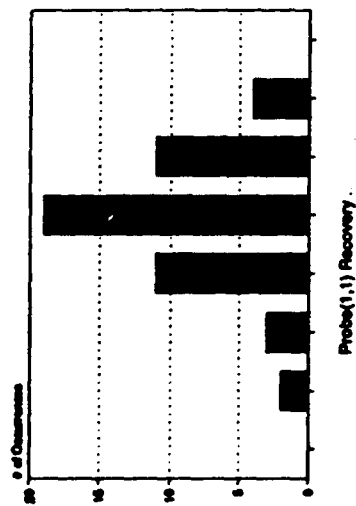


Figure 117. FJ59.022 Dynamic Ring and Face Average Recovery Distributions

FJ59.022 Probe Recovery Distributions



Smallest X-axis
division=0.001 (.1%)
recovery

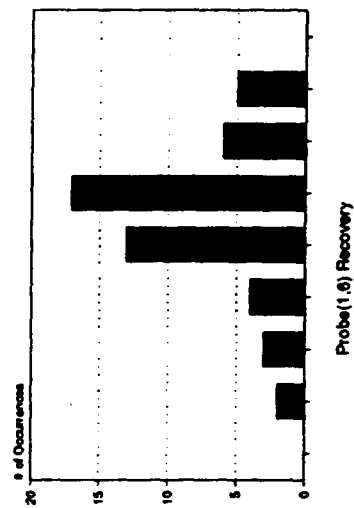
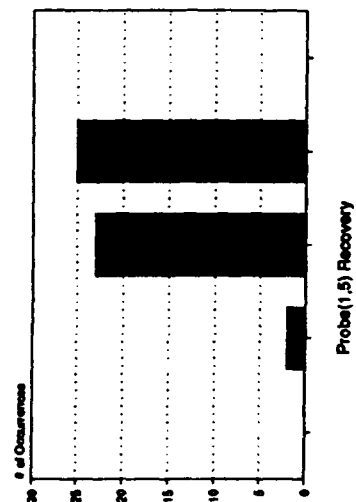
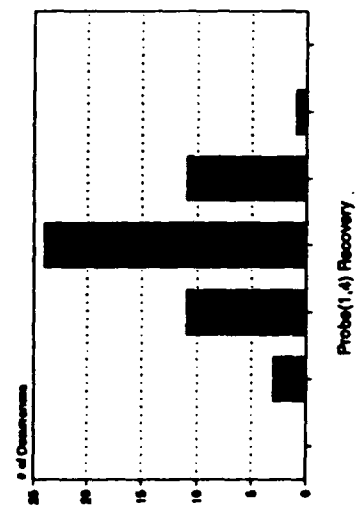
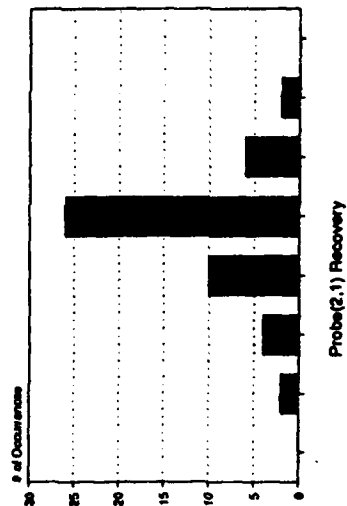
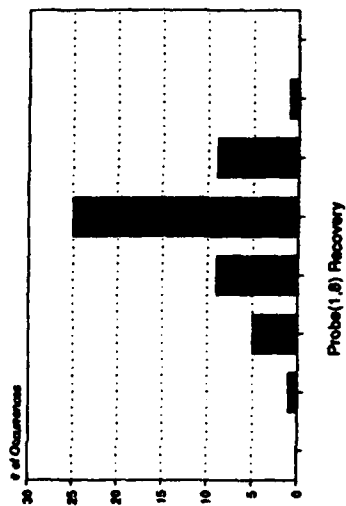
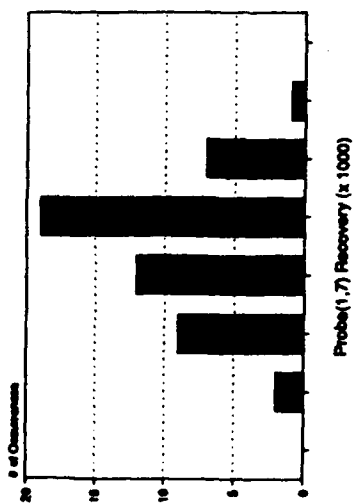


Figure 118. FJ59.022 Probe Recovery Distributions

Figure 118. (Continued)



Smallest X-axis
division=0.001 (.1%)
recovery

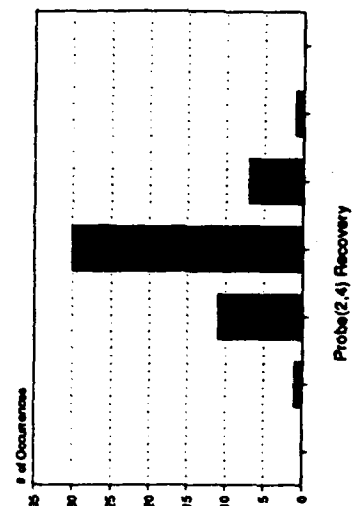
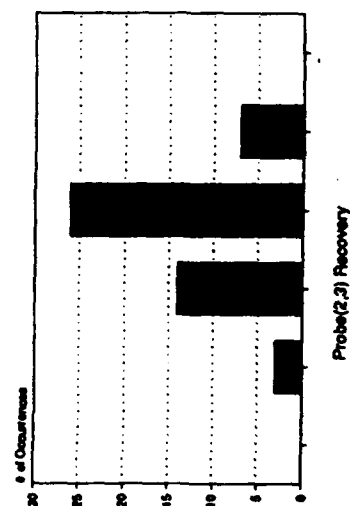
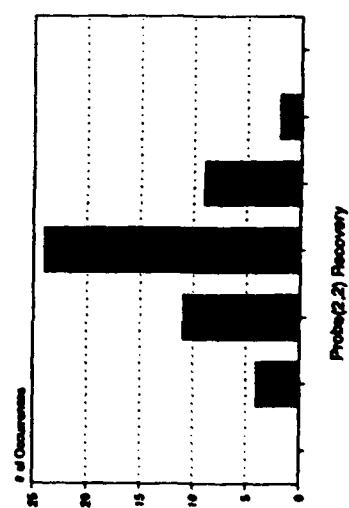


Figure 118. (Continued)

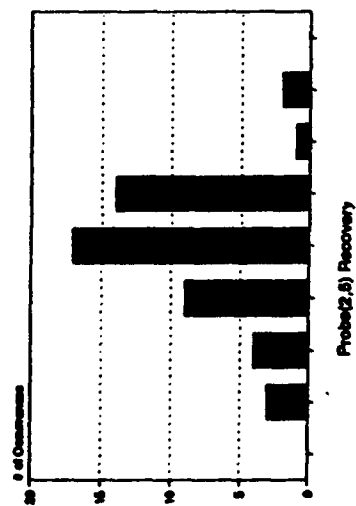
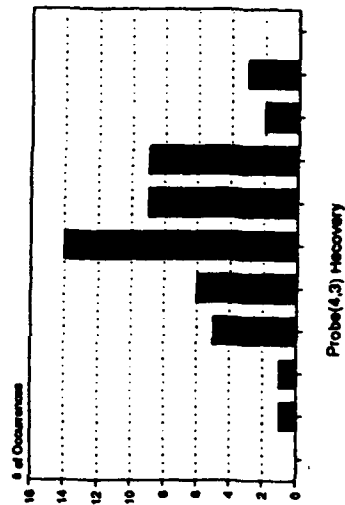
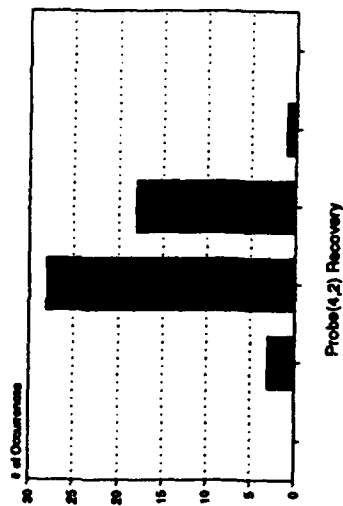


Figure 118. (Continued)



Smallest x-axis
division=0.001 (.1%)
recovery

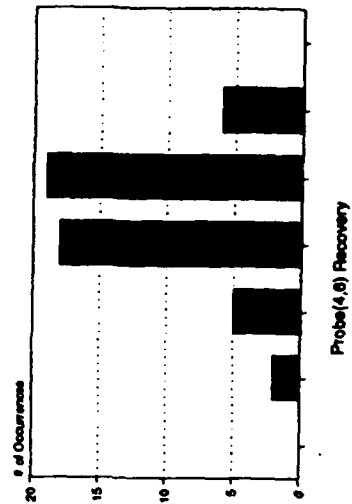
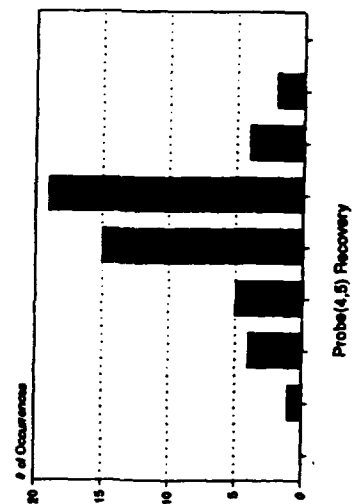
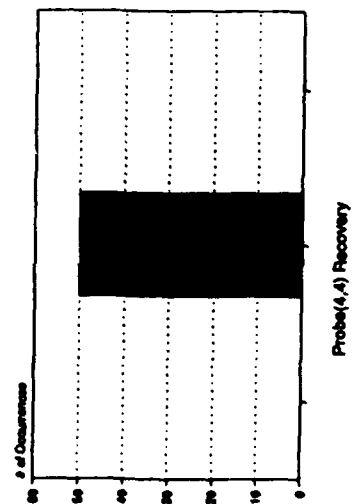
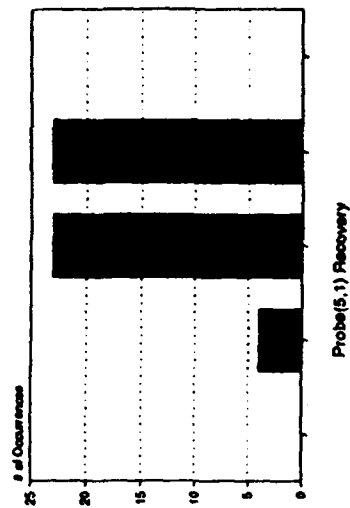
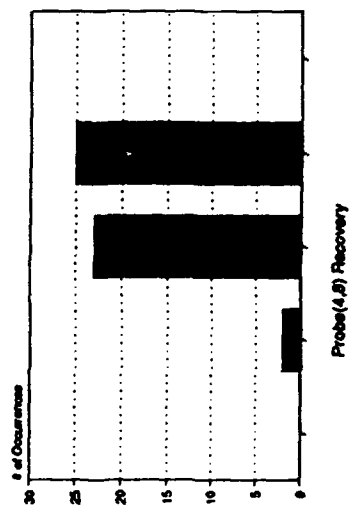
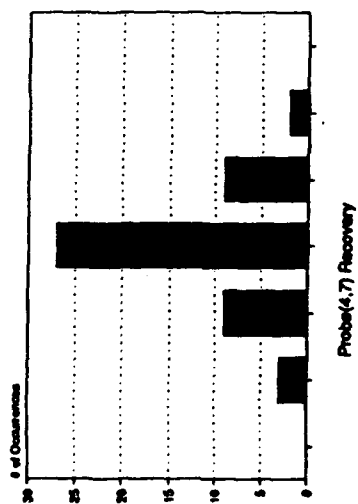


Figure 118. (Continued)



Smallest X-axis
division=0.001 (.1%)
recovery

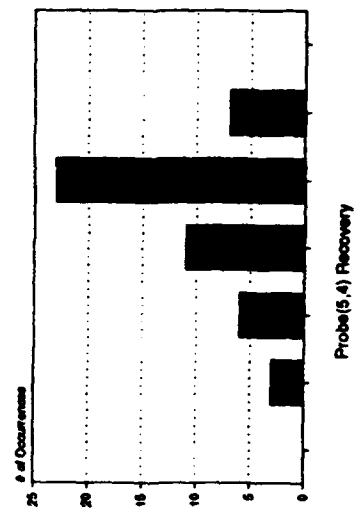
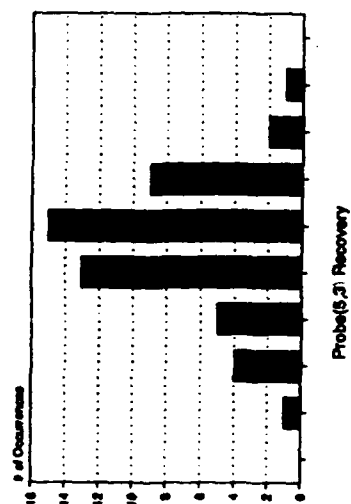
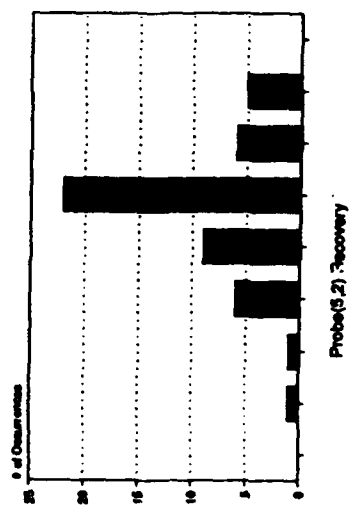
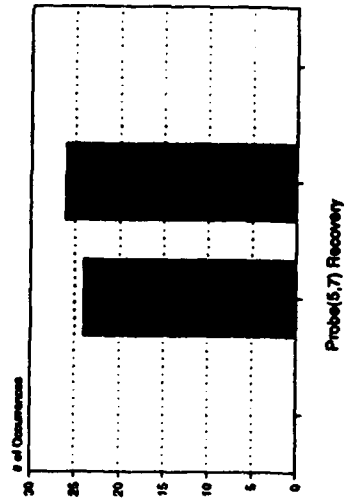
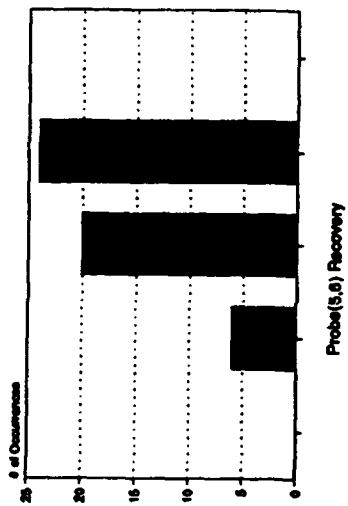
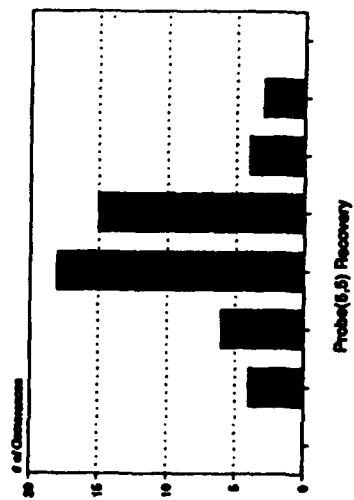
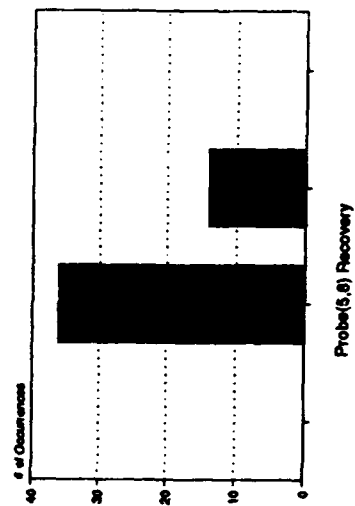


Figure 118. (Continued)



Smallest X-axis
division=0.001 (.1%)
recovery



FJ59.022 1419 Indices
Pcp Intensity Distributions

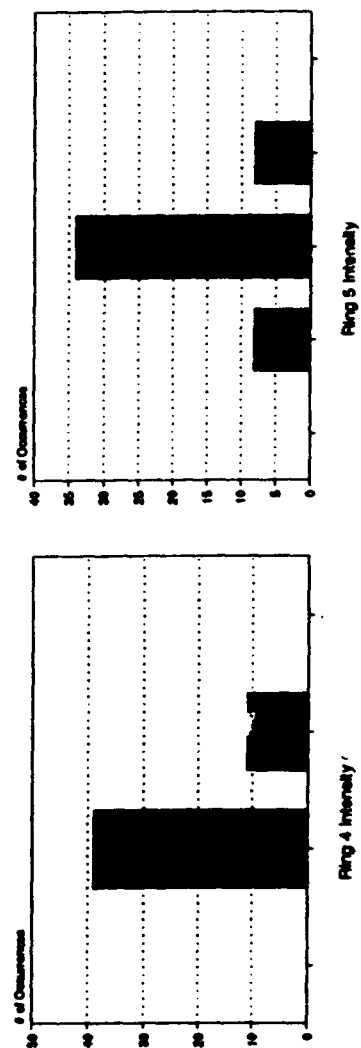
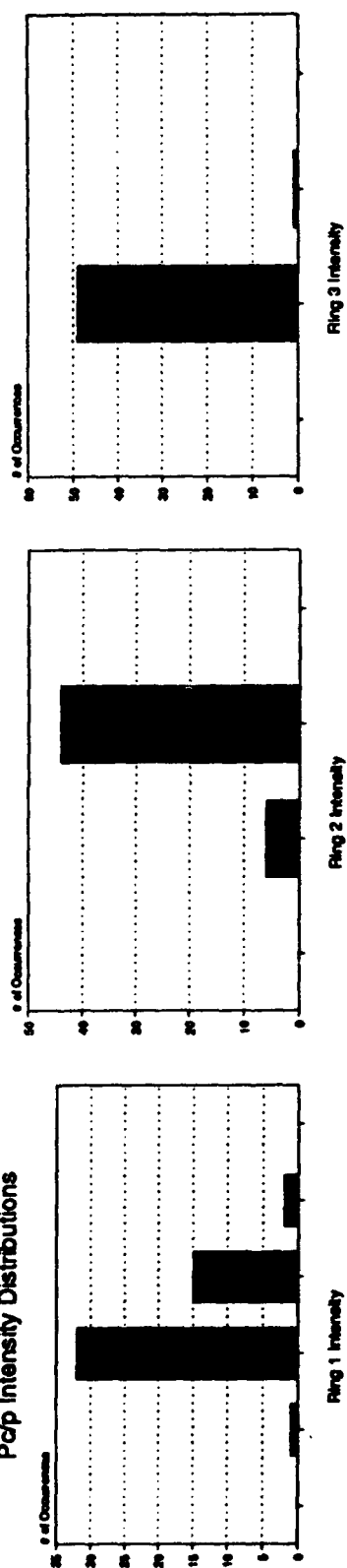


Figure 119. FJ59.022 Δ Pc/P, Intensity Distributions

FJ59.022 Dynamic 1419 Indices
Multiple Per Rev Distributions

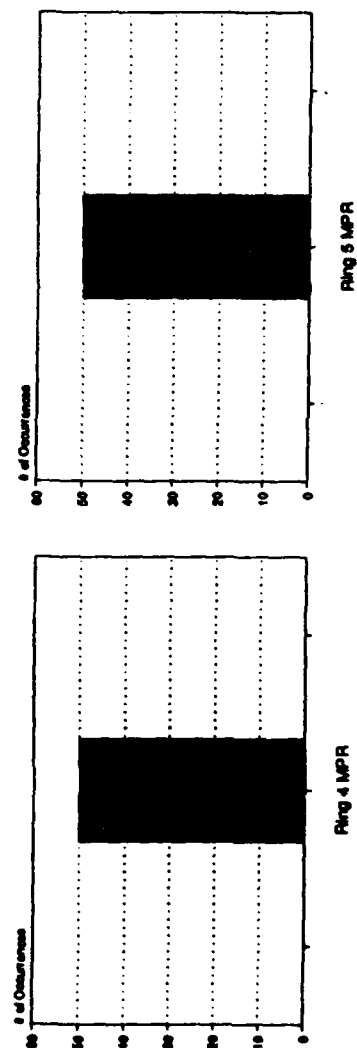
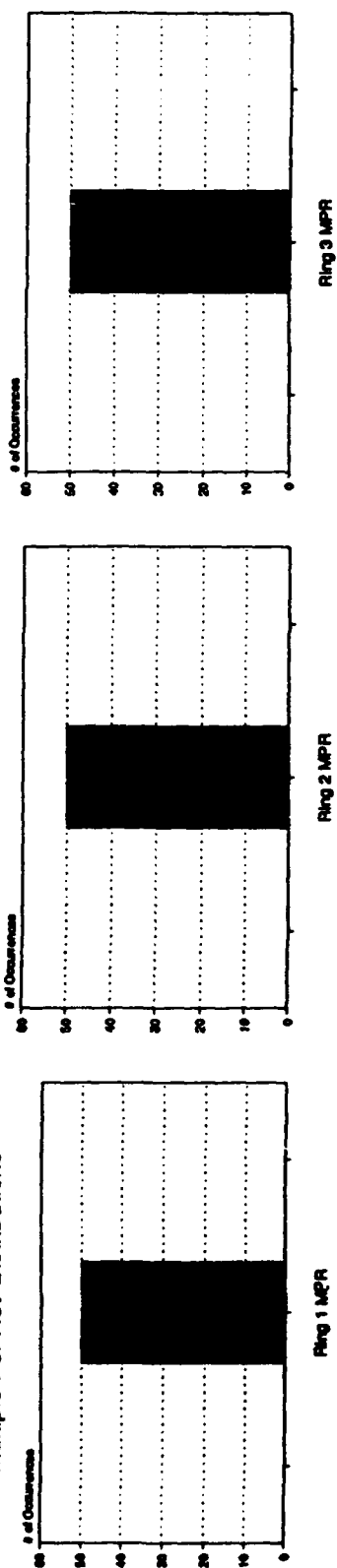


Figure 120. FJ59.022 MPR
Distributions

FJ59.022 1419 Indices
Extent Distributions

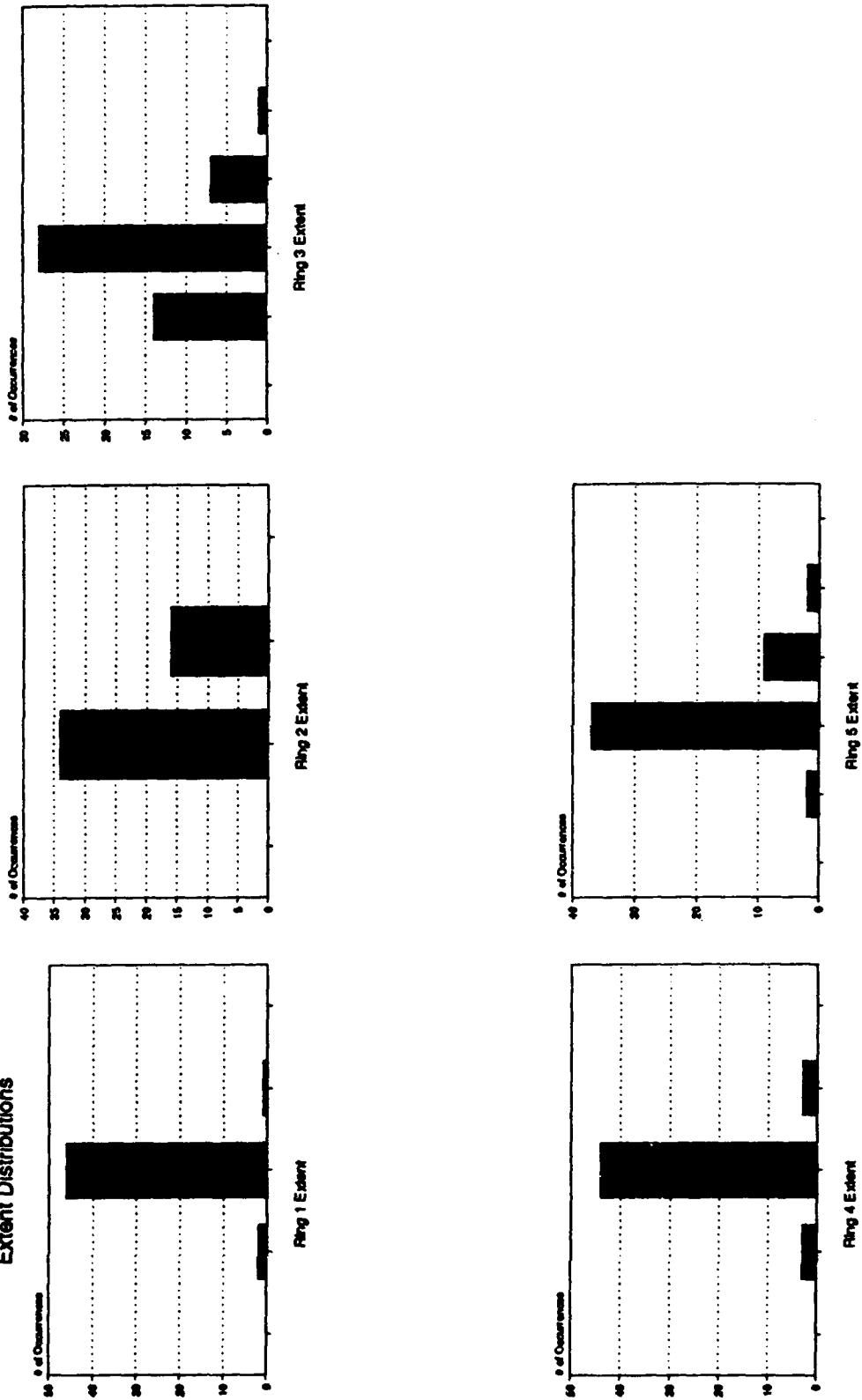


Figure 121. FJ59.022 Extent
Distributions

FJ59.022 1419 Indices
Pr/P (IDR) Distributions

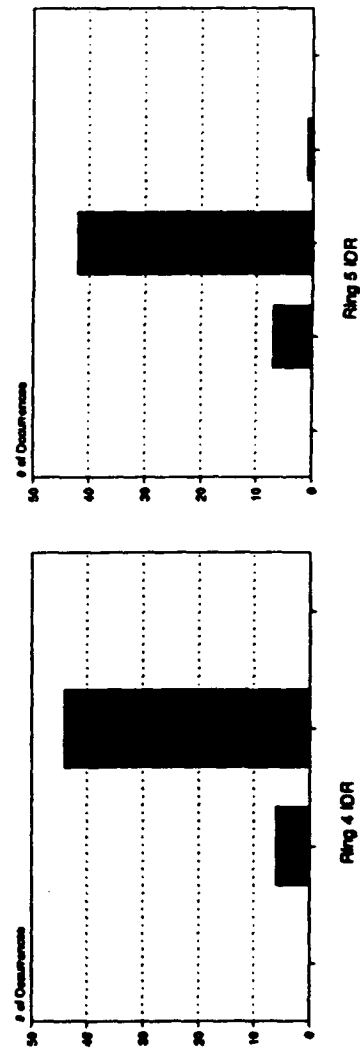
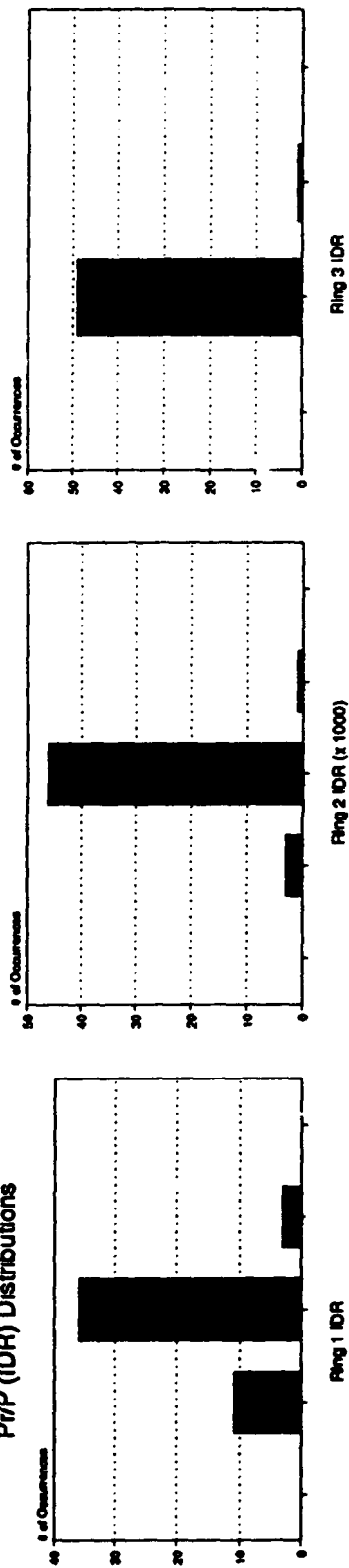


Figure 122. FJ59.022 $\Delta Pr/P$, IDR
Distributions

WT1170.1 Analog Parameter Distributions

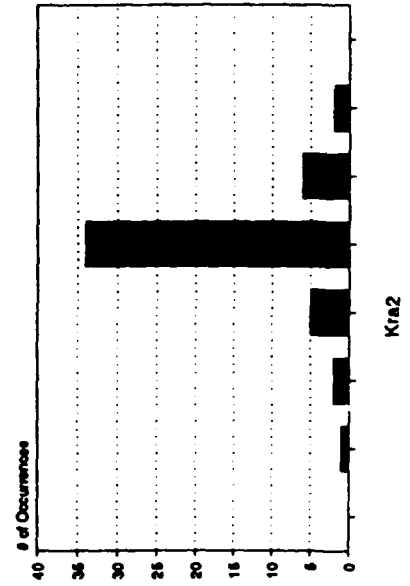
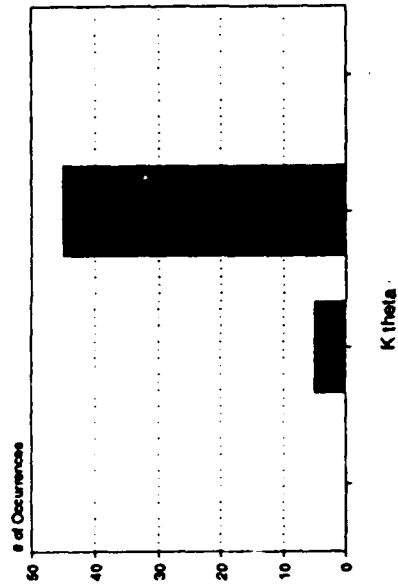
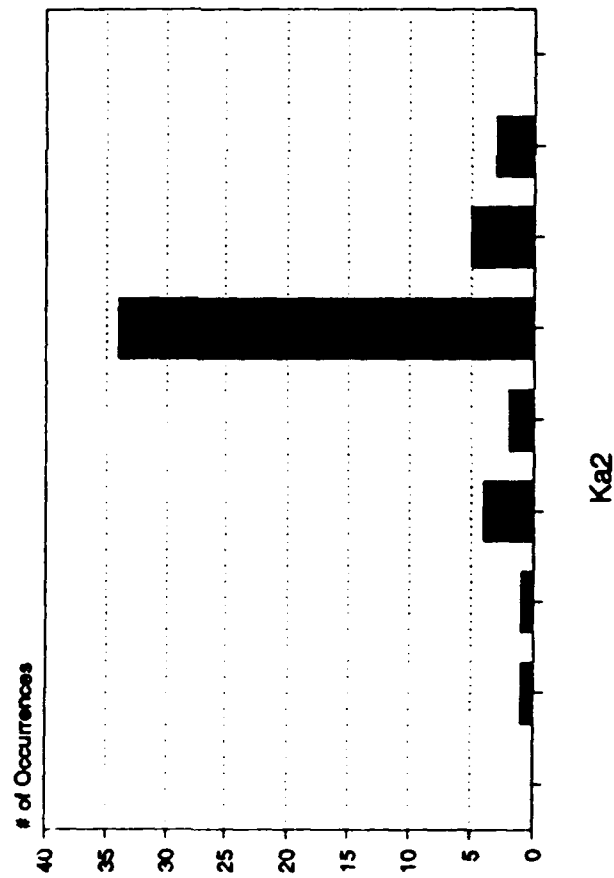


Figure 123. WT1170.1 Analog Parameter

WT1170.1 Digital Parameter Distributions

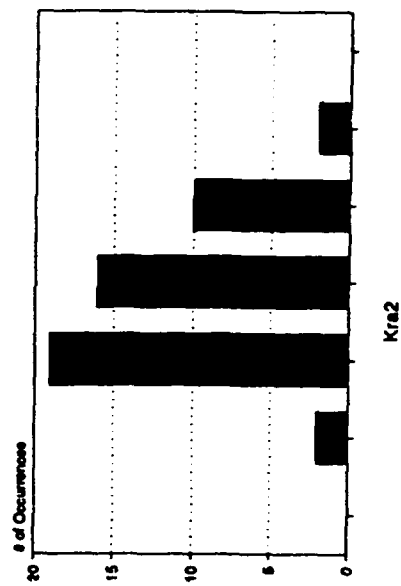
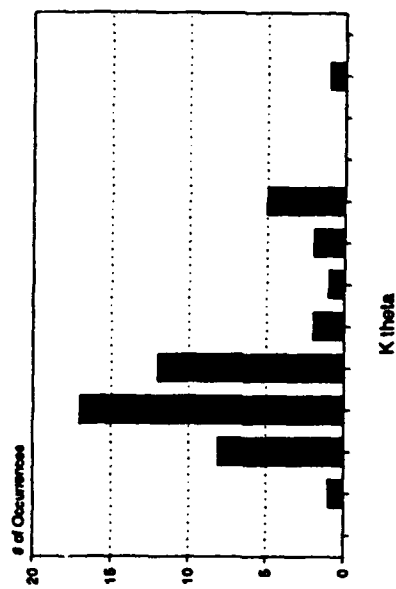
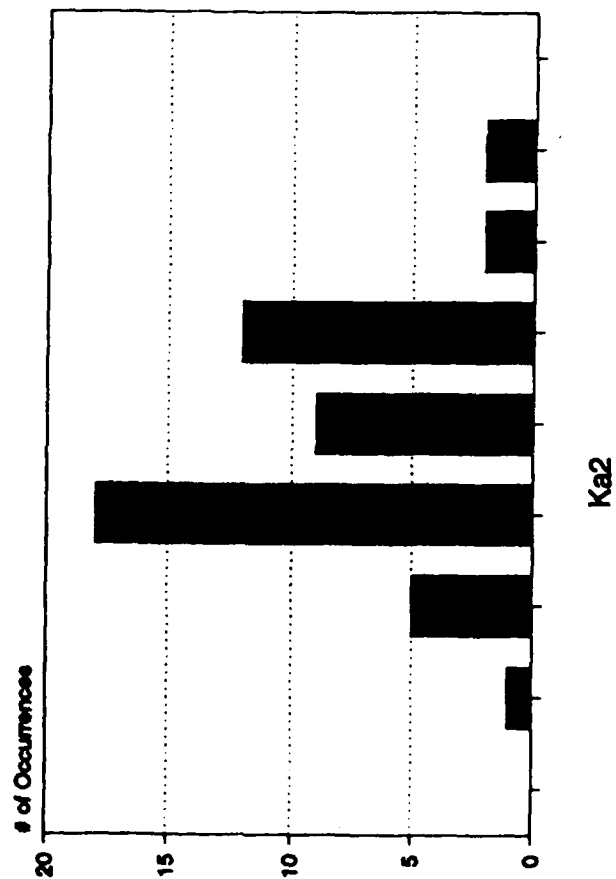
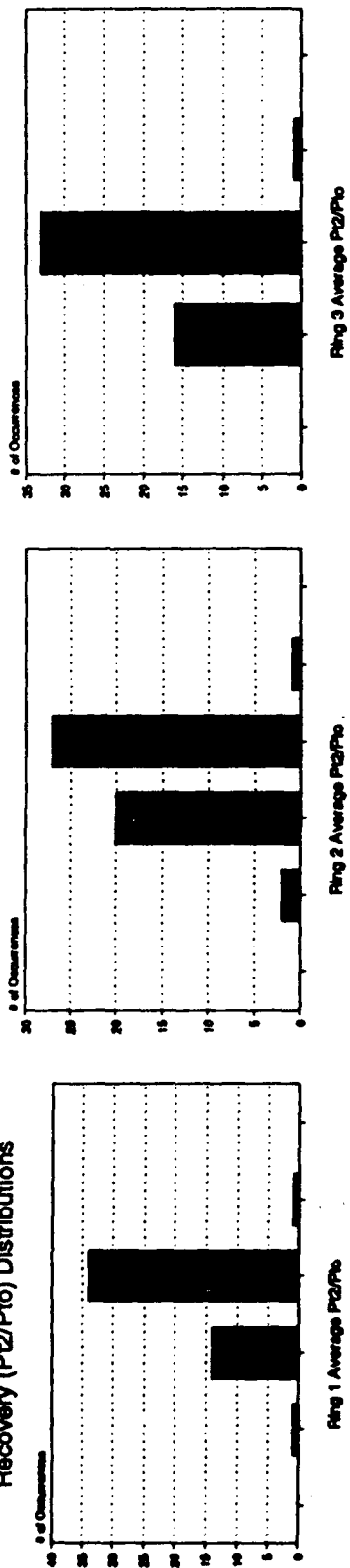


Figure 124. WT1170.1 Digital Parameter Distributions

WT1170.1 Dynamic Ring & Face Average
Recovery (P2/Pto) Distributions



Smallest X-axis
division=0.001 (.1%)
recovery

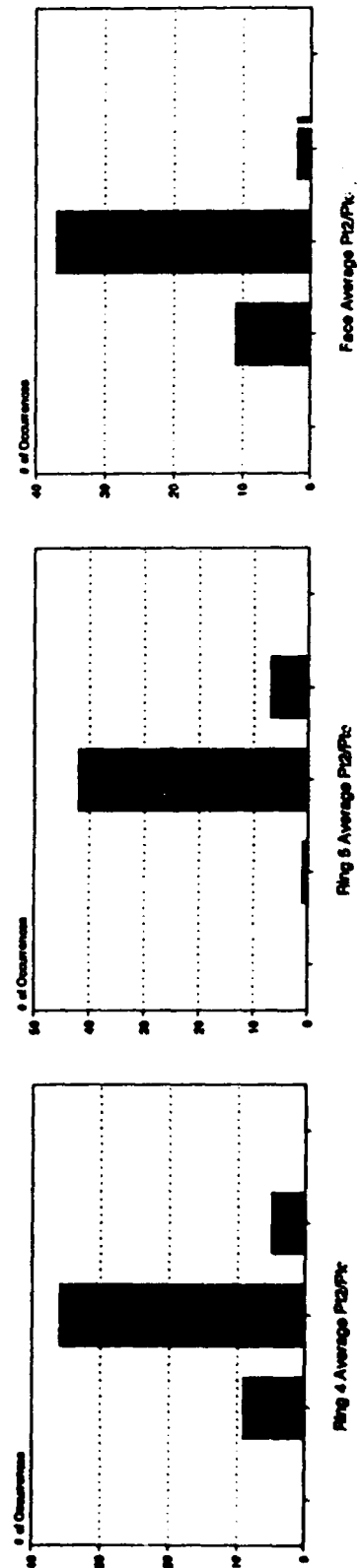


Figure 125. WT1170.1 Dynamic Ring and
Face Average Recovery Distributions

WT1170.1 Probe Recovery Distributions

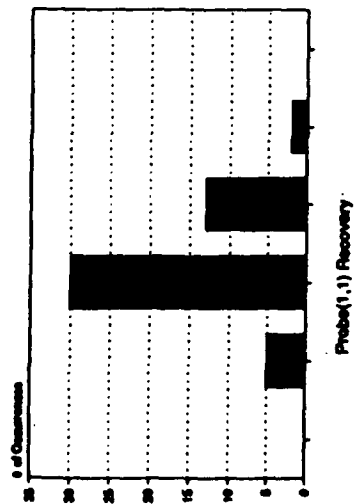
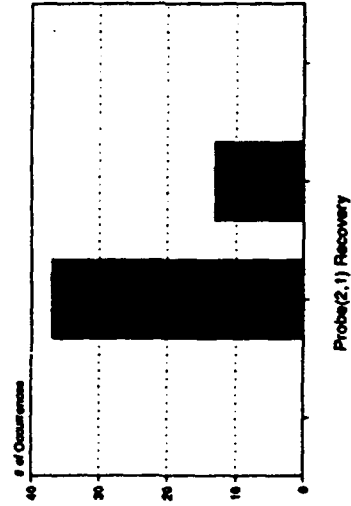
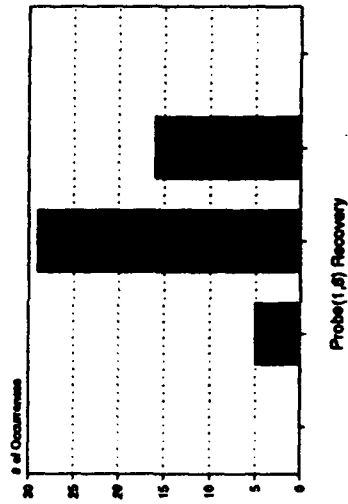


Figure 126. (Continued)



Smallest X-axis
division=0.001 (.1%)
recovery

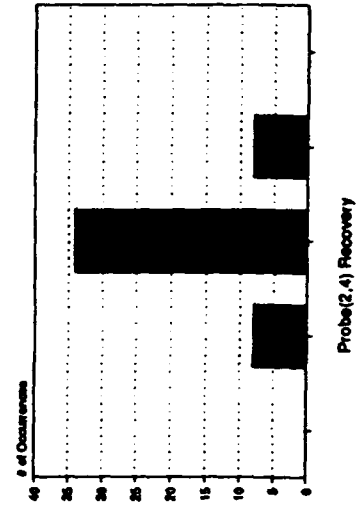
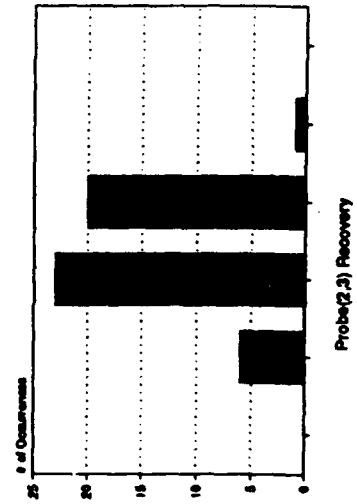
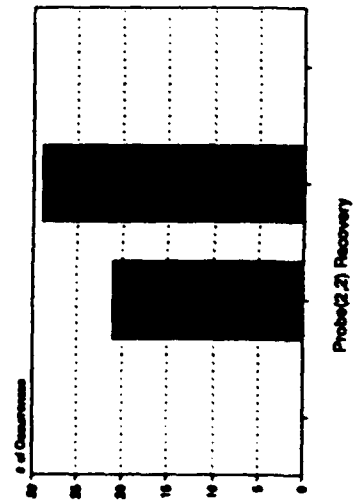
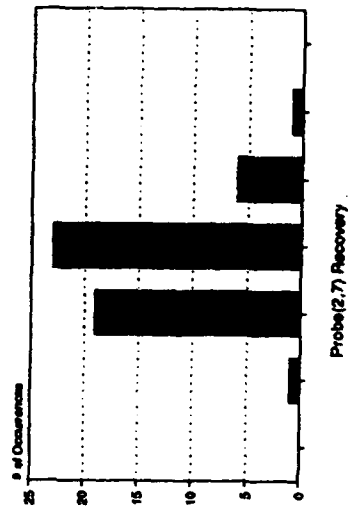
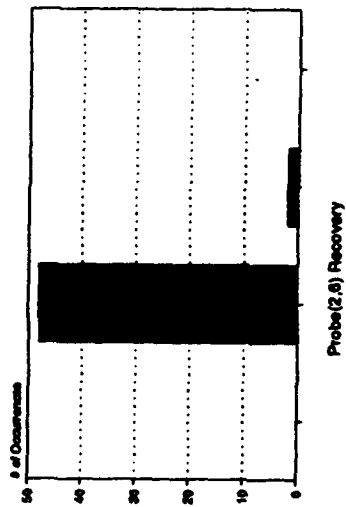
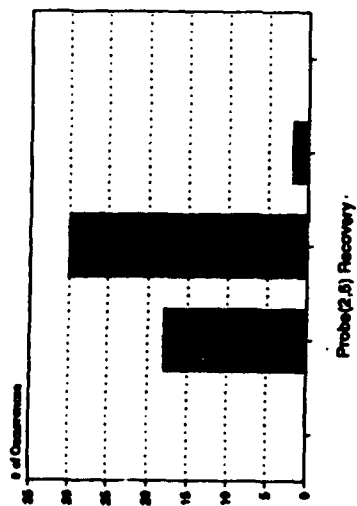


Figure 126. (Continued)



Smallest X-axis
division=0.001 (.1%)
recovery

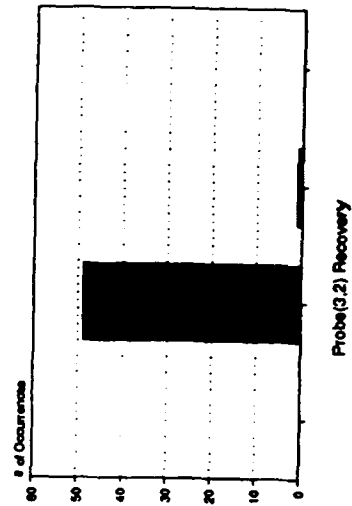
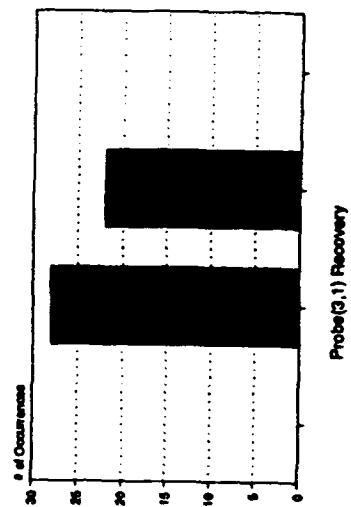
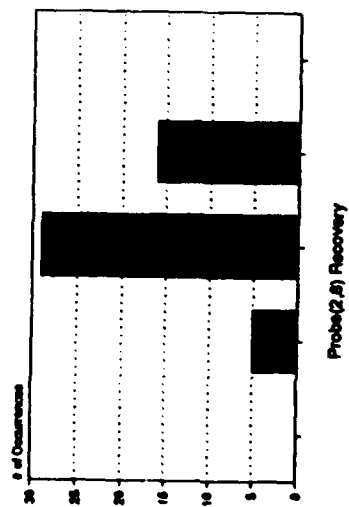
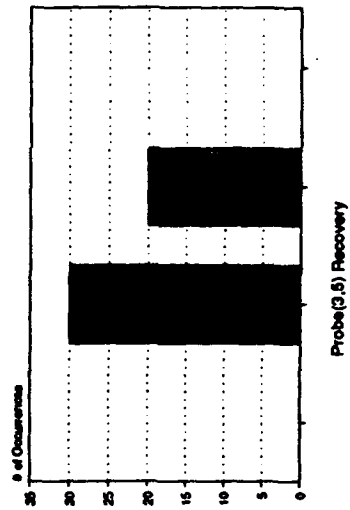
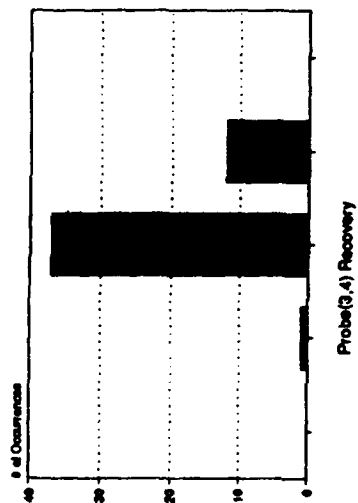
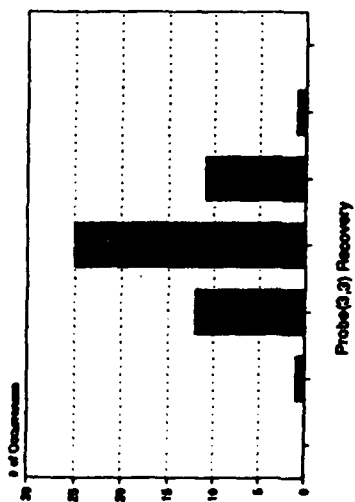


Figure 126. (Continued)



Smallest X-axis
division=0.001 (.1%)
recovery

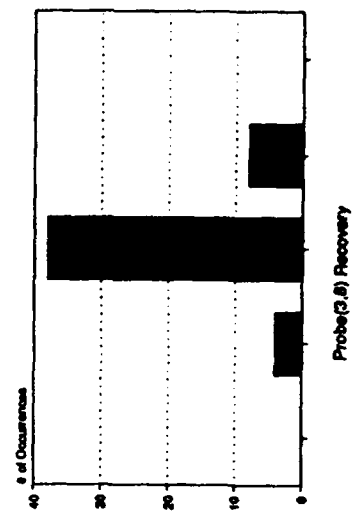
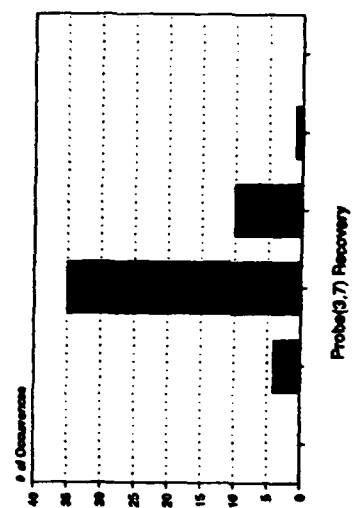
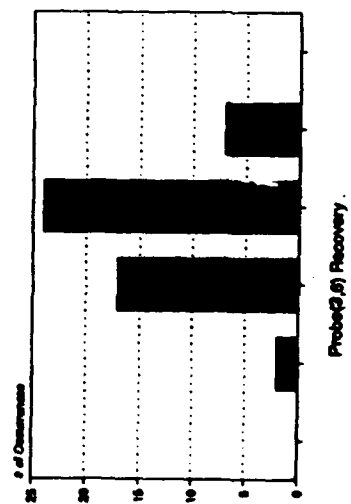
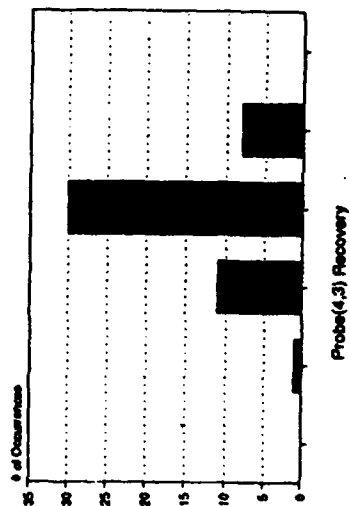
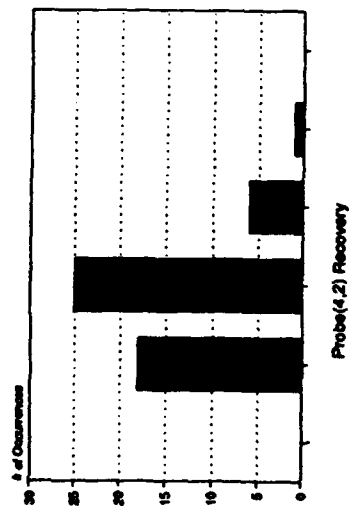
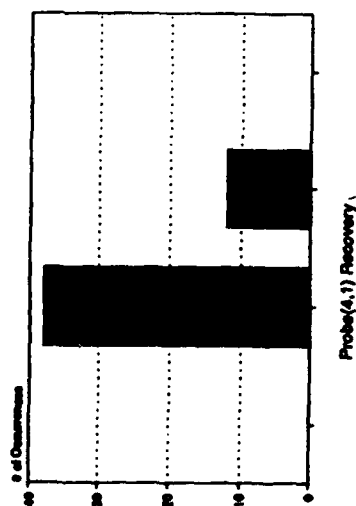


Figure 126. (Continued)



Smallest X-axis
division=0.001 (.1%)
recovery

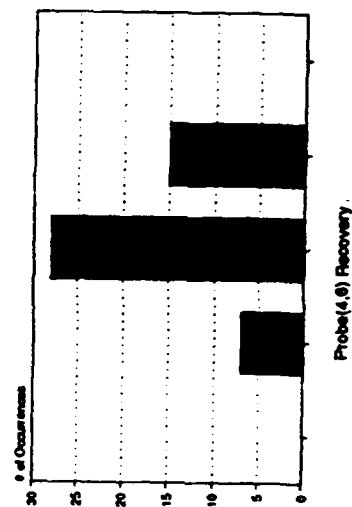
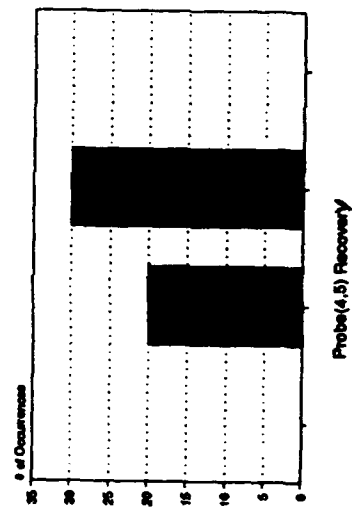
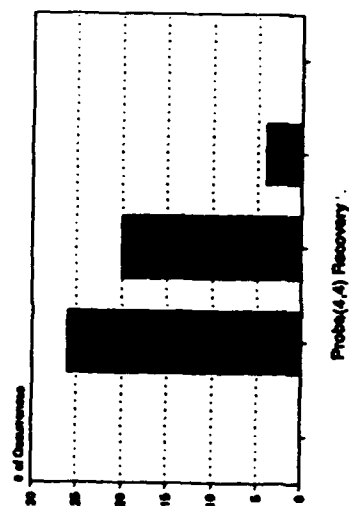


Figure 126. (Continued)

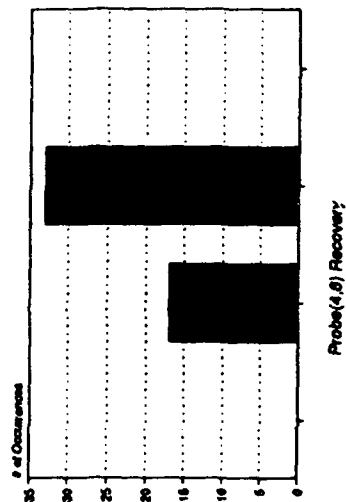
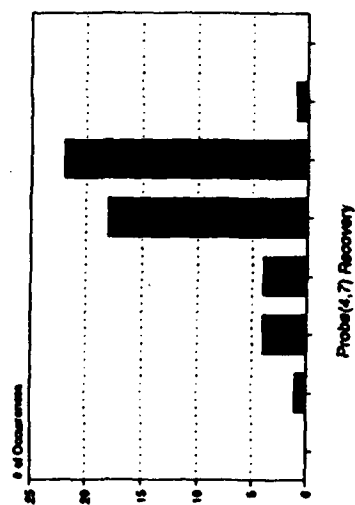
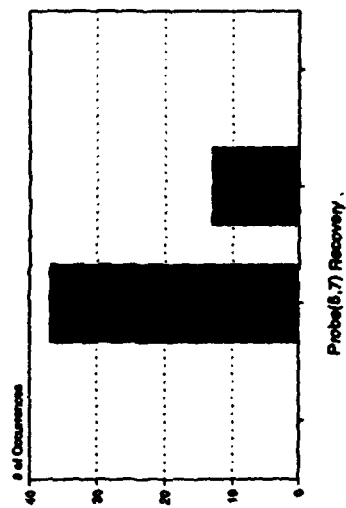
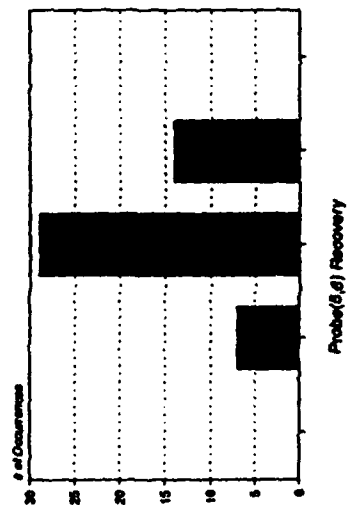
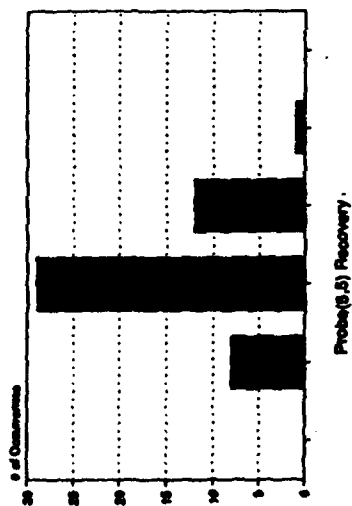
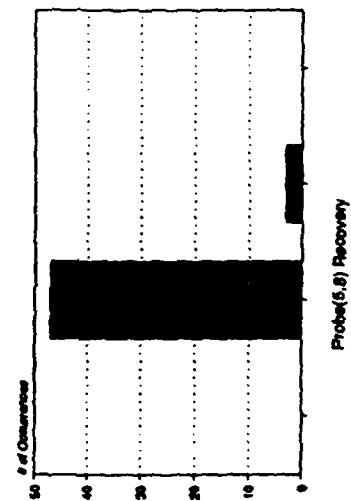


Figure 126. (Continued)



Smallest X-axis
division=0.001 (.1%)
recovery



WT1170.1 1419 Indices
Pc/p Intensity Distributions

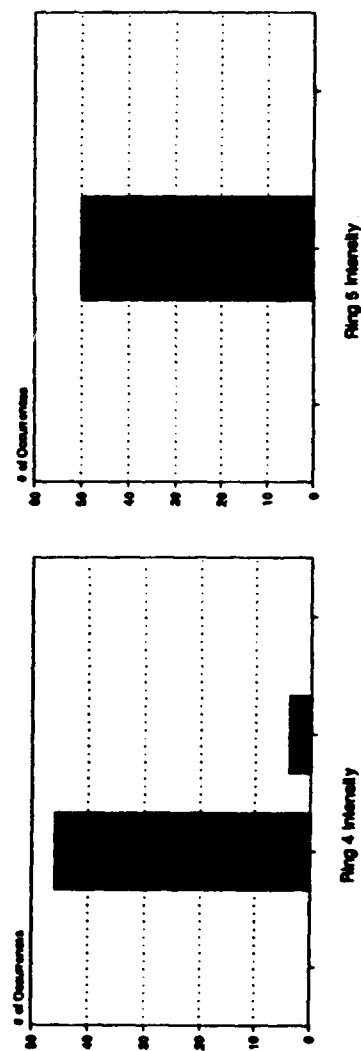
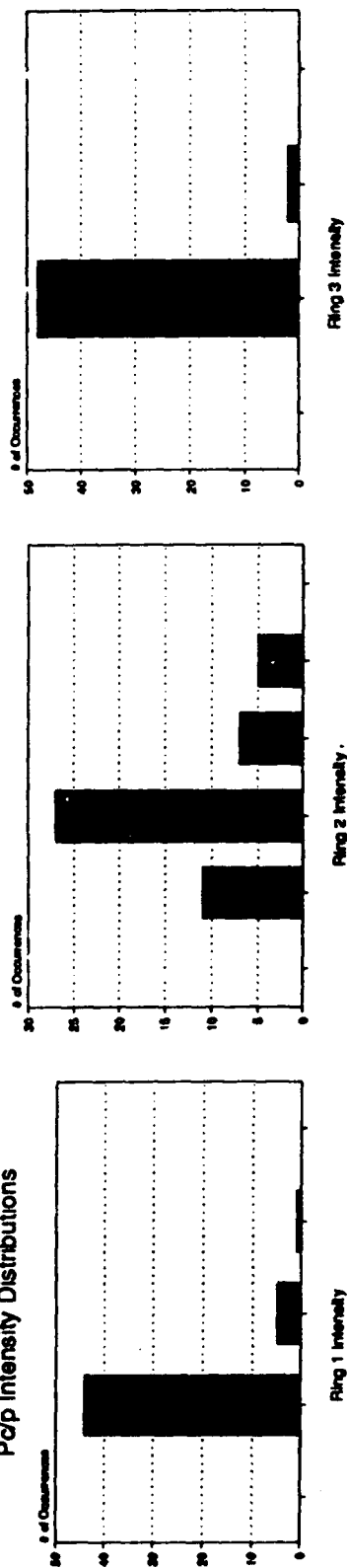
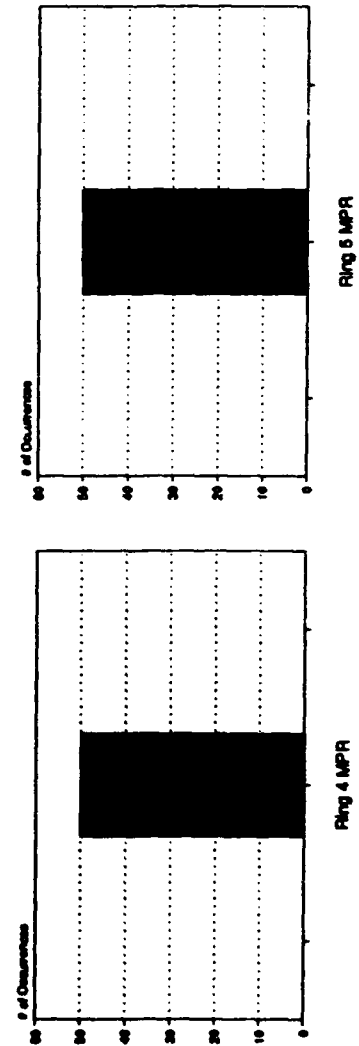
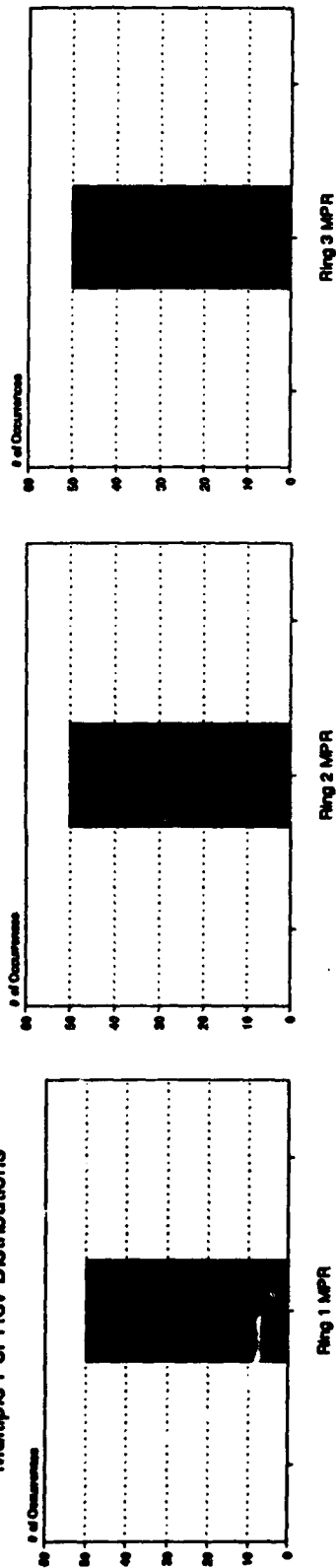


Figure 127. WT1170.1 Δ Pc/P, Intensity Distributions

**WT1170.1 Dynamic 1419 Indices
Multiple Per Rev Distributions**



**Figure 128. WT1170.1 MPR
Distributions**

WT1170.1 1419 Index Extent Distributions

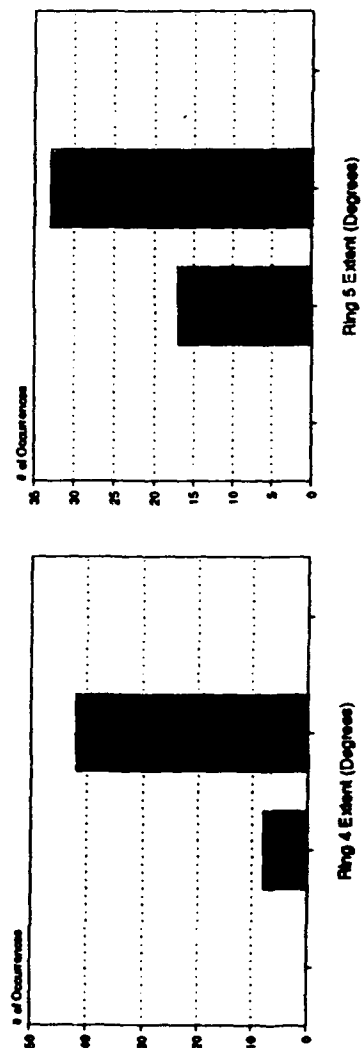
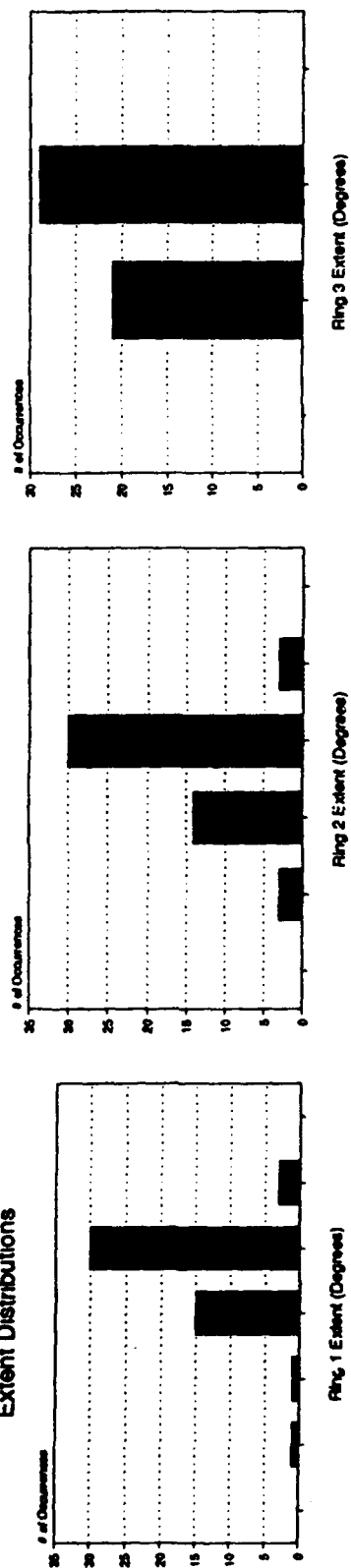


Figure 129. WT1170.1 Extent Distributions

WT1170.1 1419 Indice
Pr/P (IDR) Distributions

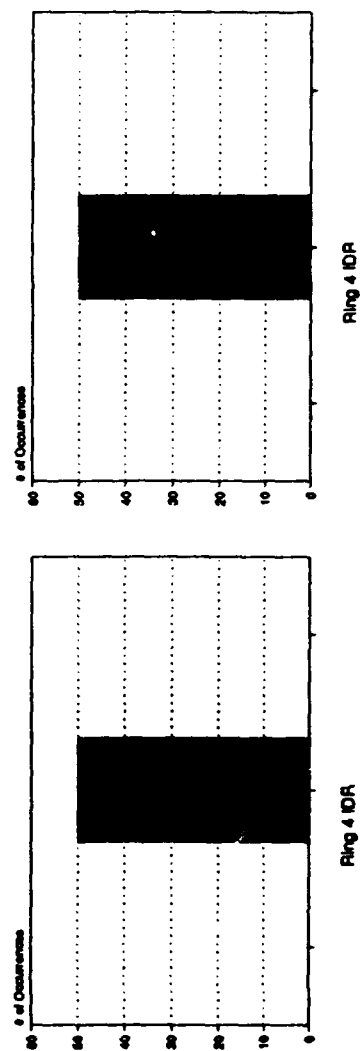
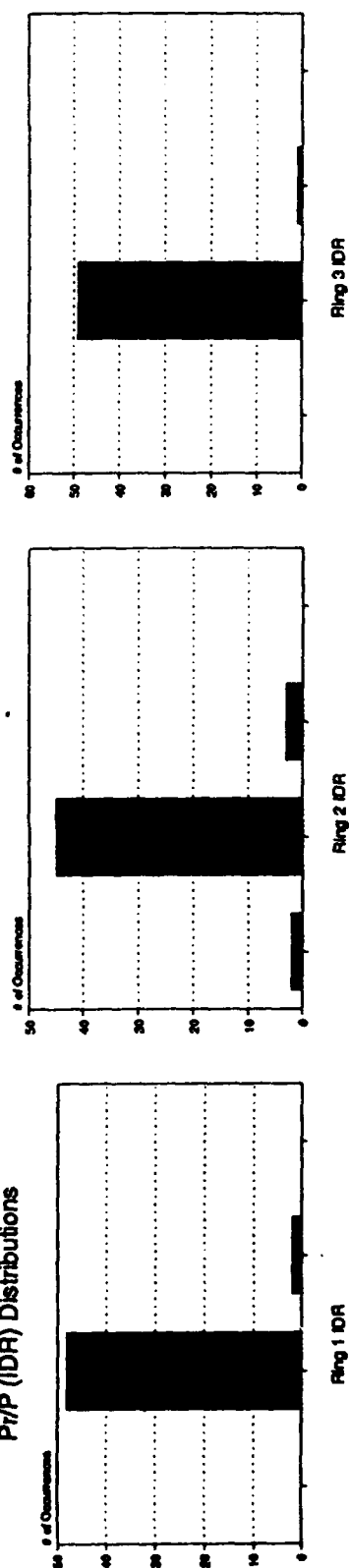


Figure 130. WT1170.1 Δ Pr/P, IDR
Distributions

APPENDIX C BIAS ERROR DATA

Table 30.
DYNADEC System Bias Errors,
Raw Output

	A	B	C	D	E	F
1	Date	91/6/20				
2	Time	8:17:11	8:21:26	8:32:58	8:45:12	9:16:56
3	Point	None	14.129	14.05	11.187	9.09
4	Diff (1,1)	0.002	0.00116	0.00183	0.00164	0.00034
5	(1,2)	0	0.00191	0.00027	0.00332	0.00564
6	(1,3)	0.001	0.00078	0.00018	0.00162	0.00011
7	(1,4)	0	0.00025	0.00066	0.00062	0.00107
8	(1,5)	0	0.00304	0.00093	0.00021	0.00388
9	(1,6)	0	0.00284	0.00241	0.00427	0.00145
10	(1,7)	0	0.00025	0.00163	0.00024	0.00122
11	(1,8)	0	0.00099	0.00202	0.00252	0.00183
12	(2,1)	0.002	0.00315	0.00111	0.00039	0.00285
13	(2,2)	0.001	0.00113	0.00083	0.00178	0.00343
14	(2,3)	0.003	0.00131	0.00174	0.00023	0.00254
15	(2,4)	0.001	0.00159	0.00072	0.00181	0.00303
16	(2,5)	0	0.00087	0.00086	0.00206	0.00031
17	(2,6)	0.002	0.00138	0.00111	0.00119	0.00116
18	(2,7)	0.001	0.00088	0.00393	0.00282	0.00283
19	(2,8)	0	0.00137	0.0032	0.00092	0.00187
20	(3,1)	0	0.00254	0.00033	0.0014	0.00158
21	(3,2)	0.002	0.00364	0.00062	0.00397	0.00102
22	(3,3)	0.002	0.00049	0.00227	0.00043	0.00078
23	(3,4)	0.001	0.00026	0.0015	0.00008	0.00027
24	(3,5)	0.003	0.00135	0.00103	0.00087	0.00169
25	(3,6)	0.001	0.00034	0.00246	0.00186	0.00028
26	(3,7)	0.001	0.0038	0.00335	0.00025	0.00273
27	(3,8)	0.002	0.00048	0.00305	0.00091	0.00142
28	(4,1)	0.002	0.00342	0.00013	0.00598	0.00124
29	(4,2)	0.001	0.00088	0.00161	0.00192	0.00044
30	(4,3)	0.001	0.00042	0.0018	0.00193	0.00263
31	(4,4)	0.001	0.00104	0.00179	0.003	0.00203
32	(4,5)	0.004	0.00018	0.00188	0.00125	0.00086
33	(4,6)	0.001	0.00444	0.00224	0.00195	0.00386
34	(4,7)	0	0.00165	0.00099	0.00199	0.00071
35	(4,8)	0.004	0.00318	0.00512	0.00317	0.0001
36	(5,1)	0.001	0.00189	0.0007	0.00277	0.0022
37	(5,2)	0.001	0.00094	0.00186	0.00255	0.00006
38	(5,3)	0	0.00288	0.00237	0.00176	0.0038
39	(5,4)	0.003	0.00085	0.00082	0.00096	0.00055
40	(5,5)	0.001	0.00523	0.00037	0.0044	0.00117
41	(5,6)	0.002	0.00362	0.00165	0.00123	0.00253
42	(5,7)	0	0.00102	0.00123	0.00021	0.00133
43	(5,8)	0.005	0.00099	0.00165	0.00461	0.00023
44	Counter	1	2	3	4	5
45	Avg	0.0013	0.0017108	0.0016063	0.0018773	0.0016768
46						
47						

Table 30. (Continued)

	G	H	I	J	K	L
1	91/6/27					
2	9:58:51	10:09:55	10:57:34	11:23:14	11:40:03	11:50:26
3	None	3.106	11.06	11.071	11.09	11.092
4	0.002	0.00138	0.00044	0.00227	0.00088	0.00588
5	0	0.00616	0.0017	0.00366	0.00388	0.00124
6	0.004	0.00217	0.00611	0.00049	0.00009	0.00475
7	0.001	0.00046	0.00062	0.00339	0.00501	0.00031
8	0.002	0.00337	0.00373	0.00009	0.0022	0.00212
9	0.002	0.00255	0.00385	0.00336	0.00071	0.00343
10	0	0.00131	0.00315	0.00016	0.00087	0.00035
11	0.004	0.00452	0.00451	0.00106	0.00045	0.00015
12	0.002	0.0021	0.00068	0.00272	0.00163	0.00108
13	0.001	0.00509	0.00021	0.00093	0.00389	0.00173
14	0.001	0.00373	0.00085	0.0036	0.00159	0.00433
15	0.002	0.00103	0.00012	0.00307	0.00215	0.00428
16	0.001	0.00124	0.00028	0.00134	0.00295	0.00023
17	0	0.00137	0.00117	0.00364	0.00306	0.00025
18	0.005	0.00291	0.00297	0.00188	0.00083	0.00346
19	0	0.00324	0.0007	0.00193	0.00127	0.00021
20	0	0.00003	0.00054	0.00029	0.00072	0.00204
21	0.002	0.00048	0.00143	0.001	0.00348	0.00138
22	0.002	0.00149	0.00093	0.0027	0.00155	0.00147
23	0.001	0.00191	0.00077	0.0015	0.00006	0.00062
24	0.001	0.00072	0.0004	0.00124	0.00125	0.00063
25	0	0.00322	0.00136	0.00174	0.0045	0.00146
26	0.001	0.0034	0.00038	0.00137	0.00022	0.00153
27	0.001	0.00047	0.0025	0.00024	0.00118	0.00059
28	0.001	0.00183	0.00181	0.00386	0.00192	0.00011
29	0	0.00157	0.00007	0.00025	0.00177	0.00077
30	0.002	0.00205	0.00175	0.00353	0.00109	0.00156
31	0.001	0.00044	0.0012	0.00294	0.00037	0.00089
32	0.001	0.00053	0.00098	0.00248	0.0003	0.00058
33	0.001	0.00113	0.00021	0.00055	0.00051	0.00132
34	0.003	0.00406	0.00399	0.00185	0.00109	0.00282
35	0.001	0.00023	0.00131	0.00089	0.00022	0.00215
36	0.001	0.00016	0.00043	0.00029	0.00323	0.00118
37	0.003	0.00363	0.00357	0.00441	0.00379	0.00315
38	0.002	0.00258	0.00323	0.00288	0.0026	0.00457
39	0.002	0.00045	0.00014	0.0012	0.0046	0.00326
40	0.003	0.00571	0.00049	0.00026	0.00205	0.00308
41	0.002	0.00294	0.00096	0.00081	0.00031	0.00062
42	0.001	0.00043	0.00178	0.00235	0.00031	0.00128
43	0.002	0.00024	0.00469	0.00024	0.00164	0.00262
44	6	7	8	9	10	11
45	0.001525	0.0020583	0.0016503	0.0018115	0.0017555	0.001837
46						
47						

Table 30. (Continued)

	M	N	O	P	Q	R
1					91/7/9	
2	11:58:21	12:03:28	12:18:17	12:27:27	14:16:28	14:57:30
3	11.09	11.111	11.113	11.133	None	None
4	0.00212	0.0036	0.00006	0.00083	0.002	0.00063
5	0.00188	0.00335	0.00005	0.00414	0	0.00095
6	0.00291	0.00012	0.0021	0.00061	0.004	0.0012
7	0.00401	0.00232	0.00161	0.00288	0.003	0.00057
8	0.0022	0.00068	0.0058	0.0224	0	0.0044
9	0.00029	0.00083	0.00295	0.00417	0.003	0.00179
10	0.00013	0.00034	0.0012	0.00425	0	0.00224
11	0.00055	0.0011	0.00067	0.00279	0.003	0.00359
12	0.00163	0.00576	0.00133	0.00204	0.003	0.00191
13	0.00089	0.00241	0.00116	0.00307	0.001	0.00234
14	0.00059	0.00419	0.00153	0.00291	0.001	0.00458
15	0.00315	0.00481	0.0018	0.00188	0.002	0.00164
16	0.00295	0.00273	0.006	0.00122	0.002	0.00441
17	0.00006	0.00031	0.00035	0.00349	0.001	0.00335
18	0.00383	0.00209	0.0036	0.00337	0.004	0.00046
19	0.00427	0.00184	0.00426	0.00024	0.002	0.00096
20	0.00028	0.00151	0.00231	0.00251	0.001	0.00166
21	0.00248	0.00031	0.00151	0.00103	0.001	0.00038
22	0.00355	0.00302	0.00236	0.0021	0.002	0.00046
23	0.00006	0.00178	0.00383	0.0026	0	0.0016
24	0.00175	0.00249	0.00137	0.00405	0	0.00039
25	0.0035	0.00295	0.00122	0.00077	0	0.00257
26	0.00078	0.0019	0.00255	0.0005	0	0.00072
27	0.00082	0.00204	0.0019	0.00061	0	0.0017
28	0.00192	0.00159	0.00124	0.00393	0.001	0.00206
29	0.00377	0.00098	0.00309	0.00042	0.001	0.00278
30	0.00109	0.00079	0.00209	0.00044	0.001	0.00157
31	0.00063	0.00143	0.00256	0.00157	0.001	0.00044
32	0.0023	0.00139	0.0018	0.00047	0.001	0.00204
33	0.00051	0.00116	0.00149	0.00001	0.001	0.00053
34	0.00091	0.00462	0.00314	0.00144	0.002	0.00131
35	0.00022	0.0017	0.0027	0.00113	0.002	0.00193
36	0.00323	0.00047	0.00277	0.00077	0.002	0.00338
37	0.00479	0.00087	0.00105	0.00134	0.002	0.00356
38	0.0026	0.00641	0.00355	0.00133	0.004	0.00379
39	0.0046	0.00057	0.00566	0.00039	0.002	0.003
40	0.00005	0.00494	0.00089	0.0034	0.002	0.00238
41	0.00069	0.00043	0.00195	0.00176	0	0.00055
42	0.00131	0.00025	0.00021	0.00111	0	0.00065
43	0.00164	0.000215	0.00267	0.00097	0.001	0.00037
44	12	13	14	15	16	17
45	0.0018735	0.0020074	0.0022095	0.0023735	0.00145	0.001871
46						
47						

Table 30. (Continued)

	S	T	U	V	W	X
1				91/7/10		
2	15:08:43	15:12:03	15:28:37	12:51:35	13:13:36	14:10:23
3	60.037	61.016	None	None	61.016	61.009
4	0.00019	0.00019	0.003	0.002	0.00019	0.00281
5	0.00337	0.00537	0.001	0.001	0.00537	0.00013
6	0.00083	0.00083	0.002	0.001	0.00183	0.00046
7	0.00074	0.00174	0.002	0.001	0.00074	0.00322
8	0.00322	0.00222	0	0	0.00222	0.00052
9	0.00018	0.00118	0.003	0.002	0.00018	0.00049
10	0.00124	0.00076	0.003	0.001	0.00076	0.00277
11	0.00023	0.00023	0.001	0.002	0.00023	0.00219
12	0.00247	0.00247	0.004	0.002	0.00247	0.00119
13	0.00216	0.00016	0.001	0.002	0.00016	0.00149
14	0.00024	0.00076	0	0	0.00076	0.00229
15	0.00005	0.00095	0.002	0.003	0.00195	0.00254
16	0.0013	0.0023	0.002	0.003	0.0023	0.00076
17	0.00018	0.00018	0.002	0	0.00082	0.00093
18	0.00351	0.00251	0.002	0.004	0.00151	0.00059
19	0.00245	0.00445	0.003	0.002	0.00245	0.00185
20	0.00092	0.00192	0.001	0	0.00008	0.00191
21	0.00204	0.00204	0.001	0.001	0.00204	0.00269
22	0.003	0.003	0.002	0.002	0.001	0.00066
23	0.00446	0.00246	0.002	0.002	0.00246	0.00387
24	0.00185	0.00185	0	0.001	0.00185	0.00096
25	0.00383	0.00183	0.001	0.001	0.00283	0.0029
26	0.00023	0.00023	0	0.001	0.00177	0.00377
27	0.00101	0.00001	0.001	0.001	0.00001	0.00045
28	0.00024	0.00024	0.002	0.001	0.00076	0.00177
29	0.00043	0.00243	0.002	0.001	0.00243	0.00276
30	0.0013	0.0003	0.001	0.001	0.0013	0.00271
31	0.0019	0.00091	0.001	0.001	0.0019	0.00288
32	0.00353	0.00253	0	0.002	0.00253	0.00273
33	0.00072	0.00072	0	0	0.0028	0.00143
34	0.00307	0.00407	0.002	0.001	0.00307	0.00015
35	0.00375	0.00475	0.002	0.002	0.00475	0.00111
36	0.00165	0.00065	0.001	0.004	0.00065	0.00055
37	0.00249	0.00149	0.002	0.003	0.00349	0.00112
38	0.00043	0.00257	0.003	0.001	0.00043	0.0058
39	0.0039	0.0019	0.002	0.004	0.0029	0.00162
40	0.00038	0.00162	0.003	0	0.00038	0.00396
41	0.00253	0.00353	0.002	0.001	0.00253	0.00517
42	0.00106	0.00194	0	0.001	0.00094	0.0031
43	0.00046	0.00254	0.001	0.003	0.00054	0.00538
44	18	19	20	21	22	23
45	0.0016885	0.0017958	0.001575	0.001525	0.0016845	0.002092
46						
47						

Table 30. (Continued)

	Y	Z	AA	AB	AC	AD
1				91/7/11		
2	14:27:10	14:46:10	14:58:40	12:55:02	13:13:41	13:36:08
3	61.02	61.024	61.022	None	61.049	61.053
4	0.00035	0.00247	0.00095	0.003	0.00052	0.00323
5	0.00107	0.00205	0.00401	0.001	0.00021	0.00167
6	0.00156	0.00122	0.00102	0.004	0.00109	0.00305
7	0.00302	0.00287	0.00042	0.001	0.00101	0.00234
8	0.00274	0.00159	0.00186	0.002	0.00229	0.00163
9	0.0007	0.00238	0.00067	0.003	0.00063	0.0026
10	0.00029	0.001	0.001	0	0.00242	0.00152
11	0.00216	0.00008	0.00356	0.004	0.00237	0.00062
12	0.00507	0.00114	0.00419	0.001	0.00019	0.00499
13	0.00389	0.00336	0.00221	0.003	0.00326	0.00119
14	0.00158	0.00025	0.0013	0.002	0.00216	0.00098
15	0.0007	0.00147	0.00382	0.001	0.00047	0.00103
16	0.00016	0.0045	0.0062	0	0.00219	0.0007
17	0.00021	0.00198	0.00112	0	0.00311	0.00272
18	0.00031	0.00044	0.00394	0.002	0.00258	0.0026
19	0.00058	0.00003	0.00028	0.001	0.0008	0.00132
20	0.00142	0.00003	0.00259	0.001	0.00007	0.00249
21	0.00139	0.00109	0.00163	0.001	0.00173	0.0024
22	0.00105	0.00039	0.00279	0	0.00026	0.00133
23	0.00205	0.00115	0.00324	0	0.00309	0.00111
24	0.00088	0.00173	0.0012	0	0.0027	0.00186
25	0.00115	0.00069	0.00042	0	0.00194	0.00055
26	0.00214	0.00375	0.00193	0.001	0.00152	0.00139
27	0.00019	0.00029	0.00299	0.001	0.00018	0.00089
28	0.00392	0.00492	0.0018	0	0.00026	0.00041
29	0.0016	0.0009	0.00057	0	0.00194	0.00166
30	0.0031	0.00159	0.00057	0.003	0.0032	0.00094
31	0.0003	0.00046	0.00173	0.001	0.00048	0.00123
32	0.00037	0.00138	0.00393	0.001	0.00448	0.00383
33	0.00317	0.00294	0.00001	0.002	0.00331	0.00064
34	0.00496	0.00038	0.00099	0.003	0.00413	0.0004
35	0.00577	0.00612	0.00341	0.002	0.00461	0.0061
36	0.00372	0.00176	0.00444	0.001	0.00128	0.00233
37	0.00135	0.00361	0.00208	0.001	0.0007	0.00251
38	0.00162	0.00072	0.0013	0.004	0.00052	0.00291
39	0.00534	0.00011	0.00279	0.001	0.00065	0.00294
40	0.00094	0.00152	0.00003	0.002	0.00269	0.00076
41	0.00038	0.0006	0.0002	0.001	0.00067	0.00082
42	0.00359	0.00232	0.00148	0.002	0.00095	0.00052
43	0.0014	0.00312	0.00228	0.001	0.00141	0.00156
44	24	25	26	27	28	29
45	0.0019048	0.00171	0.0020238	0.001425	0.0017018	0.0018443
46						
47						

Table 30. (Continued)

	AE	AF	AG	AH	AI	AJ
1			91/7/15			
2	13:51:35	14:05:24	12:25:27	12:38:22	12:59:14	13:10:49
3	61.054	61.056	None	60.049	60.041	60.037
4	0.00286	0.00007	0.003	0.00055	0.00087	0.00156
5	0.0004	0.0013	0.002	0.00142	0.00248	0.00201
6	0.00007	0.00037	0.001	0.00517	0.00699	0.00235
7	0.00076	0.00192	0.001	0.00084	0.00239	0.00126
8	0.00035	0.00532	0	0.00289	0.00453	0.00174
9	0.00267	0.00089	0.003	0.00245	0.00135	0.0023
10	0.00005	0.00189	0.002	0.00296	0.00135	0.00057
11	0.00469	0.00391	0.001	0.0014	0.0005	0.00157
12	0.00186	0.00089	0.004	0.00078	0.00024	0.00155
13	0.00257	0.00017	0	0.0029	0.00429	0.00021
14	0.00272	0.00159	0.001	0.00403	0.00353	0.00049
15	0.00572	0.00232	0.002	0.00396	0.00094	0.00209
16	0.00012	0.00119	0.001	0.00128	0.00296	0.00032
17	0.00032	0.00221	0	0.00166	0.00066	0.00209
18	0.00359	0.00221	0.002	0.00276	0.0027	0.00326
19	0.00056	0.00042	0.001	0.0035	0.00079	0.00009
20	0.00377	0.00259	0.001	0.00157	0.00352	0.00185
21	0.00188	0.0001	0.001	0.00054	0.00219	0.0019
22	0.0038	0.00084	0.003	0.00211	0.00276	0.00134
23	0.00247	0.00202	0.002	0.00141	0.00003	0.0013
24	0.00111	0.00001	0.001	0.00055	0.00046	0.00069
25	0.00137	0.00344	0.001	0.00257	0.00139	0.00049
26	0.00078	0.00133	0	0.00199	0.00036	0.00032
27	0.00022	0.0011	0.001	0.0038	0.00423	0.00075
28	0.00337	0.00148	0.002	0.00208	0.00032	0.00255
29	0.00099	0.00147	0.001	0.00104	0.00309	0.00276
30	0.00321	0.00119	0.001	0.00127	0.00155	0.00148
31	0.00158	0.00033	0.001	0.00331	0.0004	0.00198
32	0.00264	0.00031	0.003	0.00146	0.00025	0.00145
33	0.00044	0.00023	0	0.00017	0.00213	0.00154
34	0.00212	0.00168	0.001	0.00144	0.00189	0.00321
35	0.00252	0.00061	0.003	0.00217	0.00392	0.00423
36	0.00303	0.00009	0.003	0.00217	0.00244	0.0018
37	0.00191	0.0006	0.002	0.00332	0.00302	0.0009
38	0.00376	0.00488	0.003	0.00257	0.00225	0.00152
39	0.00141	0.002	0.003	0.00236	0.00064	0.00132
40	0.00229	0.0007	0.001	0.00118	0.00143	0.00036
41	0.00035	0.00233	0	0.00059	0.00145	0.00219
42	0.00131	0.00043	0	0.00124	0.00197	0.0003
43	0.00039	0.0005	0.002	0.00019	0.00208	0.00019
44	30	31	32	33	34	35
45	0.0019008	0.0014233	0.0015	0.0019913	0.0020085	0.001497
46						
47						

Table 30. (Continued)

	AK	AL	AM	AN	AO	AP
1						
2	13:32:56	13:35:29	13:42:34	13:59:31	14:13:24	14:39:51
3	60.035	60.035	60.033	60.031	59.032	59.022
4	0.00092	0.00092	0.00137	0.00083	0.00179	0.00053
5	0.00208	0.00408	0.00035	0.00039	0.0027	0.00119
6	0.00074	0.00126	0.00253	0.00036	0.00354	0.00083
7	0.00187	0.00013	0.00171	0.00275	0.00161	0.00001
8	0.00167	0.00133	0.00068	0.00406	0.00285	0.00004
9	0.00089	0.00189	0.00004	0.0022	0.00187	0.00234
10	0.00028	0.00072	0.00152	0.00265	0.00079	0.00505
11	0.00183	0.00117	0.00001	0.00069	0.00215	0.00167
12	0.00142	0.00242	0.00162	0.00003	0.00071	0.00095
13	0.00027	0.00127	0.00057	0.00182	0.00267	0.00258
14	0.00082	0.00282	0.00208	0.0005	0.00224	0.00173
15	0.00097	0.00103	0.00039	0.00138	0.00031	0.00055
16	0.00007	0.00207	0.00273	0.00037	0.00061	0.00281
17	0.00002	0.00002	0.00474	0.00005	0.00003	0.00001
18	0.00115	0.00185	0.00018	0.00548	0.00287	0.00019
19	0.00077	0.00177	0.00428	0.00081	0.00079	0.00005
20	0.00198	0.00002	0.00014	0.00031	0.0008	0.00298
21	0.00077	0.00077	0.00024	0.00014	0.00163	0.00227
22	0.00072	0.00072	0.00038	0.00296	0.00279	0.00178
23	0.00034	0.00266	0.00189	0.00067	0.00239	0.00067
24	0.00227	0.00127	0.00066	0.00067	0.00153	0.00194
25	0.00107	0.00093	0.00282	0.00002	0.00384	0.00132
26	0.00187	0.00187	0.00373	0.00115	0.00111	0.00343
27	0.0012	0.0012	0.00042	0.00299	0.00102	0.00221
28	0.00102	0.00098	0.00242	0.00156	0.00464	0.00252
29	0.00258	0.00158	0.00063	0.00006	0.00046	0.00136
30	0.00212	0.00012	0.00254	0.00322	0.00028	0.00279
31	0.00179	0.00179	0.00061	0.00064	0.00404	0.00187
32	0.00193	0.00193	0.00184	0.00052	0.00041	0.00189
33	0.00475	0.00275	0.0006	0.00181	0.00156	0.00202
34	0.00009	0.00091	0.00381	0.00121	0	0.0008
35	0.00246	0.00346	0.00183	0.00276	0.00074	0.00222
36	0.00095	0.00195	0.00169	0.00286	0.00016	0.00371
37	0.00108	0.00092	0.00201	0.00128	0.00161	0.00187
38	0.0063	0.0033	0.0074	0.00489	0.00264	0.00144
39	0.00002	0.00098	0.0003	0.00396	0.0004	0.00314
40	0.00069	0.00169	0.00039	0.0012	0.00443	0.00023
41	0.00247	0.00047	0.00117	0.00191	0.00157	0.00003
42	0.00431	0.00231	0.00087	0.00353	0.00073	0.00286
43	0.00146	0.00154	0.00008	0.00103	0.0005	0.00234
44	36	37	38	39	40	41
45	0.0015003	0.0015218	0.0015818	0.001643	0.0016703	0.0017055
46						
47						

Table 30. (Continued)

	AQ	AR	AS	AT	AU	AV
1	91/7/19				91/12/11	
2	13:17:27	13:27:52	14:18:24	14:32:28	14:43:10	9:51:25
3	None	59.016	59.015	59.012	57.034	70.055
4	0.001	0.00354	0.00007	0.00292	0.00041	0.00131
5	0.003	0.00333	0.00342	0.00332	0.00045	0.00332
6	0	0.00084	0.0004	0.00292	0.0049	0.00446
7	0.003	0.00031	0.00392	0.00268	0.0005	0.00111
8	0.001	0.00068	0.00052	0.00536	0.0025	0.00166
9	0.001	0.00131	0.00148	0.00062	0.00073	0.00142
10	0.002	0.00009	0.00243	0.00361	0.00158	0.00295
11	0	0.00138	0.00041	0.00045	0.00443	0.00303
12	0.003	0.00323	0.00065	0.0046	0.00149	0.00158
13	0.003	0.00104	0.00066	0.00229	0.00124	0.00175
14	0	0.00021	0.00094	0.00054	0.00222	0.002
15	0.003	0.00045	0.00195	0.00023	0.00174	0.00313
16	0.001	0.00065	0.00257	0.00003	0.00183	0.00134
17	0	0.00117	0.00173	0.00156	0.0004	0.00119
18	0.002	0.00099	0.00146	0.00366	0.00447	0.00386
19	0.001	0.00199	0.00381	0.00278	0.00258	0.00107
20	0	0.00025	0.00327	0.00064	0.00176	0.00472
21	0.001	0.00166	0.00117	0.00103	0.00049	0.00473
22	0.003	0.0052	0.00122	0.00202	0	0.00107
23	0.002	0.00396	0.00027	0.00021	0.00056	0.00292
24	0.001	0.00043	0.00023	0.00214	0.00221	0.00545
25	0.001	0.00095	0.00011	0.0001	0.00179	0.00062
26	0.001	0.00277	0.00082	0.00292	0.00306	0.00037
27	0.001	0.0024	0.00239	0.00297	0.00346	0.00166
28	0.002	0	0.00134	0.00044	0.00068	0.00142
29	0.001	0.00185	0.00063	0.00453	0.00089	0.00088
30	0.001	0.00096	0.00243	0.00254	0.00181	0.00521
31	0.001	0.00179	0.00274	0.00038	0.00125	0.00106
32	0.003	0.00161	0.00025	0.00137	0.00054	0.00376
33	0	0.00086	0.00087	0.00106	0.00126	0.00446
34	0.002	0.00235	0.00228	0.0004	0.00194	0.00375
35	0.003	0.00456	0.00323	0.00317	0.00304	0.00235
36	0.003	0.00374	0.00071	0.00022	0.00156	0.00281
37	0.002	0.00459	0.00415	0.00034	0.00063	0.00598
38	0.001	0.00329	0.00182	0.00345	0.00701	0.00706
39	0.005	0.00256	0.00155	0.00321	0.0032	0.00527
40	0.001	0.00098	0.00091	0.0027	0.00114	0.00849
41	0	0.00202	0.00085	0.00239	0.00093	0.00376
42	0	0.00094	0.00228	0.003	0.00161	0.0048
43	0.003	0.00057	0.00056	0.00077	0.00106	0.0073
44	42	43	44	45	46	47
45	0.00155	0.0017875	0.0015625	0.0019893	0.0018338	0.003127
46						
47						

Table 30. (Continued)

	AW	AX	AY	AZ	BA	BB
1	91/12/17					
2	10:30:47	10:46:49	8:22:40	9:08:19	9:16:24	9:24:03
3	70.057	71.037	None	71.037	71.037	71.037
4	0.00235	0.00228	0.002	0.00128	0.00228	0.00228
5	0.00177	0.00005	0	0.00105	0.00005	0.00105
6	0.00227	0.00307	0.004	0.00107	0.00107	0.00107
7	0.00281	0.00212	0	0.00412	0.00412	0.00512
8	0.00438	0.00356	0.003	0.00056	0.00156	0.00356
9	0.00135	0.00198	0.002	0.00298	0.00298	0.00098
10	0.0022	0.00247	0.002	0.00047	0.00047	0.00147
11	0.00396	0.00345	0.004	0.00245	0.00345	0.00245
12	0.00249	0.00215	0.002	0.00415	0.00315	0.00315
13	0.00381	0.00362	0.001	0.00262	0.00362	0.00562
14	0.00013	0.00258	0.001	0.00258	0.00158	0.00158
15	0.0058	0.00412	0.002	0.00312	0.00312	0.00212
16	0.00344	0.00125	0	0.00075	0.00125	0.00075
17	0.00146	0.00535	0.002	0.00435	0.00435	0.00635
18	0.00064	0.00226	0.004	0.00026	0.00226	0.00126
19	0.00075	0.00261	0.001	0.00361	0.00061	0.00061
20	0.00543	0.00327	0.003	0.00128	0.00327	0.00428
21	0.00279	0.00272	0.003	0.00072	0.00172	0.00272
22	0.00041	0.0007	0.003	0.0003	0.0003	0.0003
23	0.00082	0.00251	0.002	0.00151	0.00151	0.00051
24	0.00075	0.00093	0.001	0.00093	0.00193	0.00093
25	0.00359	0.00344	0.003	0.00044	0.00244	0.00244
26	0.00315	0.0033	0.001	0.0023	0.0013	0.0013
27	0.00021	0.00084	0.001	0.00084	0.00016	0.00084
28	0.00068	0.0052	0.003	0.0012	0.0042	0.0042
29	0.00032	0.00408	0.001	0.00208	0.00108	0.00208
30	0.0021	0.00231	0.002	0.00131	0.00131	0.00131
31	0.00103	0.00034	0.002	0.00134	0.00234	0.00234
32	0.00266	0.0012	0.003	0.0002	0.0002	0.0022
33	0.00647	0.00518	0.003	0.0003	0.0003	0.0003
34	0.00376	0.00257	0.003	0.00457	0.00357	0.00257
35	0.0025	0.00057	0.003	0.00057	0.00057	0.00057
36	0.00619	0.00839	0.004	0.00239	0.00239	0.00439
37	0.0097	0.00469	0.006	0.00569	0.00469	0.00569
38	0.00619	0.00365	0.003	0.00265	0.00265	0.00065
39	0.00355	0.00637	0.003	0.00737	0.00437	0.00637
40	0.00711	0.00589	0.007	0.00589	0.00389	0.00589
41	0.00092	0.00201	0.003	0.0001	0.00201	0.00099
42	0.00791	0.00639	0.009	0.00439	0.00439	0.00339
43	0.00589	0.00278	0.002	0.00378	0.00378	0.00378
44	48	49	50	51	52	53
45	0.00309351	0.0030563	0.0026	0.0021893	0.0022573	0.0024865
46						
47						

Table 30. (Continued)

	BC	BD	BE	BF	BG	BH
1					91/12/18	92/1/6
2	9:38:43	9:49:33	9:55:24	10:25:21	11:25:26	13:11:27
3	71.038	None	71.038	71.083	71.083	None
4	0.00152	0.004	0.00052	0.00276	0.00276	0.001
5	0.00335	0	0.00235	0.00031	0.00069	0.001
6	0.00441	0.003	0.00541	0.00074	0.00174	0.004
7	0.00158	0.001	0.00258	0.00249	0.00249	0
8	0.00208	0.004	0.00108	0.00464	0.00364	0.004
9	0.00378	0.004	0.00378	0.004	0.004	0.003
10	0.00345	0.001	0.00145	0.00386	0.00286	0.001
11	0.00348	0.004	0.00448	0.00338	0.00438	0.003
12	0.00043	0.001	0.00143	0.00198	0.00198	0.001
13	0.00526	0.002	0.00626	0.00096	0.00196	0.001
14	0.00196	0.002	0.00496	0.00151	0.00151	0.001
15	0.00268	0.002	0.00368	0.00025	0.00175	0.002
16	0.00155	0.002	0.00155	0.00269	0.00269	0
17	0.00246	0.002	0.00346	0.00495	0.00295	0.002
18	0.00111	0.002	0.00111	0.00307	0.00307	0.003
19	0.00394	0.001	0.00294	0.0036	0.0036	0.001
20	0.00609	0.002	0.00509	0.00207	0.00207	0.001
21	0.00288	0.003	0.00388	0.00539	0.00439	0.003
22	0.00071	0.001	0.00071	0.00093	0.00193	0.002
23	0.00215	0.002	0.00215	0.00486	0.00486	0.001
24	0.00113	0.002	0.00313	0.0053	0.0043	0.001
25	0.00103	0.003	0.00203	0.00407	0.00507	0.003
26	0.001	0.002	0.002	0.0012	0.0008	0.002
27	0.00026	0.001	0.00074	0.00122	0.00022	0.001
28	0.00506	0.004	0.00506	0.00258	0.00158	0.004
29	0.00098	0.001	0.00102	0.00217	0.00417	0.002
30	0.0062	0.002	0.0052	0.00339	0.00239	0.003
31	0.00036	0.002	0.00036	0.00084	0.00016	0.002
32	0.00328	0.004	0.00328	0.00455	0.00555	0.003
33	0.00153	0.002	0.00147	0.00221	0.00506	0.002
34	0.00231	0.003	0.00331	0.00167	0.00167	0.001
35	0.00007	0.002	0.00007	0.00099	0.00101	0
36	0.00691	0.004	0.00091	0.00332	0.00532	0.004
37	0.00557	0.007	0.00457	0.00844	0.00744	0.007
38	0.00368	0.005	0.00368	0.00189	0.00289	0.001
39	0.00423	0.006	0.00323	0.00654	0.00254	0.001
40	0.00377	0.005	0.00577	0.00498	0.00398	0.004
41	0.00266	0.003	0.00234	0.00094	0.00094	0.003
42	0.00968	0.008	0.00968	0.00868	0.00667	0.005
43	0.00851	0.005	0.00851	0.00555	0.00655	0.002
44	54	55	56	57	58	59
45	0.0030773	0.00285	0.0032058	0.0031243	0.0030908	0.00215
46						
47						

Table 30. (Continued)

	BI	BJ	BK	BL	BM	BN
1						
2	13:01:29	13:07:10	13:44:27	13:18:51	14:19:26	14:29:06
3	None	71.128	71.128	71.128	59.022	59.022
4	0.003	0.00349	0.00249	0.0026	0.00047	0.00336
5	0	0.0018	0.0028	0.00112	0.00019	0.00195
6	0.004	0.0011	0.0011	0.00223	0.00017	0.00073
7	0.001	0.00052	0.00052	0.00161	0.00099	0.0017
8	0.003	0.00014	0.00086	0.00332	0.00004	0.00305
9	0.002	0.00047	0.00053	0.00286	0.00434	0.00426
10	0.003	0.0035	0.0025	0.00237	0.00405	0.00016
11	0.005	0.00262	0.00462	0.0021	0.00567	0.00031
12	0.002	0.00325	0.00325	0.00144	0.00105	0.00443
13	0.002	0.00487	0.00387	0.00056	0.00042	0.00074
14	0.002	0.00071	0.00171	0.00181	0.00127	0.00034
15	0.002	0.00223	0.00223	0.00103	0.00055	0.00274
16	0.002	0.00052	0.00152	0.00289	0.00281	0.00124
17	0.004	0.00334	0.00334	0.00054	0.00099	0.0027
18	0.003	0.00166	0.00266	0.00137	0.00019	0.00241
19	0.001	0.003	0.001	0.00083	0.00205	0.00122
20	0.004	0.00462	0.00362	0.00478	0.00398	0.00037
21	0.003	0.00317	0.00317	0.00415	0.00328	0.00203
22	0.002	0.00108	0.00192	0.00184	0.00578	0.00034
23	0.001	0.00446	0.00446	0.00241	0.00033	0.00094
24	0.002	0.00227	0.00327	0.00377	0.00106	0.00075
25	0.003	0.00419	0.00619	0.0037	0.00168	0.00544
26	0.001	0.0013	0.0023	0.00174	0.00043	0.00273
27	0	0.00095	0.00005	0.00132	0.00121	0.002
28	0.005	0.00126	0.00226	0.00575	0.00052	0.00005
29	0	0.00012	0.00012	0.00065	0.00336	0.00159
30	0.003	0.0057	0.0037	0.00017	0.00379	0.00292
31	0.002	0.00138	0.00038	0.00525	0.00087	0.00071
32	0.003	0.00494	0.00594	0.00408	0.00511	0.00266
33	0.003	0.00084	0.00084	0.0003	0.00102	0.0045
34	0.002	0.0023	0.0003	0.00082	0.0002	0.00277
35	0.003	0.00019	0.00119	0.00092	0.00278	0.00187
36	0.004	0.00288	0.00188	0.00171	0.00471	0.00235
37	0.006	0.00419	0.00419	0.00646	0.00087	0.00555
38	0	0.00554	0.00454	0.00293	0.00244	0.00121
39	0.004	0.00414	0.00014	0.00303	0.00114	0.00148
40	0.003	0.00499	0.00299	0.00451	0.00523	0.00004
41	0	0.00026	0.00026	0.00051	0.00197	0.00268
42	0.006	0.00187	0.00187	0.00424	0.00286	0.00402
43	0.002	0.00916	0.00616	0.00627	0.00366	0.00341
44	60	61	62	63	64	65
45	0.002525	0.0026255	0.0024185	0.0024998	0.0020883	0.002105
46						
47						

Table 30. (Continued)

	BO	BP	BQ	BR	BS	BT
1		92/1/9	92/1/13			
2	14:48:26	14:59:03	12:46:22	13:22:26	13:25:33	13:38:13
3	59.022	59.022	None	None	None	None
4	0.00053	0.00147	0.002	0.002	0.004	0.003
5	0.00019	0.00181	0.003	0.002	0	0
6	0.00017	0.00117	0.001	0.002	0.003	0.004
7	0.00099	0.00099	0.003	0.003	0.001	0
8	0.00004	0.00004	0.002	0.003	0.004	0.005
9	0.00434	0.00434	0.003	0.002	0.002	0.003
10	0.00405	0.00405	0.003	0.003	0.001	0.003
11	0.00267	0.00367	0.002	0.003	0.004	0.003
12	0.00105	0.00105	0.003	0.002	0.001	0.002
13	0.00258	0.00058	0.002	0.004	0.002	0.002
14	0.00173	0.00027	0.001	0	0.002	0.002
15	0.00055	0.00255	0.001	0.001	0.003	0.001
16	0.00481	0.00181	0.003	0.003	0.002	0.001
17	0.00099	0.00099	0.004	0.002	0.002	0.005
18	0.00081	0.00119	0.001	0.002	0.004	0.001
19	0.00105	0.00105	0.003	0.003	0.001	0.002
20	0.00498	0.00498	0.005	0.004	0.002	0.004
21	0.00527	0.00328	0.002	0.003	0.003	0.004
22	0.00278	0.00478	0.002	0.001	0.002	0.003
23	0.00033	0.00067	0.002	0.004	0.002	0.001
24	0.00206	0.00094	0.004	0.004	0.003	0.003
25	0.00068	0.00168	0.003	0.002	0.004	0.004
26	0.00143	0.00043	0.001	0.003	0.001	0.002
27	0.00221	0.00221	0.002	0.001	0.001	0.001
28	0.00048	0.00052	0.002	0.003	0.005	0.004
29	0.00236	0.00236	0	0.001	0	0.002
30	0.00379	0.00579	0.004	0.002	0.002	0.003
31	0.00187	0.00087	0.002	0.002	0.003	0.002
32	0.00411	0.00441	0.003	0.001	0.003	0.003
33	0.00102	0.00098	0.001	0.002	0.002	0.001
34	0.0008	0.0002	0.003	0.005	0.003	0.002
35	0.00378	0.00178	0.002	0.001	0.002	0.003
36	0.00371	0.00571	0.003	0.004	0.003	0.002
37	0.00287	0.00387	0.004	0.003	0.003	0.004
38	0.00344	0.00044	0.001	0.005	0.001	0.001
39	0.00114	0.00314	0.001	0.005	0.005	0.003
40	0.00523	0.00023	0.004	0.004	0.004	0.002
41	0.00003	0.00197	0.001	0.003	0.002	0
42	0.00486	0.00486	0.005	0.005	0.004	0.002
43	0.00566	0.00266	0.003	0.003	0.003	0.005
44	66	67	68	69	70	71
45	0.002286	0.0021448	0.002425	0.0027	0.002475	0.00245
46						
47						

Table 30. (Continued)

	BU	BV	BW	BX	BY	BZ
1			92/1/14	92/1/15	92/1/30	
2	13:39:27	14:55:03	15:15:16	14:36:36	11:55:02	12:48:38
3	72.026	None	72.026	None	72.067	None
4	0.00243	0.001	0.00043	0.001	0.00243	0.003
5	0.00133	0.001	0.00133	0.003	0.00133	0.002
6	0.00355	0.003	0.00455	0.003	0.00455	0.001
7	0.00254	0.001	0.00154	0.001	0.00054	0.003
8	0.00728	0.004	0.00728	0.004	0.00728	0.002
9	0.00081	0.001	0.00281	0.004	0.00081	0.004
10	0.00495	0.002	0.00295	0.001	0.00295	0.002
11	0.00191	0.004	0.00191	0.004	0.00191	0.002
12	0.00019	0.001	0.00019	0.002	0.00019	0.004
13	0.00267	0.002	0.00367	0.002	0.00367	0.003
14	0.00349	0.003	0.00349	0.001	0.00349	0.002
15	0.00516	0.001	0.00316	0.002	0.00316	0.001
16	0.00207	0.003	0.00407	0.003	0.00307	0.003
17	0.00172	0.004	0.00071	0.001	0.00028	0.001
18	0.00186	0.003	0.00086	0.005	0.00186	0.001
19	0.00149	0.001	0.00051	0.004	0.00249	0.004
20	0.00352	0.003	0.00352	0.003	0.00152	0.003
21	0.00268	0.004	0.00468	0.003	0.00268	0.002
22	0.0052	0.001	0.00419	0.003	0.00419	0.002
23	0.00469	0	0.00369	0.002	0.00469	0.003
24	0.00175	0.004	0.00275	0.002	0.00175	0.004
25	0.00665	0.003	0.00565	0.002	0.00665	0.003
26	0.00136	0.002	0.00236	0.002	0.00236	0.003
27	0.00055	0	0.00055	0.001	0.00045	0.001
28	0.00543	0.004	0.00443	0.002	0.00643	0.002
29	0.00107	0.002	0.00207	0.003	0.00207	0.002
30	0.00205	0.003	0.00105	0.003	0.00005	0.005
31	0.00353	0.004	0.00653	0.002	0.00453	0.002
32	0.00511	0.004	0.00711	0.003	0.00611	0.003
33	0.00479	0.002	0.00279	0.003	0.00379	0.003
34	0.00161	0.003	0.00361	0.003	0.00161	0.003
35	0.00048	0.002	0.00048	0	0.00052	0.001
36	0.00318	0.002	0.00318	0.004	0.00418	0.004
37	0.00626	0.007	0.00726	0.003	0.00626	0.003
38	0.00197	0.003	0.00397	0.001	0.00397	0.004
39	0.0011	0.007	0.0001	0.002	0.0021	0.006
40	0.00457	0.006	0.00357	0.003	0.00557	0.005
41	0.00216	0.004	0.00316	0	0.00084	0.006
42	0.00283	0.008	0.00483	0.003	0.00383	0.002
43	0.00487	0.002	0.00687	0.004	0.00387	0.004
44	72	73	74	75	76	77
45	0.0030215	0.002875	0.0031965	0.00245	0.0030008	0.00285
46						
47						

Table 30. (Continued)

	CA	CB	CC	CD	CE	CF
1						92/1/31
2	12:53:25	13:00:41	13:23:30	13:31:28	14:20:08	14:24:37
3	None	72.026	None	72.067	None	None
4	0.003	0.00243	0.003	0.00043	0.003	0.004
5	0.002	0.00133	0.001	0.00333	0.002	0.002
6	0.002	0.00455	0.003	0.00255	0.001	0.003
7	0.003	0.00254	0.002	0.00354	0.003	0.003
8	0.002	0.00628	0.002	0.00628	0.003	0.002
9	0.005	0.00081	0.003	0.00081	0.004	0
10	0.002	0.00495	0.002	0.00495	0.003	0.005
11	0.002	0.00291	0.004	0.00009	0.002	0.002
12	0.005	0.00019	0.003	0.00081	0.004	0
13	0.002	0.00467	0.002	0.00367	0.001	0.004
14	0.001	0.00349	0.001	0.00349	0	0.002
15	0.002	0.00316	0.004	0.00216	0.003	0.001
16	0.003	0.00307	0.001	0.00507	0.001	0.003
17	0.002	0.00071	0.001	0.00172	0.002	0.003
18	0.002	0.00086	0.004	0.00114	0.003	0.003
19	0.004	0.00149	0.002	0.00149	0.003	0.002
20	0.003	0.00552	0.003	0.00252	0.004	0.002
21	0.003	0.00368	0.003	0.00368	0.003	0.003
22	0.003	0.00419	0.003	0.0032	0.003	0.002
23	0.003	0.00669	0.002	0.00469	0.003	0.001
24	0.004	0.00275	0.003	0.00175	0.001	0.001
25	0.002	0.00565	0.005	0.00565	0.003	0.002
26	0.002	0.00036	0.002	0.00236	0.002	0.004
27	0.002	0.00145	0.001	0.00055	0.001	0.003
28	0.002	0.00543	0.004	0.00343	0.003	0.002
29	0.002	0.00007	0.002	0.00107	0.001	0
30	0.005	0.00305	0.004	0.00105	0.004	0
31	0.002	0.00553	0.001	0.00253	0.001	0.004
32	0.003	0.00411	0.002	0.00611	0.001	0.001
33	0.004	0.00479	0.003	0.00379	0.003	0.001
34	0.003	0.00261	0.001	0.00261	0.003	0.003
35	0.001	0.00048	0	0.00052	0.001	0.004
36	0.002	0.00718	0.005	0.00518	0.004	0
37	0.007	0.00626	0.002	0.00626	0.007	0.003
38	0.001	0.00597	0.001	0.00697	0.007	0.001
39	0.006	0.0029	0.002	0.0019	0.006	0.002
40	0.003	0.00857	0.003	0.00557	0.004	0.001
41	0.004	0.00216	0	0.00216	0.004	0.002
42	0.008	0.00683	0.003	0.00683	0.009	0.002
43	0.005	0.00687	0.004	0.00587	0.002	0
44	78	79	80	81	82	83
45	0.00305	0.0036635	0.002425	0.0031945	0.00295	0.002075
46						
47						

Table 30. (Continued)

	CG	CH	CI	CJ	CK	CL
1	92/2/3	92/2/4		92/2/5		
2	13:29:33	12:17:16	12:58:11	13:05:37	12:34:16	12:56:55
3	None	None	None	72.026	None	563.4
4	0.004	0.004	0.003	0.00043	0.004	0.0031
5	0	0	0.001	0.00333	0.003	0.00287
6	0.005	0.005	0.003	0.00155	0.002	0.00368
7	0	0.002	0.002	0.00354	0.003	0.00337
8	0.004	0.002	0.003	0.00528	0.003	0.00075
9	0.002	0.005	0.003	0.00281	0.004	0.00242
10	0.004	0.001	0.002	0.00495	0.005	0.00381
11	0.005	0.003	0.004	0.00009	0.002	0.00221
12	0.002	0.005	0.003	0.00281	0.003	0.00357
13	0.003	0.002	0.002	0.00167	0.002	0.00543
14	0.002	0.004	0.001	0.00049	0.002	0.00127
15	0.002	0.004	0.004	0.00516	0.003	0.00117
16	0.002	0.002	0.002	0.00407	0.003	0.00328
17	0.004	0.002	0.001	0.00071	0.003	0.00302
18	0.003	0.002	0.004	0.00014	0.002	0.00077
19	0	0.003	0.002	0.00051	0.003	0.00297
20	0.004	0.003	0.003	0.00452	0.003	0.00631
21	0.004	0.002	0.003	0.00168	0.002	0.00304
22	0.002	0.003	0.003	0.0062	0.003	0.00033
23	0.002	0.003	0.004	0.00669	0.003	0.00001
24	0.003	0.003	0.003	0.00175	0.002	0.00041
25	0.004	0.005	0.005	0.00665	0.003	0.00104
26	0.002	0.002	0.004	0.00236	0.004	0.00022
27	0.001	0.002	0.001	0.00145	0.002	0.00095
28	0.005	0.005	0.004	0.00543	0.004	0.00318
29	0.001	0.002	0.003	0.00007	0.003	0.00013
30	0.002	0.002	0.004	0.00305	0.004	0.00415
31	0.003	0.003	0.002	0.00453	0.001	0.0026
32	0.003	0.004	0.002	0.00411	0.003	0.00232
33	0.002	0.002	0.003	0.00479	0.003	0.00419
34	0.002	0.004	0.001	0.00261	0.002	0.00282
35	0.002	0.004	0	0.00048	0.002	0.0022
36	0.004	0.002	0.004	0.00518	0.003	0.00588
37	0.005	0.009	0.006	0.00626	0.004	0.00641
38	0.004	0.004	0.004	0.00497	0.002	0.00267
39	0.005	0.006	0.006	0.0001	0.007	0.00214
40	0.004	0.008	0.004	0.00457	0.002	0.00476
41	0.003	0.002	0.003	0.00416	0	0.00117
42	0.01	0.006	0.009	0.00683	0.003	0.00466
43	0.002	0.003	0.002	0.00387	0.004	0.00523
44	84	85	86	87	88	89
45	0.003025	0.003375	0.003075	0.0032463	0.0029	0.0027628
46						
47						

Table 30. (Continued)

	CM	CN	CO	CP	CQ	CR
1			92/2/6			
2	13:34:23	14:37:46	15:28:04	13:06:04	13:17:20	13:44:01
3	14.148	14.148	72.026	None	72.026	72.03
4	0.00004	0.00104	0.00057	0	0.00243	0.00419
5	0.00325	0.00125	0.00234	0.002	0.00033	0.0037
6	0.00582	0.00582	0.00155	0.001	0.00455	0.00286
7	0.00279	0.00279	0.00454	0.001	0.00154	0.00279
8	0.0047	0.0057	0.00528	0.004	0.00628	0.00331
9	0.00104	0.00104	0.00281	0.002	0.00081	0.00027
10	0.00435	0.00435	0.00495	0.003	0.00395	0.00402
11	0.00027	0.00127	0.00009	0.004	0.00009	0.00214
12	0.00433	0.00433	0.00181	0.002	0.00181	0.00019
13	0.00415	0.00215	0.00067	0.003	0.00367	0.00593
14	0.00217	0.00217	0.00149	0.001	0.00249	0.00027
15	0.000098	0.00298	0.00516	0.002	0.00316	0.00347
16	0.00142	0.00158	0.00407	0.001	0.00307	0.00133
17	0.00583	0.00383	0.00071	0.003	0.00172	0.0047
18	0.00166	0.00134	0.00086	0.004	0.00214	0.00242
19	0.00247	0.00053	0.00051	0.001	0.00249	0.00216
20	0.0025	0.0015	0.00452	0.004	0.00452	0.00401
21	0.00539	0.00539	0.00268	0.004	0.00168	0.00569
22	0.00009	0.00191	0.00719	0.002	0.00419	0.00063
23	0.0037	0.0037	0.00669	0.001	0.00469	0.00414
24	0.00505	0.00505	0.00025	0.001	0.00175	0.00163
25	0.00339	0.00639	0.00665	0.003	0.00565	0.00546
26	0.00098	0.00102	0.00336	0	0.00136	0.00217
27	0.00245	0.00045	0.00045	0	0.00045	0.00035
28	0.00068	0.00368	0.00343	0.004	0.00243	0.00114
29	0.0034	0.00241	0.00007	0	0.00093	0.00067
30	0.0055	0.0045	0.00205	0.002	0.00205	0.00293
31	0.00391	0.00291	0.00253	0.002	0.00353	0.00423
32	0.00035	0.00235	0.00511	0.003	0.00511	0.00275
33	0.00006	0.00094	0.00579	0.003	0.00379	0.0007
34	0.00052	0.00147	0.00161	0.002	0.00361	0.00049
35	0.00015	0.00085	0.00048	0.003	0.00048	0.00175
36	0.00066	0.00234	0.00518	0.004	0.00418	0.00391
37	0.00566	0.00766	0.00626	0.005	0.00326	0.0039
38	0.0013	0.0053	0.00797	0.003	0.00697	0.00479
39	0.00212	0.00512	0.0019	0.007	0.0009	0.00753
40	0.00099	0.00299	0.00457	0.002	0.00557	0.00347
41	0.00312	0.00512	0.00316	0	0.00116	0.00119
42	0.00663	0.00733	0.00483	0.007	0.00483	0.00769
43	0.00605	0.00405	0.00787	0.004	0.00187	0.00763
44	90	91	92	93	94	95
45	0.002726	0.003165	0.0033003	0.0025	0.0028873	0.003065
46						
47						

Table 30. (Continued)

	CS	CT	CU	CV	CW	CX
1			92/2/7			92/2/10
2	14:11:16	14:35:04	15:11:40	12:51:48	13:09:52	15:15:11
3	72.051	72.052	14.148	None	14.148	None
4	0.00018	0.00203	0.00104	0.002	0.00204	0.002
5	0.00291	0.00095	0.00225	0.002	0.00225	0.003
6	0.00334	0.00018	0.00382	0.002	0.00482	0
7	0.00008	0.00114	0.00279	0.002	0.00379	0.004
8	0.00604	0.00108	0.0027	0.002	0.0027	0.002
9	0.00119	0.00663	0.00204	0.004	0.00204	0.005
10	0.00247	0.00005	0.00235	0.003	0.00235	0.004
11	0.00456	0.00233	0.00127	0.003	0.00127	0.001
12	0.00086	0.00298	0.00633	0.004	0.00633	0.003
13	0.00009	0.00297	0.00215	0.001	0.00215	0.001
14	0.00469	0.00017	0.00017	0.003	0.00017	0.001
15	0.00046	0.00025	0.00298	0.004	0.00398	0.001
16	0.00284	0.00258	0.00058	0.002	0.00042	0.003
17	0.00054	0.00303	0.00183	0.002	0.00183	0.004
18	0.00192	0.00293	0.00034	0.002	0.00034	0.001
19	0.00037	0.00247	0.00247	0.002	0.00347	0.003
20	0.00211	0.00249	0.0005	0.002	0.0005	0.005
21	0.00453	0.00245	0.00439	0.003	0.00439	0.003
22	0.00585	0.00469	0.0191	0.004	0.00191	0.002
23	0.00023	0.00245	0.0037	0.001	0.0047	0.003
24	0.00039	0.00369	0.00305	0.002	0.00405	0.003
25	0.00175	0.00374	0.00339	0.003	0.00239	0.002
26	0.0042	0.00112	0.00002	0.002	0.00002	0.001
27	0.00113	0.00379	0.00155	0.002	0.00155	0.001
28	0.00023	0.00282	0.00168	0.004	0.00168	0.002
29	0.00236	0.0006	0.0034	0	0.00241	0.002
30	0.00329	0.00214	0.0035	0.004	0.0035	0.005
31	0.00047	0.00407	0.00291	0.001	0.00291	0.002
32	0.00602	0.0036	0.00235	0.001	0.00135	0.003
33	0.00095	0.0021	0.00006	0.003	0.00094	0.004
34	0.00088	0.00058	0.00048	0.002	0.00052	0.003
35	0.00261	0.001	0.00115	0.001	0.00015	0
36	0.0022	0.00376	0.00134	0.003	0.00034	0.001
37	0.00231	0.00796	0.00666	0.007	0.00466	0.003
38	0.00486	0.00173	0.0063	0.003	0.0013	0.005
39	0.00165	0.00263	0.00212	0.003	0.00212	0.007
40	0.00245	0.00002	0.00199	0.002	0.00299	0.002
41	0.00036	0.00202	0.00312	0	0.00012	0.004
42	0.00199	0.00312	0.00633	0.007	0.00833	0.002
43	0.00763	0.00358	0.00605	0.005	0.00305	0.005
44	96	97	98	99	100	101
45	0.0023248	0.002448	0.0030063	0.002625	0.0023958	0.0027
46						
47						

Table 30. (Continued)

	CY	CZ	DA	DB	DC	DD
1				92/2/12		
2	12:46:50	13:42:19	14:24:44	14:51:08	12:43:43	12:53:15
3	None	14.148	72.058	72.06	None	563.4
4	0.003	0.00204	0.00187	0.00529	0.002	0.0031
5	0.001	0.00125	0.00063	0.00184	0	0.00287
6	0.003	0.00582	0.00098	0.00582	0.004	0.00368
7	0.002	0.00279	0.00065	0.00201	0.001	0.00337
8	0.001	0.0047	0.00399	0.00195	0.004	0.00025
9	0.003	0.00104	0.0025	0.00077	0.001	0.00242
10	0.003	0.00335	0.00479	0.00154	0.003	0.00381
11	0.003	0.00127	0.00203	0.00553	0.004	0.00221
12	0.003	0.00433	0.0037	0.00364	0.001	0.00157
13	0.002	0.00215	0.00446	0.00216	0.003	0.00443
14	0	0.00217	0.00276	0.00178	0.001	0.00327
15	0.002	0.00198	0.00115	0.00019	0.002	0.00183
16	0.004	0.00158	0.00348	0.00192	0.001	0.00128
17	0.002	0.00583	0.00384	0.00254	0.004	0.00502
18	0.003	0.00166	0.0002	0.00178	0.002	0.00122
19	0.003	0.00047	0.00047	0.00162	0	0.00097
20	0.004	0.0025	0.00381	0.00629	0.004	0.00631
21	0.002	0.00539	0.00326	0.00514	0.004	0.00404
22	0.002	0.00091	0.0027	0.00059	0.002	0.00133
23	0.004	0.0037	0.00335	0.00458	0.002	0.00101
24	0.003	0.00605	0.00714	0.0026	0.003	0.00259
25	0.001	0.00539	0.00092	0.00188	0.003	0.00104
26	0.003	0.00002	0.00335	0.00199	0.001	0.00178
27	0.001	0.00245	0.00015	0.00215	0	0.00005
28	0.004	0.00068	0.00222	0.0014	0.005	0.00418
29	0	0.0004	0.00043	0.00149	0.001	0.00013
30	0.002	0.0045	0.00118	0.00095	0.002	0.00215
31	0.002	0.00391	0.00564	0.00114	0.003	0.0026
32	0.001	0.00135	0.00535	0.00034	0.003	0.00332
33	0.002	0.00006	0.00435	0.00039	0.002	0.00119
34	0.004	0.00052	0.00493	0.0038	0.001	0.00182
35	0.001	0.00085	0.00017	0.00026	0.001	0.0032
36	0.001	0.00034	0.00236	0.00324	0.004	0.00288
37	0.005	0.00666	0.00645	0.00894	0.004	0.00241
38	0.003	0.00333	0.00287	0.00366	0.002	0.00133
39	0.002	0.00412	0.00902	0.00349	0.002	0.00014
40	0.002	0.00399	0.00276	0.0067	0.001	0.00176
41	0.002	0.00312	0.0044	0.0045	0	0.00217
42	0.004	0.00833	0.00584	0.00508	0.003	0.00266
43	0.003	0.00205	0.0006	0.00725	0.002	0.00723
44	102	103	104	105	106	107
45	0.0024	0.0028263	0.0030188	0.0029558	0.0022	0.0024655
46						
47						

Table 30. (Continued)

	DQ	DR	DS	DT	DU	DV
1					92/2/20	
2	13:25:39	13:47:32	14:20:42	14:47:19	15:30:30	12:59:43
3	563.4	603.4	1170.1	71.037	71.038	None
4	0.0041	0.00328	0.00489	0.0012	0.00083	0.002
5	0.00387	0.00022	0.0018	0.00452	0.00115	0
6	0.00268	0.00085	0.00192	0.00159	0.00181	0.003
7	0.00436	0.00045	0.00022	0.00411	0.00001	0.001
8	0.00025	0.00037	0.00556	0.00124	0.00172	0.003
9	0.00242	0.00151	0.00072	0.00172	0.00243	0.002
10	0.00381	0.00384	0.00231	0.0031	0.00104	0.002
11	0.0012	0.00418	0.00173	0.00115	0.00482	0.004
12	0.00257	0.00304	0.00121	0.00204	0.0018	0.001
13	0.00443	0.00085	0.00324	0.00015	0.0013	0.002
14	0.00127	0.00169	0.00046	0.00036	0.00295	0.003
15	0.00017	0.00014	0.00213	0.00275	0.00078	0.001
16	0.00128	0.00182	0.00177	0.00093	0.00348	0.002
17	0.00402	0.00419	0.00118	0.00124	0.00464	0.003
18	0.00122	0.00326	0.00399	0.00188	0.00372	0.003
19	0.00297	0.00042	0.00114	0.00142	0.00434	0.002
20	0.00631	0.00457	0.00375	0.00079	0.00404	0.002
21	0.00204	0.0022	0.00387	0.00145	0.00295	0.004
22	0.00233	0.00074	0.00181	0.00473	0.00514	0.002
23	0.00001	0.00011	0.00336	0.00065	0.00343	0.001
24	0.00041	0.0018	0.00219	0.0013	0.00195	0.003
25	0.00104	0.00336	0.0041	0.00698	0.00246	0.003
26	0.00078	0.0016	0.00201	0.00239	0.00147	0.003
27	0.00105	0.00149	0.00181	0.00232	0.0011	0
28	0.00218	0.00512	0.00537	0.0025	0.00475	0.003
29	0.00087	0.00016	0.00114	0.00264	0.00155	0.003
30	0.00515	0.00329	0.00089	0.00008	0.00275	0.003
31	0.0006	0.00553	0.00121	0.00018	0.00038	0.002
32	0.00332	0.00183	0.00116	0.00718	0.00568	0.003
33	0.00319	0.00052	0.00064	0.00418	0.00277	0.003
34	0.00018	0.00286	0.00252	0.00377	0.00258	0.003
35	0.0022	0.00281	0.00037	0.0004	0.00007	0.001
36	0.00388	0.00139	0.0023	0.00149	0.00109	0.003
37	0.0841	0.00359	0.00034	0.00538	0.00793	0.003
38	0.00033	0.0053	0.00174	0.00253	0.0014	0.003
39	0.00314	0.00477	0.00002	0.00686	0.005	0.004
40	0.00476	0.00095	0.00343	0.00492	0.0055	0.003
41	0.00217	0.00051	0.00004	0.0038	0.00237	0.001
42	0.00666	0.00222	0.00295	0.00628	0.00202	0.008
43	0.00623	0.00094	0.00423	0.00517	0.00426	0.004
44	120	121	122	123	124	125
45	0.0045888	0.0021943	0.002138	0.0026843	0.0027365	0.00255
46						
47						

Table 30. (Continued)

	DE	DF	DG	DH	DI	DJ
1				92/2/18		
2	13:27:36	14:04:05	14:52:57	15:18:44	13:01:12	13:12:55
3	1170.1	59.022	70.055	70.057	None	59.022
4	0.00189	0.00383	0.00235	0.00052	0.001	0.00153
5	0.0018	0.00025	0.0006	0.00122	0.003	0.00019
6	0.00108	0.00093	0.00375	0.00146	0.003	0.00217
7	0.00178	0.00062	0.00161	0.00267	0	0.00101
8	0.00356	0.00184	0.00697	0.00105	0.004	0.00304
9	0.00172	0.00067	0.00476	0.00237	0	0.00434
10	0.00231	0.00127	0.00131	0.00142	0.002	0.00405
11	0.00027	0.0001	0.00231	0.00131	0.003	0.00467
12	0.00079	0.0006	0.00265	0.00242	0	0.00195
13	0.00024	0.00266	0.00599	0.00186	0.003	0.00258
14	0.00146	0.00096	0.00315	0.00264	0	0.00127
15	0.00513	0.00001	0.00238	0.00397	0.001	0.00045
16	0.00177	0.00039	0.00364	0.00487	0.002	0.00281
17	0.00018	0.00397	0.00003	0.00305	0.004	0.00199
18	0.00399	0.00051	0.0041	0.00195	0.002	0.00019
19	0.00086	0.00266	0.00247	0.00559	0.002	0.00005
20	0.00275	0.00152	0.00006	0.00789	0.004	0.00298
21	0.00287	0.00034	0.00372	0.00189	0.003	0.00527
22	0.00119	0.00328	0.002	0.00464	0.001	0.00378
23	0.00436	0	0.00016	0.00636	0.002	0.00134
24	0.00019	0.00086	0.00466	0.00228	0.004	0.00106
25	0.0051	0.00064	0.00553	0.00423	0.002	0.00068
26	0.00101	0.00017	0.00452	0.00115	0.002	0.00043
27	0.00181	0.00083	0.00223	0.00134	0.001	0.00021
28	0.00437	0.00109	0.00597	0.00168	0.004	0.00148
29	0.00114	0.00252	0.00027	0.00155	0	0.00236
30	0.00111	0.00143	0.0015	0.00287	0.002	0.00279
31	0.00021	0.00237	0.00358	0.00339	0.002	0.00187
32	0.00084	0.00403	0.00297	0.0034	0	0.00511
33	0.00264	0.00004	0.00163	0.00058	0.001	0.00102
34	0.00152	0.00115	0.00386	0.00105	0.003	0.0002
35	0.00137	0.00256	0.00064	0.00125	0.001	0.00278
36	0.0033	0.00033	0.0002	0.00233	0.001	0.00471
37	0.00134	0.00318	0.00653	0.00411	0.004	0.00187
38	0.00274	0.00432	0.00049	0.00577	0.003	0.00344
39	0.00098	0.00595	0.00264	0.00012	0.003	0.00114
40	0.00343	0.00132	0.00166	0.00776	0.002	0.00423
41	0.00404	0.00213	0.00515	0.00169	0.002	0.00103
42	0.00395	0.00025	0.00792	0.00238	0.005	0.00586
43	0.00623	0.00633	0.00507	0.00957	0.001	0.00366
44	108	109	110	111	112	113
45	0.002183	0.0016978	0.0030258	0.0029413	0.002075	0.0022898
46						
47						

Table 30. (Continued)

	DK	DL	DM	DN	DO	DP
1				92/2/19		
2	13:16:07	14:09:56	14:26:36	15:24:56	13:01:11	13:07:25
3	59.022	72.067	72.067	59.022	None	None
4	0.00193	0.00391	0.00191	0.00393	0.002	0.003
5	0.00036	0.00106	0.00038	0.00264	0	0.001
6	0.00104	0.00507	0.00507	0.00204	0.003	0.003
7	0.00174	0.00163	0.00063	0.00026	0.001	0.002
8	0.00005	0.00638	0.00638	0.00195	0.004	0.003
9	0.00056	0.0023	0.0003	0.00156	0.002	0.004
10	0.00038	0.00051	0.00149	0.00138	0.002	0.001
11	0.00079	0.00526	0.00626	0.00221	0.004	0.003
12	0.0017	0.00087	0.00113	0.0007	0.001	0.003
13	0.00277	0.00062	0.00617	0.00277	0	0.001
14	0.00092	0.00287	0.00087	0.00108	0.002	0.001
15	0.00111	0.00332	0.00032	0.00111	0.001	0.004
16	0.00073	0.00242	0.00042	0.00227	0.001	0
17	0.00109	0.00228	0.00128	0.00309	0.003	0.001
18	0.0006	0.00155	0.00055	0.0006	0.002	0.003
19	0.00277	0.00109	0.00009	0.00077	0.002	0.001
20	0.00062	0.00289	0.00389	0.00062	0.003	0.003
21	0.00045	0.00345	0.00345	0.00145	0.004	0.001
22	0.0024	0.00037	0.00063	0.0034	0.003	0.002
23	0.00112	0.00086	0.00286	0.00012	0	0.002
24	0.00098	0.00402	0.00502	0.00198	0.003	0.001
25	0.00025	0.00557	0.00357	0.00175	0.003	0.003
26	0.00194	0.0009	0.0001	0.00106	0.002	0.003
27	0.00007	0.00208	0.00108	0.00107	0.001	0
28	0.00119	0.00232	0.00132	0.00219	0.002	0.003
29	0.00263	0.00077	0.00177	0.00163	0.001	0.002
30	0.00045	0.00376	0.00476	0.00055	0.002	0.004
31	0.00248	0.00045	0.00155	0.00348	0.002	0.001
32	0.00314	0.00399	0.00199	0.00414	0.004	0.001
33	0.00015	0.00309	0.00209	0.00015	0.002	0.003
34	0.00125	0.00213	0.00113	0.00025	0.003	0.001
35	0.00245	0.00053	0.00147	0.00045	0.002	0
36	0.00144	0.00423	0.00423	0.00044	0.01	0.004
37	0.00229	0.00351	0.00251	0.00329	0.007	0.005
38	0.00243	0.00228	0.00428	0.00143	0.006	0.001
39	0.00207	0.00063	0.00263	0.00507	0.005	0.003
40	0.00343	0.00066	0.00534	0.00143	0.003	0.001
41	0.00124	0.00154	0.00046	0.00524	0.003	0.001
42	0.00235	0.00601	0.00401	0.00435	0.005	0.002
43	0.00644	0.00551	0.00751	0.00544	0.002	0.003
44	114	115	116	117	118	119
45	0.001545	0.0025673	0.0025225	0.0019835	0.0027	0.0021
46						
47						

Table 30. (Continued)

	DW	DX	DY	DZ	EA	EB
1						
2	13:14:21	13:34:22	13:58:43	14:15:12	14:34:26	15:33:17
3	71.05	71.083	71.108	71.128	72.067	59.022
4	0.00337	0.00315	0.00227	0.00245	0.00291	0.00147
5	0.00273	0.0037	0.00413	0.00083	0.00238	0.00019
6	0.00318	0.00105	0.00374	0.00143	0.00207	0.00017
7	0.00033	0.00011	0.00495	0.00447	0.00363	0.00099
8	0.00454	0.00067	0.00011	0.00248	0.00438	0.00004
9	0.00034	0.00255	0.00012	0.00346	0.0043	0.00334
10	0.0028	0.00109	0.0031	0.00107	0.00149	0.00605
11	0.00004	0.00268	0.00321	0.00142	0.00526	0.00267
12	0.00498	0.00512	0.00444	0.0014	0.00187	0.00095
13	0.0007	0.00328	0.00323	0.00384	0.00417	0.00158
14	0.00254	0.0016	0.00029	0.00247	0.00013	0.00027
15	0.00266	0.005	0.00419	0.00059	0.00432	0.00045
16	0.00052	0.00241	0.00294	0.0031	0.00058	0.00381
17	0.00298	0.00131	0.00737	0.00372	0.00028	0.00399
18	0.0001	0.00212	0.00022	0.00001	0.00045	0.00181
19	0.00391	0.001	0.0019	0.00508	0.00091	0.00105
20	0.00232	0.00562	0.00528	0.00703	0.00289	0.00498
21	0.00251	0.00363	0.0053	0.00269	0.00245	0.00527
22	0.00376	0.00272	0.00019	0.00314	0.00037	0.00378
23	0.00346	0.00255	0.00342	0.00493	0.00386	0.00033
24	0.00019	0.00107	0.00191	0.00497	0.00402	0.00106
25	0.00442	0.00283	0.00249	0.0022	0.00457	0.00032
26	0.00126	0.00173	0.00024	0.0001	0.0019	0.00143
27	0.00076	0.00275	0.00381	0.00231	0.00092	0.00221
28	0.00255	0.00414	0.00273	0.00317	0.00132	0.00148
29	0.00352	0.00041	0.00005	0.00188	0.00077	0.00236
30	0.00575	0.00515	0.00025	0.0001	0.00576	0.00379
31	0.00296	0.0005	0.00241	0.00041	0.00145	0.00287
32	0.00153	0.00138	0.00201	0.00284	0.00099	0.00311
33	0.00425	0.00171	0.00042	0.00421	0.00309	0.00002
34	0.00239	0.00285	0.00368	0.00459	0.00213	0.0008
35	0.00137	0.00083	0.00428	0.00301	0.00147	0.00178
36	0.00455	0.00375	0.00141	0.00112	0.00323	0.00671
37	0.00297	0.00119	0.00414	0.00915	0.00651	0.00187
38	0.00134	0.00121	0.00289	0.00201	0.00228	0.00044
39	0.00049	0.00324	0.00687	0.00464	0.00063	0.00214
40	0.00507	0.00768	0.00259	0.00717	0.00334	0.00023
41	0.0029	0.00476	0.00417	0.00108	0.00354	0.00003
42	0.00169	0.00263	0.00477	0.00426	0.00801	0.00486
43	0.00638	0.00572	0.00312	0.00751	0.00751	0.00466
44	126	127	128	129	130	131
45	0.0026028	0.0026723	0.002866	0.0030585	0.0028035	0.002134
46						
47						

Table 30. (Continued)

	EC	ED	EE	EF	EG	EH
1	92/2/21				92/2/24	
2	15:36:23	13:05:18	13:14:56	14:39:29	15:07:07	13:10:34
3	59.022	None	603.4	563.4	1170.1	None
4	0.00293	0.002	0.00328	0.0011	0.00389	0
5	0.00064	0	0.00178	0.00187	0.00281	0.002
6	0.00096	0.003	0.00015	0.00368	0.00092	0.002
7	0.00274	0.002	0.00145	0.00136	0.00178	0.001
8	0.00095	0.002	0.00164	0.00275	0.00356	0.003
9	0.00044	0.003	0.00051	0.00058	0.00172	0.002
10	0.00238	0.002	0.00584	0.00481	0.00231	0.002
11	0.00179	0.003	0.00018	0.0012	0.00273	0.003
12	0.0037	0.003	0.00504	0.00357	0.00079	0.002
13	0.00177	0.001	0.00015	0.00543	0.00224	0.003
14	0.00092	0.001	0.00031	0.00227	0.00154	0
15	0.00211	0.004	0.00086	0.00083	0.00413	0
16	0.00027	0.001	0.00018	0.00128	0.00023	0.003
17	0.00309	0.002	0.00419	0.00502	0.00318	0.002
18	0.0004	0.003	0.00226	0.00023	0.00499	0.001
19	0.00277	0.002	0.00158	0.00097	0.00214	0.002
20	0.00162	0.003	0.00557	0.00731	0.00175	0.004
21	0.00055	0.001	0.0008	0.00204	0.00387	0.003
22	0.0044	0.002	0.00274	0.00033	0.00019	0.001
23	0.00112	0.002	0.00189	0.00099	0.00236	0.003
24	0.00198	0.001	0.0008	0.00159	0.00019	0.004
25	0.00075	0.004	0.00236	0.00204	0.0051	0.002
26	0.00106	0.004	0.0016	0.00278	0.00401	0.002
27	0.00007	0	0.00349	0.00005	0.00081	0.002
28	0.00119	0.004	0.00212	0.00418	0.00537	0.004
29	0.00263	0.002	0.00016	0.00113	0.00014	0
30	0.00055	0.004	0.00529	0.00415	0.00011	0.002
31	0.00248	0.002	0.00353	0.0036	0.00121	0.002
32	0.00514	0.001	0.00017	0.00232	0.00184	0.001
33	0.00015	0.002	0.00352	0.00219	0.00064	0.001
34	0.00075	0.001	0.00286	0.00082	0.00052	0.003
35	0.00045	0	0.00081	0.0032	0.00037	0
36	0.00044	0.005	0.00139	0.00688	0.0023	0.001
37	0.00429	0.003	0.00559	0.00941	0.00234	0.008
38	0.00143	0.005	0.0043	0.00033	0.00026	0.003
39	0.00607	0.005	0.00277	0.00314	0.00098	0.006
40	0.00143	0.001	0.00495	0.00576	0.00143	0.003
41	0.00224	0.004	0.00049	0.00317	0.00104	0.003
42	0.00135	0.007	0.00322	0.00566	0.00095	0.008
43	0.00544	0.005	0.00094	0.00523	0.00323	0.005
44	132	133	134	135	136	137
45	0.001886	0.00255	0.002269	0.0028813	0.0019993	0.002475
46						
47						

Table 30. (Continued)

	EI	EJ	EK	EL	EM	EN
1						
2	13:18:51	13:20:58	14:02:01	14:28:17	14:30:03	14:54:16
3	1170.1	1170.1	603.4	None	603.4	72.067
4	0.00189	0.00289	0.00428	0.001	0.00428	0.00191
5	0.00481	0.00281	0.00222	0.001	0.00222	0.00338
6	0.00008	0.00108	0.00015	0.002	0.00285	0.00207
7	0.00078	0.00278	0.00145	0.002	0.00155	0.00363
8	0.00356	0.00156	0.00063	0.001	0.00237	0.00338
9	0.00072	0.00372	0.00251	0.004	0.00051	0.0023
10	0.00031	0.00131	0.00584	0.002	0.00384	0.00049
11	0.00173	0.00173	0.00118	0.002	0.00318	0.00526
12	0.00021	0.00021	0.00504	0.003	0.00404	0.00087
13	0.00424	0.00124	0.00215	0	0.00015	0.00517
14	0.00154	0.00046	0.00069	0	0.00069	0.00087
15	0.00213	0.00413	0.00014	0.002	0.00086	0.00332
16	0.00177	0.00177	0.00018	0.002	0.00182	0.00058
17	0.00218	0.00082	0.00419	0.004	0.00219	0.00028
18	0.00399	0.00399	0.00126	0.001	0.00426	0.00045
19	0.00014	0.00014	0.00058	0.003	0.00242	0.00091
20	0.00075	0.00075	0.00657	0.005	0.00457	0.00289
21	0.00487	0.00287	0.0012	0.002	0.0002	0.00145
22	0.00119	0.00081	0.00274	0.002	0.00274	0.00037
23	0.00236	0.00336	0.00289	0.003	0.00289	0.00186
24	0.00219	0.00219	0.0018	0.003	0.0008	0.00402
25	0.0051	0.0031	0.00236	0.002	0.00436	0.00357
26	0.00101	0.00101	0.0006	0.001	0.0026	0.0019
27	0.00081	0.00381	0.00249	0.001	0.00149	0.00008
28	0.00337	0.00437	0.00212	0.002	0.00312	0.00132
29	0.00114	0.00014	0.00016	0	0.00016	0.00077
30	0.00089	0.00011	0.00529	0.003	0.00429	0.00376
31	0.00079	0.00121	0.00353	0.002	0.00253	0.00045
32	0.00184	0.00084	0.00283	0.002	0.00083	0.00099
33	0.00064	0.00064	0.00352	0.001	0.00252	0.00008
34	0.00152	0.00252	0.00286	0.002	0.00086	0.00213
35	0.00037	0.00137	0.00081	0.002	0.00019	0.00147
36	0.0023	0.0013	0.00239	0.002	0.00439	0.00223
37	0.00066	0.00134	0.00459	0.004	0.00459	0.00551
38	0.00374	0.00126	0.0033	0.003	0.0043	0.00228
39	0.00202	0.00098	0.00677	0.006	0.00477	0.00063
40	0.00543	0.00243	0.00495	0.002	0.00495	0.00066
41	0.00096	0.00004	0.00151	0.004	0.00049	0.00154
42	0.00395	0.00005	0.00422	0.001	0.00322	0.00701
43	0.00423	0.00423	0.00106	0.003	0.00006	0.00751
44	138	139	140	141	142	143
45	0.0020553	0.0017843	0.0025763	0.0022	0.0024538	0.0022338
46						
47						

Table 30. (Continued)

	EU	EV	EW	EX	EY	EZ
1	92/3/5			92/3/6		
2	15:19:55	12:48:44	13:15:41	13:57:27	7:57:37	8:54:14
3	72.02	None	71.021	603.4	None	603.4
4	0.00152	0.002	0.00021	0.00328	0.003	0.00228
5	0.00161	0	0.00019	0.00122	0.003	0.00122
6	0.00098	0.002	0.00466	0.00015	0	0.00185
7	0.00164	0.001	0.00038	0.00145	0.003	0.00055
8	0.00051	0.002	0.0065	0.00063	0.001	0.00037
9	0.0036	0.003	0.00038	0.00149	0.003	0.00151
10	0.00151	0.002	0.00647	0.00684	0.003	0.00384
11	0.00082	0.003	0.00427	0.00018	0.001	0.00318
12	0.00414	0.003	0.00097	0.00504	0.003	0.00304
13	0.00005	0.002	0.00311	0.00115	0.001	0.00115
14	0.00072	0.001	0.00233	0.00069	0	0.00269
15	0.00371	0.003	0.00388	0.00086	0.001	0.00014
16	0.00237	0.002	0.00356	0.000118	0.002	0.00182
17	0.00235	0.001	0.00258	0.00419	0.003	0.0052
18	0.00012	0.002	0.00442	0.00026	0.001	0.00226
19	0.00272	0.002	0.00102	0.00242	0.002	0.00242
20	0.00594	0.003	0.00422	0.00557	0.004	0.00457
21	0.00256	0.002	0.00261	0.0002	0.002	0.0012
22	0.00272	0.001	0.00154	0.00174	0.002	0.00374
23	0.00104	0.002	0.00225	0.00189	0.002	0.00089
24	0.00092	0.001	0.00489	0.0018	0.004	0.0028
25	0.00424	0.002	0.00481	0.00236	0.002	0.00436
26	0.00309	0.004	0.00065	0.0006	0.001	0.0016
27	0.00338	0	0.0012	0.00149	0.002	0.00249
28	0.001	0.003	0.0012	0.00312	0.003	0.00412
29	0.00134	0.001	0.0019	0.00116	0	0.00016
30	0.00658	0.004	0.00042	0.00529	0.004	0.00229
31	0.00117	0.001	0.00435	0.00453	0.002	0.00353
32	0.002	0.002	0.00505	0.00183	0.002	0.00183
33	0.00559	0.004	0.00141	0.00152	0.001	0.00152
34	0.00343	0.002	0.00315	0.00286	0.002	0.00286
35	0.00261	0	0.00012	0.00281	0.002	0.00281
36	0.00362	0.004	0.00299	0.00439	0.001	0.00139
37	0.00084	0.007	0.00478	0.00559	0.006	0.00559
38	0.00359	0.003	0.00852	0.0033	0.004	0.0063
39	0.00155	0.005	0.00454	0.00477	0.006	0.00477
40	0.00561	0.007	0.00208	0.00495	0.002	0.00495
41	0.00103	0.002	0.00078	0.00051	0.004	0.00251
42	0.00246	0.008	0.00869	0.00622	0.002	0.00322
43	0.00159	0.008	0.00847	0.00294	0.005	0.00194
44	150	151	152	153	154	155
45	0.0024068	0.002675	0.0031388	0.0025352	0.002375	0.002624
46						
47						

Table 30. (Continued)

	FA
1	
2	9:27:06
3	1170.1
4	0.00389
5	0.00281
6	0.00092
7	0.00078
8	0.00456
9	0.00072
10	0.00431
11	0.00027
12	0.00021
13	0.00424
14	0.00046
15	0.00313
16	0.00177
17	0.00218
18	0.00499
19	0.00114
20	0.00375
21	0.00487
22	0.00019
23	0.00436
24	0.00219
25	0.0051
26	0.00301
27	0.00181
28	0.00537
29	0.00014
30	0.00011
31	0.00121
32	0.00084
33	0.00064
34	0.00252
35	0.00063
36	0.0043
37	0.00034
38	0.00174
39	0.00202
40	0.00543
41	0.00096
42	0.00195
43	0.00623
44	156
45	0.0024023
46	
47	

Table 30. (Continued)

	A	B	C	D	E	F
48						
49	Date	91/6/20	91/6/27	91/7/9		
50	Time	8:18:04	9:59:33	14:17:15	14:39:52	14:51:02
51	Err A075	0.071	0.081	0.13	0.134	0.1
52	Err A076	0.05	0.048	0.061	0.061	0.055
53	Err A065	0.044	0.038	0.042	0.039	0.044
54	Err K the	0.01775	0.02025	0.0325	0.0335	0.025
55	Err K a2	0.05	0.048	0.061	0.061	0.055
56	Err K ra2	0.0352	0.0304	0.0336	0.0312	0.0352
57	Diff (1,1)	0.002	0.004	0.004	0.002	0.003
58	(1,2)	0.001	0.003	0.003	0.004	0.003
59	(1,3)	0.002	0.005	0.005	0.004	0.004
60	(1,4)	0.002	0.004	0.003	0.003	0.003
61	(1,5)	0.001	0.003	0.002	0.003	0.004
62	(1,6)	0.003	0.004	0.005	0.002	0.002
63	(1,7)	-0.004	0.004	0.004	0.004	0.002
64	(1,8)	0.002	0.005	0.002	0.004	0.005
65	(2,1)	0.001	0.002	0.002	0.002	0.003
66	(2,2)	0.002	0.002	0.005	0.002	0.004
67	(2,3)	0.001	0.003	0.003	0.004	0.002
68	(2,4)	0.002	0.004	0.004	0.004	0.005
69	(2,5)	0.002	0.002	0.003	0.004	0.004
70	(2,6)	0.001	0.004	0.004	0.004	0.001
71	(2,7)	0.005	0.003	0.003	0.002	0.004
72	(2,8)	0	0.002	0.002	0.001	0.003
73	(3,1)	-0.001	0.001	0.003	0.003	0.001
74	(3,2)	-0.003	0.004	-0.004	0.001	0.001
75	(3,3)	0.001	0.004	0.003	0.003	0.003
76	(3,4)	0.002	0.004	0.003	0.003	0.004
77	(3,5)	0.002	0.002	0.002	0.003	0.002
78	(3,6)	-0.003	-0.002	0.002	0.001	-0.004
79	(3,7)	-0.003	0.002	0	-0.001	0.001
80	(3,8)	0	0.002	0.002	0.002	0.001
81	(4,1)	0	0.0003	0.0002	0	0.0002
82	(4,2)	-0.0001	0.0002	0	0.0003	0.0001
83	(4,3)	0	0.0003	0.0001	-0.0001	0.0002
84	(4,4)	0	0.0004	0.0002	0	0.0002
85	(4,5)	-0.0003	-0.0001	-0.0001	0	-0.0002
86	(4,6)	-0.0002	0.0001	0.0002	0	-0.0001
87	(4,7)	0.0006	0.0008	0.0009	0.0006	0.0009
88	(4,8)	-0.0001	0	-0.0001	-0.0001	-0.0002
89	(5,1)	-0.003	0.001	0.002	0.003	0.001
90	(5,2)	0.003	0.006	0.002	0.002	0.004
91	(5,3)	0.001	0.003	0.003	0.003	0.004
92	(5,4)	-0.004	0.003	-0.004	-0.001	-0.005
93	(5,5)	-0.002	0.002	0.002	0.004	0.004
94	(5,6)	-0.003	-0.004	-0.002	-0.003	-0.004

Table 30. (Continued)

	A	B	C	D	E	F
95	(5,7)	-0.002	0.003	-0.004	-0.001	0.001
96	(5,8)	-0.004	-0.004	-0.004	-0.006	-0.002
97	Counter	1	2	3	4	5
98	Avg	9.75E-05	0.002075	0.001535	0.0016425	0.0016275

Table 30. (Continued)

	G	H	I	J	K	L
48						
49		91/7/10		91/7/11		91/7/15
50	15:29:21	12:52:43	13:08:91	12:55:43	13:10:10	12:26:24
51	0.127	0.131	0.093	0.129	0.096	0.132
52	0.06	0.065	0.055	0.064	0.056	0.069
53	0.041	0.045	0.045	0.042	0.043	0.049
54	0.03175	0.03275	0.02325	0.03225	0.024	0.033
55	0.06	0.065	0.055	0.064	0.056	0.069
56	0.0328	0.036	0.036	0.0336	0.0344	0.0392
57	0.001	0.004	0.002	0.003	0.003	0.003
58	0.003	0.002	0.004	0.003	0.003	0.003
59	0.004	0.004	0.004	0.004	0.003	0.004
60	0.003	0.003	0.003	0.003	0.004	0.002
61	0.003	0.003	0.003	0.002	0	0.002
62	0.002	0.002	0.002	0.003	0.004	0.003
63	0.003	0.003	0.004	0.003	0.004	0.003
64	0.004	0.003	0.004	0.005	0.002	0.004
65	0.002	0.005	0.002	0.004	0.002	0.004
66	0.002	0.002	0.002	0.001	0.002	0.001
67	0.004	0.002	0.004	0.003	0.004	0.004
68	0.004	0.005	0.004	0.003	0.002	0.004
69	0.002	0.003	0.004	0.004	0.002	0.001
70	0.003	0.004	0.004	0	0.003	0.003
71	0.003	0.002	0.002	0.004	0.006	0.005
72	0.002	0.004	0.001	0.002	0.002	0
73	0.001	-0.004	0.003	0.001	0	-0.003
74	0.001	0.001	0.001	0.001	0.002	0.002
75	0.003	0.003	0.003	0.002	0.002	0.003
76	0.004	0.003	-0.003	0.002	0.003	0.002
77	0.002	0.001	0.003	0.001	0.001	0.001
78	0.001	-0.001	0.001	-0.002	-0.001	0.001
79	0.002	0.001	-0.001	0.001	0.001	0.001
80	0.002	0.001	0.002	0.002	0.002	0.001
81	0	0.0002	0	0	0	0.0001
82	0.0003	0.0001	0.0003	0	0.0001	0.0001
83	0	0	-0.0001	-0.0002	-0.0001	-0.0001
84	0.0003	0.0001	0	0.0003	0.0001	0.0002
85	0	-0.0002	0	-0.0001	0	0
86	-0.0001	-0.0001	0	-0.0002	0	0.0001
87	0.0007	0.0007	-0.0006	0.0007	0.0007	0.0007
88	-0.0002	-0.0001	-0.0001	-0.0001	-0.0002	-0.0002
89	0.003	0.002	0.003	0.003	0.002	0.004
90	0.002	0	0.002	0.003	0.002	0.002
91	0.004	-0.004	0.003	0.002	0.004	0.003
92	0.003	0.002	0.001	0.001	0.002	0.002
93	0.004	0.002	0.004	-0.004	0.002	0.004
94	-0.002	-0.001	-0.003	-0.001	-0.003	-0.002

Table 30. (Continued)

	G	H	I	J	K	L
95	-0.002	-0.001	-0.001	0.003	-0.003	-0.002
96	-0.002	-0.004	-0.006	-0.004	-0.003	-0.003
97	6	7	8	9	10	11
98	0.0018	0.0013175	0.0015125	0.00146	0.00149	0.0015725

Table 30. (Continued)

	M	N	O	P	Q	R
48						
49		91/7/19		91/12/11	91/12/17	
50	12:33:24	13:18:09	13:22:43	9:00:51	8:27:44	9:52:40
51	0.1	0.122	0.093	0.019	0.001	0.008
52	0.061	0.064	0.056	-0.005	-0.007	-0.002
53	0.048	0.046	0.044	-0.012	-0.011	-0.015
54	0.025	0.0305	0.02325	0.00475	0.00025	0.002
55	0.061	0.064	0.056	-0.005	-0.007	-0.002
56	0.0384	0.0368	0.0352	-0.0096	-0.0088	-0.012
57	0.003	0.003	0.003	0.004	0.002	0.004
58	0.003	0.002	0.004	0.003	0.002	0.004
59	0.004	0.001	0.005	0.003	0.003	0.002
60	0.003	0.001	0.002	0.003	0.004	0.003
61	0.004	0.003	0.001	0.004	0.001	0.004
62	0.002	0.004	0.005	0.005	0.004	0.005
63	0.002	0.004	0.004	0.003	0.004	0.004
64	0.004	0.002	0.001	0.004	0.003	0.004
65	0.003	0.002	0.003	0.003	0.004	0.004
66	0.002	0.003	0.003	0.003	0.004	0.002
67	0.003	0.002	0.002	0.003	0.001	0.003
68	0.003	0.003	0.003	0.005	0.002	0.003
69	0.003	0.003	0.003	0.004	0.004	0.003
70	0.004	0.004	0.002	0.004	0.005	0.005
71	0.004	0.003	0.005	0.002	0.002	0.003
72	0.003	0.002	0.003	0.003	0.003	0.003
73	0.001	0	-0.001	0.005	0.004	0.004
74	0.001	0.002	-0.002	0.002	0.004	0.004
75	0.003	0.003	0.003	0.005	0.002	0.004
76	0.003	0.002	0.003	0.005	0.004	0.005
77	0.001	0.001	0.002	0.005	0.004	0.003
78	-0.001	0.001	-0.003	0.003	0.005	0.005
79	0	0.002	-0.003	0.004	0.004	0.003
80	0.001	0.001	-0.001	0.002	0.003	0.002
81	0	0.0002	-0.0001	0.0007	0.0005	0.0006
82	0.0002	0.0001	0.0003	0.0004	0.0008	0.0003
83	0.0001	0.0002	0.0001	0.0009	0.0009	0.0009
84	0	0.0001	0.0003	0.0004	0.0005	0.0004
85	-0.0002	-0.0002	0	0.0008	0.001	0.0005
86	0.0001	0.0001	0	0.0008	0.0009	0.0008
87	0.0009	0.0009	0.0009	0.0009	0.0008	0.001
88	-0.0001	0	0.0001	0.0002	0.0005	0.0004
89	0.002	0.003	0.002	0.004	0.004	0.004
90	0.003	0.004	0.003	0.003	0.004	0.004
91	0.003	0.002	0.004	0.004	0.001	0
92	-0.004	0.002	0.003	0.001	-0.002	0.002
93	0.002	0.004	0.002	0.005	0.003	0.003
94	-0.002	0	-0.002	0.001	-0.002	-0.003

Table 30. (Continued)

	M	N	O	P	Q	R
95	-0.004	0	-0.005	0.005	0.006	0.003
96	-0.003	-0.002	-0.001	0.003	0.003	0.003
97	12	13	14	15	16	17
98	0.001425	0.00171	0.001365	0.0029525	0.0025225	0.0026725

Table 30. (Continued)

	S	T	U	V	W	X
48						
49	91/12/18	92/1/6	92/1/9	92/1/13	92/1/14	92/1/15
50	13:23:43	13:00:09	12:47:03	13:26:20	14:37:17	13:00:04
51	0.01	0.01	-0.007	0.014	0.01	0.053
52	-0.008	-0.004	0.005	-0.004	-0.005	0.66
53	-0.015	-0.016	0.015	-0.013	-0.015	0.013
54	0.0025	0.0025	-0.00175	0.0035	0.0025	0.01325
55	-0.008	-0.004	0.005	-0.004	-0.005	0.66
56	-0.012	-0.0128	0.012	-0.0104	-0.012	0.0104
57	0.003	0.004	0.004	0.004	0.003	0.003
58	0.002	0.003	0.001	0.001	0.004	0.005
59	0.003	0.004	0.004	0.004	0.005	0.005
60	0.003	0.003	0.004	0.004	0.003	0.007
61	0.003	0.005	0.004	0.004	0.003	0.007
62	0.004	0.003	0.003	0.003	0.005	0.001
63	0.003	0.003	0.006	0.006	0.005	0.005
64	0.004	0.005	0.005	0.005	0.003	0.001
65	0.003	0.004	0.005	0.005	0.005	0.004
66	0.003	0.003	0.005	0.005	0.004	0.003
67	0	0.002	0.002	0.002	0.001	0.003
68	0.004	0.004	0.003	0.003	0.004	0.004
69	0.003	0.003	0.004	0.004	0.005	0.006
70	0.004	0.005	0.004	0.004	0.004	0.001
71	0.002	0.004	0.002	0.002	0.004	-0.004
72	0.002	0.003	0.003	0.003	0.003	0.002
73	0.005	0.004	0.005	0.005	0.004	0.006
74	0.005	0.005	0.004	0.004	0.004	0.004
75	0.003	0.004	0.003	0.003	0.004	0.007
76	0.004	0.003	0.005	0.005	0.003	0.007
77	0.004	0.004	0.003	0.003	0.004	0.003
78	0.003	0.005	0.005	0.005	0.004	0.007
79	0.003	0.003	0.004	0.004	0.003	0.002
80	0.002	0.001	0.002	0.002	0.001	0.003
81	0.0006	0.0006	0.0007	0.0007	0.0004	0.0011
82	0.0003	0.0006	0.0007	-0.0007	0.0004	0.0007
83	0.0006	0.0008	0.0005	0.0005	0.0006	0.0006
84	0.0004	0.0003	0.0004	0.0004	0.0004	0.0011
85	0.0005	0.0005	0.0005	0.0005	0.0004	0.001
86	0.0007	0.0006	0.0006	0.0006	0.0004	0.00006
87	0.0007	0.001	0.001	0.001	0.0013	0.0009
88	0.0002	0.0004	0.0005	0.0005	0.0003	0.0003
89	0.004	0.002	0.002	0.002	0.003	0.005
90	0.002	0.003	0.002	0.002	0.003	0.003
91	-0.002	-0.003	-0.003	-0.003	-0.003	0.003
92	0.001	0.003	-0.003	-0.003	0.001	-0.001
93	0.003	0.004	0.003	0.003	0.002	0.004
94	-0.003	-0.003	-0.003	-0.003	-0.003	-0.002

Table 30. (Continued)

	S	T	U	V	W	X
95	0.004	0.004	0.004	0.004	0.004	0.002
96	0.004	0.004	0.003	0.003	0.003	-0.004
97	18	19	20	21	22	23
98	0.0023	0.002645	0.0024975	0.0024625	0.002555	0.002694

Table 30. (Continued)

	Y	Z	AA	AB	AC	AD
48						
49	92/1/30				92/1/31	92/2/3
50	12:00:01	12:00:03	13:00:05	14:00:52	13:00:22	12:00:07
51	0.13	0.01	0.002	0.014	0.01	0.011
52	0.026	-0.007	-0.008	-0.005	-0.003	-0.006
53	-0.014	-0.014	-0.017	-0.014	-0.015	-0.015
54	0.0325	0.0025	0.0005	0.0035	0.0025	0.00275
55	0.026	-0.007	-0.008	-0.005	-0.003	-0.006
56	-0.0112	-0.0112	-0.0136	-0.0112	-0.012	-0.012
57	0.005	0.003	0.003	0.004	0.003	0.004
58	0.003	0.0	0.003	0.004	0.003	0.003
59	0.004	0.0	0.003	0.003	0.003	0.005
60	0.004	0.004	0.003	0.004	0.004	0.004
61	0.004	0.004	0.004	0.004	0.004	0.005
62	0.004	0.002	0.005	0.005	0.005	0.005
63	0.002	0.005	0.004	0.003	0.003	0.003
64	0.004	0.004	0.004	0.005	0.005	0.004
65	0.006	0.002	0.003	0.005	0.005	0.005
66	0.002	0.003	0.004	0.002	0.002	0.004
67	0.003	0.004	0.004	0.003	0.002	0.002
68	0.005	0.004	0.003	0.004	0.005	0.004
69	0.003	0.003	0.003	0.004	0.004	0.004
70	0.006	0.006	0.004	0.003	0.003	0.005
71	0.003	0.005	0.004	0.004	0.004	0.003
72	0.002	0.002	0.002	0.004	0.003	0.005
73	0.005	0.005	0.005	0.003	0.005	0.005
74	0.005	0.004	0.005	0.005	0.004	0.004
75	0.004	0.005	0.004	0.005	0.004	0.004
76	0.003	0.004	0.004	0.003	0.004	0.005
77	0.004	0.004	0.005	0.005	0.005	0.004
78	0.004	0.005	0.003	0.004	0.005	0.004
79	0.004	0.004	0.003	0.004	0.002	0.003
80	0.002	0	0.001	0.002	0.003	0.003
81	0.0008	0.0007	0.0007	0.0004	0.0008	0.0006
82	0.0008	0.0003	0.0007	0.0007	0.0009	0.0004
83	0.0009	0.0004	0.0007	0.0006	0.0005	0.0006
84	0.0008	0.0005	0.0005	0.0005	0.0005	0.0005
85	0.0008	0.0007	0.0006	0.0008	0.0005	0.0005
86	0.001	0.0005	0.0005	0.0009	0.0005	0.0009
87	0.0008	0.0007	0.0008	0.0008	0.001	0.0014
88	0.0004	0.0003	0.0005	0.0004	0.0004	0.0005
89	0.004	0.003	0.005	0.003	0.003	0.002
90	0.003	0.003	0.005	0.004	0.004	0.004
91	0.002	0.002	0.002	-0.001	-0.001	0.002
92	-0.004	0.002	0.003	-0.005	0.002	0.003
93	0.006	0.004	0.004	0.002	0.004	0.005
94	0.004	-0.003	-0.003	-0.003	-0.002	-0.001

Table 30. (Continued)

	Y	Z	AA	AB	AC	AD
95	0.005	0.004	0.005	0.005	0.002	0.004
96	0.003	0.004	0.004	0.004	0.003	0.004
97	24	25	26	27	28	29
98	0.0030075	0.0028025	0.0029	0.0026525	0.0027525	0.003135

Table 30. (Continued)

	AE	AF	AG	AH	AI	AJ
48						
49	92/2/4	92/2/5	92/2/6	92/2/7		92/2/10
50	12:00:12	12:00:04	13:06:45	12:52:29	15:15:55	12:47:32
51	0.013	0.015	0.015	0.01	0.009	0.013
52	-0.004	0.018	-0.004	0.012	0.013	0.014
53	-0.015	0.014	-0.015	0.021	0.015	0.018
54	0.00325	0.00375	0.00375	0.0025	0.00225	0.00325
55	-0.004	0.018	-0.004	0.012	0.013	0.014
56	-0.012	0.0112	-0.012	0.0168	0.012	0.0144
57	0.006	0.004	0.001	0.003	0.005	0.004
58	0.004	0.002	0.002	0.004	0.004	0.005
59	0.003	0.005	0.003	0.003	0.003	0.004
60	0.003	0.004	0.003	0.004	0.004	0.005
61	0.005	0.005	0.005	0.006	0.006	0.004
62	0.005	0.003	0.002	0.003	0.003	0.004
63	0.002	0.005	0.003	0.004	0.003	0.004
64	0.005	0.005	0.005	0.004	0.006	0.005
65	0.005	0.004	0.003	0.003	0.005	0.003
66	0.002	0.002	0.002	0.003	0.002	0.003
67	0.004	0.004	0.004	0.004	0.003	0.004
68	0.005	0.004	0.004	0.004	0.005	0.004
69	0.002	0.003	0.001	0.003	0.003	0.003
70	0.005	0.005	0.005	0.004	0.004	0.005
71	0.005	0.005	0.004	0.005	0.004	0.005
72	0.003	0.003	0.001	0.002	0.004	0.002
73	0.005	0.005	0.005	0.004	0.003	0.005
74	0.006	0.004	0.004	0.005	0.006	0.004
75	0.004	0.004	0.003	0.004	0.005	0.002
76	0.004	0.003	0.004	0.005	0.003	0.005
77	0.005	0.005	0.002	0.004	0.005	0.005
78	0.004	0.005	0.006	0.003	0.006	0.005
79	0.004	0.003	0.004	0.005	0.003	0.003
80	0.003	0.003	0.003	0.004	0.004	0.003
81	0.0006	0.0007	0.0005	0.0007	0.0005	0.0006
82	0.0008	0.0004	0.0008	0.0006	0.0004	0.0007
83	0.0006	0.0006	0.0005	0.0007	0.0005	0.0008
84	0.0005	0.0004	0.0003	0.0003	0.0004	0.0005
85	0.001	0.0009	0.0004	0.0006	0.0007	0.0007
86	0.0004	0.0005	0.0004	0.0003	0.0005	0.0002
87	0.0009	0.0007	0.0008	0.0007	0.0009	0.0008
88	0.0003	0.0003	0.0004	0.0003	0.0004	0.0004
89	0.004	0.003	0.003	0.004	0.002	0.004
90	0.002	0.003	0.004	0.004	0.003	0.004
91	-0.003	-0.003	-0.001	0.001	0.002	0.001
92	0.002	0.003	-0.003	0.001	-0.003	0.002
93	0.005	0.005	0.003	0.005	0.003	0.003
94	-0.002	-0.001	-0.003	-0.002	-0.002	-0.003

Table 30. (Continued)

	AE	AF	AG	AH	AI	AJ
95	0.003	0.005	0.004	0.003	0.003	0.004
96	0.003	0.002	0.003	0.003	0.004	0.006
97	30	31	32	33	34	35
98	0.0029525	0.0029125	0.0023275	0.002905	0.0028825	0.0030425

Table 30. (Continued)

	AK	AL	AM	AN	AO	AP
48						
49	92/2/12	92/2/18	92/2/19	92/2/20	92/2/21	92/2/24
50	12:00:05	13:00:03	13:00:02	13:00:25	13:00:59	13:00:309
51	0.017	0.012	0.012	0.013	0.003	0.018
52	-0.006	-0.006	0.016	-0.005	0.014	0.019
53	-0.015	-0.015	0.02	-0.015	0.019	0.017
54	0.00425	0.003	0.003	0.00325	0.00075	0.0045
55	-0.006	-0.006	0.016	-0.005	0.014	0.019
56	-0.012	-0.012	0.016	-0.012	0.0152	0.0136
57	0.004	0.003	0.003	0.003	0.004	0.004
58	0.004	0.002	0.003	0.003	0.004	0.002
59	0.004	0.004	0.004	0.004	0.003	0.003
60	0.004	0.002	0.002	0.003	0.003	0.003
61	0.006	0.004	0.003	0.004	0.004	0.004
62	0.004	0.005	0.006	0.005	0.006	0.005
63	0.003	0.003	0.004	0.005	0.002	0.003
64	0.006	0.005	0.003	0.003	0.004	0.003
65	0.004	0.004	0.004	0.005	0.006	0.006
66	0.002	0.004	0.002	0.003	0.002	0.003
67	0.003	0.001	0.002	0.003	0.002	0.003
68	0.004	0.004	0.004	0.004	0.005	0.004
69	0.002	0.003	0.004	0.004	0.004	0.005
70	0.006	0.004	0.004	0.006	0.002	0.004
71	0.005	0.003	0.002	0.002	0.004	0.004
72	0.002	0.004	0.003	0.003	0.002	0.004
73	0.005	0.005	0.004	0.004	0.005	0.004
74	0.006	0.004	0.003	0.004	0.004	0.004
75	0.002	0.004	0.005	0.004	0.005	0.002
76	0.005	0.004	0.004	0.004	0.004	0.004
77	0.005	0.003	0.005	0.004	0.004	0.005
78	0.005	0.005	0.003	0.006	0.005	0.004
79	0.003	0.004	0.004	0.004	0.002	0.001
80	0.002	0.002	0.003	0	0.003	0.002
81	0.0006	0.0006	0.0006	0.0007	0.0006	0.0004
82	0.0003	0.0001	0.0002	0.0002	0.0007	0.0008
83	0.0006	0.0003	0.0009	0.0004	0.0005	0.001
84	0.0004	0.0003	0.0004	0.0004	0.0003	0.0005
85	0.0008	0.0005	0.0004	0.0005	0.0004	0.001
86	0.0006	0.0003	0.0005	0.0003	0.0003	0.0008
87	0.0021	0.0015	0.001	0.001	0.0008	0.001
88	0.0003	0.0005	0.0004	0.0003	0.0003	0.0002
89	0.003	0.003	0.004	0.001	0.004	0.004
90	0.003	0.002	0.003	0.0004	0.002	0.005
91	-0.001	-0.004	-0.002	0	-0.002	-0.001
92	0.001	0.002	0.002	-0.003	0.001	0.001
93	0.002	0.004	0.004	0.003	0.005	0.002
94	-0.003	-0.003	-0.003	-0.003	-0.001	-0.003

Table 30. (Continued)

	AK	AL	AM	AN	AO	AP
95	0.003	0.005	0.004	0.003	0.003	0.003
96	0.003	0.003	0.003	0.005	0.004	0.002
97	36	37	38	39	40	41
98	0.0028175	0.0025525	0.002585	0.002505	0.0027225	0.0026175

Table 30. (Continued)

	AQ	AR	AS	AT	AU	AV
48						
49	92/2/28	92/3/5	92/3/6			7/91 Error
50	12:59:45	12:00:05	7:00:09	8:00:01		Used
51	0.017	0.01	0.018	0.01		0.0015724
52	-0.004	-0.002	0.003	0.006		0.0021749
53	-0.014	-0.012	0.017	0.018		0.0017889
54	0.00425	0.0025	0.0045	0.0025		0.0016453
55	-0.004	-0.002	0.003	0.006		0.0024524
56	-0.0112	-0.0096	0.0136	0.0144		0.0018491
57	0.003	0.004	0.004	0.003		0.0013569
58	0.003	0.003	0.003	0.002		0.0016722
59	0.004	0.003	0.002	0.005		0.0021002
60	0.005	0.003	0.004	0.003		0.001824
61	0.004	0.004	0.004	0.004		0.0016951
62	0.003	0.005	0.003	0.003		0.00183
63	0.005	0.002	0.003	0.006		0.0016809
64	0.005	0.004	0.005	0.005		0.0012091
65	0.002	0.006	0.003	0.002		0.0024044
66	0.003	0.002	0.002	0.004		0.00162
67	0.004	0.003	0.002	0.004		0.0012636
68	0.003	0.003	0.005	0.003		0.0014682
69	0.004	0.005	0.003	0.003		0.001816
70	0.005	0.004	0.005	0.006		0.0015782
71	0.005	0.003	0.004	0.005		0.0012238
72	0.001	0.004	0.004	0.001		0.0015509
73	0.005	0.005	0.003	0.006		0.001548
74	0.004	0.004	0.005	0.005		0.0013073
75	0.002	0.004	0.005	0.003		0.0018018
76	0.005	0.004	0.003	0.004		0.001446
77	0.005	0.005	0.004	0.005		0.0016544
78	0.005	0.006	0.005	0.005		0.0014082
79	0.003	0.001	0.003	0.003		0.0016713
80	0.002	0.004	0.002	0.002		0.0013653
81	0.0007	0.0006	0.0006	0.0006		0.0019551
82	0.0007	0.0007	0.0006	0.0006		0.0026956
83	0.0004	0.0008	0.0003	0.0009		0.0018227
84	0.0004	0.0005	0.0003	0.0002		0.002178
85	0.0004	0.0009	0.0007	0.0008		0.002848
86	0.0003	0.0009	0.0008	0.0003		0.0021122
87	0.0008	0.0007	0.0007	0.001		0.0017529
88	0.0004	0.0004	0.0002	0.0004		0.0014282
89	0.004	0.004	0.003	0.001		0.0013211
90	0.001	0.004	0.002	0.007		0.0015926
91	-0.004	0.003	0.001	0.003		
92	0.001	0.002	0.001	0.001		0.0017421
93	0.003	0.004	0.003	0.002		
94	-0.002	0.003	-0.003	0.001		

Table 30. (Continued)

	AQ	AR	AS	AT	AU	AV
95	0.004	0.002	0.002	0.003		
96	0.003	0.002	0.004	0.003		
97	42	43	44	45		
98	0.0026025	0.0030125	0.00258	0.002945		

Table 30. (Continued)

	AW	AX	AY	AZ	BA	BB
48						
49	12/92-2/3/	2/4/92 on	7/91 Error	12/92-2/3/	2/4/92 on	
50	Not Used	Used	Used	Not Used	Used	
51	0.0021874	0.002345	0.0028571	0.0035333	0.003625	K the
52	0.0013321	0.0018392	0.0029286	0.0029333	0.003125	Ka2
53	0.0026315	0.0024068	0.0037857	0.0036667	0.0035625	K ra2
54	0.0018477	0.0019489	0.0027857	0.0038	0.0034375	
55	0.003131	0.0028108	0.0024286	0.004	0.0045	
56	0.0025428	0.0022083	0.0030714	0.0039333	0.0040625	
57	0.0026323	0.0027544	0.0028571	0.0039333	0.0035625	
58	0.0031367	0.0024375	0.0033571	0.004	0.0045625	
59	0.0019505	0.002569	0.0026429	0.0042	0.0040625	
60	0.0026587	0.0025163	0.0023571	0.0032667	0.0025625	
61	0.0018179	0.0013814	0.0029286	0.0023333	0.003125	
62	0.0023126	0.0022036	0.0035714	0.0038	0.0040625	
63	0.0021549	0.0018973	0.0028571	0.0038	0.00325	
64	0.0024692	0.0028253	0.0029286	0.0042	0.004625	
65	0.00216	0.0019088	0.0036429	0.0026667	0.0040625	
66	0.0019638	0.0018167	0.0019286	0.0028667	0.0026875	
67	0.0034169	0.0036017	0.0003571	0.0046667	0.0045625	
68	0.0031585	0.0029722	0.0005714	0.0042	0.0045	
69	0.0020987	0.0026054	0.0027857	0.0040667	0.003625	
70	0.0023951	0.0024819	0.0025	0.0042667	0.0040625	
71	0.0024067	0.0024808	0.0017143	0.004	0.0044375	
72	0.0033274	0.0032967	-0.000714	0.0044667	0.004875	
73	0.001819	0.0017069	0.0002143	0.0033333	0.003125	
74	0.0010756	0.0013282	0.0012857	0.0019333	0.002625	
75	0.0031359	0.0029192	7.857E-05	0.00066	0.0006	
76	0.0014528	0.00125	0.0001429	0.0004867	0.0005375	
77	0.0028885	0.0029403	2.857E-05	0.0006667	0.0006125	
78	0.0020872	0.0023232	0.0001571	0.0005067	0.0003813	
79	0.0033339	0.0027115	-0.0001	0.00064	0.0006688	
80	0.0024356	0.0019414	-7.14E-06	0.0006507	0.0004625	
81	0.0024136	0.0020943	0.0006714	0.00094	0.0009625	
82	0.0014692	0.001341	-0.0001	0.0003867	0.0003438	
83	0.0036777	0.0028868	0.002	0.0033333	0.0031875	
84	0.0051382	0.0056722	0.0027143	0.0032667	0.0030875	
85	0.0031895	0.0031643	0.0025	-5.78E-20	-0.000625	
86	0.0035731	0.0036292	7.143E-05	0	0.0006875	
87	0.0043556	0.0034722	0.0021429	0.0036667	0.0035	
88	0.0018913	0.0021296	-0.002286	-0.001933	-0.001875	
89	0.0052903	0.0047522	-0.001286	0.0040667	0.003375	
90	0.00438	0.0046178	-0.003429	0.0029333	0.0033125	
91						
92	0.0026836	0.0026047	0.0014736	0.0027034	0.0027477	
93						
94						

Table 30. (Continued)

	BC	BD	BE	BF	BG	BH
48						
49				Bias Error	Bias Error	
50				Used	Not Used	
51	0.1099286	0.0196667	0.0128125	0.0022966	0.0025613	
52	0.0589286	0.0418	0.00525	0.0021856	0.0017769	
53	0.0435714	-0.010533	0.003625	0.0024748	0.0029191	
54				0.0020977	0.00239	
55				0.0028486	0.0033724	
56				0.0023824	0.0029291	
57				0.0024244	0.0029937	
58				0.0025221	0.0033765	
59				0.0025951	0.0025754	
60				0.0022942	0.0028276	
61				0.0018146	0.0019611	
62				0.0024218	0.0027257	
63				0.0020697	0.0026119	
64				0.0025363	0.00295	
65				0.0024601	0.0023007	
66				0.0018619	0.0022146	
67				0.0026815	0.0037641	
68				0.0024495	0.0034478	
69				0.0024919	0.0026454	
70				0.002379	0.002915	
71				0.002236	0.0028493	
72				0.002552	0.0036439	
73				0.0016705	0.0022396	
74				0.0014589	0.0013139	
75				0.0020542	0.0024481	
76				0.001127	0.0011844	
77				0.002016	0.0022713	
78				0.0016254	0.0016481	
79				0.001903	0.0025893	
80				0.0014185	0.0019398	
81				0.001793	0.0020043	
82				0.0015099	0.0011685	
83				0.0025093	0.003582	
84				0.0040395	0.0046183	
85				0.0025918	0.0023035	
86				0.0025058	0.0025806	
87				0.0028223	0.0041643	
88				0.0010585	0.0008289	
89				0.0029769	0.0049504	
90				0.0027833	0.0039781	
91						
92				0.0022485	0.0026891	
93						
94						

LIST OF REFERENCES

1. William W. Bathie. **Fundamentals of Gas Turbines.** John Wiley & Sons, Inc., 1984.
2. Leland M. Nicolai. **Fundamentals of Aircraft Design.** METS, Inc., 1984.
3. E. L. Crosthwait, I. G. Kennon, Jr., and H. L. Roland, et al. **Preliminary Design Methodology for Air-Induction Systems.** SEG-TR-67-1, General Dynamics Ft. Worth Division, 1967.
4. Gordon C. Oates. **Aerothermodynamics of Gas Turbine and Rocket Propulsion.** AIAA, Inc., 1984.
5. J. A. Forner and J. M. Manter. **Prediction of Cruise Missile Inlet Peak Instantaneous Distortion Patterns from Steady State and Turbulence Data Using a Statistical Technique.** AIAA Paper 82-1085, AIAA, Inc., 1982. 18th Joint Propulsion Conference, 1982/Cleveland, Ohio.
6. Frank L. Csavina and Russel K. Denney. **A Global Approach in Evaluating Inlet/Engine Compatibility.** ASME Paper 91-GT-402. International Gas Turbine and Aeroengine Congress and Exposition, 1991/Orlando, Florida.
7. Society of Automotive Engineers, Inc. **Inlet Total-Pressure Distortion Considerations for Gas-Turbine Engines.** Aerospace Information Report 1419. May, 1983.
8. Society of Automotive Engineers, Inc. **Gas Turbine Engine Inlet Flow Distortion Guidelines.** Aerospace Recommended Practice 1920. March, 1978.
9. R. C. Crites and M. V. Heckert. **Applications of Random Data Techniques on Aircraft Inlet Diagnostics.** AIAA Paper 70-597, AIAA, Inc. AIAA 5th Aerodynamic Testing Conference, 1970/Tulahoma, Tennessee.

10. R. W. King, J. A. Schuerman, and R. G. Muller. **Analysis of Distortion Data from TF30-P-3 Mixed Compression Inlet Test.** NASA-CR-2686. NASA Lewis Research Center, 1976.
11. H. Clyde Melick, Jr., Andres H. Ybarra, and Daniel P. Bencze. **Estimating Maximum Instantaneous Distortion from Inlet Total Pressure RMS Measurements.** AIAA Paper 78-790, AIAA, Inc., 1978. AIAA/SAE 14th Joint Propulsion Conference, 1978/Las Vegas, Nevada.
12. R. Borg. **A Synthesis Method for Estimating Maximum Instantaneous Inlet Distortion Based on Measured Inlet Steady State and RMS Pressures.** AGARD-CP-201. Aerodynamics of Power Plant Installation, 1981.
13. D. L. Motyka. **Determination of Maximum Expected Instantaneous Distortion from Inlet Pressure RMS Measurements.** AIAA Paper 78-970, AIAA, Inc.
14. C. H. Stevens, E. D. Spong, and R. C. Oliphant. **Evaluation of a Statistical Method for Determining Peak Inlet Flow Distortion Using F-15 and F-18 Data.** AIAA Paper 80-1109, AIAA, Inc. AIAA/SAE/ASME 16th Joint Propulsion Conference, 1980/Hartford, Connecticut.
15. D. Sedlock. **Improved Statistical Analysis Method for Prediction of Maximum Inlet Distortion.** AIAA Paper 84-1274, AIAA, Inc., 1984. AIAA/SAE/ASME 20th Joint Propulsion Conference, 1984/Cincinnati, Ohio.
16. P. V. Maywald and D. K. Beale. **Development of a Freejet Capability for Evaluating Inlet-Engine Compatibility.** ASME Paper 91-GT-401. International Gas Turbine and Aeroengine Congress and Exposition, 1991/Orlando, Florida.
17. D. K. Beale. **Evaluation of a Freejet Technique for Testing Fighter Aircraft Propulsion Systems.** AIAA Paper 86-1460, AIAA, Inc. AIAA/ASME/SAE/ASEE 22nd Joint Propulsion Conference, 1986/Huntsville, Alabama.
18. D. K. Beale. **Validation of a Freejet Technique for Evaluating Inlet-Engine Compatibility.** AIAA Paper 89-2325, AIAA, Inc. AIAA/ASME/SAE/ASEE 25th Joint Propulsion Conference, 1989/Monterey, California.

19. D. K. Beale and M. Zelenak. **Development and Validation of a Freejet Technique for Inlet-Engine Compatibility Testing.** AIAA Paper 92-3921, AIAA, Inc., 1992. AIAA 17th Aerospace Ground Testing Conference, 1992/Nashville, Tennessee.
20. G. Cooper and W. Phares. **CFD Applications in an Aerospace Engine Test Facility.** AIAA Paper 90-2003, AIAA, Inc., 1990. AIAA/SAE/ASME/ASEE 26th Joint Propulsion Conference, 1990/Orlando, Florida.
21. W. J. Dardis, E. R. Mayhew, and D. K. Beale. **An Acceptance Process for the Evaluation of Inlet Distortion.** AIAA Paper 92-3918, AIAA, Inc., 1992. AIAA 17th Aerospace Testing Conference, 1992/Nashville, Tennessee.
22. J. J. Marous and D. E. Sedlock. **An Analog Editing System for Inlet Dynamic Flow Distortion, DYNADEC Past, Present and Future.** AIAA Paper 80-1108, AIAA, Inc., 1980. AIAA/SAE/ASME 16th Joint Propulsion Conference, 1980/Hartford, Connecticut.
23. G. R. Adams, J. W. Thompson, Jr., R. B. Abernethy, T. Biesiadny, C. T. Harvey, J. W. Steurer, J. C. Ascough, and D. D. Williams. **Uncertainty Methodology for In-Flight Thrust Determination.** SAE Paper 831438. Aerospace Congress and Exposition, 1983/Long Beach California.
24. Richard J. Larsen and Morris L. Marx. **An Introduction to Mathematical Statistics and Its Applications.** Prentice-Hall, Inc., 1981.
25. Society of Automotive Engineers, Inc. **Uncertainty of In-Flight Thrust Determination.** SAE Aerospace Information Report 1678. July, 1985.